Leg 198 Preliminary Report

Extreme Warmth in the Cretaceous and Paleogene: A Depth Transect on Shatsky Rise, Central Pacific

27 August–23 October 2001

Shipboard Scientific Party

Ocean Drilling Program
Texas A&M University
1000 Discovery Drive
College Station TX 77845-9547
USA

January 2002

PUBLISHER'S NOTES

This report was prepared from shipboard files by scientists who participated in the cruise. The report was assembled under time constraints and does not contain all works and findings that will appear in the *Initial Reports* of the ODP *Proceedings*. Reference to the whole or to part of this report should be made as follows:

Shipboard Scientific Party, 2002. Leg 198 Preliminary Report. *ODP Prelim. Rpt.,* 98 [Online]. Available from World Wide Web: <http://www-odp.tamu.edu/publications/prelim/198_prel/198PREL.PDF>. [Cited YYYY-MM-DD]

Distribution: Electronic copies of this series may be obtained from the Ocean Drilling Program's World Wide Web site at http://www-odp.tamu.edu/publications.

This publication was prepared by the Ocean Drilling Program, Texas A&M University, as an account of work performed under the international Ocean Drilling Program, which is managed by Joint Oceanographic Institutions, Inc., under contract with the National Science Foundation. Funding for the program is provided by the following agencies:

Australia/Canada/Chinese Taipei/Korea Consortium for Ocean Drilling
Deutsche Forschungsgemeinschaft (Federal Republic of Germany)
Institut National des Sciences de l'Univers-Centre National de la Recherche Scientifique (INSU-CNRS; France)
Ocean Research Institute of the University of Tokyo (Japan)
National Science Foundation (United States)
Natural Environment Research Council (United Kingdom)
European Science Foundation Consortium for Ocean Drilling (Belgium, Denmark, Finland, Iceland, Ireland, Italy, The Netherlands, Norway, Spain, Sweden, and Switzerland)
Marine High-Technology Bureau of the State Science and Technology Commission of the People's Republic of China

DISCLAIMER

The following scientists and personnel were aboard the *JOIDES Resolution* for Leg 198 of the Ocean Drilling Program:

SHIPBOARD SCIENTIFIC PARTY

Timothy J. Bralower
Co-Chief Scientist
Department of Geological Sciences
University of North Carolina at Chapel Hill
CB 3315
Mitchell Hall
Chapel Hill NC 27599-3315
USA
Work: (919) 962-0704
Fax: (919) 966-4519
bralower@email.unc.edu

Isabella Premoli-Silva
Co-Chief Scientist
Dipartimento di Scienze della Terra
Università degli Studi di Milano
Via Mangiagalli 34
20133 Milano
Italy
Work: (39) 02-23698248
Fax: (39) 02-70638261
Isabella.Premoli@unimi.it

Mitchell J. Malone
Staff Scientist/Inorganic Geochemist
Ocean Drilling Program
Texas A&M University
College Station TX 77845-9547
Work: (979) 845-5218
Fax: (979) 845-0876
malone@odpemail.tamu.edu

Michael A. Arthur
Sedimentologist
Department of Geosciences
Pennsylvania State University
503 Deike Building
University Park PA 16875
USA
Work: (814) 863-6054
Fax: (814) 863-7823
arthur@geosc.psu.edu

Kristen Averyt
Inorganic Geochemist
Department of Geological and Environmental Sciences
Stanford University
320 Braun Hall
Stanford CA 94305
USA
Work: (650) 723-4885
Fax: (650) 725-0979
kaveryt@pangea.stanford.edu

Simon C. Brassell
Organic Geochemist
Department of Geological Sciences
Indiana University, Bloomington
1001 East 10th Street
Bloomington IN 47405-1403
USA
Work: (812) 855-3786
Fax: (812) 855-7961
simon@indiana.edu

Paul R. Bown
Paleontologist (nannofossisl)
Department of Geological Sciences
University College London
Gower Street
London WC1E 6BT
United Kingdom
Work: (44) 020-7679-2431
Fax: (44) 020-7388-7614
p.bown@ucl.ac.uk

James E.T. Channell
Paleomagnetist
Department of Geological Sciences
University of Florida
241 Williamson Hall
PO Box 112120
Gainesville FL 32611-2120
USA
Work: (352) 392-3658
Fax: (352) 392-9294
jetc@nersp.nerdc.ufl.edu

Leon J. Clarke
Physical Properties Specialist
School of Ocean Sciences
University of Wales, Bangor
Askew Street
Menai Bridge
Anglesey LL59 5EY
United Kingdom
Work: (44) 1248-382858
Fax: (44) 1248-716637
l.clarke@bangor.ac.uk

Andrea Dutton
Sedimentologist
Department of Geological Sciences
University of Michigan
2534 C.C. Little Building
425 East University
Ann Arbor MI 48109-1063
USA
Work: (734) 647-7924
Fax: (734) 763-4690
adutton@umich.edu

Jason W. Eleson
Paleontologist (nannofossil)
Department of Geological Sciences
University of North Carolina at Chapel Hill
CB 3315
216 Mitchell Hall
Chapel Hill NC 27599-3315
USA
Work: (919) 962-0704
Fax: (919) 966-4519
jasoneleson@mailcity.com

Tracy D. Frank
Inorganic Geochemist
Department of Earth Sciences
University of Queensland
St. Lucia QLD 4072
Australia
Work: (61) 7-3365-8379
Fax: (61) 7-3365-1277
t.frank@earth.uq.edu.au

Susanne Gylesjö
Sedimentologist
Department of Geology and Geochemistry
Stockholm Universitet
106 91 Stockholm
Sweden
Work: (46) 8-164723
Fax: (46) 8-6747897
susanne.gylesjo@geo.su.se

Haidi Hancock
Sedimentologist
Department of Earth Sciences
James Cook University of North Queensland
Townsville QLD 4811
Australia
Work: (61) 7 47 81 4079
Fax: (61) 7 47 25 1501
haidi.hancock@jcu.edu.au

Harumasa Kano
Sedimentologist
Institute of Geology and Paleontology
Tohoku University
Aoba, Aramaki, Aoba-ku
Sendai, Miyagi 980-8587
Japan
Work: (81) 22-217-6625
Fax: (81) 22-217-6634
harumasa@mail.cc.tohoku.ac.jp

R. Mark Leckie
Paleontologist (foraminifers)
Department of Geosciences
University of Massachusetts
Morrill Science Center
611 North Pleasant Street
Amherst MA 01003-5820
USA
Work: (413) 545-1948
Fax: (413) 545-1200
mleckie@geo.umass.edu

Kathleen M. Marsaglia
Sedimentologist
Department of Geological Sciences
California State University, Northridge
18111 Nordhoff Street
Northridge CA 91330-8266
USA
Work: (818) 677-6309, Ext. 3541
Fax: (818) 677-2820
kathie.marsaglia@csun.edu

Jennifer McGuire
Physical Properties Specialist
Department of Geology and Geophysics
Texas A&M University
Mail Stop 3115
College Station TX 77843-3115
USA
Work: (979) 845-8482
Fax: (979) 845-3138
mcguire@odpemail.tamu.edu

Maria Rose Petrizzo
Paleontologist (foraminifers)
Dipartimento di Scienze della Terra
Università degli Studi di Milano
Via Mangiagalli 34
20133 Milano
Italy
Work: (39) 2-2369 8240
Fax: (39) 2-7063 8261
mrose@e35.gp.terra.unimi.it

Stuart Robinson
Physical Properties Specialist
Department of Earth Sciences
University of Oxford
Parks Road
Oxford OX1 3PR
United Kingdom
Work: (44) 1865 272019
Fax: (44) 1865 272072
stuartr@earth.ox.ac.uk

Ursula Röhl
Stratigrapher
Fachbereich Geowissenschaften
Universität Bremen
Klagenfurter Strasse
28359 Bremen
Germany
Work: (49) 421-218-2482
Fax: (49) 421-218-3116
uroehl@allgeo.uni-bremen.de

William W. Sager
Paleomagnetist
Department of Oceanography
Texas A&M University
317A Eller Building
Mail Stop 3146
College Station TX 77843-3146
USA
Work: (979) 845-9828
Fax: (979) 845-6331
wsager@ocean.tamu.edu

Kotaro Takeda
Paleontologist (foraminifers)
Institute of Geology and Paleontology
Tohoku University
Aoba, Aramaki, Aoba-ku
Sendai, Miyagi 980-8578
Japan
Work: (81) 22-217-6627
Fax: (81) 22-217-6634
kotaro-t@mail.cc.tohoku.ac.jp

Deborah Thomas
Sedimentologist
Department of Geological Sciences
University of North Carolina at Chapel Hill
CB 3315
Mitchell Hall
Chapel Hill NC 27599-3315
USA
Work: (919) 225-7463
Fax: (919) 966-4519
dthomas1@email.unc.edu

James C. Zachos
Sedimentologist
Earth Sciences Department
University of California, Santa Cruz
Earth and Marine Sciences Building
Santa Cruz CA 95064
USA
Work: (831) 459-4644
Fax: (831) 459-3074
jzachos@es.ucsc.edu

Trevor Williams
Logging Staff Scientist
Lamont-Doherty Earth Observatory
Borehole Research Group
Route 9W
Palisades NY 10964
USA
Work: (845) 365-8626
Fax: (845) 365-3182
trevor@ldeo.columbia.edu

K.T. Moe
Logging Trainee
Institute for Frontier Research on Earth Evolution (IFREE)
Japan Marine Science and Technology Center
2-15 Natsushima Cho
Yokosuka 237-0061
Japan
Work: (0468) 67-5517
Fax: (0468) 67-3409
moe@jamstec.go.jp

TRANSOCEAN SEDCO FOREX OFFICIALS

Peter Mowat
Master of the Drilling Vessel
Overseas Drilling Ltd.
707 Texas Avenue South, Suite 213D
College Station TX 77840-1917
USA

Scott Pederson
Drilling Superintendent
Overseas Drilling Ltd.
707 Texas Avenue South, Suite 213D
College Station TX 77840-1917
USA

ODP SHIPBOARD PERSONNEL

Kim Bracchi
Marine Laboratory Specialist (Curator)

Tim Bronk
Marine Laboratory Specialist (Chemistry)

Shannon Center
Marine Laboratory Specialist (Photographer)

Lisa Crowder
Marine Laboratory Specialist (Yeoperson)

Sandy Dillard
Marine Laboratory Specialist (Downhole Tools, Thin Sections)

David Fackler
Information Services Representative

Burney Hamlin
Laboratory Officer

Steven W. Kittredge
Schlumberger Engineer

Jurie Kotze
Marine Electronics Specialist

Alexis Lambeck
Marine Laboratory Specialist (Core)

David Morley
Marine Computer Specialist

Anne Pimmel
Marine Laboratory Specialist (Chemistry)

Pieter Pretorius
Marine Electronics Specialist

Mads Radsted
Marine Laboratory Specialist (Paleomagnetism)

Patrick Riley
Marine Laboratory Specialist (Physical Properties)

Michael Storms
Operations Manager

Johanna Suhonen
Marine Laboratory Specialist (Underway Geophysics)

Steve Tran
Marine Computer Specialist

Bob Wheatley
Marine Laboratory Specialist (Physical Properties)

OVERVIEW

The mid-Cretaceous (~125-85 Ma) and early Paleogene (~60-45 Ma) were characterized by some of the most equable climates of the Phanerozoic and are among the best known ancient "greenhouse" climate intervals. In addition, these intervals contain some of the most abrupt and transient climatic changes in the geologic record, including the late Paleocene thermal maximum (LPTM), the mid-Maastrichtian deep-water event (MME), and the early Aptian oceanic anoxic event (OAE1a). These critical transitions involved dramatically modified oceanic circulation patterns, profound changes in geochemical cycling, and abrupt turnover in marine biotas. Recent ocean drilling efforts have led to profound advances in our understanding of the ocean and climate dynamics of a warm Earth; however, we have yet to gain a firm grip on how atmospheric or deep ocean circulation operates in the apparent absence of substantial thermal gradients, how rapid removal of important elements such as nutrients in some of these events is maintained for long period of time, and exactly how environmental changes cause extinction and speciation of marine biotas.

Ocean Drilling Program (ODP) Leg 198 on Shatsky Rise was designed to address the causes and consequences of Cretaceous and Paleogene global warmth. The objectives were to address the origin of the long-term climatic transition into and out of "greenhouse" climate as well as abrupt climatic events. Shatsky Rise, a medium-sized large igneous province (LIP) in the west-central Pacific, contains sediments of Cretaceous and Paleogene age at relatively shallow burial depths on three prominent highs. As a result, sediments of both ages can be reached readily through drilling, and fossil materials are sufficiently well preserved for stable isotope and trace element analyses and for faunal and floral assemblage studies.

Eight sites were drilled during Leg 198 on a broad depth transect (Table T1) designed to characterize changes in the nature of surface and deep waters through time, including vertical gradients of temperature, oxygenation, and corrosiveness. Six sites were cored on the Southern High, and one each on the Central and Northern Highs. The Southern High had been cored during previous Deep Sea Drilling Program (DSDP) and ODP legs; thus, the general stratigraphy of this area was known prior to drilling. The Central and Northern Highs, however, had not been cored previously.

A virtually complete section from the Holocene to the Jurassic/Cretaceous boundary interval was cored on Shatsky Rise. Leg 198 also cored the first igneous rocks from Shatsky Rise, predominantly diabase sills that may represent a regional intrusive event. Multiple coring produced a composite section for all but a small portion of the Cenozoic. Prominent orbital cycles throughout the Cenozoic hold significant potential for precise correlation between holes and sites.

A number of critical transitions were cored during Leg 198, most in multiple holes from several sites. Dark-colored, organic carbon (C_{org})-rich claystones and porcellanites of early Aptian OAE1a were recovered at three different sites. Samples from two of these sites have extremely high organic carbon contents, up to 25.2 and 34.6 wt%. This organic matter is marine in origin and of exceptional preservation, containing evidence for cyanobacteria and the oldest known alkenones, compounds produced by haptophyte algae. The preservation of organic matter and common lamination suggests deposition and diagenesis in highly dysoxic or anoxic environments. Nannofossil and radiolarian biostratigraphy indicate that the three sections correlate with sediments representing OAE1a at other sites in the Pacific and southern Europe, including the well-known Selli level of Italy. The recovered organic-rich sequences are possibly the best pelagic records of OAE1a.

A significant representation of the MME was recovered at two sites. Clusters of large *Inoceramus* prisms are seen in the cores for several meters but disappear abruptly. This disappearance is in the same stratigraphic position in two holes at ~69 Ma and correlates to the *Inoceramus* extinction and the isotopic shifts that mark the MME at other deep-sea locations. Prisms have been noticed in washed samples from a third site. The significance of the short range of visible specimens in this open-ocean setting is not currently understood. Benthic foraminiferal data from the Shatsky Rise depth transect will help to accurately characterize the changes in deep-water properties across this event.

A remarkable set of cores was taken across the Cretaceous/Tertiary (K/T) boundary at four sites on the Southern High and in nine separate holes. The lithostratigraphy of the boundary succession is remarkably similar in all of the holes, allowing precise correlation between records. The uppermost Maastrichtian whitish nannofossil foraminiferal ooze contrasts strongly with the pale orange, clay-rich lowermost Danian foraminiferal ooze. The contact is mixed by bioturbation, but otherwise the boundary interval is undisturbed.

Preliminary biostratigraphy shows the well-established, abrupt change in nannofossil and planktonic foraminiferal assemblages across the boundary at all sites. Careful sampling of burrows of Danian ooze within the top of the Maastrichtian yields spherules that are probably altered tektites. The same reaches of the burrows contain highly abundant, minute planktonic foraminiferal assemblages that possibly represent basal Paleocene Zone P0. This is the first time the basal Paleocene zone has been identified in the deep sea. Even though the K/T boundaries on Shatsky Rise have been mixed by bioturbation, the substantial thickness of the uppermost Maastrichtian *Micula prinsii* (CC26) Zone and the lowermost Danian *Parvularugogloberina eugubina* (Pα) Zones indicates that the boundary is paleontologically complete. The Shatsky Rise sections represent one of the best preserved and least disrupted deep-sea records of this major extinction event, as well as the subsequent radiation.

The late Paleocene thermal maximum, one of the primary targets of Shatsky Rise coring, was recovered in 10 separate holes at four sites on the Southern High. These sites provide a depth range of about 500 m, designed to test the response of the ocean to the hypothesized massive input of methane hydrate. In all but one of the holes, the LPTM corresponds to an 8- to 23-cm-thick layer of yellowish brown, clayey nannofossil ooze with a sharp base and a gradational top. At several sites, an extremely thin (1 mm) dark brown clay seam lies at the base of the LPTM, corresponding to a sharp drop in carbonate content as indicated by color reflectance data. One hole at the deepest site, Site 1211, has an unconformity right above the clay seam. In all of the other holes, preliminary biostratigraphy suggests that the LPTM interval is complete. The Paleocene/Eocene boundary interval was also recovered at Site 1208 on the Central High, although it is currently uncertain whether this record contains the LPTM. This deep site will extend the depth transect another 450 m.

The LPTM interval in all of the Southern High sites contains a clear record of nannofossil and planktonic foraminiferal assemblage transformation at this time of major environmental upheaval. Planktonic foraminiferal assemblages within the clay-rich interval contain an ephemeral group of ecophenotypes or short-lived species of the genera *Acarinina* and *Morozovella* observed in other tropical and subtropical locations. All sites show a general deterioration in nannofossil preservation at the onset of the event and contain abundant 10- to 20-µm-sized, bladey calcite crystals that are thought to have been derived from precipitation of dissolved carbonate.

The general changes in lithology suggest a transition from paleodepths at the shallower sites that were less sensitive to changes in carbonate solubility in the deep ocean (Sites 1209, 1210, and 1212),

to those that were at depth ranges highly sensitive to changes across the LPTM interval (Sites 1208 and 1211). The decrease in carbonate content and deterioration in nannofossil preservation are evidence for an abrupt rise in the level of the calcite compensation depth (CCD) and lysocline during the LPTM, the predicted response for a massive release of methane into the ocean-atmosphere system.

A major deep-water cooling event that coincides with intensification of glaciation on Antarctica occurred during the Eocene–Oligocene transition. Leg 198 recovered records in a total of nine holes at four sites across a large depth range to test the response of the tropical Pacific Ocean to this cooling event. Cooling is thought to have indirectly led to a gradual deepening in the CCD as a result of increased physical weathering on continents or intensification of deep-sea circulation. In all of the holes, the transition is associated with a lightening in the color of the sediment associated with an increase in carbonate content. This transition takes place over 4 to 7.5 m at the Southern High sites, but over 1–2 cm at Site 1208 on the Central High. The distinctive color change in the all of the Leg 198 records reflects a pronounced deepening in the CCD at or during the Eocene–Oligocene transition. The sharp boundary at Site 1208 indicates a considerable deepening in the CCD in this region. Preliminary data show that the prominent change in lithologic signature occurs just before or within the time of cooling. However, further analysis is required to determine the exact timing of this event and the nature of the deep-water changes on Shatsky Rise.

Coring on Shatsky Rise also provided a number of surprises. On the Central and Northern Highs, expanded, mixed siliceous-calcareous Neogene sequences were recovered that are potentially significant for advances in biochronology and magnetochronology. These sections are strongly cyclic and have potentially significant high-quality paleoceanographic records. Site 1208 on the Central High is an excellent candidate for the development of a paleomagnetic intensity record for the Pacific Ocean. At the opposite end of the stratigraphic column, an organic-rich horizon in the Valanginian may represent the first deep ocean record of an event that was previously confined to Tethys.

INTRODUCTION

Leg 198 was designed to obtain a depth transect of the Cretaceous through Paleogene Pacific Ocean to advance our understanding of the behavior of Earth's climate during "greenhouse" intervals. The Cretaceous and Paleogene are an extended interval of global warmth, on which are superimposed some of the most abrupt and transient climatic changes in the Phanerozoic, including the late Paleocene thermal maximum (e.g., Kennett and Stott, 1991; Zachos et al., 1993), the MME (e.g., MacLeod and Huber, 1996), and the early Aptian OAE1a (e.g., Bralower et al., 1994; Erba et al., 1999). These transient events, less than a million years in duration, are associated with abrupt changes in sea-surface temperatures (SSTs) (e.g., Zachos et al., 1994), switches in the mode of deep sea circulation (e.g., Frank and Arthur, 1999), drastic changes in primary production in surface waters and in marine environments, profound turnover in marine communities (e.g., Erba, 1994; Kelly et al., 1996; Thomas, 1998), and sharp changes in geochemical cycling and burial of organic and inorganic materials (e.g., Arthur et al., 1985; Dickens et al., 1995). A surge in interest in transient climate events has accompanied the recognition that they may have involved rates of input of greenhouse gases similar to modern emissions (e.g., Dickens et al., 1997; Norris and Röhl, 1999).

The last couple of decades of ocean drilling have involved recovery of a number of high-quality records of the mid-Cretaceous and Paleogene interval of global warmth. Stable isotopic and

micropaleontological investigations of these sections allowed us to compile detailed long-term records of sea-surface and deep-water temperatures and to identify times of peak warmth, as well as transitional intervals into and out of this "greenhouse" interval (e.g., Huber et al., 1995; Jenkyns et al., 1995; Clarke and Jenkyns, 1999; Norris and Wilson, 1998; Erbacher et al., 2001; Wilson and Norris, 2001). Combination of data from low- and high-latitude sites can help us determine thermal gradients; however, we can still only speculate about the nature of deep sea circulation. Moreover, we still do not have a complete understanding of how global warmth was maintained for long periods of time with apparently low thermal gradients (e.g., Sloan and Thomas, 1998; Huber and Sloan, 2000), nor do we completely understand how these thermal gradients affected deep sea circulation patterns. We have also yet to determine how the ocean maintains apparently high or low fertility states for extended intervals and how this affected the balance of key nutrients. Finally, we do not fully understand the detailed mechanisms that transform marine communities during times of abrupt environmental change.

One of the largest obstacles facing our understanding of Cretaceous and Paleogene climate and ocean circulation is that many good stratigraphic sections have been buried at depths where diagenetic alteration has obscured stable isotope and other climate proxies. In other sequences, spot-coring, coring gaps, and drilling disturbance hinder detailed paleoceanographic studies. The result is that site coverage is uneven and almost nonexistent in some areas. This is especially the case for the Pacific Ocean. The areal extent and importance of the Pacific in global circulation, however, makes it a critical target for drilling of warm climatic intervals.

One of the most promising locations in the Pacific for recovering Cretaceous and Paleogene sediments at relatively shallow burial depths is Shatsky Rise, a medium-sized LIP, in the west-central Pacific (Fig. F1). Shatsky Rise has been the target of three DSDP expeditions—Legs 6, 32, and 86—and ODP Leg 132. The highest quality record was obtained during Leg 86 at Site 577, which was limited to the Paleogene and uppermost Maastrichtian. Some sites in the older legs were spot-cored, and chert has lowered recovery in others, especially in the Cretaceous. Rotary coring of the unindurated Cenozoic section has led to considerable disturbance. Yet even with an extremely patchy record, SST estimates obtained from isotopic analyses of Shatsky Rise sediments have provided scarce but important data for our understanding of Cretaceous and Paleogene climates. The Leg 198 depth transect was designed to provide additional data from the tropical Pacific as well as a representative open-ocean signal.

The majority of sites used in current paleoceanographic investigations were situated at relatively shallow paleodepths, mostly less than 2000 m. The selected Shatsky sites provide a depth transect spanning 1500 m of the water column, providing us the opportunity to sample true intermediate and deep waters. Even though the paleodepth estimates for the Leg 198 sites are somewhat uncertain, their broad depth range ensures that the deepest sites will lie below previously drilled sites. Existing recovery from Shatsky demonstrates that pristine isotope-grade material will be recovered for most of the entire interval of interest due to its relatively shallow burial depth. This will allow the following specific objectives to be addressed:

1. Filling the Pacific gap in current paleoenvironmental data sets to complete global reconstructions and modeling of the physical and chemical parameters of warm oceans.
2. Reconciling the nature of climatic forcing during the Cretaceous and Paleogene by monitoring changes in the properties of surface and deep waters. This will help to constrain

the character and stability of intermediate and deep-water circulation, vertical thermal gradients, and basin fractionation during ancient intervals of extreme warmth.
3. Understanding how apparently cooler tropical SSTs and low meridional thermal gradients were maintained during "greenhouse" climate intervals.
4. Shedding light on the origin of transient climatic events such as the Eocene/Oligocene boundary, the LPTM, late Paleocene and early Eocene hyperthermals, and the MME. The depth transect will also help address questions concerning the nature of chemical (i.e., CCD, nutrients, and oxygenation) and physical oceanographic changes (temperature gradients) during these events.
5. Understanding water column stratification during mid-Cretaceous oceanic anoxic events (OAEs) as well as obtaining complete records of organic-rich sediments suitable for detailed paleontological and geochemical investigations. These data will allow us to more fully determine the response of marine biotas to abrupt environmental changes and to constrain changes in carbon and nutrient cycling during the OAEs.
6. Examining Lower Cretaceous sedimentary rocks from Shatsky Rise would allow us to address (1) how evolutionary records of microplankton from the Pacific compare with those derived elsewhere; (2) if there is any record for C_{org}-rich levels in the Valanginian that might correlate with carbonaceous levels in Europe; and (3) the record of the CCD through time in this part of the ocean and the major forces driving these changes.
7. Determining the age, composition, and nature of basement rocks would add valuable information to models of the origin of Shatsky Rise and LIPs in general.

The Shatsky Rise sedimentary section should also allow a number of additional questions to be addressed. These questions include (1) determining the origin of orbital cycles expressed in the sedimentary record, (2) reconstructing the history of the CCD in the northern Pacific, (3) determining the subsidence track of Shatsky Rise through time and comparing it with tracks for other features in the Pacific, (4) recreating Paleogene and Neogene atmospheric circulation patterns from the distribution and composition of eolian materials, and (5) refining the geologic timescale based on orbital chronology and the correlation between biostratigraphy and magnetostratigraphy.

Finally, drilling of basement on Shatsky Rise will provide samples to determine the age and composition of basement under the rise. The compositional data from Shatsky Rise basement and other LIPs will be compared in light of the different models for their formation.

Tectonic Evolution of Shatsky Rise

Shatsky Rise, a broad elevation in the west-central Pacific, is the oldest existing oceanic plateau. The rise is 1650 km long, 450 km wide, and consists of three prominent highs (Southern, Central, and Northern) arranged in a southwest-northeast trend (Fig. F2). The Southern High, also known as Shatsky Plateau, is the largest high with a length of about 700 km and a width of about 300 km. Central and Northern Highs are less than half the size of the Southern High. The highs have tops at 2.5–3.5 km and gentle flanks that rise from the surrounding seafloor at 5.5–6 km. This topography is consistent with production by effusive flood basalt–style volcanism. The highs are volcanic edifices that are surrounded by normal oceanic lithosphere and a group of about 80 seamounts (Sager et al., 1999). Although there has been no basement drilling of Shatsky Rise, altered basalts have been dredged (Sager et al., 1999).

Southern High is elongated southwest to northeast with a subcircular summit that rises to ~2400 m (Fig. F2). The sediment pile on the high is up to ~1200 m thick. Jurassic/Cretaceous rudists and corals have been dredged from the south edge of the Southern High summit, suggesting that the Southern High was emergent early in its history (Sager et al., 1999).

Central High is subcircular with a broad summit rising to depths of ~3000 m Nakanishi et al., 1999). The sedimentary section is up to 1 km in thickness. Underneath the sediments are a series of basement ridges and faults. The Central High flanks appear to follow lineation and fracture patterns, and thus were likely shaped by ridge tectonics (Sager et al., 1999). The smallest of the highs, Northern High, has a domed summit rising to 3100 m. The sediment package on this high reaches about 1 km in thickness (Sager et al., 1999). The shape and orientation of the flanks also suggest that they were formed by ridge tectonics (Nakanishi et al., 1999; Sager et al., 1999).

Shatsky Rise intersects the southwest-northeast trending Japanese magnetic lineations and the northwest-southeast trending Hawaiian lineations (Nakanishi et al., 1989). Thus the regional magnetic anomalies of the abyssal Pacific seafloor surrounding Shatsky Rise exhibit a nearly orthogonal pattern (Sager et al., 1988; Nakanishi et al., 1992) with the presumed intersection of the anomalies near the crest of the rise. The observation of lineations continuing through Shatsky Rise indicates that it formed on oceanic lithosphere (Nakanishi et al., 1999).

The rise is bracketed by magnetic polarity Zones M21 and M10N (Fig. F3), with a progression of ages and decreasing volume of highs from southwest to northeast (Southern to Northern High) (Sager and Han, 1993). Because the rise lies at the triple junction of the Hawaiian and Japanese magnetic lineation sequences, its formation is thought to be related to the evolution of the junction between them (e.g., Larson and Chase, 1972; Hilde et al., 1976). Magnetic lineations cross only the lower part of the three highs, suggesting that they are volcanic edifices separated by normal lithosphere (Nakanishi et al., 1999). Nakanishi et al. (1989) proposed that Shatsky Rise formed by a magmatic pulse at a hotspot triple-junction intersection beginning in polarity Chron CM21 in the Tithonian (Late Jurassic) and ending at ~ polarity Chron CM12 in the Valanginian (Early Cretaceous). Age gaps between the highs suggest that plateau volcanism was episodic. Sager and Han (1993) noted uniform reversed magnetization on the Southern Rise and proposed that it formed rapidly during one reversed polarity chron, although the calculated rate of formation was somewhat slower than Ontong Java Plateau (Tarduno et al., 1991). The rise was likely formed by eruption of a large igneous pile during initial plume head activity (Sager and Han, 1993; Sager et al., 1999).

A number of lineations form magnetic bights in the middle of the rise. These bights indicate past locations of triple junctions (Nakanishi et al., 1999; Sager et al., 1999). Bights older than M22 occur south of Shatsky Rise. Bights between M19 and M14 are found between the Southern and Northern Highs. Gaps between magnetic lineation bights indicate large triple-junction jumps (Nakanishi et al., 1999). It is possible that the triple-junction movement was caused by ridge jumps as the triple junction moved to stay over the plume, which drifted northeast relative to the Pacific plates as the plates moved over the mantle. The formation of Shatsky Rise occurred about the same time as an 800 km eastward jump of the Pacific-Izanagi-Farallon Triple Junction and reorganization of Pacific-Izanagi Ridge between Chrons CM21 and CM19. The ridge jump was possibly caused by the eruption of Shatsky Rise. Other ridge jumps occurred around the time of the formation of the Central and Northern Highs (Sager et al., 1999).

Although paleoreconstructions have a great deal of uncertainty, Shatsky Rise appears to have formed in equatorial latitudes in the Southern Hemisphere and gradually drifted northward during the last 90 m.y. (Larson et al., 1992) (Fig. F4).

Stratigraphy of Shatsky Rise

All previous DSDP and ODP drill sites are located on the Southern High (Fig. F3). The sedimentation history of the Central and Northern Highs was not known prior to Leg 198. Pelagic sedimentation on the Southern Rise began in the latest Jurassic or earliest Cretaceous and shows a moderately stratified section overlying acoustic basement. The section is up to 1.2 km thick in places (Ewing et al., 1966; Sliter and Brown, 1993). Sedimentation appears to have been interrupted by episodic, regional, or local erosional events identified by previous drilling (Sliter and Brown, 1993). Some of the unconformities show up as major reflectors observed in seismic records. Quaternary channeling of the sediment pile is evident on seismic records, and in some places Lower Cretaceous sediments crop out at the seafloor (Sliter et al., 1990), for example near Site 306 (Site 1214). Seismic profiles show abrupt changes in stratigraphy over short distances.

Divergence of deep reflectors suggests that there was more rapid basement subsidence in the Early Cretaceous prior to the deposition of Upper Cretaceous and Cenozoic sediments. However, the subsidence history of Shatsky Rise is not well known. Thierstein (1979) backtracked Sites 305 and 306 (currently at 2903 and 3416 m, respectively) to close to 1000 m paleodepth in the Early Cretaceous sediments. Recently, rudists, corals and echinoid spines were dredged from a ridge on the Southern High at 3000 m (Sager et al., 1999), suggesting paleodepths close to sea level. Detailed studies of benthic foraminiferal assemblages are required to more accurately constrain the subsidence history of Shatsky Rise and compare it to other features in the Pacific with a clearer subsidence history.

A total of eight previous DSDP and ODP drill sites lie on the Southern High (Fig. F3). At Site 47 atop the southwest flank of the Southern High, the highly discontinuous, ~130-m Cenozoic and Maastrichtian section that was recovered consists of ooze and chalk. Nearby, at Site 48, the ~85-m section contains Miocene ooze resting directly on Maastrichtian chalk (Fischer, Heezen, et al., 1971). At Site 49, on the lower southwestern flank, a thin (~5 m) Pleistocene zeolitic clay unit sits directly on ~15 m of Tithonian–Berriasian cherty chalk. The nearby section at Site 50 includes ~35 m of Pleistocene zeolitic clay and siliceous ooze overlying ~9 m of Tithonian–Berriasian chalk. At Site 305, on the southern flank of Southern High, 640 m of section was cored. The section includes Campanian to Holocene ooze and chalk with minor, disseminated chert overlying Santonian to Coniacian and Cenomanian to Barremian chalk with regular chert nodules (Larson, Moberly, et al., 1975; Sliter, 1992). Nearby, drilling at Site 306 recovered Holocene ooze directly overlying chalk of Albian age. Alternating chalk and chert extend down to the Berriasian, where the hole was terminated at 475 meters below seafloor (mbsf) (Fig. F5). Scraps of C_{org}-rich sediments of early Aptian age were recovered at Sites 305 and 306 (Larson, Moberly, et al., 1975). Sliter (1989) refined the biostratigraphy of the mid-Cretaceous of Site 305 and placed the organic-rich units in the *Globigerinelloides blowi* planktonic foraminiferal zone, correlating them with OAE1a, the lowermost mid-Cretaceous OAE (Bralower et al., 1993). Additional fragments of carbonaceous shale from Core 37 at Site 305 are early Cenomanian to early Turonian in age and apparently underlie a major unconformity that extends to the Coniacian.

Drilling at Site 577, which is located near Site 47, recovered ~120 m of nannofossil ooze (Heath et al., 1985). The section includes a thin upper Miocene to Holocene interval overlying a relatively expanded upper Maastrichtian–Paleocene interval. The K/T boundary at Site 577 is nearly complete biostratigraphically and contains an Ir anomaly (Wright et al., 1985). The boundary interval has been the subject of a host of paleoceanographic investigations (e.g., Gerstel et al., 1986; Zachos and

Arthur, 1986; Zachos et al., 1989). The LPTM lies between cores at Site 577 (Pak and Miller, 1992). Site 810, the most recently cored Shatsky site that was drilled during Leg 132 primarily as an engineering test, recovered a highly discontinuous Cenozoic and upper Maastrichtian section composed of ooze, chalk, and chert (Storms, Natland, et al., 1991; Premoli Silva et al., 1993).

Two regional reflectors or sets of reflectors divide the sedimentary column of the Southern High. Sliter and Brown (1993) defined R1 as a prominent unconformity near the Cenomanian/Turonian boundary and R2 as a prominent chert horizon that lies close to the Barremian/Aptian boundary. Less prominent reflectors occur near the Paleogene/Neogene and K/T boundaries. Sliter and Brown (1993) also divided the Southern High stratigraphic section into five main stratigraphic units, a scheme that is also applied here: Units 1 and 2 are Neogene and Paleogene in age, respectively; Unit 3 is Turonian–Maastrichtian (between R0 and R1); Unit 4 is Aptian–Cenomanian (between R1 and R2); and Unit 5 is Berriasian–Barremian (below R2). The sedimentary sections on the Central and Northern Highs can be very tentatively correlated with the Southern High section based on the major reflectors. However, the absence of thick sedimentary sections between the highs lessens the credibility of these correlations (A. Klaus, W. Sager, and L. Khankishieva, pers. comm., 1997). Thus, the detailed sedimentary history of the Central and Northern Highs remained largely unknown prior to Leg 198.

The sedimentary history of Shatsky Rise appears to have been greatly affected by crossing the equatorial high-productivity zone in the mid- to Late Cretaceous (Fig. F4). This crossing led to the accumulation of substantial amounts of siliceous material that was concentrated in chert horizons during burial.

Oceanography

Shatsky Rise lies in the path of surface-water currents transporting two very different water masses. The first, the Kuroshio Extension, is the arm of the Kuroshio Current extending eastward into the Pacific Ocean off the coast of Japan. This current is the Pacific equivalent of the Gulf Stream after it leaves the coastline of North America (Kawai, 1970). The second current, the Oyashio, transports water from the subarctic water mass. These currents converge near the Northern High. However, depending on the exact location of the currents, which changes significantly over time, temperature and current velocity vary substantially over the rise. Average salinity for these surface waters ranges between 34 and 35 g/kg.

The Kuroshio and Oyashio Currents impose structure on underlying intermediate waters, marking a strong vertical gradient in temperature and salinity. At 1000 m depth, temperatures average 3°C. These waters also have salinities near 34 g/kg. The intermediate waters flow toward the east as part of a clockwise gyre in the North Pacific.

DETAILED SCIENTIFIC OBJECTIVES

Long- and Short-Term Warming in the Paleogene

The exact causes of the long- and short-term Paleogene warm episodes remain enigmatic. Several pieces of geochemical evidence, including changes in the mean ocean $\delta^{13}C$ and alkalinity, point toward greenhouse forcing (Shackleton, 1986; Kennett and Stott, 1991; Zachos et al., 1993; Thomas and Shackleton, 1996). Samples recovered during Leg 198 will help constrain the nature and causes of these warm episodes.

LPTM

In terms of the rate and degree of warming, the LPTM is unprecedented in Earth history (Fig. F6). The deep-sea and high-latitude oceans warmed by 4°C and 8°C, respectively. The carbon isotopic composition of the ocean decreased by 3‰–4‰ coeval with the warming event, suggesting a massive perturbation to the global carbon cycle (Fig. F7) (Kennett and Stott, 1991; Bains et al., 1999). The large magnitude and rate (~–3‰–4‰/5 k.y.) of the carbon isotope excursion (CIE) is consistent with the sudden injection of a large volume of methane from clathrates stored in continental slope sediments (Dickens et al., 1995, 1997). Much of this methane would have quickly converted to CO_2, stripping O_2 from deep waters, contributing to the major extinction event of benthic foraminifers (Thomas, 1990), and lowering alkalinity. The result should be a sharp rise in the level of the lysocline and CCD (Dickens, 2000). Both CO_2 and CH_4 would also have immediately contributed to greenhouse warming.

The Leg 198 depth transect will help us determine (1) the magnitude of the tropical Pacific sea-surface and deep-water temperatures increase during the LPTM; (2) whether or not the Pacific lysocline and CCD shoaled during the CIE, whether or not bottom-water oxygenation decreased, and how these changes fit with geochemical models of clathrate release; (3) the response of planktonic and benthic populations to the LPTM in the subtropical Pacific; and (4) whether or not there is a change in the distribution of bottom-water carbon isotopes prior to and/or during the LPTM signaling possible circulation changes.

Paleogene Deep-Water Circulation

Several investigators have suggested that early Cenozoic global warming would have altered deep-ocean circulation patterns by reducing the density of surface waters in high latitudes (Kennett and Shackleton, 1976; Wright and Miller, 1993; Zachos et al., 1993). This, in turn, would permit increased downwelling of highly saline but warmer waters in subtropical oceans. Such reversals or switches in circulation probably occurred suddenly rather than gradually. In fact, it has been suggested that a sudden change in intermediate-water circulation patterns may have occurred just prior to the LPTM, possibly triggering the dissociation of clathrates (Bralower et al., 1997a). There may have been additional, abrupt warming intervals in the late Paleocene and early Eocene (Thomas and Zachos, 1999; Thomas et al., 2000). These “hyperthermals” were characterized by changes in the assemblage composition of benthic foraminifers corresponding to negative shifts in planktonic and benthic foraminiferal $\delta^{18}O$ and $\delta^{13}C$ values. The ultimate cause of the hyperthermals may be similar to the LPTM, driven by the release of greenhouse gas.

Leg 198 samples will be used to assess regional and global circulation changes during the Paleogene. Major changes in the sources of waters bathing Shatsky Rise might be reflected in the spatial and vertical distribution of carbon isotope ratios in bottom waters as well as in benthic foraminiferal assemblage patterns. Several studies have shown that throughout the late Paleocene and early Eocene, the most negative deep-ocean carbon isotope values were consistently recorded by benthic foraminifers from Shatsky Rise (Miller et al., 1987b; Pak and Miller, 1992; Corfield et al., 1992). Such a pattern is similar to that in the modern ocean, implying older, nutrient-enriched waters in the Pacific, and younger, nutrient-depleted waters in the high latitudes. Although Site 577 is discontinuous across the Paleocene/Eocene boundary, isotope data from Site 865 on Allison Guyot in the equatorial Pacific suggest a possible reduction, if not reversal, in the $\delta^{13}C$ gradient between the shallow Pacific and the rest of the ocean (Bralower et al., 1995). If this was true, it would be

consistent with increased production of intermediate waters in low latitudes. In summary, Leg 198 samples will help address whether there is evidence of warmer, more saline deep waters at times during the Paleogene and how export production in the Pacific changed from the Paleocene to the Eocene.

Eocene–Oligocene Paleoceanography

The Eocene–Oligocene represents the final transition from a "greenhouse" to an "icehouse" world. Although this transition occurred over a period of 18 m.y., stable isotopic records reveal that much of the cooling occurred over relatively brief intervals in the late early Eocene (~50–51 Ma) and earliest Oligocene (~33 Ma) (Fig. F6) (e.g., Kennett, 1977; Miller et al., 1987a; Stott et al., 1990; Miller et al., 1991; Zachos et al., 1996). Furthermore, small, ephemeral ice sheets were probably present on Antarctica sometime after the first event (Browning et al., 1996). The first large permanent ice sheets became established much later, most likely during the early Oligocene event (Zachos et al., 1992a). Current reconstructions of ocean temperature and chemistry for the Eocene and Oligocene, however, are based primarily on pelagic sediments collected in the Atlantic and Indian Oceans (Miller et al., 1987a; Zachos et al., 1992b, 1996). Very few sections suitable for such work have been recovered from the Pacific (Miller and Thomas, 1985; Miller and Fairbanks, 1985). As a consequence, we still lack a robust understanding of how global ocean chemistry and circulation evolved in response to high-latitude cooling and glaciation.

Leg 198 sections across the Eocene–Oligocene transition will provide a vertical depth transect of ocean chemistry and temperature changes during this important climatic transition. These sections will allow us to determine whether the basin-to-basin deep carbon isotope gradient changed during the Eocene–Oligocene transition in response to high-latitude cooling and glaciation, and how the lysocline/CCD in the Pacific responded to the rapid high-latitude cooling/glaciations.

Mid- and Late Cretaceous Climate

The mid-Cretaceous (Barremian–Turonian [125–90 Ma]) Earth experienced some of the warmest temperatures and lowest thermal gradients of the entire Phanerozoic Eon. This time interval, therefore, represents one of the best ancient approximations of "greenhouse" climate. The Late Cretaceous was characterized by significant global cooling, but available oxygen isotopic records differ on the exact timing of the end of the "greenhouse" conditions. Records from DSDP Site 511 on the Falkland Plateau, South Atlantic (Huber et al., 1995), and the chalk from England (Jenkyns et al., 1994) suggest that peak warmth occurred in the early Turonian, at ~90 Ma (Fig. F8). Data from Shatsky Rise DSDP sites (e.g., Douglas and Savin, 1975; Savin 1977), however, indicate that peak "greenhouse" conditions existed in the Albian, at ~105 Ma. In addition, these stratigraphies differ on whether peak warming was immediately followed by long-term cooling (English chalk) or sustained warmth then cooling beginning in the mid-Campanian (Site 511 data). Differences between the various records may reflect real latitudinal climatic variations or diagenetic alteration of stable isotopic proxies.

There is also significant disparity as to exactly how much cooling occurred in the Late Cretaceous, especially in the tropics. Savin (1977) and D'Hondt and Arthur (1996) concluded that the Maastrichtian was characterized by surprisingly cool tropical SSTs (20°–21°C) based on $\delta^{18}O$ analyses of planktonic foraminifers, the "cool tropics paradox" (D'Hondt and Arthur, 1996). Wilson and Opdyke (1996), on the other hand, measured $\delta^{18}O$ values on rudists recovered from Pacific guyots

and concluded that tropical SSTs in the same interval were extremely warm (between 27°C and 32°C). More recently, Pearson et al. (2001) have also found evidence for high Maastrichtian temperatures in planktonic foraminifers from clay units in Tanzania. The climate history of the Cretaceous is based on a limited number of oxygen isotope data points from few sites with little information from the tropics. In fact, Shatsky Rise Site 305 (Douglas and Savin, 1975) is among a handful of low-latitude sites that form the basis of most Cretaceous thermal gradient estimates that are used as inputs in climate models (e.g., Barron and Peterson, 1991).

There is a limited understanding of the evolution of bottom-water circulation in the mid- and Late Cretaceous, in particular, of how and when the transition from low-latitude (e.g., Brass et al., 1982) to high-latitude (e.g., Zachos et al., 1993) deep-water sources took place. Benthic foraminiferal $\delta^{18}O$ records are even sparser than those based on planktonic foraminifers, and there are very few benthic data from the entire Pacific. Thus, the role of this giant basin in the evolution of deep waters during the mid- and Late Cretaceous is poorly understood.

The long-term cooling of the Late Cretaceous was interrupted by a significant event in the mid-Maastrichtian, when the source of deep waters appears to have changed abruptly from low- to high-latitude sources (e.g., MacLeod and Huber, 1996; Barrera et al., 1997; Frank and Arthur, 1999). This event appears to have coincided with the extinction of the inoceramid bivalves (MacLeod et al., 1996) and possibly also the rudistid bivalves (Johnson et al., 1996). Growing evidence, however, suggests that this benthic event is distinctly diachronous (MacLeod et al., 1996). The change to high-latitude deep-water sources appears to have been long-lived, lasting until the LPTM. However, more benthic data are required to accurately characterize Late Cretaceous and Paleocene deep-water properties.

The Upper Cretaceous sections recovered during Leg 198 will help us determine (1) whether peak "greenhouse" conditions occurred in the Albian (Savin, 1977) or the early Turonian (Jenkyns et al., 1994; Huber et al., 1995); (2) if peak warming was immediately followed by long-term cooling (Jenkyns et al., 1994) or by sustained warmth and then by cooling beginning in the mid-Campanian (Huber et al., 1995), or whether cooling history varied between latitudes; (3) whether apparent cool tropical temperatures in the Maastrichtian (the "cool tropics paradox" of D'Hondt and Arthur [1996]) were real or the result of diagenetic alteration of planktonic foraminiferal tests; (4) the properties and age of mid- and Late Cretaceous deep water and from what oceanic region it was derived; (5) the timing and rate of changes in the sources of deep waters from low- to high-latitude sources; (6) the changes in deep-water mass properties that accompanied the MME and their effect on benthic faunas; (7) whether the MME led to a permanent change in deep-water source; and (8) the changes in vertical thermal gradients through time and whether climate and deep-water circulational changes were coupled.

Mid-Cretaceous Oceanic Anoxic Events

The beginning of "greenhouse" climate conditions in the mid-Cretaceous (Barremian–Turonian) was associated with widespread deposition of C_{org}-rich sediments, informally known as "black shales," in the oceans. These C_{org}-rich deposits are known to occur primarily at specific stratigraphic horizons, namely, the lower Aptian, the uppermost Aptian to lowermost Albian, the upper Albian and in the upper Cenomanian, close to the Cenomanian/Turonian boundary (e.g., Jenkyns, 1980; Schlanger et al., 1987; Sliter, 1989; Arthur et al., 1990; Bralower et al., 1993) (Fig. F9). Schlanger and Jenkyns (1976) hypothesized that these OAEs resulted from the vertical expansion of oxygen

minimum zones linked to transgressive sea-level pulses and the reduced oxygenation of bottom waters. Others have theorized that oxygen depletion and the deposition of C_{org}-rich sediments instead was the consequence of other paleoceanographic changes such as salinity stratification (Ryan and Cita, 1977; Thierstein and Berger, 1978) and increased flux of C_{org} from surface productivity or terrestrial sources (e.g., Dean and Gardner, 1982; Parrish and Curtis, 1982; Pedersen and Calvert, 1991).

The deposition of mid-Cretaceous C_{org}-rich sediments coincided with a worldwide pulse in ocean crustal production (Fig. F10) (Larson, 1991a; Tarduno et al., 1991; Arthur et al., 1991; Erba and Larson, 1991). The release of mantle CO_2 from this enormous volcanic episode may have directly caused mid-Cretaceous "greenhouse" warming. The increased preservation and production of organic carbon may have resulted from this warming (e.g., Arthur et al., 1985) combined with increases in nutrients, while sea level rose as the result of the creation of an anomalously young, and therefore shallow ocean floor (Hays and Pitman, 1973; Schlanger et al., 1981).

Regardless of their origin, the burial of C_{org}-rich sediments enriched in ^{12}C led to significant positive $\delta^{13}C$ excursions. These have been documented for the Cenomanian/Turonian boundary (Scholle and Arthur, 1980), the early Aptian, and the late Aptian–early Albian (e.g., Weissert, 1989; Bralower et al., 1999). Short-lived negative $\delta^{13}C$ excursions at the onset of the events may be related to input of mantle CO_2 during volcanic events (e.g., Bralower et al., 1994) or to the dissociation of methane hydrates (Jahren and Arens, 1998; Opdyke et al., 1999; Jahren et al., 2001). OAEs are known to be times of rapid turnover among marine biotas as a result of complex changes in habitats (Coccioni et al., 1992; Erba, 1994; Premoli Silva and Sliter, 1999; Premoli Silva et al., 1999; Leckie et al., in press).

Complicating the development of paleoceanographic models are apparent differences in the stratigraphic extent and paleobathymetry of C_{org}-rich deposits from the Pacific compared to the Atlantic and Tethys Oceans. In the Atlantic and Tethys, C_{org}-rich deposits occur mostly in basinal settings characterized by major inputs of terrestrial C_{org} by turbidity currents that led to vertically widespread, long-lived episodes of deep-water anoxia (e.g., Arthur and Premoli-Silva, 1982; Arthur et al., 1984; Stein et al., 1986). Terrestrial C_{org}-rich deposits in the Atlantic and Tethys occur in intervals besides the OAEs (e.g., Bralower et al., 1993). The record of carbonaceous strata in the Pacific is concentrated in the OAEs, dominated by marine C_{org}, and almost exclusively restricted to paleobathymetric highs (e.g., Dean et al., 1981; Thiede et al., 1982). However, our understanding of the Pacific record is based on scattered occurrences of carbonaceous strata from Shatsky, Hess, and Magellan Rises, the Mid-Pacific Mountains (MPM), the Manihiki Plateau, the Mariana Basin, and the accreted oceanic limestone from the Franciscan Complex along the western margin of North America (Sliter, 1984).

Recovery of mid-Cretaceous C_{org}-rich deposits at relatively shallow burial depth from Shatsky Rise will help determine

1. How sedimentation (i.e., lithology, amount and type of C_{org}) differs between OAE intervals and non-OAE intervals;
2. The biotic, sedimentologic, and geochemical similarities and differences between the different OAE episodes;
3. Whether an oxygen minimum zone model is applicable for OAEs on Shatsky Rise;

4. Whether there are any differences between the recovery of C_{org}-rich sediments on the Northern and Southern Highs that might indicate that the intensity of upwelling differed as a function of latitude;
5. The effect of the worldwide, mid-Cretaceous volcanic pulse on the deposition of C_{org} and the timing of OAEs;
6. If volcanism was a direct cause of "greenhouse" climate conditions and whether volcanism or methane dissociation is a more likely trigger; and
7. How microplankton and microbenthos respond to the physical, chemical, and biological oceanographic changes associated with OAEs.

General Early Cretaceous Paleoceanography

Microplankton Evolution

The Early and mid-Cretaceous were critical times in the evolution of planktonic foraminifers and calcareous nannoplankton (e.g., Roth, 1987; Leckie, 1989; Premoli Silva and Sliter, 1999). Nannoplankton underwent dramatic radiations close to the Jurassic/Cretaceous and Barremian/Aptian boundaries (e.g., Bralower et al., 1989, 1994). Both of these events have been documented in the Atlantic and Tethys, but not yet from the Pacific. Pacific sites recording these diversification events would help provide an understanding of their causes.

Planktonic foraminifers appear to have evolved in the Bajocian (Middle Jurassic), but their occurrence is sporadic below the Lower Cretaceous. The diversification of this group was, until recently, thought to have occurred in the early Aptian. Coccioni and Premoli Silva (1994), however, found the evolutionary appearance of a number of taxa far below their previous ranges in the lower Valanginian of the Rio Argos section of Spain. Documentation of this diversification event in other locations and oceanographic settings will help our understanding of its causes.

Shatsky Rise drilling will help us answer the following questions: (1) How did the evolution of nannoplankton correlate to changes in ocean thermal structure and circulation? and (2) Is there evidence for diversification of planktonic foraminifers in the early Valanginian as in Spain, and if so, did this event correlate with any obvious changes in circulation or climate?

Valanginian Greenhouse Event

A major change in stable carbon isotope ratios of marine carbonates and organic matter has been observed in the Valanginian (e.g., Lini et al., 1992). The event appears to correlate with a major burial event of C_{org}, an increase in atmospheric CO_2, and global warming, perhaps the earliest indications of the Cretaceous "greenhouse" climate (Lini et al., 1992). Increased crustal production rates at this time (e.g., Larson, 1991b) suggest that the event may have a volcanic origin. Warming in the Valanginian is at odds with the evidence of Stoll and Schrag (1996) and others for glaciation in this part of the Cretaceous. Recovery of high-quality stratigraphic sections from additional locations will help resolve this issue. Shatsky drilling will help us address how the Valanginian carbon isotope record correlates to indicators of climate change and volcanism and whether there is evidence for warming or cooling in this time interval.

Early Cretaceous CCD Fluctuations

The Early and mid-Cretaceous were characterized by major changes in the level of the CCD (e.g., Thierstein, 1979; Arthur and Dean, 1986). These changes likely resulted from changes in fertility, sea level, ocean floor hypsometry, and ocean circulational patterns. One of the most dramatic events occurred in the early Aptian, at around the same time as the massive Pacific volcanic event, suggesting that volcanism played a direct role, perhaps through increased pCO_2. The few data that exist for the Pacific suggest a different CCD history from the Atlantic (Thierstein, 1979), and more data will help resolve the history of the Pacific CCD. Shatsky Rise drilling will help us address the following questions: (1) What was the gradient of carbonate dissolution in the mid-Cretaceous Pacific Ocean? (2) What was the history of variation in the lysocline and CCD in the Early and mid-Cretaceous? and (3) Was a major early Aptian CCD shoaling episode observed for the Atlantic Ocean basins characteristic of the global ocean, or were the oceans out of phase as the result of the pattern of deep-water aging?

Nature and Age of Shatsky Rise Basement

LIPs such as the Ontong Java Plateau and Shatsky Rise were constructed during voluminous magmatic events that took place over geologically brief (<1 m.y.) time intervals (e.g., Duncan and Richards, 1991; Tarduno et al., 1991; Coffin and Eldholm, 1994). These events are thought to be associated with massive thermal anomalies in the mantle known as "superplumes" (Larson, 1991b). A likely possibility is that the voluminous phase of superplume activity was associated with the ascent of a plume "head" and that activity declined as the magma source dried up as the lithosphere rode over the plume "tail." One of the major questions concerning the origin of LIPs such as Shatsky Rise is whether they formed in a midplate setting or at a divergent boundary, possibly a triple junction, at times of changing plate geometry (e.g., Sager et al., 1988).

Trace element geochemistry of most samples from Shatsky Rise are close to mid-ocean-ridge basalt (MORB) (Tatsumi et al., 1998), indicating that they were generated at a divergent boundary, but a few samples have an affinity closer to Polynesian alkalic basalts, suggesting a midplate origin. The latter result is not unexpected, since Shatsky Rise is thought to have formed in the South Pacific (McNutt and Fischer, 1987) near crust with the distinctive Polynesian chemistry. Additional basement drilling at Shatsky Rise will help us address whether it had some kind of a hybrid origin or whether there are other explanations for the few anomalous samples.

Although volcanic basement crops out at several localities on Shatsky Rise (Sliter et al., 1990), basement samples obtained are from dredges, and one pebble in a core-catcher sample from DSDP Site 50, and all of these are heavily weathered. Ozima et al. (1970) dated volcanic rocks dredged from Shatsky Rise as Tertiary in age. Either these rocks were derived from late stage volcanism identified in seismic data from the rise, or possibly their pervasive alteration precludes reliable age determination. Maximum estimates for the age of basement on Shatsky Rise can be obtained by adjacent magnetic anomalies (Nakanishi et al., 1989). These ages range from 148 Ma (Late Jurassic polarity Zone CM21) at the Southern High to 136 Ma (Berriasian–Valanginian polarity Zone CM14) at the Northern High based on the timescale of Gradstein et al. (1994). Fresh basement samples will provide valuable age information.

PRINCIPAL RESULTS

Site 1207

Site 1207 is the northernmost site in the Shatsky transect, lying some 5° north of the sites on the Southern High. The site is located in lower bathyal (3103 m) water depth close to the most elevated, central part of the Northern High of Shatsky Rise. The paleodepth history of this site is not well known, but subsidence was likely rapid in the interval immediately after its formation in the Valanginian (135 Ma), then slowed considerably. Paleoreconstructions suggest that the site was formed and remained in equatorial latitudes for the first 50 m.y. of its history.

The Northern High has not been drilled before; thus, the stratigraphy was unknown prior to drilling Site 1207. The sedimentary section at Site 1207 is approximately 1200 m thick. Seismic profiles show a generally horizontal stratigraphy, with several prominent reflectors. Drilling objectives were to recover a Paleogene and Cretaceous section to investigate climate change during an interval of long-term global warmth. Correlation with reflectors on the Southern High defined by Sliter and Brown (1993) was tentative. The most prominent reflectors on the Southern High, Reflectors R1 of Cenomanian–Coniacian age and R2 of Barremian–Aptian age, are apparent on seismic profiles. The drilling strategy was to core through R2 in a first hole using the advanced piston corer /extended core barrel (APC/XCB), to core a second APC hole to refusal, and then to core a hole using the rotary core barrel (RCB) through R2. Finally, a full suite of logs were to be collected through the whole sequence.

A 622.5-m upper Barremian to Holocene section was penetrated at Site 1207 (Table T1). Recovery was excellent in the upper Campanian to Holocene section, but poor in the upper Barremian to lower Campanian where chert horizons were extremely common. Results show a surprisingly different sedimentary sequence than the one previously documented at DSDP and ODP sites on the Southern High of Shatsky Rise. The Paleogene and uppermost Cretaceous sequence likely is missing as a result of major early Neogene slumping and erosion (Fig. F11). Thus, we were unable to achieve our Paleogene objectives at this site. The middle Miocene to Pliocene section, on the other hand, is expanded (161 m thick), apparently complete, and composed of nannofossil ooze with diatoms that also contain planktonic foraminifers and radiolarians (Fig. F12). The section contains prominent carbonate cycles that appear to record orbital climate fluctuations. The section should provide a valuable biochronology as well as important information on the nature of ocean circulation changes.

At the opposite end of the stratigraphic column, a horizon of highly carbonaceous (up to 34.7 wt% C_{org}) lower Aptian claystone that correlates to the global OAE1a, including the Selli level of the southern Alps and Apennines of Italy, was recovered. Organic matter in these horizons is exceptionally well preserved. Organic geochemical, stable isotopic, and paleontological analyses of this C_{org}-rich interval will help constrain the environmental changes during OAE1a in the Pacific Ocean. Drilling at Site 1207 was impeded by the presence of chert throughout the lower Campanian to Barremian section. Drilling and logging at Site 1207 revealed important information about the nature and stratigraphy of this chert that will help develop strategies to improve recovery in such chalk/chert sequences.

Unique Neogene Section

Upper Miocene to Holocene sediments (lithologic Subunit IA) recovered at Site 1207 contain common to abundant diatoms (between 10% and 40%), a far higher proportion than in

contemporaneous units from sites on the Southern High of Shatsky Rise. At Southern High Site 305, the relative proportion of diatoms is 5%–15% in the Miocene to Holocene section, but it decreases rapidly at the unconformity between the late Miocene and the late Oligocene (Larson, Moberly, et al., 1975). Diatoms were described as rare in samples from Sites 47 and 577 (Koizumi, 1975; Koizumi and Tanimura, 1985). Approximately 5° of latitude separates Site 1207 from the previously drilled sites on the Southern High, and it is feasible that this distance is associated with a significant change in oceanographic regime.

The abundance of diatoms in lithologic Subunit IA (0–131.3 mbsf) sediments suggests that surface waters over Site 1207 were moderately to highly productive from the late Miocene to the Holocene. Alternatively, high biosiliceous production at Site 1207 may be an effect of local topographic upwelling. This option is not appealing given the absence of significant diatom concentration in sediments on the Southern High. More likely, the abundance of diatoms at Site 1207 reflects a component of productive subarctic surface waters over the site in the late Neogene. The relative proportion of diatoms is considerably lower in Subunit IB (131.5–162.5 mbsf) sediments, likely as a result of lower surface-water productivity in the early middle to early late Miocene. The abundance of *Discoaster,* a nannoplankton genus thought to thrive in oligotrophic waters (e.g., Chepstow-Lusty et al., 1989) appears to be antithetical to the proportion of diatoms in the Neogene section.

One of the most prominent features of the Neogene section at Site 1207 is the decimeter-scale lithologic cycles in Cores 198-1207A-1H to 18H between dominantly darker green-gray horizons and lighter tan-gray-white horizons. These cycles show significant changes in the relative percentage of diatoms (see "Lithostratigraphy," in "Specialty Syntheses") and marked differences in the nature of carbonate preservation. Reconstructions suggest that the site was above the CCD until at least the early Pliocene but close to this level until the early Miocene (Rea et al., 1995); thus, the cycles could represent variations in dissolution as a result of changes in the depth of the lysocline. Variation in biosiliceous production may also be responsible for the cycles.

Today, Site 1207 lies in a subtropical water mass toward the north of the range of the warm water Kuroshio Extension current. To the north of the site lies a significant front, a transition region between subtropical and subarctic water masses. Transition zone waters are derived from off the coast of northern Japan, where the cold, nutrient-rich Oyashio Current mixes with the warm, nutrient-poor Kuroshio Current. These water move eastward across the Pacific in the West Wind Drift at a latitude of 40°–42°N. The location of Site 1207 is highly sensitive to past climatic variations because of its proximity to the transition zone.

Significant oceanographic changes occurred during the Neogene that had profound effects on circulation and distribution of water masses in the Pacific Ocean; these changes appear to be reflected in the sedimentary record at Site 1207. An event at 14.5 Ma has been associated with the formation of the East Antarctica Ice Sheet (Kennett et al., 1985); another event at 11 Ma is related to the closure of the Indo-Pacific seaway (Romine and Lombari, 1985). These events led to a steepening of temperature gradients and intensification of North Pacific gyral circulation including the ancestral Kuroshio Current. The modified circulation resulted in the development of a distinct North Pacific transitional water mass, separated from the northern subpolar region, and the northward displacement of temperate organisms. The development of distinct water masses in the North Pacific combined with long-term cooling may also be responsible for the marked facies change between lithologic Subunits IB and IA that corresponds to a sharp increase in biosiliceous material in sediments at ~9 Ma.

Koizumi (1985) correlated fluctuations in Pliocene–Pleistocene diatom communities at DSDP Sites 579 and 580 in the abyssal plain northwest of Shatsky Rise to climatic fluctuations that caused variation in the amount of subarctic waters at these sites. In colder intervals of the late Miocene to Pleistocene, Site 1207 may have been within the transition zone between the subtropical water mass and the subarctic water mass (Fig. F13), even though the site was well to the south of its current location (32°N at 10 Ma; R. Larson, pers. comm., 2001). Thus, fluctuations in the proportion of diatoms, which are more abundant in subarctic than subtropical waters, may reflect latitudinal shifts in the position of the transition zone.

Shipboard biostratigraphic data suggest that nannofossils have suffered a greater amount of dissolution in greenish layers that are enriched in diatoms; preservation is considerably better in the white-gray ooze layers that have fewer diatoms. If the greenish layers correspond to cool intervals as argued above, then the pattern of preservation is opposite to that of most sites in the Pacific (e.g., Farrell and Prell, 1991; Zahn et al., 1991). A body of evidence suggests that during glacial stages intermediate deep waters were produced in the Pacific and that these young, nutrient-poor waters caused little dissolution close to their source. An opposite pattern was noted at Site 882 on Emperor Seamount by Haug et al. (1995), who argued that the upwelling of nutrient- and CO_2-rich waters during glacial stages increased carbonate dissolution. Microfossils suggest a similar mechanism for dissolution patterns in the upper Miocene to Pleistocene at Site 1207.

A significant peak in opal accumulation rates occurs between 3.2 and 2.75 Ma at other sites from the northern Pacific (Haug et al., 1995; Maslin et al., 1995). The origin of this peak and subsequent decline is uncertain, but the base of this peak corresponds to the beginning of long-term global cooling that culminated in Northern Hemisphere glaciation, and the top of the peak corresponds with the rapid advance of Northern Hemisphere glaciers. Although qualitative in nature, a sharp rise in the abundance of diatoms occurs in the middle of Core 198-1207A-6H and continues up to the lower part of Core 198-1207A-3H. The age model indicates that this interval corresponds approximately to the 3.2–2.75 Ma period.

Origin of the 57-m.y. Hiatus

One of the surprises of drilling at Site 1207 was a major unconformity between the middle Miocene and upper Campanian. This hiatus represents approximately 57 m.y. of stratigraphic record. The unconformity lies at the base of a 3.3-m interval of zeolitic nannofossil clay (lithologic Subunit IC [162.5–163.8 mbsf]), at the center of which are a 5-cm Mn nodule and a few chert nodules. The interval has common micronodules of phosphate, volcanic glass, and grains of quartz, feldspar, and heavy minerals, as well as authigenic phillipsite crystals. Microfossils of Campanian and Miocene ages are mixed throughout the clay interval, possibly because of drilling disturbance. Very rare Paleogene nannofossils and foraminifers were observed in a few samples from this interval.

The age of the event(s) that caused the unconformity is difficult to interpret from the fossil record. The most likely age is an interval prior to the middle Miocene (15 Ma), the age of immediately overlying sediments. The presence of an Mn crust and micronodules, chert nodules, and zeolite crystals suggests an extended interval of seafloor exposure. A mixture of nannofossils of Campanian and Miocene ages suggests winnowing of underlying and overlying units after the hiatus. Paleogene microfossils hint at the presence of some intermediate section before removal during the hiatus interval.

Major unconformities are also found at Sites 49 and 50 near the base of the southwestern flank of the Southern High (4282 and 4487 m, respectively) (Table T2). At these sites, Pleistocene ooze directly overlies uppermost Jurassic or lowermost Cretaceous chalk. At Site 306 on the southern flank of the Southern High, Pleistocene sediments directly overlie those of Albian age. All of these sites are located on significant slopes; thus, it is likely that unconformities were produced by the removal of sediments by mass wasting. The unconformities at Sites 49 and 50 are characterized by zeolitic clay, common phillipsite, and Mn-coated rock fragments, chert and ash pebbles. The core with mixed Albian and Quaternary at Site 306 contains Mn nodules and chert fragments.

Several possibilities exist for the origin of the major unconformity at Site 1207. A number of prominent unconformities in the deep sea are caused by changes in the CCD resulting from shifts of carbonate deposition to shallow-water environments coincident with sea-level rise (e.g., Loutit et al., 1988) or changes in deep-water circulation that increases the age of a water mass. Although the subsidence history of Site 1207 is undetermined at the current time, and the history of the CCD in the Pacific is still somewhat uncertain, available information (Thierstein, 1979; Rea et al., 1995) suggests that the CCD was substantially deeper than the current depth of Site 1207 in early Miocene to late Eocene times (Rea et al., 1995). The curve of Rea et al. (1995) for the northwest Pacific indicates that Site 1207 was likely near or slightly below the CCD at some point in the Maastrichtian–middle Eocene. However, the sediment record on the Southern Rise suggests that the CCD history for Shatsky Rise is different from the history for the northwest Pacific developed by Rea et al. (1995). Indeed, a separate study (Thierstein, 1979) shows that the current depth of Site 1207 was substantially above the Pacific CCD in the Campanian–Maastrichtian. Given that the site must have been shallower than its current depth throughout the Campanian to Miocene interval, it is unlikely that dissolution is responsible for the unconformity.

A second possible mechanism for the unconformity is that sediments were removed from the top of the Northern Rise during one or a series of erosion, slumping, or mass wasting events. Seismic line TN037-5A shows an interval of disturbed, diagonal reflectors with thicknesses ranging to 100 m up to 10 km to the north and south of Site 1207. These disturbed horizons may represent beds truncated by erosion or slumping (Fig. F14).

The depth and age distribution of Neogene deep-sea hiatuses have been studied in detail by Keller and Barron (1987). These authors found a prominent hiatus between 15 and 16 Ma in CN4, which corresponds to the minimum age of the major unconformity at Site 1207. Keller and Barron (1987) also observed that hiatuses in the depth range of Site 1207 are concentrated on plateaus, rises, and seamounts and suggested that they were most likely due to slumping events.

Site 1207 lies between basement highs to the east and west. The unconformity lies substantially below the level of the highs. Thus it is possible that this paleotrough served as a north-south conduit for bottom-water flow from the Cretaceous to the early Neogene. This flow may have steepened and undercut the sediments leading to slumping on the north and south of the present summit. In fact, a prominent canyon, which may have been produced by mass wasting, lies just to the north of Site 1207. Erosion would have been efficient while sedimentation rates were lower in the middle Miocene, but once productivity and, hence, sedimentation rates increased in the late Miocene, a sediment drape was established over the paleotrough.

In summary, results from Site 1207 show a drastically different sequence than anywhere on the Southern High of Shatsky Rise. Available seismic profiles suggest that sediments of Paleogene and latest Cretaceous age are not present on the Northern High as opposed to the Southern High, where

these units are widespread. Conversely, the Miocene–Holocene section on Northern High is relatively expanded, whereas this sequence is thin or absent on the Southern High.

Early Aptian Oceanic Anoxic Event

A major highlight of Site 1207 is the recovery of a 45-cm-thick, dark brown, finely laminated C_{org}-rich claystone of early Aptian age in lithologic Unit III (335.3–622.8 mbsf). The presence of lamination indicates dysoxic or anoxic conditions at the seafloor for the duration of the event. Organic carbon contents are extremely high (up to 34.7%); characterization of this organic matter indicates it is algal and bacterial in origin. Gamma ray logging data suggest that an additional 50 cm of claystone was not recovered. Biostratigraphy indicates that this distinct horizon was deposited during OAE1a (Schlanger and Jenkyns, 1976; Bralower et al., 1993).

C_{org}-rich horizons of OAE1a age are also found at Sites 305 on Southern High, Shatsky Rise, 463 (MPM), and 866 (Resolution Guyot) (Sliter, 1989; Jenkyns, 1995). Only Sites 463 and 866 have decent recovery. The Site 1207 record extends the latitudinal and depth transect of this event in the Pacific Ocean. At Site 463 (2525-m water depth), carbonaceous limestones with up to 7.6% C_{org} are associated with volcanic ash. At Site 866 (1373-m water depth), thin organic carbon-rich (14.2%) claystones are found in a sequence of shallow-water carbonates. Organic matter characterization, including stable carbon isotope analysis indicate that the C_{org} in both sites is of algal marine origin (Dean et al., 1981; Baudin et al., 1995), similar to that at Site 1207.

Detailed microfossil biostratigraphic studies (Sliter, 1989; Bralower et al., 1994; Erba, 1994) have demonstrated that Site 463 C_{org}-rich horizons correlate exactly with carbonaceous units of early Aptian age known as the Niveau Goguel in southeastern France (Bréhéret, 1988), the Livello Selli type-level in central Italy (Coccioni et al., 1987), and the Livello Selli equivalents from the Italian and Swiss Alps, Sicily, DSDP Site 641 in the eastern North Atlantic and northern Mexico (i.e., Weissert and Lini, 1991; Bralower et al., 1994; Erba, 1994; Menegatti et al., 1998; Erba et al., 1999; Bralower et al., 1999).

OAE1a is associated with abrupt changes in calcareous nannofossil assemblages, especially among a rock-forming group known as the nannoconids, which decline sharply in abundance just prior of the onset of the event (Erba, 1994). Other robust nannofossil taxa radiate and increase in size (Tremolada and Erba, in press). Diversity and abundance of planktonic foraminifers decline rapidly prior to OAE1a. Planktonic foraminifers are absent at the base of the event as a result of dissolution then fluctuate from rare to few and low to moderate diversity through the rest of the event. When present, taxa are mainly adapted to the poor oxygen contents in the upper water column (Magniez-Jannin, 1998; Premoli Silva et al., 1999). Radiolarians are abundant throughout but exhibit a marked compositional change at the beginning of the event (Premoli Silva et al., 1999).

The early Aptian event is marked by a distinctive carbon isotopic profile consisting of a ~2‰–3‰ negative shift at the base of the event followed by a ~4‰–5‰ increase. The pronounced negative excursion has been recognized at Site 866 on Resolution Guyot (Jenkyns, 1995), the southern Alps of Italy (Menegatti et al., 1998; Erba et al., 1999), the Isle of Wight (Gröcke et al., 1999), and northern Mexico (Bralower et al., 1999).

Early Aptian C_{org}-rich units that correlate to OAE1a have been found in a limited number of locations compared to the Cenomanian–Turonian OAE (OAE2). This has led to some uncertainty as to whether the event was global in scale. Recovery of the early Aptian C_{org}-rich horizon at Site 1207 provides additional evidence that OAE1a was a global event. The record of OAE1a at Site 1207 is

more complete than any other deep-sea record except possibly Site 463. The C_{org} contents are exceedingly high, and the horizon is found at a relatively shallow burial depth (565.5 mbsf). Hence, the organic geochemical and stable isotopic records should be nearly pristine and highly informative. These and biotic records should provide key information on the environmental changes that occurred during the anoxic event.

Chert

Chert is a fundamental part of the Cretaceous stratigraphic section on Shatsky Rise. Unfortunately, little was known about the distribution and nature of chert. For example, it was unclear whether these units are nodular or layered, or whether they are distributed randomly through the section or in individual zones.

The occurrence of chert in the Shatsky Rise section is thought to reflect the path of the site across the equatorial divergence, where high productivity led to accumulation of opaline siliceous microfossils in the sediment. As the sediment was subsequently buried, this opal was progressively transformed to quartz. The stratigraphic distribution of chert in the sediment may yield important information about the width and strength of the equatorial divergence and whether this productivity varied in a predictable fashion (i.e., on orbital timescale); chert morphology may provide indications of the nature of the diagenetic process.

The uppermost chert horizon at Site 1207 lies in upper Campanian sediments at 76 Ma. Common chert is found from the lower Campanian (79–80 Ma) to the base of the hole (lithologic Units II and III [163.8–335.3 and 335.3–622.8 mbsf, respectively]). Assuming the reconstruction of R. Larson (pers. comm., 2001), these data suggest that the equatorial divergence was significantly wider at this time than today ranging to ~15° north of the equator (Fig. F4). The presence of chert throughout the section indicates that the site remained within the equatorial divergence from the Aptian up to the early Campanian. In fact, the reconstructed path predicts that the site remained within the divergence for at least the first 60 m.y. of its history.

Anecdotal drilling information and logging data show that chert levels are extremely close together for the entire lower Campanian to upper Barremian section. Formation MicroScanner (FMS) data show that the cherts are generally finely layered as opposed to nodular and that most layers are less than 10 cm thick. However, interbedded soft sediment layers are less than 1 m thick and most often under 30 cm. These interbeds are mainly composed of ooze or very soft chalk down to the Aptian, suggesting that the burial depths were never much greater than those at present. The softness of these interbeds exacerbated recovery efforts in the mid- and Upper Cretaceous interval.

Site 1208

Background

Site 1208 is located at lower bathyal (3346 m) water depth, close to center of the Central High of Shatsky Rise. The site lies on seismic line Sager line 8 (Fig. F15). Sediments of the Central High have not been cored before; thus, the stratigraphy was unknown prior to drilling at Site 1208. Moreover, correlation of reflectors and the major seismic units with the Southern and Northern Highs, where units and reflectors are calibrated with drill holes, is speculative. Site 1208 coring was designed to provide knowledge of the stratigraphy of the Central Rise, as well as correlation of units and reflectors with the Southern and Northern Highs. The site was located at the point where the stratigraphic sequence appears to be most complete.

The objective at Site 1208 was to recover a Paleogene through Upper Cretaceous section for paleoceanographic investigation. Highly tentative predrilling correlation with the Southern High seismic units of Sliter and Brown (1993) suggested relatively thick seismic Units 1 (Neogene) and 2 (Paleogene) characterized by predominantly weak, largely horizontal reflectors and a relatively thin Unit 3 (Upper Cretaceous). The Upper Cretaceous to Holocene sequence was expected to contain a number of minor disconformities as indicated by prominent, but horizontal reflectors. At depth, a major angular unconformity suggests erosion of a significant part of the mid-Cretaceous sequence (Fig. F15). The total thickness of the sedimentary section at Site 1208 was estimated at ~785 m. Basement underlying the site was formed during magnetochron CM15 in the Berriasian (Nakanishi et al., 1989). The drilling strategy was to double core down to the uppermost chert horizon in the Upper Cretaceous using the APC/XCB.

Coring at Site 1208 revealed a dramatically different sequence than predicted. The upper ~260 m is an expanded upper Miocene to Holocene section below which lies almost 60 m of a less expanded lower and middle Miocene section. Reflectors that were thought to represent transitions between different units are probably individual horizons with substantially different bulk density values, probably diatom-rich levels. The Paleogene is almost entirely missing at this site and only a short segment of the Upper Cretaceous was encountered beneath a prominent, deep reflector at 328.2 mbsf (Fig. F15). We drilled a total of 392.3 m through a major angular unconformity where Campanian ooze and chalk rests unconformably on middle Albian chalk and chert (Table T1). This chert prevented further drilling with the XCB. Because only a small portion of the section will contribute to the major goals of the leg, we decided not to core a second hole.

Summary of Results

A thick, apparently complete upper Miocene to Holocene section was recovered between 0 and 251.6 mbsf (Fig. F16; lithologic Subunit IA). This section is composed of nannofossil ooze and nannofossil clay. Most intervals have significant (5%–20%) amounts of diatoms and minor amounts of foraminifers, radiolarians, and silicoflagellates. This unit contains numerous discrete ash horizons. The entire Neogene section is composed of prominent lithologic cycles on a decimeter to meter scale. These cycles were also detected in multisensor track (MST) data throughout the section; preliminary biochronology suggests that they have dominant frequencies of ~40 and 100 k.y. and thus represent obliquity and eccentricity rhythms. The section shows highly promising magnetostratigraphy as well as properties suitable for paleointensity records. The average sedimentation rate of the upper Miocene to Holocene section is approximately 42 m/m.y; thus, it will be an excellent candidate for high-resolution biochronologic and paleoceanographic investigations.

The recovered section contains an interval (lithologic Subunit IC; 311.65 to 328.15 mbsf) with at least four unconformities separated by sediments (claystone to nannofossil ooze and chalk) deposited at extremely slow rates (0.08 to 4.2 m/m.y.). These highly condensed claystones contain some zeolite minerals (phillipsite), manganese micronodules, and rare foraminifers. Nannofossil biostratigraphy allows us to piece together the history of this highly disjointed section. The section shows some striking similarities to the major unconformity at Site 1207, as well as some minor differences. Combining results from both sites, will enable us to reconstruct the regional depositional history for the Central and Northern Highs of Shatsky Rise.

The zeolitic claystone at the base of lithologic Subunit IC at Site 1208 suggests that the site was close to or below the CCD for much of the late Paleocene, Eocene, and Oligocene. Directly above the unconformity between the Campanian and Paleogene, distinct nannofossils allow us to identify a narrow time slice across the Paleocene/Eocene boundary in Section 198-1208A-36X-CC. This section may contain a highly condensed interval of the LPTM and thus may provide important information on the response of the deep ocean to this abrupt global warming event. An overlying interval of nannofossil ooze indicated an abrupt drop in the CCD in the earliest Oligocene coincident with the earliest Oligicene time (Oi-1) cooling step (Zachos et al., 1993, 1996).

Highlights

Expanded Neogene Section for Paleoceanography and Chronology

Sedimentation rates at Site 1208 averaged 42.4 m/m.y. from the Holocene to late early Pliocene (0 to 3.82 Ma), 22.3 m/m.y. from the late early Pliocene to the early late Miocene (3.82 Ma to 8.28 Ma), then decreased to 5.9 m/m.y. in the early late Miocene to late early Miocene (8.28 to 18.2 Ma). The rates in the late Miocene to Holocene are far higher than typical pelagic sedimentation. The detrital clay and silt component of the sediment may have been derived by eolian transport. However, a large component of the sediment must have been delivered by sediment drift. A number of recent ODP legs have targeted sediment drifts for high-resolution paleoceanographic investigation. These include Leg 162 in the Iceland Basin and Norwegian-Greenland Sea and Leg 172 on the Blake-Bahama Outer Ridge and Bermuda Rise. The Site 1208 sedimentation rates, although significant, are not as high as the rates in the majority of these sites.

Sedimentation rates in the lower Pliocene to Holocene interval are more or less constant. Sedimentation rates in contemporaneous intervals at sites drilled during Leg 145 in the North Pacific peak in the Pliocene and decrease above this interval (Barron et al., 1995). The Pliocene peak, which is considerably higher than rates at Site 1208, is associated with a massive flux of diatoms, the so-called “diatom dump.”

The Neogene section at Site 1208 has a number of additional advantages for high-resolution biochronology. These include a combination of siliceous and calcareous microfossils, a high-resolution magnetostratigraphy, a marked orbital cyclicity, numerous ash layers with potential for radiometric dating and intrasite correlation, and a potential magnetic paleointensity record.

Foraminiferal preservation is generally poor, but sufficient for stable isotope stratigraphy in selected intervals. Nannofossil and planktonic foraminiferal assemblages show considerable variation that appears to record climatic change. Diatoms, radiolarians, and silicoflagellates also show sharp changes in abundance that are likely related to changing water-mass properties. Thus, the section also has significant potential for high-resolution paleoceanographic investigations.

Orbital Rhythms: A Strong Climate Signal

Marked cyclic variations are observed in MST data throughout the upper Miocene to Holocene section at Site 1208. These variations are expressed as strong lithologic cycles that have frequencies at the decimeter to meter scale. Preliminary shipboard biochronology suggests that the dominant periodicities correspond to eccentricity (~100 k.y.) cycles for the last 0.8 m.y. and to a combination of eccentricity and obliquity (~40 k.y.) cycles in the interval from 0.6 to 2.7 Ma. These cycles are marked by relatively subtle to sharp changes in color that are associated with variations in the amount of clay, pyrite, and different biogenic particles. For most of the upper Miocene to Holocene section the cycles are predominantly between nannofossil clay with diatoms and nannofossil ooze

with clay and diatoms. The darker gray to green interbeds tend to have more abundant diatoms and clay, more dissolved nannofossil assemblages, and more abundant reduced iron minerals (i.e., pyrite). The lighter, gray, tan, and white interbeds contain fewer diatoms, less clay, and a better preserved nannofossil assemblage.

Upper Miocene to Holocene sediments (lithologic Subunit IA) recovered at Site 1208 contain few to common diatoms (up to 20%)—lower percentages than sediments recovered at Site 1207, but higher percentages than contemporaneous units from sites on the Southern High of Shatsky Rise, where diatoms are usually less than 5%. Site 1208 is ~1° south of Site 1207 and ~4° north of the Southern High sites. As at Site 1207 (see "Site 1207" in "Principal Results"), diatom-rich layers are thought to represent intervals during which colder, more productive, transitional, and subarctic water masses shifted southward over the site (Fig. F13). Lighter-colored layers that are poorer in diatoms represent warmer intervals during which Site 1208 was located in a subtropical water mass, similar to its location today and similar to sites on the Southern High through most of the Neogene. As the site is considerably higher than the surrounding deep-ocean floor, there may also be a topographic effect to the productivity and productivity variation.

Diatoms increase markedly in abundance across the transition from lithologic Subunit IB to IA at 251.6 mbsf (~8 Ma). This interval lies just after a change in Pacific Ocean circulation associated with the closure of the Indonesian seaway that caused intensification of North Pacific gyral circulation (Fig. F17) (Kennett et al., 1985); a strengthened west wind drift likely increased upwelling along this boundary and created a more well-established North Pacific transitional water mass separated from the northern subpolar region.

Changes in the geographic distribution of water masses through time also affected other fossil groups at Site 1208. In particular, Neogene planktonic foraminifers show distinct stratigraphic changes between assemblages dominated by subtropical and tropical taxa and those dominated by taxa with cool, temperate affinities. Moreover, faunas at Site 1208 are considerably richer in warmer, tropical taxa than at Site 1207, which is located only ~1° to the north. This suggests that for much of the Neogene, Sites 1207 and 1208 were located in a region with sharp temperature gradients.

Origin of Regional Unconformities

The interval between the lower Miocene and the upper Campanian (lithologic Subunit IC; Cores 198-1208A-35X and 36X, 311.65–328.15 mbsf) is marked by at least three distinct unconformities. These unconformities separate the upper Oligocene and lower Oligocene, the upper Eocene and lower Eocene, and the Paleocene/Eocene boundary interval and the upper Campanian. Additionally, most of these intervals are characterized by extremely slow sedimentation that locally resulted in the postdepositional precipitation of zeolites and manganese micronodules. Carbonate layers occur sporadically and are generally composed of dissolved nannofossils and sparse benthic and planktonic foraminifers. The only coring gap that affects interpretation lies between Sections 198-1208A-36X-2 and 36X-CC in the lower Eocene between nannofossil Subzone CP9b and combined Zones CP10 and CP11. The estimated sedimentation rates for the key intervals containing unconformities are 0.09 m/m.y. for the late Paleocene to early Eocene transition and 4.2 m/m.y. for the earliest Oligocene.

The lower Miocene to Campanian interval at Site 1208 shows stratigraphic and lithologic similarities to the contemporaneous interval at Site 1207 on the Northern High of Shatsky Rise. This suggests that events that caused the unconformity were regional in scale. However, the unconformity record at Site 1208 is more complex than that at Site 1207. The continuous record at

Site 1208 allows us to distinguish highly condensed intervals from major breaks in sedimentation. The presence of carbonate provides a record of CCD variations through time.

Several of the unconformities at Site 1208 appear to result from shoaling of the CCD. The history of the CCD in the North Pacific shows a slow rise from 50 to 70 Ma (early Maastrichtian to early Eocene), a rapid rise from 30 to 50 Ma (early Eocene to early Oligocene), and a long-term deepening from 14 to 30 Ma (early Oligocene to middle Miocene) (Rea et al., 1995). The CCD remained above the current depth of Site 1208 from 15 to 39 Ma (middle Miocene to middle Eocene). One of the clearest lithologic changes lies close to the Eocene/Oligocene boundary in interval 198-1208A-36X-2, 0–20 cm where a distinct color change reflects a sharp upsection increase in carbonate content that likely corresponds to an abrupt drop in the CCD. This interval, within nannofossil Subzone CP16a and the lower part of Subzone CP16b, corresponds to a global deepening of the CCD (Zachos et al., 1996) that is thought to correspond to the Oi-1 cooling event.

The uppermost Paleocene to lowermost Eocene interval appears highly condensed. Preliminary biostratigraphy suggests that this interval is complete to the limits of resolution. The presence of highly dissolved nannofossil assemblages and depauperate foraminifers in some samples and other samples that are devoid of carbonate suggests that the site rested close to the CCD through this interval.

The absence of zonal markers in the lower Miocene to lower Oligocene transition complicates age interpretation. Thus, it is not possible to determine whether this section contains one or more unconformities or if it is merely highly condensed. This transition lies in an interval of nannofossil ooze, chalk, and claystone that is dark orange to brown in color, indicative of slow sedimentation. However, given poor biostratigraphic resolution, it is also possible that one or more unconformities lie within this transition. The similarity in the age of the sediment overlying this interval (early Miocene foraminiferal Zone N9, 14.7–15.1 Ma) at Sites 1207 and 1208 also suggests that the unconformity represents a regional event. Seismic reflection profiles at Site 1207 indicate that a major Oligocene–early Miocene interval of erosion and slumping removed much of the section underlying this unconformity. The stratigraphy at Site 1208 suggests that this erosive event may have been regional, perhaps driven by the intensification of deep-water circulation during long-term early Neogene cooling (e.g., Kennett et al., 1985).

The record of hiatuses at Site 1208 and other sites in the North Pacific also shows a number of similarities. The section at Site 883 on Emperor Seamount has unconformities in the upper to middle Miocene (9.8 to 14 Ma), the lower Miocene to lower Oligocene and the lower Eocene (Barron et al., 1995). Keller and Barron (1987) show four widespread hiatuses in the latest Oligocene to earliest middle Miocene interval. Thus, the early Miocene to early Oligocene erosive event is not limited to Shatsky Rise but is a regional phenomenon.

A major angular unconformity occurs between the Campanian and the middle Albian (Fig. F15). This unconformity contact was not recovered at Site 1208, but its nature can be inferred from regional seismic interpretations. Seismic stratigraphy indicates that the age of the units overlying the Campanian becomes younger to the east of Site 1208. In this direction, the truncation of the inferred mid-Cretaceous section beneath the unconformity suggests a lengthy phase of nondeposition and erosion at some stage during the Late Cretaceous or Paleogene (Fig. F18). Campanian horizons appear to depositionally onlap the unconformity surface at Site 1208. The mid-Cretaceous horizons appear to have draped the rough basement topography across the Central Rise and the Campanian horizons appear to have smoothed out this topography. The horizons on either side of the unconformity between the upper Campanian and the upper Paleocene are parallel. This suggests

most likely that the unconformity resulted from an interval when the site was below the CCD, an interval that was not recovered in Core 198-1208A-36X. We cannot rule out the possibility that a minor amount of erosion complimented this dissolutional episode. The similarity in age of the Campanian horizons underlying the unconformity at Sites 1207 and 1208 (nannofossil Zone CC22; 75–76 Ma) suggests that the Late Cretaceous and early Paleogene interval of dissolution was regional in scope.

Deep-Water Record of the Paleocene–Eocene Transition

The interval of time surrounding the Paleocene/Eocene boundary was characterized by rapid changes in climate and ocean circulation that led to profound changes in marine and terrestrial biotas (i.e., papers in Aubry et al., 1998). Superimposed on this interval of long-term transition was an abrupt global warming event in the late Paleocene, known as the LPTM. The deep sea and high latitude oceans warmed by 4° and 8°C, respectively, during the LPTM. The warming, in turn, led to profound changes in precipitation and continental weathering patterns (Robert and Kennett, 1994; Gibson et al., 1993). The climatic changes also affected biota on a global scale triggering rapid turnover of benthic and planktonic organisms in the ocean (i.e., Thomas, 1990; Kelly et al., 1996).

The carbon isotopic composition of the ocean decreased by 3‰–4‰ coeval with the warming event, suggesting a massive perturbation to the global carbon cycle (Kennett and Stott, 1991; Bains et al., 1999). The large magnitude and rate (~–3‰–4‰ /5 k.y.) of the carbon isotope excursion is consistent with a sudden injection of a large volume of isotopically depleted carbon into the ocean/atmosphere system. Dickens et al. (1995, 1997) suggested that the largest source of depleted carbon was the vast reservoir of methane clathrates stored in continental slope sediments. Much of this methane would have quickly converted to CO_2, stripping O_2 from deep waters and lowering alkalinity. The expected response of this massive input of CO_2 into the ocean-atmosphere system is a sharp rise in the level of the CCD. The response of the CCD in the Pacific can be determined by comparison of carbonate preservation in Shatsky Rise sediments at various water depths.

At Site 1208, the upper Paleocene–lower Eocene transition rests unconformably above the Campanian in Section 198-1208A-36X-CC. Preliminary nannofossil biostratigraphy suggests that this section lies close to the Paleocene/Eocene boundary and the LPTM. Assemblages appear to contain a small component derived from downhole contamination during drilling or core handling. The contaminated component can be separated from the in situ component by observing the continuity of ranges; contaminated taxa tend to be highly abundant upsection and occur discontinuously. Three events that lie close to the boundary—the last occurrence (LO) of the genus *Fasciculithus* and the first occurrences of *Tribrachiatus bramlettei* and *Discoaster diastypus*—occur within 6 cm of each other. These events lie just within or just above the LPTM and are separated by ~330 k.y. (Aubry et al., 1996; Bralower et al., 1995).

Poorly preserved nannofossil assemblages and intervals barren of carbonate suggest that the CCD was close to the depth of the site during the Paleocene/Eocene boundary transition interval. Combined with results from other Leg 198 drill sites, the recovered section may hold important clues about the Paleocene–Eocene transition in the North Pacific. High-resolution bulk carbon isotope analyses and carbonate variations will be used to identify the event. In addition, the clay-rich lithology will provide an excellent opportunity to derive detailed clay mineralogical records that could be used to monitor changes in atmospheric circulation.

Site 1209

Background

Site 1209 is located in middle bathyal (2387 m) water depth close to the most elevated, central part of the Southern High of Shatsky Rise. The site is located on seismic line TN037-14A (Fig. F19). This profile is hard to correlate with other profiles on the southern and western flanks of the Southern High that are tied to drill holes. A tentative predrilling correlation with the Southern High seismic units of Sliter and Brown (1993) suggests a moderately thick Unit 1 (Neogene), an expanded Unit 2 (Paleogene), and a moderately thick Unit 3 (Upper Cretaceous). The site is close to the point where the stratigraphic sequence appears to be most complete; however, the section was expected to contain a number of minor disconformities as indicated by prominent horizontal reflectors. The total thickness of the sedimentary section at Site 1209 is estimated at ~1147 m. Basement underlying the site was formed during magnetochron CM20 in the Tithonian (Nakanishi et al., 1989).

The major goals of Site 1209 drilling were to core a shallow, relatively expanded Paleogene and uppermost Cretaceous section. Holes 1209A and 1209B were cored largely with the APC (Table T1). Only two cores were taken with the XCB. Hole 1209C was drilled down to the lower Miocene, and then the Oligocene to Maastrichtian section was cored. The three holes terminated at different levels in the Maastrichtian due to difficulty penetrating chert horizons with the XCB center bit. The deepest recovered sediment was early Maastrichtian in age from 297.6 mbsf in Hole 1209B.

Coring recovered a relatively thin (111.2 m) lower Miocene to Holocene (0–16.4 Ma) section of nannofossil ooze, clayey nannofossil ooze, and nannofossil ooze with clay (lithologic Unit I) (Fig. F20). This unit has an unconformity (11.19 to 15.1 Ma) separating the uppermost middle Miocene and the uppermost lower Miocene. Lithologic Unit I rests unconformably on lithologic Unit II (111.2 and 235 mbsf), which consists of nannofossil ooze and nannofossil ooze with clay of early Oligocene to early Paleocene age (28.6–65 Ma). Preliminary nannofossil and planktonic foraminiferal biostratigraphy suggests that the succession is largely complete. However, minor unconformities may be present, especially in the upper to middle Eocene interval (between 38 and 42 Ma) that is characterized by low sedimentation rates. Underlying lithologic Unit III of Maastrichtian age (65 to 70 Ma) is composed of nannofossil ooze and chert. Three prominent chert layers were encountered in the ~50-m Maastrichtian section in Hole 1209C. However, no horizons were found in the same interval in Hole 1209B, suggesting that chert layers are laterally discontinuous. The ooze surrounding the chert at the bottom of each hole was often still fluid and almost completely unlithified.

Summary of Results

The upper middle Miocene to Holocene section at Site 1209 was apparently continuous and similar to contemporaneous sequences at Sites 1207 and 1208. Unconformities from the lower to middle Miocene and the lower Miocene to the lower Oligocene are partially equivalent to those observed at Sites 1207 and 1208 (Fig. F21), suggesting that regional oceanographic processes controlling erosion and dissolution had a major effect on sedimentation. The Neogene section at Site 1209 was deposited at much lower sedimentation rates than at the other sites, at least partially as a result of the lower production of biosiliceous and carbonate materials. Moreover, sedimentation at Site 1209 was exclusively pelagic, whereas the other two sites appear to have received a large supply of fine sediment from contour current and eolian transport. A progression of decimeter- to meter-scale orbital cycles is observed in the sedimentary record at Site 1209. Preliminary ages suggest that

dominant frequencies are eccentricity (100 k.y.) subsequent to 0.6 Ma, obliquity (40 k.y.) from 0.6 to 2.5 Ma, and then a gradual transition from long obliquity (1.25 m.y.) to long eccentricity (400 k.y.) to eccentricity (100 k.y.) through the lower Neogene and Paleogene section.

The upper Campanian to lower Oligocene section at Site 1209 is also apparently complete. The highlights of Site 1209 coring were clearly associated with the recovery of the sedimentary record of several critical events in this interval, most of them in multiple holes. These include the Eocene–Oligocene transition, the LPTM, the K/T boundary, and the MME. Sediments are almost completely unlithified, and the site appears to have remained above the CCD for most of this time interval; hence, foraminiferal preservation is good to excellent. The stable isotope and paleontological records from Site 1209 will provide important information on the nature of environmental changes during these events and their effect on marine biotas. Site 1209 will provide a firm shallow end-member in the Shatsky Rise depth transect.

Highlights

Eocene–Oligocene Transition

The Eocene to Oligocene transition represents the true end of the "greenhouse" world of the Mesozoic and Early Cenozoic. Although this transition occurred over a period of several million years, stable isotopic records reveal that much of the cooling occurred over a relatively brief (350 k.y.) interval in the earliest Oligocene known as Oi-1 (33.15–33.5 Ma) (e.g., Miller et al., 1991; Zachos et al., 1996). The deep oceans cooled by ~3°C during Oi-1, and large permanent ice-sheets became established in Antarctica (Zachos et al., 1992a; Zachos et al., 1992b). Current reconstructions of ocean temperature and chemistry for the Eocene–Oligocene transition, however, are based primarily on pelagic sediments collected in the Atlantic and Indian Oceans (Miller et al., 1987a; Zachos et al., 1996). Very few sections suitable for such work have been recovered from the Pacific (e.g., Miller and Thomas, 1985). As a consequence, we still lack a robust understanding of how global ocean chemistry or circulation evolved in response to high latitude cooling and glaciation.

The Eocene/Oligocene boundary was recovered in Cores 198-1209A-14H, 198-1209B-14H and 15H, and 198-1209C-4H. This boundary is identified by the LO of the planktonic foraminiferal genus *Hantkenina* at 33.7 Ma. Preliminary nannofossil and planktonic foraminiferal biostratigraphy suggests that the boundary interval is complete. The most marked feature in the transition record at Site 1209 is a gradual change, over ~7.5 m in the lowermost Oligocene and uppermost Eocene, from light brown to tan nannofossil ooze with clay to a light gray to white nannofossil ooze. A similar lithologic transition was observed in an identical stratigraphic position at Site 1208. However, the Site 1208 record is far more condensed than the Site 1209 record.

The distinctive color change in the Site 1209 record reflects a pronounced deepening in the CCD. This oceanwide event is thought to be related to the intensification of ocean circulation and/or to increased continental weathering (Zachos et al., 1996). Cycles from within the transition show that the transition was nonlinear and likely affected by climatic variations controlled by orbital cycles. This observation will help constrain the cause of deepening of the CCD. Planktonic and benthic foraminiferal preservation in this interval is moderate. Thus, stable isotope stratigraphies from Site 1209 have the potential to provide a firm understanding of the evolution of Pacific surface and deep waters through this important climatic transition.

Late Paleocene Thermal Maximum

At the other end of the climatic spectrum from the Eocene–Oligocene transition, the LPTM is an abrupt and short-term (~210 k.y.) warming event at 55.5 Ma that led to major transformation of marine plankton and benthos. This climatic event involved an increase of some 8°C of high-latitude surface waters and some 5°C of deep ocean waters. Warming is thought to have been driven by the input of a massive quantity of greenhouse gas, most likely methane, into the ocean-atmosphere system (e.g., Dickens et al., 1995). The response of the tropics and the Pacific Ocean to this climatic event is currently poorly known (Bralower et al., 1995).

The LPTM at Site 1209 corresponds to a 12.5-cm-thick medium brown layer of clayey nannofossil ooze with a sharp basal contact and a gradational upper contact. This horizon was recovered in Sections 198-1209A-21H-7, 198-1209B-22H-1, and 198-1209C-11H-3. The detailed lithostratigraphy of the three LPTM records recovered varies significantly on a millimeter scale as a result of deformation of the soft horizons during coring and splitting. Section 198-1209B-21H-5 shows the most complete record of the interval directly surrounding the LPTM, whereas Core 198-1209A-21H shows the most complete upper Paleocene to lower Eocene transition as indicated by MST data. The event corresponds to a sharp change from a white nannofossil ooze to a brown nannofossil ooze with clay (Fig. F22). In Hole 1209B, these two lithologies are separated by an extremely thin (1 mm) dark brown clay seam. In the other two holes, this seam has been disturbed during coring and splitting.

The micropaleontologcal record of the LPTM interval is summarized in Figure F22. Preliminary biostratigraphy shows that the event lies toward the top of nannofossil Zone CP8 and planktonic foraminiferal Zone P5. In addition, a single specimen of *Gavelinella beccariiformis,* a benthic foraminiferal species that goes extinct at the onset of the LPTM (e.g., Thomas, 1990) was found in Section 198-1209A-21H-CC, several decimeters below the event. The abrupt decrease in the nannofossil *Fasciculithus* that occurs just above the LPTM in other sections (Bralower et al., 1995; Bralower et al., 1997b; Aubry et al., 1996; Monechi et al., 2000) lies at the top of the clayey nannofossil ooze layer at Site 1209 (Fig. F22). The LPTM layer corresponds to a prominent magnetic susceptibility peak followed by a 6- to 7-m interval of relatively high susceptibility that shows cyclic variation. The top of the event is currently undefined. However, preliminary biostratigraphy—in particular the first occurrence (FO) of the nannofossil *Discoaster diastypus* that lies 1.73 m above the base of the LPTM (between Samples 198-1209A-21H-5, 130 cm, and 21H-6, 30 cm), and the LO of the plantkonic foraminifer *Morozovella velascoensis* that lies 2.38 m above the base of the event (between 198-1209A-21H-5, 129–130 and 49–50 cm)—indicates that the section is condensed compared to continental margin records from the Atlantic and Tethys (i.e., Kennett and Stott, 1991; Norris and Röhl, 1999).

The LPTM interval is associated with dramatic turnover in nannofossil assemblages. One of the dominant nannolith genera, *Fasciculithus,* is replaced by *Zygrhablithus bijugatus,* a nannolith that is often a highly abundant or dominant component of Eocene assemblages (Fig. F22). The genus *Discoaster* is often highly abundant within the event itself, likely as a result of warming or increased oligotrophy (Bralower, unpubl. data). Common to abundant calcispheres are found in sediments from the LPTM interval at Site 1209. These fossils are likely produced by calcareous dinoflagellates during intervals of adverse surface-water conditions.

Low-latitude planktonic foraminiferal assemblages in the LPTM also experienced a significant transformation with the sudden appearance of an ephemeral group of ecophenotpyes or new species of the genera *Acarinina* and *Morozovella* (Kelly et al., 1996). The range of these transient taxa is

limited to the interval of the carbon isotope excursion; hence, they are known as the "excursion" taxa. Although preliminary observations did not yield any of the end-member excursion taxa, several forms that are intermediate between the true excursion taxa and their ancestors were observed. No detailed observations were made on benthic foraminifers at Site 1209 due to sampling limitations.

The response of the CCD is a sensitive indicator of a changing carbon cycling during the LPTM, likely as a result of the input of large quantities of methane into the ocean-atmosphere system (e.g., Dickens et al., 1997). This response can be monitored by changes in carbonate content and preservation. Nannofossil preservation below the event at Site 1209 is moderate, indicating that the site was located in the broad range of the lysocline. Preservation declines markedly in the 1-mm clay lens at the base of the event as shown by pervasive etching of coccolith shields and nannolith rims. Preservation remains poor for several centimeters above this level, but nannofossils never completely disappear from the record. This interval of poor preservation is accompanied by a high abundance of bladey rhombs that may be reprecipitated calcite. The deterioration in nannofossil preservation is evidence for an abrupt rise in the level of the CCD and lysocline during the LPTM. The effects of this rise are not nearly as dramatic at Site 1209 as at Site 1208, which was situated almost 1 km deeper (see "Site 1208" in "Principle Results").

Cretaceous/Tertiary Boundary

At Site 1209 the base of lithologic Unit II coincides with the Cretaceous/Paleocene boundary, marked by a significant lithologic change from uppermost Maastrichtian, white to very pale orange nannofossil ooze to basal Paleocene, darker grayish orange foraminiferal nannofossil ooze. This boundary is located in Sections 198-1209A-25H-6 and 198-1209C-15H-3 but occurs within an unrecovered interval in Hole 1209B. The most complete boundary sequence is found in Hole 1209C. Here the top of the Maastrichtian is slightly indurated, possibly indicating an incipient hardground, and overlain by lowermost Paleocene mottled, light orange, slightly indurated foraminiferal nannofossil ooze that grades into softer and paler tan-gray nannofossil ooze. The lowermost Paleocene layer is strongly bioturbated as shown by the pale orange roots within the irregular surface of the top of the white Maastrichtian ooze (Fig. F23). The basal Paleocene unit is about 14 cm thick and overlain by a 23-cm-thick pure white ooze. In Hole 1209A, the uppermost Maastrichtian white nannofossil ooze is separated from the lowermost Paleocene light orange foraminiferal nannofossil ooze by a watery, disturbed, orange brown clay horizon. This horizon was formed by disturbance during coring and splitting and does not correspond to the "clay horizon" that defines the K/T boundary in classic sections such as El-Kef, Tunisia; Caravaca, southern Spain; and Gubbio (Bottaccione), Italy.

The micropaleontological record of the K/T interval is summarized in Figure F23. Preliminary biostratigraphy shows the well-known abrupt change in nannofossil and planktonic foraminiferal assemblages. The white nannofossil ooze (Hole 1209A: sample F2) yields a diverse, but dissolved, highly fragmented fauna of the latest Maastrichtian *Abathomphalus mayaroensis* planktonic foraminiferal Zone; the washed residue also contains rare, minute, well-preserved heterohelicids, predominantly *Guembelitria,* that suggest a possible preservation of Zone P0 fauna in the deepest burrows. Nannofossil assemblages in this interval (sample N1) are diverse, well-preserved, and include relatively common *Micula prinsii* indicating correlation to the uppermost Maastrichtian nannofossil Zone CC26. The light orange foraminiferal nannofossil ooze burrows (Hole 1209C: sample F1) yield highly abundant, minute (<100 mm), and well-preserved planktonic foraminiferal

assemblages that are dominated by heterohelicids and belong to the basal Paleocene *Parvularugoglobigerina eugubina* (Pα) Zone. Nannofossils in the gray-orange ooze (sample N2) are limited to "disaster" taxa (calcispheres) and reworked Cretaceous taxa. In the overlying pale nannofossil ooze horizon, the average size of the foraminiferal assemblage increases associated with increasing abundance of trochospiral forms with respect to heterohelicids (Hole 1209A: sample F3; Hole 1209C: sample F2). The lower part of the white ooze unit (sample N3) is dominated by ultrafine micrite, calcispheres, and the survivor coccolith taxon *Cyclagelosphaera reinhardtii*. Finally, the upper part of the white ooze unit contains fine micrite, small species of the coccolith *Neobiscutum, C. reinhardtii,* and another survivor, *Markalius inversus*. This whole interval thus belongs to nannofossil Subzone CP1a. In Hole 1209A, the orange-brown soupy clay, containing a late Danian planktonic fauna, coats indurated ooze above the burrows fragmented by drilling.

The lowermost 2–3 cm of basal Paleocene darker grayish orange foraminiferal nannofossil ooze contains common spherules, probably altered tektites. The thin (1–2 cm) boundary clay unit that corresponds to planktonic foraminiferal Zone P0 in a few deep-sea and shelf sites (e.g., El Kef, Tunisia; and Caravaca, southern Spain) is not found at this site, however. On the other hand, the rare well-preserved minute heterohelicids—especially *Guembelitria* in Hole 1209A sample F1—seem to suggest a possible preservation of Zone P0 fauna in the deepest burrows.

We postulate that this interval has been mixed by bioturbation soon after the boundary (Fig. F23). Nevertheless, the substantial thickness of the uppermost Maastrichtian *M. prinsii* (CC26) Zone and the lowermost Danian *G. eugubina* (Pα) Zones at Site 1209 indicates that the K/T boundary is paleontologically complete. In most deep sea-sites, the Pα Zone is either unrecovered or poorly preserved. Thus, the section represents one of the best preserved and least disrupted deep-sea records of this major extinction event, as well as of the subsequent radiation.

Mid-Maastrichtian Event

The long-term cooling of the Late Cretaceous was interrupted by a dramatic event in the mid-Maastrichtian (~69–70 Ma; nannofossil Zone CC24), when oceanic deep waters appear to have switched abruptly from low- to high-latitude sources (e.g., MacLeod and Huber, 1996; Frank and Arthur, 1999). This event appears to have coincided with the extinction of the inoceramid bivalves. Growing evidence, however, suggests that this biotic event is distinctly diachronous in the Atlantic, Tethys, and Pacific Oceans (MacLeod et al., 1996). Moreover, the magnitude and direction of stable isotope changes are quite variable from site to site (Frank and Arthur, 1999), possibly as a result of uncertainties in stratigraphic correlation or of true differences in deep-water properties.

The MME appears to have been recovered in Section 198-1209C-19H-1, which lies in nannofossil Zone CC24. In this section (Fig. F24) and several below it, large inoceramid prisms can be seen with the naked eye. Although the LO of inoceramids has not yet been determined in Hole 1209C, the abrupt disappearance in Core 198-1209C-19H is a likely sign of the event. Shore-based stable isotopic and benthic assemblage studies will help us refine our understanding of the origin and implications of this deep-water change.

Site 1210

Background

Site 1210 is located on the southern flank of the Southern High of Shatsky Rise on seismic line TN037-17A. Because of the proximity of this site to the seismic lines that are calibrated with drill

holes and characteristic sets of reflectors on these profiles, the seismic units of Sliter and Brown (1993) can be identified with confidence. Seismic Unit 1 (Neogene) is relatively condensed, and Units 2 (Paleogene) and 3 (Upper Cretaceous) are moderately expanded (Fig. F25). Although the site was selected at a location where the sedimentary section looks relatively expanded, the section was expected to contain a number of minor disconformities as indicated by prominent horizontal reflectors.

At 2574 m, Site 1210 is the second shallowest site in the Shatsky Rise Paleogene–Late Cretaceous depth transect that ranges from 2387 to 3346 m. As part of this depth transect, cores from Site 1210 will be used to address a number of leg-related objectives focused on abrupt and long-term climate change during the Cretaceous and Paleogene.

Holes 1210A and 1210B were cored largely with the APC. XCB center bit drilling was used to punch through chert layers in the Upper Cretaceous section (Table T1). Hole 1210A terminated at 249.30 mbsf in the core below a major chert horizon in the upper Maastrichtian. In Hole 1210B, a greater effort was made to penetrate the chert layers and to core the surprisingly soft sediment in between them with the APC. In this hole, 11 chert layers were penetrated with XCB center bit drilling, and a total depth of 376.36 mbsf was achieved.

Summary of Results

Coring at Site 1210 recovered three lithologic units that have been separated based on composition (Fig. F26). Lithologic Unit I ranges from Holocene to lower Oligocene (0 to ~32 Ma, 0–115.8 mbsf) and consists of clayey nannofossil ooze, nannofossil ooze with clay, and nannofossil ooze. This unit is split into three subunits. Subunit IA (Holocene to upper Miocene; 0 to 5.5 Ma; 0–83.4 mbsf) is olive-gray to gray and was deposited at higher rates than Subunit IB (upper Miocene to upper middle Miocene; 5.5 to 11.5 Ma; 83.4–112.0 mbsf), whose color ranges from shades of yellowish brown to pale orange to grayish orange. Subunit IC (upper middle Miocene to lower Oligocene; 11.5 to ~32 Ma; 112.0 to 115.8 mbsf) encompasses several dark yellowish brown clay-rich intervals that represent condensed sections or unconformities, interbedded with pale orange nannofossil ooze. A significant unconformity from lower Miocene to lower Oligocene occurs within this interval (see "Biostratigraphy" in "Specialty Syntheses"). Lithologic Unit II ranges from lower Oligocene to lower Paleocene (~32 to 65 Ma; 115.8–219.9 mbsf) and consists of shades of orange and yellowish brown nannofossil ooze, nannofossil ooze with clay, and minor amounts of clay with nannofossil ooze. The unit has a generally higher carbonate content than Unit I. Lithologic Unit III ranges from upper Maastrichtian to lower Campanian (65 to ~77 Ma; 219.8–377.0 mbsf) and consists of white nannofossil ooze, nannofossil ooze with foraminifers, and chert. This ooze has extremely high carbonate contents. Eleven chert layers were penetrated in lithologic Unit III.

The recovered section at Site 1210 is remarkably similar to that cored at Site 1209 located 29 km to the northeast on the summit of the Southern High. On a large scale, the ages of unconformities at the two sites are similar. On a small scale, critical boundaries—for example, the Paleocene/Eocene and Cretaceous/Paleocene boundaries—show a similar, detailed sequence of lithologies. Thus, the two sites have highly comparable sedimentation histories. There are a number of subtle differences between the Site 1209 and 1210 sedimentary section that provide for important interpretation in the depth transect framework of Leg 198. Site 1210 is 200 m deeper than Site 1209. Preliminary biostratigraphy suggests that the middle Miocene to upper Miocene interval at Site 1209 is highly condensed with a number of diastems, whereas the same interval at Site 1210 more likely

corresponds to an unconformity. Increased dissolution at Site 1210 in the middle to late Miocene is the most likely mechanism to explain this difference.

The highlights of coring at Site 1210 are also similar to those at Site 1209, namely the recovery of all of the critical intervals, most in both holes. These include the Eocene/Oligocene boundary, the LPTM, the Cretaceous/Paleocene boundary, and the MME.

Highlights

Recovery of Critical Events

As at Site 1209, a number of critical events have been recovered at Site 1210 in multiple holes. The lithologic record of each of these intervals at Site 1210 appears to be remarkably similar to that at Site 1209. The correlation is especially compelling based on magnetic susceptibility data of the composite section (Fig. F27). These data show similar shaped peaks for the events at the two sites, but perhaps more remarkably, a broadly similar number of peaks in between them. MST data will provide precise correlations between the two sites as well as an internal chronology. Site 1210 in general shows a slightly more expanded as well as more complete section in certain intervals. However, in the absence of detailed data and analysis, discussion of the significance of these events would be broadly similar for both Sites 1209 and 1210. More detail on the critical events is presented in "1209 Principal Results."

The Eocene–Oligocene transition has been recovered in an interval of continuous recovery from Holes 1210A and 1210B. The record for both holes show a gradual increase in carbonate content (Fig. F28) that is indication for a deepening in the CCD, similar to Site 1209 and sites from the Atlantic and Indian Oceans (e.g., Zachos et al., 1996). The Site 1210 record shows alternating dark and light lithologic cycles throughout this interval that indicate an overriding orbital control on dissolution. In intervals of the uppermost Eocene at Site 1210, planktonic foraminifers are extremely dissolved, suggesting that the site was close to the CCD. Comparison of carbonate content and microfossil records between the Leg 198 sites will provide important information on changes in the level of the lysocline and CCD through this major cooling event.

The interval recording the LPTM was recovered in Holes 1210A and 1210B. The lithologic record of this event is very similar in the two holes; this similarity is borne out by the magnetic susceptibility records (Fig. F27). The sharp base of the event coincides with an abrupt change from a very pale orange nannofossil ooze to a thin (1–2 mm), dark yellowish brown clayey nannofossil ooze. This is overlain by ~18 cm of moderate yellowish brown nannofossil ooze with clay that grades slowly into a pale orange nannofossil ooze. There is a noticeable color change from below the LPTM clay-rich horizon to directly above it that persists upsection for at least 10 m. The significance of this color change has not been determined. The clay-rich units show signs of dissolution, although this does not appear to be more pervasive than at Site 1209. Nannofossils appear highly dissolved in the lowest 1 cm of the event, but preservation improves significantly in the middle and upper part of the nannofossil ooze with clay. Blade-shaped, ~10–20 µm calcite grains are observed throughout the clay-rich units. Transient "excursion" planktonic foraminifers that correlate with the interval represented by the negative carbon isotope shift (e.g., Kelly et al., 1996) are observed within and just above the clay-rich units. Although based on preliminary observations, the lack of significant difference between the LPTM records at Sites 1209 and 1210 suggests that these sections were located in a depth range that was relatively insensitive to carbonate solubility changes across the LPTM. The Paleocene–Eocene transition at Site 1208, on the other hand shows a significant amount of

dissolution and intervals lacking carbonate, suggesting that it was at a depth (~800 m deeper than Site 1210) far more sensitive to saturation changes.

The record of the K/T boundary at Site 1210 is similar to that at Site 1209. The boundary succession includes uppermost Maastrichtian (nannofossil Zone CC26) pale orange nannofossil ooze overlain by lowermost Paleocene (foraminiferal Zone Pα) grayish orange foraminiferal ooze that grades into a white foraminiferal nannofossil chalk then back into a grayish orange nannofossil ooze. The boundary between the uppermost Maastrichtian and the lowermost Paleocene is clearly bioturbated, and careful sampling of burrows yields planktonic foraminifers dominated by *Guembelitria* with rare *Hedbergella holmdelensis* that suggest a possible Zone P0 age. Light brown to amber, spherical particles about 50 µm in diameter found in a sample from these burrows may be altered tektites. As at Site 1209, perhaps the most exciting aspect of this boundary succession is the excellently preserved, and apparently expanded, Danian section that will allow us to investigate the detailed record of the recovery and adaptive radiation of floras and faunas after this major extinction event.

The MME also appears to have been recovered at Site 1210. Large *Inoceramus* prisms can be seen over a 2-m interval of the mid-Maastrichtian in Core 198-1210B-28H but disappear above this level. The FO of the planktonic foraminifer *Abathomphalus mayaroensis* lies in Section 198-1210B-26H-CC, which is consistent with the age of the event at other sites (i.e., MacLeod and Huber, 1996).

Anomalous Lithification of Shatsky Rise Sediments

One of the most interesting results to emerge from Site 1210 and other Southern Rise sites is that the sediment has undergone little lithification, even at comparable burial depths to sediment at other sites that are indurated. For example, at the base of Hole 1210B at 377 mbsf, the predominant lithology is a nannofossil foraminiferal ooze. This sediment is soft, plastic in behavior, and almost uncemented. Nannofossils and foraminifers at this level have suffered a greater amount of dissolution than overgrowth. At a comparable depth in a typical carbonate sequence on the Ontong Java Plateau, chalk is found at this level; in fact, the chalk/ooze boundary is located between 181 and 339 mbsf. The soft nature of the upper part of the Shatsky Rise section has been discussed by Matter et al. (1975).

At Site 1210 between 200 and 300 mbsf, there are not the expected changes in physical properties that go hand-in-hand with compaction (e.g., Schlanger and Douglas, 1974). In this interval, gamma ray attenuation (GRA) density decreases, *P*-wave velocity is constant, and porosity increases. What are the major anomalies at Shatsky Rise that might be responsible for the relative lack of induration of the Cretaceous and Paleogene section? One possible factor that may have played a role in keeping the sediment soft is that sedimentation for most of the burial history of the deep section rates have been relatively slow, except for the last 5 m.y. Thus, the time integrated overburden for the deep section has been far less than most comparable sections.

A second factor is sediment composition. Cretaceous and Paleocene sediments at Site 1210 and other Leg 198 sites on the Southern High of Shatsky Rise are unusually enriched in foraminifers. Qualitative estimates of the foraminiferal abundance range up to 30% by volume, whereas typical deep sea sediments never exceed 15%–20% foraminifers. The bulk of the remaining volume is composed of nannofossils. The Site 1210 foraminiferal nannofossil oozes do not have anomalous porosities, densities, or *P*-wave velocities. However, the predominantly subspherical shape of foraminifers (vs. the predominantly flat shape of nannofossils) provides a smaller surface of exposed carbonate grains and a lower amount of grain-to-grain contact than in typical nannofossil ooze.

Thus, typical nannofossil ooze will experience more pressure solution, and this will lead to a greater amount of available carbonate for overgrowth on particles and for cement. This general relationship is borne out by results from the Ontong Java Plateau, where the ooze–chalk transition was drilled at five sites during Leg 130 (Berger, Kroenke, et al., 1991). The transition was recovered at depths ranging from 181 mbsf (Site 804) to 339 mbsf (Site 806). Shipboard microfossil abundance estimates show a substantial difference in the relative abundance of nannofossils and planktonic foraminifers, especially around the ooze–chalk transition. Although these data are semiquantitative, an apparent relationship exists between the depth of the transition and the relative abundance of foraminifers. Sections with generally higher abundances of foraminifers (Sites 805, 806, and 807) have deeper ooze–chalk transitions, between 264 and 339 mbsf, than those with lower percentages of foraminifers (Sites 803 and 804) where this transition is at 217 and 181 mbsf, respectively. The general lack of overgrowth and lithification is beneficial for paleoceanographic studies that rely on stable isotope analyses as the extent of diagenesis is less at Shatsky Rise than in comparable sections elsewhere.

Site 1211

Background

Site 1211 is located in lower bathyal (2907 m) water depth on the southern flank of the Southern High of Shatsky Rise. The site is on seismic line TN037-17A (Fig. F29) at the location of DSDP Site 305, which was RCB cored. The drilled sequence at Site 305 contains a relatively thick sequence of Lower Cretaceous chalk and chert, Upper Cretaceous ooze and chert, and Cenozoic ooze (Larson, Moberly et al., 1975). The unindurated part of the sequence at Site 305 was highly disturbed by rotary drilling and the record of the Eocene–Oligocene transition, the LPTM, and the Cretaceous/Tertiary boundary has been lost. Thus, the triple APC coring strategy for Site 1211 was designed to recover a complete and undisturbed record of the Site 305 sequence.

Site 1211 is the second deepest site in the Upper Cretaceous–Paleogene part of the Shatsky Rise depth transect. The site is more than 200 m deeper than Site 1212, the next shallowest site, and more than 500 m deeper than Site 1209, the shallowest site. Thus, drilling results from Site 1211 will contribute to broad, leg-based objectives that are aimed at understanding changes in Late Cretaceous and Paleogene ocean circulation at a time of global warmth. Results from Site 305 show that the site is located in a depth range that appears to be rather sensitive to changes in ocean chemistry, particularly carbonate solubility.

Holes 1211A, 1211B, and 1211C were cored with the APC (Table T1). Hole 1211A terminated at 158.9 mbsf at the highest chert layer in the upper Maastrichtian. In Hole 1211B, this chert layer was penetrated with XCB center bit drilling and a total of 169.9 m was cored reaching the lower Maastrichtian. Because there is some recovery of coherent Maastrichtian and Campanian ooze from Site 305, we decided not to spend the time to penetrate multiple chert layers to core the lowermost Maastrichtian and Campanian sequence with APC. Hole 1211C was cored to immediately below the K/T boundary at 138.3 mbsf to fill stratigraphic gaps in the composite sequence constructed from Holes 1211A and 1211B. The lack of overlap between the first two holes resulted from double coring an interval in the upper section of Hole 1211B.

Summary of Results

Coring at Site 1211 recovered three lithologic units that have been separated based on sediment composition (Fig. F30). Lithologic Unit I ranges from Holocene to lower Miocene (0 to ~17.3 Ma; 0–53.4 mbsf) and consists of nannofossil ooze, clayey nannofossil ooze, and nannofossil clay, shades of gray, green, yellow, orange, and brown in color. This unit has a higher clay content than underlying units. Two subunits are distinguished. Subunit IA (Holocene to lower Pliocene; 0 to ~4.8 Ma; 0–41.4 mbsf) is olive-gray and yellowish gray in color, contains siliceous microfossils and rare ash layers, and often shows a marked decimeter-scale cyclicity. Subunit IB (lower Pliocene to lower Miocene; ~4.8 to ~17.3 Ma; 41.4–53.4 mbsf) is yellowish orange and grayish orange in color and contains centimeter to decimeter-scale cycles. An unconformity from lower Miocene to upper Oligocene separates lithologic Unit I from Unit II (see "Biostratigraphy" in "Specialty Syntheses"). Lithologic Unit II ranges from upper Oligocene to lower Paleocene (~27 to 65 Ma; 53.38–133.80 mbsf) and consists of yellowish brown and dark yellowish brown nannofossil ooze with minor amounts of nannofossil ooze with clay, clayey nannofossil ooze, and clay with nannofossils. A number of minor diastems occur in this interval as indicated by thin, darker horizons. More significant unconformities are found in the middle Eocene (~40–45 Ma) and upper Paleocene (~56–59 Ma). The unit has a generally higher carbonate content than Unit I. Color reflectance data show decimeter-scale carbonate cyclicity. Lithologic Unit III ranges from upper to lower Maastrichtian (65 to ~70 Ma; 133.8–169.9 mbsf) and consists of pale orange nannofossil ooze and chert. The unit has extremely high carbonate contents. One chert layer was penetrated in lithologic Unit III.

The Site 1211 stratigraphic section shows broad similarity to the sections recovered at Sites 1209 and 1210 suggesting, in general, common sedimentation histories. In particular, the critical boundaries, for example the Paleocene/Eocene and Cretaceous/Paleocene boundaries, show a similar sequence of lithologies. However, sedimentation rates throughout the section are generally significantly lower at Site 1211 than at the previous two sites (Fig. F31), and there are additional unconformities and condensed intervals. All of these differences appear to reflect changes in carbonate preservation coincident with the greater water depth.

Highlights

The major highlight of coring at Site 1211 is similar to the highlights at Sites 1209 and 1210, namely the recovery of all of the critical intervals, most of which were recovered in all three holes. These include the Eocene/Oligocene boundary, the LPTM, the Cretaceous/Paleocene boundary, and probably the MME. In the first part of this section we describe the general stratigraphy of these intervals. In the absence of detailed data and analysis, however, a discussion of the significance of these events would be broadly similar to Sites 1209 and 1210.

The stratigraphic record at Site 1211 reveals differences from that at Sites 1209 and 1210 that appear to be related to increased water depth. In the second part of this section, we integrate results from the three sites and explores the significance of these differences in the framework of the Shatsky Rise depth transect.

Recovery of Critical Events

Sediment recovered at Site 1211 contains the record of the Eocene–Oligocene transition, the LPTM, the K/T boundary, and possibly the MME. Several of these events were recovered in all three holes. The lithologic record of each of these intervals at Site 1211 appears to be similar to Sites 1209 and 1210, but also to show significant differences.

The Eocene–Oligocene transition has been recovered in Holes 1211A, 1211B, and 1211C. Cores and reflectance data from the boundary transition show a subtle gradual upward lightening in color, likely as a result of an increase in carbonate content (Fig. F32). This change is evidence for a deepening of the lysocline and CCD. Prominent color cycles in the transition interval suggest an orbital control on dissolution. The amplitude of the reflectance variations is higher than at previously drilled Southern High sites, suggesting greater variation in dissolution intensity at the deeper Site 1211.

The LPTM was recovered in Holes 1211A, 1211B, and 1211C; however, the lithologic record in the three holes is different (Fig. F33), and magnetic susceptibility records are hard to correlate. Part of this problem arises from the fact that the event in Holes 1211A and 1211C was cut by section breaks. In these two holes, the LPTM was recovered in a yellowish brown clayey nannofossil ooze. The contact of this layer with the underlying grayish orange nannofossil ooze is mixed by bioturbation (Fig. F33). The lower part of the clayey nannofossil ooze in Hole 1211A also appears to have been cut by a burrow that contains grayish orange ooze. The clayey nannofossil ooze layer is ~11-cm thick in Hole 1211A and 8-cm thick in Hole 1211C and is overlain abruptly by grayish orange nannofossil ooze. In Hole 1211B, the base of the LPTM corresponds to a sharp change from a pale orange nannofossil ooze to a yellowish brown clayey nannofossil ooze. This color is uniform for 16 cm then grades to a grayish orange over the next ~30 cm. All sediment in the section above the base of the LPTM is darker than below.

Based on lithology and color, it is impossible to correlate between the LPTM in Holes 1211A and 1211C with the event in Hole 1211B. However, biostratigraphy suggests that there is a diastem right above the base of the event in Hole 1211B. Samples from the lower 6–7 cm of the clay-rich unit in Holes 1211A and 1211C contain the nannolith *Fasciculithus* in similar abundance to the lower part of the LPTM at Sites 1209 and 1210. Nannofossils in the lower part of the event are also poorly preserved, and abundant calcite blades are seen in samples as at the previous sites. The planktonic foraminifer *Morozovella velascoensis,* the LO of which defines the top of Zone P5, occurs 33 cm above the base of the event in Hole 1211A and ~24 cm above the base of the event in Hole 1211C. In Hole 1211B, however, *Fasciculithus* disappears 1–2 cm above the base of the event and *M. velascoensis* is absent in a sample 6 cm above the base. The nannolith *Discoaster diastypus,* the FO of which defines the base of nannofossil Zone CP9, is found 2–3 cm above the base of the event in Hole 1211B, 34 cm above the base of the event in Hole 1211C, and 10 cm above the base in Hole 1211A, which may have a slight gap at this level (this event is found 2 to 4 m above the base of the event at Sites 1209 and 1210). These preliminary data show the LPTM interval in Holes 1211A and 1211C is correlative with the lowermost 1 cm of the event in Hole 1211B. All three sections are highly condensed compared to records from Sites 1209 and 1210. The condensed nature of the LPTM at Site 1211 suggests that it was in a depth range that was sensitive to carbonate solubility changes across the LPTM.

The K/T boundary stratigraphy at Site 1211 is very similar to that at Sites 1209 and 1210. The boundary succession includes pale orange nannofossil ooze of latest Maastrichtian age (nannofossil Zone CC26) overlain by lowermost Paleocene (foraminiferal Zone Pα) yellowish orange foraminiferal ooze. This lithology grades upward into a white foraminiferal nannofossil ooze then back into a grayish orange nannofossil ooze. The boundary between the uppermost Maastrichtian and the lowermost Paleocene is clearly bioturbated, and careful sampling of burrows yields planktonic foraminifers dominated by *Guembelitria* with rare *Hedbergella holmdelensis* that suggest a possible

Zone P0 age. Light brown to amber, spherical particles about 100 µm in diameter found in a sample from these burrows may be altered tektites.

The MME is likely to have been recovered at Site 1211. Although *Inoceramus* prisms are not visible in the sediments, they are present in washed residues from Section 198-1211B-17H-CC.

Carbonate Record at Site 1211

The Shatsky Rise depth transect was designed to reconstruct the effect of short-term and long-term variations in the lysocline and CCD on the Upper Cretaceous and Paleogene sedimentary record. The total depth range of sites included in this transect is almost 1000 m, from Site 1209 (2387 m) to Site 1208 (3346 m). Site 1208 was clearly below the CCD for a significant part of the early Paleogene and the Maastrichtian, as much of this stratigraphic interval corresponds to an unconformity. Site 1211 (2907 m) is the deepest site in the Shatsky Rise transect with a nearly complete Maastrichtian to Eocene section.

The Site 1211 section shows broad similarities to its shallower neighbors, Sites 1209 and 1210 (2573 m) but is considerably more condensed (Fig. F31). Lower sedimentation rates in the major, continuous parts of the Site 1211 section as well as the longer duration of several hiatuses have reduced the thickness of the stratigraphic column. The major Miocene-Oligocene hiatus is similar in duration at all of the sites, however. This hiatus is thought to represent regionally increased erosion coincident with intensified deep-water flow during the latest Oligocene and early Miocene (see "Site 1207" and "Site 1208" in "Principle Results"). Preliminary biostratigraphy suggests unconformities in the Site 1211 section in the middle Eocene (~40–45 Ma) and upper Paleocene (~56–59 Ma) that are unique among the Southern High sites or at least much longer in duration than gaps in these intervals at the other sites.

Throughout the Paleogene section at Site 1211 are a number of 5- to 20-cm thick yellow-brown clay rich nannofossil ooze levels that have abundant phillipsite, pyrite, and manganese-coated foraminifers. Carbonate content of these layers reach as low as ~50 wt%. There are approximately 26 such intervals >5 cm in thickness. These levels are thought to result from lengthy seafloor exposure during intervals of intense dissolution when the site was located close to the lysocline/CCD. The late Paleocene to middle Eocene is an interval with a steadily falling but generally shallow CCD in the North Pacific (Rea et al., 1995). Paleodepths of Sites 1209, 1210, and 1211 are thought to be comparable to those of the present day (see "Biostratigraphy" in "Specialty Syntheses"); thus, the unconformities at Site 1211 may be intervals when the CCD shoaled to depths around 2900 m. A few clay-rich intervals in the upper Maastrichtian may also represent short-term lysocline/CCD shoaling events.

Superimposed on this long-term record for CCD variation are short-term (<1 m.y.) events that led to abrupt shoaling of the lysocline/CCD. The two most prominent events are in the mid-Paleocene. The second is at the LPTM. Both of these events are highly condensed compared to Sites 1209 and 1210 as a result of dissolution. For the mid-Paleocene event, dissolution lasted up to 1 m.y. beyond the end of the event.

Color reflectance data from Site 1211 show low-amplitude cyclic variation throughout the Paleogene. The percent total reflectance is usually closely correlated with carbonate content. For much of this interval, carbonate likely reflects the amount of dissolution. This suggests that the intensity of dissolution was controlled by a mechanism that might vary in intensity on orbital timescales. Two possible mechanisms are changing deep-water circulation and surface-water

productivity. The cycle record at Site 1211 should allow development of an orbital chronology for the Paleogene section.

Site 1212

Background

Site 1212 is located in middle bathyal (2681 m) water depth on the southern flank of the Southern High of Shatsky Rise. The site is at the location of DSDP Site 47 (Fischer, Heezen, et al., 1971). Hole 47.2 was cored with RCB penetrating 129.2 m of predominantly soft sediments, which frequently were so fluid that cores could not be opened. The hole terminated at a hard layer interpreted as chert. The recovered sediments, mainly nannofossil ooze and chalk are Pleistocene to late early Maastrichtian in age. Site 1212 also lies about 1.3 km to the northwest of DSDP Site 577.

According to the drilling record from Hole 47.2 (Fischer, Heezen, et al., 1971), the uppermost seismic reflector correlates with a major unconformity between the upper Miocene and the lower Oligocene. The next highest reflector corresponds to the uppermost chert horizon in the Maastrichtian. The interval between the two reflectors contains a Paleogene to uppermost Cretaceous section with minor unconformities. The lower Eocene to the K/T boundary section in Hole 47.2 was apparently complete and included the Paleocene–Eocene transition. The K/T boundary was described as heavily disturbed by coring but the described planktonic foraminiferal faunal succession was complete (Douglas, 1971). Abundant fragments of *Inoceramus* shells were recorded from the highly disturbed nannofossil ooze in the lowermost core taken (Core 47.2-14; 128.0 to 129.2 mbsf). Stable isotope analyses on single planktonic species have been performed on samples from this site and from other Shatsky Rise sites including Sites 305 and 306, and the first paleotemperature curves for the Northern Pacific were constructed for the entire Pleistocene to Cretaceous interval (Douglas and Savin, 1971, 1975). LPTM excursion isotope values were identified on single specimen and multispecimen analyses of foraminifers from Hole 47.2 by Stott (1992). This interval was described as highly disturbed by drilling.

Site 1212 is the third shallowest site in the Shatsky Rise depth transect. The site is approximately 300 m deeper than Site 1209 (2387 m) and 230 m shallower than Site 1211, the deepest site drilled on the Southern High; Central High Site 1208 at 3346 m is ~770 m deeper then Site 1212. The objective at Site 1212 was to recover a complete and undisturbed record of the Hole 47.2 sequence with APC double coring. As part of the Shatsky Rise depth transect, drilling at Site 1212 addresses a number of leg-related objectives.

Holes 1212A and 1212B were cored with the APC (Table T1). Hole 1212A terminated at 101.6 mbsf at the uppermost chert layer in the upper Maastrichtian. In Hole 1212B, 11 chert layers were penetrated with XCB center bit drilling and a total of 207.6 mbsf was cored, reaching the upper Albian.

Summary of Results

Coring at Site 1212 recovered three lithologic units that have been separated based on sediment composition and color variation (Fig. F34). Lithologic Unit I ranges from Holocene to middle Miocene (0 to ~15.1 Ma, 0–63.0 mbsf) and consists of nannofossil ooze with clay, clayey nannofossil ooze with foraminifers, and clayey nannofossil ooze, light gray to light olive-gray in color. This unit has a higher clay content than underlying units. Two subunits are distinguished. Subunit IA (Holocene to upper Pliocene, 0 to ~3 Ma, 0–35.9 mbsf) is characterized by interbedded light gray

nannofossil ooze with clay and light olive-gray clayey nannofossil ooze with foraminifers expressed as decimeter-scale light/dark alternations. The clay and foraminiferal content varies from 5% to 35% and from 0% to 32%, respectively. Minor components include siliceous microfossils (diatoms, radiolarians, silicoflagellates, and sponge spicules) and rare ash layers. Subunit IB (upper Pliocene to middle Miocene; ~3 to ~15.1 Ma; 35.9–63.0 mbsf) consists of light gray nannofossil ooze with clay and light olive-gray clayey nannofossil ooze and contains subtler decimeter-scale light/dark alternations. Siliceous microfossils are present but considerably rarer than in Subunit IA. Ash layers are absent.

An unconformity from middle Miocene to lower middle Eocene separates lithologic Unit I from Unit II (see "Biostratigraphy" in "Special Syntheses"). Lithologic Unit II ranges from lower middle Eocene to lower Paleocene (~43.6 to 65 Ma; 63.0–102.2 mbsf) and consists of alternating pale yellowish brown nannofossil ooze with clay and pale orange to grayish orange nannofossil ooze (Subunit IIA; lower middle Eocene to Paleocene/Eocene boundary; 43.6 to 55 Ma; 63.0–79.9 mbsf), and very pale yellowish brown nannofossil ooze with clay interbedded with very pale orange nannofossil ooze (Subunit IIB, Paleocene/Eocene boundary to K/T boundary; 55 to 65 Ma; 79.9–102.2 mbsf). A number of minor diastems occur in this interval as indicated by thin, darker horizons. The unit has a generally higher carbonate content than Unit I.

Lithologic Unit III ranges from upper Maastrichtian to upper Albian (65 to ~100 Ma, 102.2.–207.6 mbsf) and consists of soft, white nannofossil ooze and nannofossil ooze with foraminifers interbedded with chert. The unit has extremely high carbonate contents and is frequently highly disturbed by drilling because of its fluid nature. Eleven chert layers were penetrated. Two significant unconformities are found toward the base of this unit, separating the upper Campanian from the Coniacian and the Coniacian from the upper Albian.

The Site 1212 stratigraphic section shows broad similarity to the sections recovered at previously drilled Sites 1209–1211 suggesting, in general, common sedimentation histories. In particular, the critical boundaries, the Paleocene/Eocene and Cretaceous/Paleocene, show a similar sequence of lithologies. In addition, sedimentation rates throughout the Site 1212 section are generally comparable with the rates estimated at Sites 1209 and 1210, whereas they are higher than at Site 1211 in certain intervals (e.g., Paleocene–Campanian; Fig. F30). The major difference is the ~30 m.y. unconformity between lithologic Units I and II, a gap that is longer in duration than the major Neogene–Paleogene unconformity at other Southern High sites. Additional unconformities and condensed intervals in the Site 1212 section may be located in shore-based biostratigraphic investigations.

Highlights

The stratigraphic record at Site 1212 reveals differences from the records at Sites 1209, 1210, and 1211 that are not related to water depth. For example, the major Miocene–Eocene unconformity spans the lower Oligocene through mid-middle Eocene, an interval largely preserved at the other sites, including Site 1211, which is situated 230 m deeper than Site 1212. This suggests that the missing section at Site 1212 is not a result of dissolution. The absence of upper Eocene to Oligocene sediments at Site 1212 is more likely a result of local erosion or mass wasting. The site lies near the top of a canyon and in an area of the Southern High where the stratigraphy is complex (Sliter and Brown, 1993). Thus, it is possible that mass wasting has removed part of the section in the vicinity of Site 1212.

The major highlight of coring at Site 1212 is similar to the highlights at Sites 1209, 1210, and 1211, namely the recovery of all of the critical intervals, most in both holes. One exception to this is the Eocene/Oligocene boundary, which lies within the Miocene to Eocene unconformity. Even though coring of Cretaceous sediments was limited, the results from Site 1212 are meaningful with regard to the geologic history of Shatsky Rise.

Recovery of Critical Events

Coring at Site 1212 recovered the LPTM, the Cretaceous/Paleocene boundary, and the MME. The LPTM at Site 1212 is lithologically similar to Sites 1209 and 1210, corresponding to a 9-cm interval of yellowish brown clayey nannofossil ooze. This lithology has a sharp contact with underlying pale orange nannofossil ooze, and a gradational contact with overlying pale orange nannofossil ooze. Preliminary biostratigraphic investigation suggests that the sequence is similarly expanded to the Sites 1209 and 1210 LPTM sections and that similar changes in assemblages and microfossil preservation occur within the event. For example, the abundance of *Fasciculithus* decreases sharply near the onset of the event, and excursion foraminifers (e.g., Kelly et al., 1996) have been observed. The base of the LPTM event, however, appears to correspond to an unconformity. Foraminifers in Sample 198-1212B-9H-5, 77–78 cm, include *Globanomalina pseudomenardii,* the LO of which defines the top of Zone P4 at 55.9 Ma (age), ~0.4 m.y. before the onset of the event. The significance of this unconformity in terms of stratigraphy and paleoceanographic interpretation of the LPTM is currently not understood.

The K/T boundary interval is also lighter in color than at the other sites and the sediments near the boundary appear to be somewhat less indurated. Ooze immediately underlying the boundary correlates to uppermost Maastrichtian nannofossil Zone CC26 based on the presence of *Micula prinsii*. The paleontological boundary has been bioturbated, and careful sampling of burrows of lowermost Danian sediment that extend 10 cm into the uppermost Maastrichtian yields ~100-µm-sized, amber to olive-green spherules as well as tiny planktonic foraminifers possibly representing basal Paleocene Zone P0. Planktonic foraminifers in the lowermost Danian correspond to Zone Pα. The identical faunal and floral changes are observed in the boundary interval as at the other sites, and the early Danian interval, in particular, appears rather expanded and remarkably undisturbed.

Because Site 1212 is located close to Site 577 where the K/T boundary was triple cored during Leg 86 (i.e., Wright et al., 1985), comparison is necessary. Lithologically, the K/T boundary recovered in Holes 577, 577A, and 577B are similar although not identical to the Site 1212 record. The main difference between the sections is the degree of bioturbation and thickness of the bioturbated layer, and the thickness and color of the lowermost Paleocene foraminiferal ooze layer. Lighter color is associated with an increase in thickness of the basal layer from 10 cm in Hole 577A to more than 15 cm in Hole 577. Smear slide analysis for Site 577 showed that planktonic foraminifers are abundant (up to 35%) from basal Paleocene to ~60–70 cm above the K/T, whereas above and below this interval they rarely exceed 1%. At Site 1212, abundant foraminifers are found in smear slides only in the lowest 10–20 cm of the basal Paleocene.

A detailed study of planktonic foraminiferal biostratigraphy and assemblages across the K/T boundary at Site 577 was conducted by Gerstel et al. (1986). These authors illustrated the same evolutionary trends and succession of events as found at Site 1212 and other Leg 198 sites. Gerstel et al. (1986) argued that the presence of *Parvularugoglobigerina eugubina* below the K/T boundary was evolutionary. However, we have noticed that (1) the distribution of *P. eugubina* below the boundary is confined to the burrows associated with tektite-like spherules and (2) it is preceded in the deepest

burrows by the tiny *Guembelitria* assemblage reminiscent of the P0 zonal fauna. Moreover, the Site 1212 record shows that the tektite-like spherules are concentrated in the first few centimeters (2–3 cm) above the K/T boundary, and their record above is related to the intense burrowing. Nannofossil assemblages across the boundary were described in detail by Monechi (1985), who documented that the basal Paleocene yellow-brown ooze is characterized by an abrupt increase of *Thoracosphera* and the FO of *Neobiscutum romeinii,* followed by the FOs of *Markalius astoporus* and *Cyclagelosphaera reinhardtii,* similar to the sequence of events found at Site 1212 and other Leg 198 sites.

Cretaceous History of the Southern High

The Maastrichtian–Campanian section at Site 1212 is underlain by a thin layer of clay and glauconite-rich ooze of Coniacian age (planktonic foraminiferal Zone KS23, top of Section 198-1212B-24H-6), which in turn is underlain by ooze of late Albian age (Zones KS 16–17; base of Section 198-1212B-24H-6 to Section 27H-CC). This interval has been recovered at a number of other sites on Shatsky Rise, including Sites 1207 and 1213, and DSDP Sites 305 and 306 (Luterbacher, 1975). Coniacian to upper Cenomanian sediment, however, is extremely rare on Shatsky Rise as noted by Sliter (1992), who also reevaluated the planktonic foraminiferal biostratigraphy of Site 305 and found an unconformity in this interval. Sliter (1992) proposed that the Coniacian to Cenomanian interval was widely unconformable as a result of deep-sea erosion or dissolution. Coring results from Site 1212 and other Leg 198 sites confirm this conclusion. The fact that the one site where the Cenomanian to Coniacian interval is partially recovered, Site 1207 on the Northern High, lies at greater depth (3101 m) than Sites 1212 and 305 (2903 m) where it is unconformable, suggests that erosion is the likely cause of the regional unconformity. In addition, seismic line TN037-17A, which crosses Site 1209, 1210, and 1211, shows a prominent unconformity that likely correlates to the Cenomanian to Coniacian interval, where mid-Cretaceous dipping horizons are cut by horizontal uppermost Cretaceous horizons (Fig. F29). Thus, the stratigraphy of Site 1212 has important implications for the Cretaceous history of Shatsky Rise.

Site 1213

Background

Site 1213 is the southernmost and deepest site on the Shatsky Rise depth transect, located in lower bathyal (3883 m) water depth on the southern flank of the Southern High of Shatsky Rise. The site is close to the oldest part of the rise with underlying basement formed in the Tithonian (Late Jurassic). The major goals of Site 1213 drilling were to core a relatively deep-water mid- (Barremian–Cenomanian) and Lower Cretaceous sequence as well as to obtain fresh volcanic rocks from the underlying basement. The correlation of seismic lines down the southern flank of Shatsky Rise suggested that a relatively thick mid- and Lower Cretaceous section exists at relatively shallow burial depth (Fig. F35). Basement was thought to lie between 400 and 600 mbsf depending on velocity estimates. Thus both the lower part of the Cretaceous section and basement can be recovered without time-consuming drilling through extensive chalk/ooze-chert sequences.

Holes 1213A and 1213B were cored with the RCB (Table T1). Hole 1213A was terminated at 198.9 mbsf after the coring wireline parted. Lithology at the base of this hole consists of chert, porcellanite, and radiolarite of middle Albian age. A total of 447.8 m of sedimentary rock was penetrated in Hole 1213B with claystones near the base of the hole containing nannofossils and radiolarians of earliest Berriasian or latest Tithonian age. Core recovery in chert-bearing units was low. Underlying the

sedimentary package, plutonic or volcanic rocks totaling 46.6 m in thickness were penetrated and higher recovery was obtained than in the sedimentary sequence. Hole 1213B was terminated when the rate of penetration decreased significantly and the recovered material was considered sufficiently unaltered for detailed geochemical and radiometric analyses. Finally, a full suite of logs was to be collected through the whole sequence. The triple combo tool reached 431 mbsf but experienced several tight passes in the hole. With the approach of severe tropical storm Krosa combined with the poor hole conditions, it was considered too risky to deploy the FMS-sonic logging tool.

Summary of Results

Coring at Site 1213 recovered four lithologic units. Sedimentary units are divided based on composition and color. Lithologic Unit I (0–54.6 mbsf) consists of olive-gray to pale yellowish brown nannofossil ooze, clayey nannofossil ooze, and nannofossil clay that ranges from Holocene to lower Pliocene (0–5.0 Ma). This unit contains minor amounts of diatoms, foraminifers, and ash. Subunit IIA (54.6–66.1 mbsf) comprises pale orange nannofossil ooze and brown chert of Santonian age (84.8–85.5 Ma). Moderate to pale yellow brown chert and light brown and pale orange porcellanite of middle to late Cenomanian age (94.1–96.8 Ma) are grouped in Subunit IIB (66.1–85.4 mbsf).

Subunit IIIA (85.4–179.6 mbsf) of early Cenomanian to late Albian age (96.8–100.5 Ma) contains medium dark gray chert, gray, greenish gray, and pale orange porcellanite, and light greenish gray limestone. A mixture of chert, shades of brown and red in color, and pale orange to gray orange and pale yellow-brown porcellanite and radiolarite with an age range from early middle Albian to late Aptian (119–106 Ma) are grouped in Subunit IIIB (179.6–256.8 mbsf). Subunit IIIC (256.8–266.4 mbsf) corresponds to olive-black to greenish black C_{org}-rich clayey porcellanite, dusky green radiolarian porcellanite, and minor altered tuff. This unit is early Aptian in age (119.5–120.5 Ma). Gray chert, white to yellowish gray porcellanite, and light greenish gray and olive-gray nannofossil chalk to clayey nannofossil chalk of Hauterivian to late Berriasian age comprise Subunit IIID (266.4–410.3 mbsf). Subunit IIIE (410.3–447.8 mbsf) of late Berriasian to early Berriasian or latest Tithonian age contains brown, gray, grayish red, and pale to moderate brown chert, yellowish gray and light pale orange porcellanite, and brown claystone with nannofossils. A limonitic claystone breccia is found at the base of this subunit. Throughout the sedimentary section, porcellanite, limestone, and claystone have variable amounts of radiolarians and nannofossils. In many intervals nannofossil biostratigraphy was conducted on chalk adhered to the sides of chert nodules. This sediment indicates the nature of the unrecovered intervals. Finally, Unit IV (447.8–494.4 mbsf) contains at least three separate units of dark greenish gray, sparsely phyric or fine-grained diabase with chilled basaltic margins and thin interbedded pieces of altered chert.

Preliminary investigations of the almost 500-m cored sequence at Site 1213 yields a detailed 145-m.y. history of the deep south flank of Shatsky Rise. The record from this site provides a new perspective to the evolution of the plateau, from its formation by volcanic and plutonic activity, through its depositional history, to the erosional episodes that have removed sediment and sculpted its morphology. True basaltic basement was not recovered at this site; instead, we cored a sequence of diabase units with chilled margins and interbedded sediment that are interpreted as sills intruded in a late-stage, widespread plutonic event. Limonitic breccias overlie these intrusives, providing evidence for hydrothermal activity associated with sill intrusion. The earliest sediments of pelagic origin are radiolarian-rich horizons that were deposited under high-productivity surface-water conditions in well-aerated deep waters that were swept by currents. These sediments have been

transformed during burial to porcellanite and chert. At times, lower productivity conditions led to deposition of nannofossil ooze, which is now chalk in the deep record.

The early history of Shatsky Rise was interrupted by separate intervals of dysoxia/anoxia in the Valangianian and early Aptian that led to deposition of C_{org}-rich sedimentary rocks. Evidence for the Valanginian event is found in southern Europe (Lini et al., 1992). To our knowledge, however, this is the first record of this event in the Pacific Ocean as well as in the pelagic realm. C_{org}-rich rocks deposited during the well-known OAE1a were also found at Site 1207 on the Northern High. These unusual deposits with organic carbon contents from 2.9 to 25.2 wt% at Site 1213 (up to 34.6 wt% at Site 1207) show up clearly on gamma ray and U logs. The organic matter is almost exclusively of bacterial and algal origin.

The Barremian is only represented by one sample, at the top of Core 198-1213B-9R, and clearly most of the stage corresponds to an unconformity (between Cores 8R and 9R) in the Site 1213 record. This interval was also unconformable at Site 1214 (see "Site 1214" in "Principal Results"). The CCD in the Barremian is thought to have been relatively deep (e.g., Thierstein, 1979), certainly no shallower than the paleodepths of these sites at this time (2–2.5 km). Thus, the hiatus was most likely a result of a deep-water erosional event that scoured away the southern margin of Shatsky Rise.

The remainder of the mid-Cretaceous after the early Aptian was a return to better-oxygenated conditions with variation in productivity leading to deposition of radiolarian oozes (porcellanites and chert in the record) and nannofossil ooze (limestone). A hiatus occurred in the late Cenomanian to Santonian interval, the result of a widespread erosional episode that affected a wide area on the Southern High (Sliter, 1992) (see "Site 1212" in "Principal Results"). After a short depositional episode in the Santonian, a long hiatus in sedimentation lasted until the late Miocene. This episode was likely a result of a combination of erosion of the exposed, deep flank of the Southern High and carbonate dissolution at frequent times when the CCD in the Pacific shoaled above the depth of the site.

Highlights

Anoxic Events in the Early Aptian and Valanginian

Lower Aptian C_{org}-rich horizons were recovered in Core 198-1213B-8R. The horizons include olive-black to greenish black clayey porcellanites and radiolarian porcellanites with minor tuff (see "Lithostratigraphy" in "Specialty Syntheses"). Three organic carbon analyses yielded contents of 2.9, 10.2 and 25.2 wt%. The sample with the highest organic carbon content is a clayey porcellanite. Gamma ray and uranium logs show that the lower Aptian C_{org}-rich units are about 3 m thick. Total recovery of carbonaceous and noncarbonaceous in this interval (Core 198-1213B-8R) is just over 1 m. Thus, the recovery of organic-rich rocks is less than 30%.

Preliminary organic geochemistry provides information on the origin of the organic matter in lower Aptian samples from Site 1213. Characterization of the organic matter from the most C_{org}–rich samples indicates it is algal and bacterial in origin, including production of some of this organic matter by haptophytes and some by cyanobacteria. The haptophyte alkenones identified are some of the oldest known records of these compounds. The character and preservation of the bacterial material are also evidence for the existence of microbial mats at the time of deposition. Finally, the excellent preservation of organic compounds indicates deposition in highly dysaerobic conditions (see "Geochemistry" in "Specialty Syntheses").

Section 198-1213B-8H-1 is mostly noncalcareous; however, a sample at the top, Sample 198-1213B-8R-1, 3 cm, contains the nannofossil *Eprolithus floralis* but lacks *Rhagodiscus achlyostaurion* and *Prediscosphaera columnata,* and thus correlates to late Aptian Zone NC7. Sample 198-1213B-9R-1, 17 cm, lacks *Hayesites irregularis, Calcicalathina oblongata,* and *Cruciellipsis cuvillieri,* and thus correlates to upper Hauterivian–Barremian Zone NC5. Discrete intervals in Section 198-1213B-8H-1 have abundant radiolarians. Diagnostic radiolarian faunas in these samples are similar to assemblages observed in the Livello Selli in the Cismon core from the southern Alps of Italy (Premoli Silva et al., 1999). Thus, nannofossils, and particularly radiolarians, bracket the age of the carbonaceous horizons and provide a firm correlation with C_{org}-rich units of OAE1a from central Italy (the "Selli" level), the Italian and Swiss Alps, Sicily, France (the Goguel level), Site 641 in the eastern North Atlantic, and northern Mexico (i.e., Bréhéret, 1988; Weissert and Lini, 1991; Bralower et al., 1994; Erba, 1994; Menegatti et al., 1998; Erba et al., 1999; Bralower et al., 1999). In the Pacific, C_{org}-rich horizons of OAE1a age are also found at Sites 463 (MPM) and 866 (Resolution Guyot) (Sliter, 1989; Jenkyns, 1995), and elsewhere at Shatsky Rise at Sites 305 and 1207 (see "Site 1207" in "Principal Results" for a more detailed discussion). C_{org}-rich, lower Aptian sedimentary rocks from Sites 1207 and 1213 provide evidence for the nature of environmental changes in a truly pelagic regime during OAE1a.

Two C_{org}-rich levels in the Valanginian have considerably lower organic carbon contents than the lower Aptian horizons. A level in the lowermost Valanginian has 3.1 wt% C_{org}, one in the "mid" Valanginian contains 2.5 wt%. These horizons also contain clear evidence of bioturbation indicating that deep waters were sufficiently oxygenated to support a benthic community. The horizons do not show up on gamma ray logs suggesting that they are thin. The "mid" Valanginan horizon is significant as it appears to be broadly similar in age to C_{org}-rich units that had not previously been observed outside Tethys (e.g., Lini et al., 1992). The presence of a positive carbon isotope excursion that correlates to this event suggested that it was more widespread or global in extent (e.g., Weissert and Lini, 1991). Although recovery at Site 1213 does not allow us to characterize the temporal distribution of C_{org}-rich units, this record extends the known geographic distribution of organic-rich sediments considerably.

Chert Record

Although poorly recovered, pieces of chert in the Site 1213 section yield valuable information on variations in redox conditions through the Cretaceous. Nodules with orange, red, and brown hues indicate deposition and diagenesis in oxidizing environments, whereas those with olive-green to black hues indicate more reducing conditions during deposition and burial (see "Lithostratigraphy" in "Specialty Syntheses"). The color stratigraphy suggests that oxygenated conditions prevailed in the early Berriasian, late Aptian through middle Albian, and, when combined with data from other Leg 198 sites, from the late Cenomanian through the Maastrichtian. Reducing conditions prevailed in the Berriasian through the early Aptian and in the late Albian to middle Cenomanian. Similar trends were observed at Sites 1207, 305, 306, and 1214 (see "Site 1214" in "Principal Results") for coeval portions of the sequence, suggesting that for much of the Cretaceous, the entire Shatsky Rise experienced similar redox conditions at bathyal depths. Minor variations exist, however. At Site 1207, generally reducing conditions seem to persist until the late Aptian, with oxidizing conditions characterizing the early–middle Albian and from the late Albian through the Turonian.

Important Neocomian Reference Section in the Pacific

Site 1213 contains one of a handful of Neocomian pelagic sections in the Pacific Ocean. Although the section is generally poorly recovered, nannofossils are well preserved, and radiolarians are diverse and moderately well preserved. These groups should provide precise correlations with Neocomian sections worldwide. Planktonic foraminiferal occurrence is very rare. However, shore-based investigations have the potential to map out some of the earliest evolution of this group.

Shipboard nannofossil biostratigraphy has proven challenging due to the absence of important Neocomian marker taxa, especially the nannoconids. This group, which has a poorly understood affinity, are centerpieces of the biostratigraphy of the Jurassic/Cretaceous boundary interval in particular (e.g., Bralower et al., 1989). Their absence at Site 1213 is intriguing as they are abundant in samples from Site 463 in the MPM (Erba, 1994). At another site, Site 167 on Magellan Rise, nannoconids are absent except in the lowermost three cores (Roth, 1973). This group is also absent in assemblages that we interpret as Berriasian in Holes 49 and 50 on the deep western flank of Shatsky Rise (Fischer, Heezen, et al., 1971). What are the major controls on the distribution of nannoconids in the Pacific? Nannoconids are generally most common in continental-margin and epicontinental locations (e.g., Roth and Bowdler, 1981; Roth and Krumbach, 1986). In the Atlantic Ocean, this group is common in sites along the margins but absent in the deep sea except where transported by turbidity currents. Nannoconids are thought to be oligotrophic (e.g., Erba, 1994), and possibly to represent calcareous dinoflagellate cysts (Busson and Noël, 1991).

The record of nannoconids in the Pacific is complex. Their abundance at relatively shallow Site 463 and at Site 167 in its early (shallow) history, and absence at deeper Sites 1213, suggests that water depth may be a factor controlling their distribution. Alternatively, at Site 1213 and other sites, the abundance of radiolarians throughout the section might indicate high-productivity conditions hostile to oligotrophic organisms, including the nannoconids. However, at Site 463, radiolarians are often abundant along with nannoconids (Schaff, 1981; Erba, 1994). Most likely, a variety of environmental parameters influenced the distribution of this group.

Recovery of Shallow "Basement" of Shatsky Rise

Coring in Hole 1213B terminated in mafic igneous rocks on the flanks of southern Shatsky Rise. In all, 46.4 m of igneous section was drilled, with 33.4 m of recovered core (72%). Six cores, 198-1213B-28R through 33R recovered mostly massive basalt and diabase from Subunits IVA, IVB, and IVC, with each subunit thought to be a separate sill. The igneous rocks are predominantly hypocrystalline, fine-grained diabase (97.6%) with a small amount of sparsely phyric, aphanitic basalt (2%) at contacts. The diabase groundmass consists mainly of euhedral to subhedral plagioclase and intervening subhedral pyroxene and olivine, with minor glass. Alteration in the igneous section ranges from minor to moderate. Plagioclase and pyroxene crystals are locally altered to clay, and in thin section, glassy groundmass has been ubiquitously devitrified and/or altered to clay minerals. Basaltic material in the section occurs at subunit contacts, symmetrically disposed around pieces of metasediment that mark the subunit boundaries. From the chilled contacts, the basalt grades toward more coarse-grained diabase in the unit centers, where the groundmass approaches medium grained.

The sills must be early Berriasian age or younger, since this is the age of the host sediment. Paleomagnetic data show that two subunits have positive magnetic inclinations, whereas the third, basal subunit has a negative inclination, implying both normal and reversed magnetic polarities are recorded in the igneous section. This mixture indicates that the sills must have formed either before or after the long Cretaceous normal superchron (i.e., the Cretaceous Quick Zone, 121–83 Ma). On

the seismic profile along which Hole 1213B was drilled, the seismic "basement" has an odd character that may be related to the presence of intrusive, rather than extrusive, igneous rock at the sediment-igneous rock contact. The "basement" reflector, that being the deepest continuous seismic horizon, is weaker than elsewhere on Shatsky Rise, and other stronger reflectors occur beneath it. These deeper reflectors were not considered "basement" because they are not continuous all along the line, as is the weaker, shallower horizon. The cored section suggests the weak "basement" horizon denotes the top of the sills, whereas the deeper reflectors may be the top of the extrusive lava pile.

Site 1214

Background

Site 1214 is located at 3402 m water depth on the southern flank of the Southern High of Shatsky Rise. The site is at the location of DSDP Site 306 (Larson, Moberly, et al., 1975). At Site 306, we penetrated 475 m of sedimentary rocks with RCB drilling but only continuously cored from 207.5 m to total depth. Most of the upper section (28 to 207.5 mbsf) was alternately cored and washed at ~9-m intervals. The recovery was approximately 7%. The recovered sedimentary rocks, mainly calcareous porcellanite and chert with minor nannofossil chalk and ooze are late Albian to early Berriasian in age, covered by about 9 m of Holocene siliceous foraminifer-bearing nannofossil ooze.

According to the coring record from Site 306 (Larson, Moberly, et al., 1975), the uppermost Cretaceous sediments lie between Reflectors R1 and R2 of Sliter and Brown (1993). Reflector R1 (Cenomanian/Turonian boundary) crops out a few kilometers northeast of Site 306. Reflector R2 of Barremian/Aptian boundary age corresponds to the top of the porcellanite, chert, and shale section at Site 306 that rests on basement. The interval between R1 and R2 consists of chalk, chert, and porcellanite.

Site 1214 lies in the middle of the mid-Cretaceous portion of the Shatsky Rise depth transect between Site 1207 (3101 m) and Site 1213 (3883 m). The objective at Site 1214 was to recover a more complete and continuous record of the Site 306 sequence. As part of the Shatsky Rise mid-Cretaceous depth transect, drilling at Site 1214 addresses a number of leg-related objectives concerning ocean circulation and environmental change in an interval of global warmth.

Summary of Results

Hole 1214A was cored with RCB drilling terminating at 235.9 mbsf in the Hauterivian (Table T1). Average recovery of 7% was equivalent to Site 306. The sedimentary section has been divided into units based on composition and color. Lithologic Unit I (Holocene to Pleistocene; 0.0–6.9 mbsf) consists of very pale yellowish brown to moderate yellowish brown clayey foraminiferal nannofossil ooze and very pale to moderate yellowish brown clayey nannofossil ooze with foraminifers. Subunit IIA (late Albian; 6.9–34.5 mbsf) is composed of moderate yellowish brown to light olive-gray chert and very light gray to yellowish gray porcellanite, with minor white nannofossil chalk. Medium dark gray, dark gray to grayish black chert, and very light gray to light greenish gray porcellanite is grouped in Subunit IIB (late Albian to early Albian; 34.5–110.7 mbsf). Very light to light greenish gray limestone with radiolarians is a minor lithology in this subunit. Subunit IIC (early Albian to late Aptian; 110.7–207.0 mbsf) contains medium dark gray, dark gray, brownish gray, grayish brown and moderate brown chert, and yellowish gray, very light to light greenish gray porcellanite. Olive-black, greenish black and dark greenish gray claystone to clayey porcellanite is placed in Subunit IID (early Aptian; 207.0–216.6 mbsf). Finally, Subunit IIE comprises brownish gray, brownish black, and olive-

black chert and light greenish gray, greenish gray, and yellowish gray porcellanite (Hauterivian; 216.6–235.9 mbsf). Throughout the section, porcellanite and limestone have variable amounts of radiolarians and nannofossils. Most of the ages were obtained from chalk adhered to the sides of chert nodules. This sediment indicates the soft and relatively unaltered nature of the unrecovered intervals.

Highlights

The results of coring at Site 1214 provide important information on the stratigraphy of the mid-Cretaceous section on Shatsky Rise. The interpreted stratigraphy of Site 1214 are different from the stratigraphy of Site 306 from Larson, Moberly, et al. (1975) and Sliter (1992). One possibility for this difference is that Site 1214 is actually located at a distance from Site 306 given the imprecision of the coordinates of the latter site. A second possibility is that the biostratigraphy of Site 306 was carried out almost exclusively using planktonic foraminifers, whereas that of Site 1214 included nannofossils and radiolarians.

Site 1214 has an expanded Albian section, approximately 180 m in thickness, compared to 120–130 m at Site 1213. One possible reason for this disparity is that the latter site is located at greater water depth and thus subject to greater dissolution. More significantly, the stratigraphy of Site 1214 confirms that much of the Barremian corresponds to a regional unconformity on the southern part of Shatsky Rise. In both locations, lower upper Hauterivian sedimentary rocks are found in the core below lower Aptian horizons. At Site 1213, one sample at the top of Core 198-1213B-9R contained neither Aptian nor Hauterivian markers. Even with this uncertainty, combined data from Site 1213 and 1214 suggest that a significant hiatus occurred during much of the Barremian and at least part of the upper Hauterivian. The reason for this unconformity is currently unclear. This interval was present at Site 1207, which was some 800 m shallower than Site 1213 at that time; thus, a temporary change in the CCD could have led to the hiatus. However, the Barremian in most parts of the ocean, including the Pacific, is generally regarded as an interval when the CCD was relatively deep (i.e., Thierstein, 1979). Alternatively, it is possibly that this interval corresponded to an erosional event that removed sediment from the flanks of the southern high and not from the top of the northern high.

The lower Aptian section in Hole 1214A (Section 198-1214R-23R-1) contains olive-black, greenish black, and dark greenish gray claystone to clayey porcellanite. Both of these lithologies are laminated in places indicating low-oxygen conditions on the seafloor. C_{org} contents are low (<0.5 wt%) in the greenish gray lithologies. Four thin, discrete bentonite or tuff layers are observed within pieces of porcellanite. A sample from a piece of olive-black claystone toward the top of Section 198-1214R-23R-1 contains 1.4% C_{org}. Characterization of the organic matter from this sample indicates it is algal and bacterial in origin, similar to lower Aptian, highly carbonaceous lithologies from Sites 1207 and 1213 (see "Geochemistry" in "Specialty Syntheses"). This interval lies in nannofossil Zone NC6, between the FOs of *Eprolithus floralis* and *Hayesites irregularis*. Most of the sedimentary rocks in Section 198-1214R-23R-1 are noncalcareous but contain abundant radiolarians in discrete layers. Diagnostic radiolarian faunas in these levels are similar to assemblages observed in the Livello Selli in the Cismon core from the southern Alps of Italy (Premoli Silva et al., 1999) and in horizons bounding organic-rich intervals in the lower Aptian at Site 1213 (see "Biostratigraphy" in "Specialty Syntheses"). Thus, combined biostratigraphic and lithostratigraphic evidence suggests that the olive-

black claystone comes from within the general OAE1a interval, but certainly not from near the peak of the event as did samples with much higher C_{org} contents from Sites 1207 and 1213.

SPECIALTY SYNTHESES

Lithostratigraphy

Cretaceous Chert and Goo

The Cretaceous sedimentary sequence on Shatsky Rise is characterized by undercompacted nannofossil ooze to semilithified chalk that is locally partly to wholly silicified, forming porcellanite and chert, respectively (Fig. F36). The presence of chert hampered both the drilling and recovery of this section, particularly when rotary cored. The chert effectively reduced pre-Campanian recovery rates to less than 10%. Given the preferential recovery of chert and somewhat harder porcellanite over softer chalk/ooze interbeds, electric, caliper, and FMS logs through these intervals provide the best estimate of actual lithological proportions (see "Physical Properties, Downhole Measurements, and Core Logging").

The broadest temporal history of Cretaceous carbonate and biosiliceous sedimentation across the Shatsky Rise is provided by the combination of drilling results from Sites 1207 (Northern High) and 1213 (Southern High). Sediments (ooze/chalk/chert) from the Maastrichtian through the Berriasian were recovered, albeit in piecemeal fashion, with the exception of a few gaps interpreted as erosional unconformities, primarily during the Turonian–Coniacian and Barremian. The Campanian and Maastrichtian ooze was best recovered at Sites 1208, 1209, 1210, 1211, and 1212. The latter four sites record the mid-Maastrichtian *Inoceramus* extinction event.

High carbonate contents (up to 99 wt%) of the Cretaceous ooze/chalk suggest deposition above the CCD except during OAE1a (see "Geochemistry" in "Specialty Syntheses"). Where recoveries were higher at Site 1213, there is some indication of decimeter-scale cyclicity likely tied to variations in carbonate dissolution or production. Bioturbation was ubiquitous, with minor laminated intervals (radiolarites) associated with periodic reworking and winnowing by currents.

Prior to silicification, the Cretaceous sediments consisted of nannofossil ooze with variable amounts of radiolarians and foraminifers. The higher proportion and preservation of radiolarians down through the Cretaceous section is likely linked to the more equatorial position of the Shatsky Rise during the Early Cretaceous. At the equator, high productivity may have depressed the CCD, resulting in higher concentrations of biosiliceous material. These radiolarians are considered to be the major source of diagenetic silica in the section. Thin sections of chalk, porcellanite, and chert from Sites 1207 and 1213 verify the stages of silica diagenesis from Opal A (unaltered radiolarian tests), to Opal CT (lepispheres) to chert (microquartz and chalcedony).

Various lines of evidence suggest that silicification was rather early, prior to significant compaction of the sediment. Chert color, therefore, likely correlates with the original color of the presilicified sediment. Chert and porcellanite colors are generally either reddish brown or grayish to black. These color groupings are interpreted to reflect the prevailing redox conditions at the time of chert formation, with reddish brown indicative of more oxidizing conditions and grayish black reflecting a more reducing environment. Comparison of Leg 198 Sites 1207, 1213, and 1214, as well as Leg 32 Sites 305 and 306 reveals a very generalized secular trend of chert color (Fig. F37). It is likely that secular changes in prevailing redox conditions were driven by a combination of organic matter flux, sedimentation rate, and deep-water oxygen level.

Sedimentary Rocks of Early Aptian OAE1a

Coring at three sites recovered parts of sequences laid down during early Aptian OAE1a (Fig. F38). Very C_{org}-rich radiolarian claystones were recovered at Sites 1207 and 1213, whereas it appears that intervals with significant enrichment of organic carbon were either not recovered or were absent from this interval at Site 1214. The latter possibility seems unlikely given the intermediate-water depth of Site 1214 with respect to the other two sites. The lithology of the lower Aptian differs somewhat from site to site, but characteristic is the general absence of carbonate and the presence of abundant radiolarians. The C_{org}-rich, finely laminated radiolarian claystone at Site 1207, which is the shallowest of the three sites, was bracketed above and below by limestones. Cores at Sites 1213 and 1214 contained only radiolarites, radiolarian porcellanites, and claystones. The absence of carbonate indicates that the CCD rose to levels shallower than the paleodepth of Site 1207 but that the duration of the episode of severe carbonate dissolution was shorter there than at the two deeper sites.

An additional intriguing feature of the rocks at Site 1214 is the presence of at least four thin, gray layers of altered tuff interbedded with radiolarian claystones. Altered tuffaceous material was present in association with the C_{org}-rich layers recovered at Sites 1207 and 1213, but no discrete layers were noted. The presence of altered volcanic ash on Shatsky Rise reinforces the association of volcanism with OAE1a in the Pacific Basin (e.g., Larson, 1991a; Larson and Erba, 1999).

Cenozoic Carbonate Deposition

Sediment deposition for much of the Cenozoic occurred above the CCD and the lysocline. During the Paleocene and Eocene, the CCD maintained a position below Sites 1209, 1210, 1211, and 1212 resulting in the deposition of carbonate rich (>95%) oozes at those localities, and clays at deeper localities (i.e., Site 1208). Periodic lysoclinal shoaling, however, produced low-frequency and low-amplitude oscillations in carbonate deposition with a dominant cycle frequency close to that of the 100-k.y. eccentricity cycle. Carbonate deposition was further perturbed by episodic dissolution "events." One of the most prominent lies at the Paleocene/Eocene boundary (~55 Ma) as represented by a sharp, thin basal Eocene clay-rich layer at each site. These dissolution horizons probably resulted from a rapid shoaling of the lysocline and CCD brought about by the massive dissociation of methane hydrate and its subsequent oxidation to CO_2 in bottom waters (Dickens et al., 1997). From the uppermost Paleocene clays, carbonate content gradually recovers to levels that may exceed pre-event carbonate levels (Fig. F39). This suggests the lysocline overshot its original depth, consistent with the predicted silicate weathering feedback as the primary sink for the CO_2 (Dickens, 2000).

The middle Eocene is marked by a shoaling of the lysocline over the entire rise as inferred by a systematic decrease in carbonate content at Sites 1209, 1210, and 1211. Recovery occurs at the Eocene to Oligocene transition, which shows a gradual rise in carbonate content that reflects a deepening of the lysocline and CCD over the Shatsky Rise (Fig. F28). This CCD transition, which was global in extent (van Andel, 1975), initiated in the latest Eocene and peaked just above the boundary in the earliest Oligocene. At its peak, the CCD was sufficiently deep to allow carbonate to accumulate at Site 1208 (today at a depth of 3.3 km). In the mid-Oligocene, the lysocline and CCD began to shoal and, for extended intervals in the early and middle Miocene, were located above the Shatsky Rise, resulting in regional deposition of several prominent clay-rich condensed intervals. By the late middle Miocene, carbonate deposition resumed across the entire Shatsky Rise as the CCD deepened close to its present-day levels. From that point to the present, orbitally driven variations in the

lysocline together with carbonate production and clay fluxes have created distinct lithologic cycles across the entire rise.

Neogene–Quaternary Sediment Drifts and Biosiliceous Sedimentation

Based on the seismic character of the Late Neogene–Quaternary sections across the Shatsky Rise, thick sections at Sites 1207 (Northern High) and 1208 (Central High) are drift deposits, whereas those at the Southern High are thinner pelagic drape deposits. Although the drift deposits at Sites 1207 and 1208 show no distinct sedimentological evidence for current reworking, the higher than expected sediment accumulation rates at these sites are in part attributable to drift deposition. We believe that current reworking served to amplify regional variations in input of wind-borne volcanic ash and eolian terrigenous material, as well as production of biosiliceous material at these sites. The greater abundance of diatoms, radiolarians, and silicoflagellates in the upper Neogene–Quaternary sections at Sites 1207 and 1208, illustrated in Figure F40, can be attributed, in part, to a northerly increase in sea-surface productivity.

Clay Mineral Authigenesis

Green diagenetic laminae are prevalent in Quaternary and Neogene sediment at Sites 1207–1211. Similar features have been described at Ontong Java Plateau and Lord Howe Rise and were interpreted as altered layers of volcanic ash. Our observations have led us to conclude that the green laminae encountered at Shatsky Rise are diagenetic features composed primarily of saponite, a smectite group clay (see "Lithostratigraphy" in the "Site 1210" chapter). Clay was observed in discrete bands, along the edges of burrows filled with volcanic glass grains, but also as an authigenic product infilling foraminifer tests (Fig. F41). Alteration of disseminated grains of volcanic glass in the matrix and background saponite in XRD scans of bulk sediment suggest that saponite may be forming throughout the bulk sediment. Formation of this Mg and Ca bearing clay is also consistent with pore water profiles (see "Geochemistry" in "Specialty Syntheses").

Biostratigraphy

Eight sites and 16 holes (1207A and 1207B, 1208A, 1209A through 1209C, 1210A and 1210B, 1211A through 1211C, 1212A and 1212B, 1213A and 1213B, and 1214A) cored on Shatsky Rise recovered a virtually complete composite section ranging from upper Pleistocene to uppermost Tithonian representing 143 m.y. of geological history. A number of short intervals of lower and middle Miocene stratigraphy were not identified shipboard but are part of a fascinating regional sedimentation history which, grossly simplified, saw rapid deposition in the Pliocene–Pleistocene, reduced sedimentation rates in the late Miocene, condensation and hiatuses through the middle Miocene to Oligocene, complete but relatively slow deposition in the Paleogene (almost entirely on the Southern High), and rapid deposition for much of Maastrichtian to latest Tithonian time. Chert-rich sediments dominate from the mid-Campanian to lowest recovered sediments (Figs. F21, F36, F42).

With the exception of Site 1214, all sites include complete and rapidly deposited Pliocene–Pleistocene sections (8–14 m/m.y. sedimentation rates [SRs] and >1.0 g/cm^2/k.y. mass accumulation rates [MARs]) in which the noncarbonate fraction forms a significant proportion (Fig. F43). A particularly expanded drift-deposit succession (200 m and 42.4 m/m.y. SR) was recovered at Site 1208, and this section should prove to be invaluable for timescale studies allowing the integration of calcareous and siliceous biostratigraphies, cyclostratigraphy, and paleomagnetic polarity and

intensity records. The Pliocene–Pleistocene at Site 1207 was particularly rich in siliceous microfossils most likely due to cool, productive waters, which were also responsible for the paucity of tropical-subtropical species of planktonic foraminifers at this location on the Northern High. The influx of warmer water planktonic foraminifers and reduction of biosiliceous plankton to the south at Site 1209 shows the paleobiogeographic and paleoceanographic importance of the Shatsky Rise drill sites near the path of the Kuroshio Current.

The lowermost Pliocene and uppermost Miocene sections show reduced sedimentation and mass accumulation rates (<1.0 g/cm²/k.y. MAR) and overlie intervals of condensed section and unconformities that include parts of the upper, middle, and lower Miocene, the Miocene/Oligocene boundary interval as well as the upper Oligocene at most sites (Figs. F21, F43). The amount of missing section is variably expressed across Shatsky Rise and, for example, at Sites 1209 and 1211, much of the Oligocene is present. Northern and Central High Sites 1207 and 1208 and Sites 1213 and 1214 on the Southern High are also missing all or most of the Paleogene and uppermost Cretaceous. However, Southern High Sites 1209, 1210, and 1211 recovered apparently complete lower Oligocene to Paleocene sections that were deposited relatively slowly (0.2–7.6 m/m.y. SR and <1.0 g/cm2/k.y. MAR) and dominated by carbonate. These sections include complete and lithologically well-expressed LPTM and Eocene/Oligocene boundary intervals and provided excellent records of biotic response to these periods of rapid environmental change. Preliminary shipboard analysis of calcareous nannofossils through the LPTM interval reveals striking changes in assemblages, in particular the decline and extinction of *Fasciculithus* within the event and the subsequent increase in *Zygrhablithus bijugatus*.

Four Southern High Sites (1209–1212) include complete and relatively expanded K/T boundary sections characterized by a lithological switch from white Maastrichtian ooze to a thin, pale orange basal Paleocene ooze (~8–12 cm) with pyrite specks overlain by a distinctive pure white ooze. The boundary is bioturbated but otherwise undisturbed. The paleontological succession across the boundary interval is well preserved and apparently complete with the recognition of nannofossil Zones CC26 and lowermost CP1 and foraminifer Zones uppermost KS31, P0 (within burrows) and Pα. Clay spherules were observed at all sites. The calcareous plankton record above the boundary is exceptionally good, and in particular, there is only limited Cretaceous nannofossil reworking and foraminiferal mixing. Both calcareous nannofossils and planktonic foraminifers reveal the classic succession of abrupt extinction, followed by assemblages dominated by "disaster" taxa and rare "survivor" taxa, succeeded by assemblages that record the gradual introduction of new Danian "recovery" taxa. These sections represent some of the best preserved and least disrupted deep sea records of this major extinction event and the following recovery and diversification of calcareous plankton.

At the same four sites (Sites 1209–1212), we also recovered thick, carbonate-dominated, rapidly deposited sections of pure white Maastrichtian to Campanian ooze (6.5–31.6 m/m.y. SR and 1.0 g/cm²/k.y. MAR). Calcareous plankton preservation was generally good throughout, and the sections will allow the integration of calcareous plankton biostratigraphies and the study of the response of these groups to the mid-Maastrichtian and other events that include environmental changes.

Below the upper Campanian, the occurrence and stratigraphy of the Cretaceous section is variable (Fig. F21). Good lower Campanian sections were recovered below major unconformities on the Northern and Central Highs but below this interval recovery was poor and dominated by chert. Paleontological material was often limited to scraping chalk and limestone from chert pieces. However, a relatively complete Campanian to Barremian section was cored at Site 1207 with

remarkably uniform and high sedimentation rates (8.7 m/m.y. SR) and moderate recovery through the Aptian and Barremian. An outstanding record of OAE1a is well constrained by the plankton biostratigraphy.

Site 1213 yielded another thick Cretaceous section including a rapidly deposited Cenomanian to Albian succession and an Aptian section that includes OAE1a. Below this was an expanded section of Hauterivian to basal Berriasian/uppermost Tithonian. This Neocomian section yielded only few planktonic foraminifers but includes the FO in the Pacific of the tiny Hauterivian plankton foraminiferal ancestors (hedbergellids and globigerinelloidids) of the diverse Aptian assemblages. The section is rich in calcareous nannofossils and radiolarians, and the Berriasian in particular represents one of the best records of this time interval in the deep sea.

The consistent occurrence of pervasive chert lithologies from the Campanian to Tithonian across the range of sites drilled on Shatsky Rise is strongly suggestive of a long-term location beneath high-productivity surface waters related to a near paleoequator position during much of the Cretaceous. Preliminary paleontological observations support this hypothesis (e.g., very low diversity mid-Cretaceous planktonic foraminifer assemblages, indicative of high-productivity regimes, contrast strongly with peak diversities in the Campanian–Maastrichtian as Shatsky Rise drifted out of the equatorial zone). There are also intriguing and conspicuous absences within the lower Cretaceous nannofossil assemblages, particularly the almost total lack of *Nannoconus* and *Micrantholithus* nannoliths, which are such important, often rock-forming components in coeval Tethyan and Atlantic sites. Again, the location beneath highly productive surface waters may prove to have been the controlling factor.

Paleomagnetism

Magnetostratigraphic interpretations from Leg 198 sediments were restricted to upper Miocene and younger sections at all sites because cores from older sediments gave erratic magnetization directions. Despite making tens of thousands of measurements on hundreds of APC cores and using alternating field demagnetization up to 20-mT peak fields, the Oligocene to Cretaceous cores produced inclinations and declinations with poor correlation between different holes at any given site. The problem is thought to be the highly deformable nature of these sediments, which allowed disturbance and distortion of the sediments during coring, recovery, and/or splitting.

Measurements from Neogene sediments generally yielded an interpretable polarity record, typically showing polarity chrons from late Miocene to Pleistocene time (Fig. F43). Of these records, Sites 1209 to 1212 on the southern Shatsky Rise yielded a magnetostratigraphic sections of 50–100 m, going back in time to C3An (~6 Ma). The outstanding record is that from Hole 1208, on the central Shatsky Rise, where a drift deposit with high sedimentation rates was cored. This hole gave an extraordinarily expanded magnetic stratigraphy extending back to C5An in the mid-Miocene (Fig. F43).

Shipboard measurements were also made on archive-half sections from the igneous sill section drilled at the bottom of Hole 1213B. The results are unusual because two of the sills gave high positive inclinations (50°–70°) and the third yielded negative inclinations (~–30°). If it is assumed that all of the sills were formed within a relatively short geologic time span, these results imply that two of the sills are of normal polarity and the third is of reversed polarity. The steep positive values are inconsistent with the low predicted paleolatitude of Shatsky Rise during Late Jurassic and Cretaceous time.

Physical Properties, Downhole Measurements, and Core Logging

Downhole Logging

Two holes were logged during Leg 198: Hole 1207B with the triple combination tool (triple combo) and FMS-sonic tool strings, and Hole 1213B with the triple combo. Collecting data from the OAE1a black shale interval near the base of the Aptian was one of the major objectives of the leg. This sedimentary interval is clearly represented as peaks in the natural gamma radiation logs at both of the logged sites (Fig. F44). Most of the gamma radiation comes from uranium adsorbed onto the organic matter, and potassium and thorium are also high, indicating the presence of clay in the sedimentary rocks. The gamma radiation peak at OAE1a is much stronger than the other peaks in the log; other OAEs are either absent or are weaker than OAE1a on Shatsky Rise.

The Formation Micro-Scanner (FMS) resistivity images from Hole 1207B reveal the form, thickness, and depths of the chert horizons that formed the bulk of the recovered core below 230 mbsf (Fig. F45). Between 210 and 375 mbsf the chert layers occur on average every 83 cm and have an average thickness of 9 cm. The cherts typically appear as layers rather than nodules. Low core recovery in chalk/chert alternating sequences has been the subject of much discussion, and the image logs from Hole 1207B provide important data to develop better strategies for core recovery in chalk/chert sequences.

Synthetic seismograms were constructed from density and velocity data from both logs and core physical properties measurements. These reconstructions enabled the core and logs to be correlated with the seismic section and, hence, enabled ages to be assigned to the seismic reflectors.

Physical Properties

Physical properties data from Leg 198 show variation both with depth below the seafloor and with geographical location. The Northern and Central Highs of Shatsky Rise (Sites 1207 and 1208) have similar sedimentary histories dominated by major unconformities that are of ten's of millions of years in duration. The unconformities are manifested in the physical properties data as large peaks in magnetic susceptibility, *P*-wave velocity, and a downhole increase in bulk-density (both GRA and discrete measurements) (Figs. F12, F16). At Site 1207 a peak in natural gamma radiation is also apparent due to the presence of a manganese nodule proximal to the level of the major unconformity.

The Southern High of Shatsky Rise is characterized by more continuous sedimentation and shorter-duration hiatuses relative to the Northern and Central Highs. The physical properties data from Sites 1209, 1210, 1211, and 1212 suggest that compaction and dewatering, although important processes in the upper part of the sedimentary column, cannot explain all the trends observed (Figs. F20, F26, F30, F34). The Eocene–Cretaceous sediments are notable in that they appear to be underconsolidated with respect to their age and burial depth, suggesting that primary conditions, such as sediment composition, may be controlling the degree of lithification.

At Sites 1207, 1213, and 1214, a variety of lithologies of Cretaceous age, including chert, porcellanite, radiolarite, chalk, and limestone, were recovered. These sedimentary rocks exhibit a wide range of average *P*-wave velocities, from ~2200 m/s in the chalk and limestones to ~4760 m/s in the cherts (Fig. F12). Porcellanite and radiolarite have average *P*-wave velocities between this range. The high degree of variability of *P*-wave velocities in the Lower Cretaceous has significant implications for seismic data interpretation on Shatsky Rise.

Composite Depths and Cycle Stratigraphy

The recovery of complete sediment sections of APC-cored intervals was crucial to fulfilling the primary paleoceanographic objectives of Leg 198. Coring of multiple Holes at Sites 1209, 1210, 1211, and 1212 ensured the recovery of the complete (except unconformities) Cenozoic sedimentary record. Consequently, composite records of MST-derived physical properties and color reflectance data were produced for this time interval. These data compilations are unique in that previous drilling of Paleogene and Cretaceous sediments in the western Pacific failed to recover the complete and undisturbed sequences that are necessary to identify and characterize high frequency sedimentary cycles. As a result, little was understood about the influence of orbital and other periodic forcing on pre-Neogene sedimentation in the Pacific. The high-quality double and triple APC cores recovered during Leg 198 have the potential to remedy this situation. Most such sedimentary intervals exhibit pervasive lithologic cycles throughout the Cenozoic including those identified across several key transitions (Fig. F46, F47). Systematic changes in cycle amplitude and frequency are consistent from site to site, suggesting that these changes reflect regional paleoceanographic processes. The cycle packages (in all physical properties) are sufficiently distinct to allow for detailed correlation between sites (Fig. F47).

The most distinct cycles in terms of color variation and other physical properties occur in the upper Neogene. These are best represented by the total color reflectance (L*) records from Sites 1208 and 1209 as plotted along with orbital obliquity and eccentricity for the intervals 0–2 and 3–5 Ma (Fig. F48). The Pleistocene–Holocene color data at both sites exhibit the "classic" asymmetric glacial to interglacial cycle pattern. The interglacials are characterized by carbonate-rich, light-colored nannofossil oozes with clay, whereas the glacials are characterized by clay- and diatom-rich, dark-colored clayey nannofossil oozes or nannofossil clays. The transitions are mostly gradational, although several glacial to interglacial contacts are sharp. Preliminary biostratigraphic age constraints suggest that the dominant cycle frequency over the last 0.7 m.y. is near that of the 100-k.y. eccentricity cycle (Fig. F48). From 0.7 to 2.6 Ma, the dominant period shifts toward a higher frequency close to that associated with the 40-k.y. obliquity cycle. Throughout the last 2.6 m.y., the cycle amplitudes in reflectance remain remarkably similar between the Southern and Central Highs, although the mean total reflectance is higher on the Southern High. Climate-driven variations in opal and carbonate production and preservation, and in clay fluxes are responsible for these changes.

The lower Pliocene prior to the onset of Northern Hemisphere glaciaiton at 2.6 Ma is also characterized by regular lithologic cycles. As in the late Pliocene and early Pleistocene, the wavelengths indicate a dominant period close to 40 k.y. However, the cycle amplitude in this period is noticeably reduced, particularly at sites on the Southern High. The reduction in the high-frequency cycle amplitude is accompanied by an apparent increase in a low frequency cycle amplitude. In the Site 1209 color reflectance record (over the period 3 to 5 Ma), for example, there appears to be a long wavelength oscillation with a period of roughly 1.0 to 1.25 m.y. Comparison with the derived orbital curves (Laskar, 1990) suggests that this cycle may be in phase with the long period 1.25-m.y. cycle of obliquity (Fig. F48).

In the Paleogene, the sedimentation rates are sufficiently low (~3 to 5m/m.y.) over most of the Southern High that it is difficult, if not impossible, to identify cycles associated with obliquity and precessional-scale forcing. Nevertheless, prominent periodic to quasi-periodic color (light–dark) and magnetic susceptibility cycles occur throughout the upper Paleocene to late Eocene at Sites 1209,

1210, 1211, and 1212. The variations represent subtle changes in carbonate and/or Fe oxide content. The mean wavelength of the highest amplitude oscillations indicates a cycle frequency in the approximate range of the 100-k.y. eccentricity cycle. These cycles in turn exhibit an amplitude modulation with a frequency range suggestive of 400-k.y. eccentricity forcing. If so, these data would be consistent with observations elsewhere of a dominant response to precession and eccentricity forcing during the ice-free Paleogene prior to the late Eocene appearance of ice sheets on Antarctica.

Geochemistry

Interstitial Water Geochemistry

Interstitial water samples were collected from the Neogene–Campanian sediments at seven of eight sites drilled during Leg 198. The older sedimentary sequences, marked by poor recovery associated with the presence of chert, yielded no samples suitable for pore water extraction. Site 1213 samples were affected by drilling disturbance associated with rotary coring and are not considered in this synthesis. No samples were collected from Site 1214, where <1 m of unlithified sediment was cored.

Reactions involving the degradation of organic matter occur primarily in the Neogene sections. Although the sediments contain little organic matter (e.g., <0.3 wt% at Site 1207 and <0.2% at Site 1210), there is sufficient variation among the sites to lead to significant differences in the degrees of sulfate (SO_4^{2-}) reduction, ammonium (NH_4^+) production, and methane (CH_4) generation (Fig. F49). These differences correspond with contrasts in mass accumulation rates (MARs) on the Northern, Central, and Southern Highs of Shatsky Rise. The SO_4^{2-} profile is most depleted at Site 1208, located within a drift deposit atop the Central High, where the highest Neogene MARs are recorded (Fig. F49). Site 1208 is also marked by higher NH_4^+ and CH_4 production relative to other sites. By contrast, relatively minor amounts of SO_4^{2-} reduction, NH_4^+ production, and CH_4 generation were observed at Site 1211 (Southern High), where Neogene MARs are lowest (Fig. F49). The profiles from the other sites lie between the two end-members defined by Sites 1208 and 1211. These relationships suggest that organic matter preservation is enhanced slightly in areas characterized by higher MARs. In areas with relatively low MARs, it appears that most organic matter is degraded before it can be incorporated into the sediment column.

One of the most unusual aspects of the sections cored during Leg 198 is the lack of significant alteration (i.e., compaction, recrystallization, and cementation) in the Campanian–Paleogene section relative to overlying sediments. The convex-upward shape of the Sr^{2+} and Sr/Ca pore water profiles through the uppermost sediments at Sites 1207–1212 suggests that carbonate recrystallization is occurring largely within the Neogene section. By contrast, Sr^{2+} and Sr/Ca profiles through the underlying Campanian–Paleogene sediments are invariant, suggesting that carbonate dissolution and reprecipitation processes are not significant through this stratigraphic interval. This unusual downcore trend in carbonate diagenesis may be a consequence of the foraminifer-dominated nature of the Campanian–Paleogene ooze on Shatsky Rise. The relatively low surface area and associated excess surface free energy of the sediment particles may have imparted a low diagenetic potential (i.e., Schlanger and Douglas, 1974) on these sediments as compared with the overlying Neogene section, in which nannofossils (with higher surface area and excess free energy) predominate (i.e., Baker et al., 1982; Walter and Morse, 1984). A second factor may be related to the clay-rich, condensed intervals that at all sites mark the transition between the Paleogene and middle

to upper Miocene sections. The condensed horizons could have acted as crude barriers, preventing significant expulsion of pore fluids as the Campanian–Paleogene sediments underwent burial. The high water content of these sediments could have significantly reduced their compressibility, such that the load at grain-to-grain contacts remains insufficient to initiate pressure solution of carbonate. No significant inflections in pore water profiles were observed across the Neogene–Paleogene transition. This pattern suggests that although the clay-rich horizons may have played a role in controlling processes of compaction, they have not acted as an effective barrier to the diffusion of chemical elements.

Excursions to higher Mn^{2+} concentrations in the lower parts of the pore water profiles coincide with a series of condensed intervals and hiatuses within the middle–lower Miocene and Oligocene sections, which contain inferred Mn-rich phases. Excursions to higher Mn^{2+} concentrations reflect the dissolution of Mn minerals and diffusion of Mn^{2+} away from Mn-rich horizons.

Pore water profiles are also affected by reactions involving the alteration of silicate minerals and exchange with basaltic basement. Reactions associated with the formation of clays and the alteration of ash and biogenic silica are prevalent in the Neogene sediments and are reflected in the pore water profiles as sharp decreases in Mg^{2+} and elevated concentrations of K^+ and Ca^{2+} in the upper parts of profiles. These trends are overprinted on diffusion trends related to exchange with basaltic basement, including gradual downcore decreases in Mg^{2+} and K^+ and increases in Ca^{2+}.

Organic-Rich Intervals in the Lower Aptian and Valanginian

Evaluation of the abundance, character, and origin of the organic matter in the Cretaceous organic-rich intervals at Sites 1207, 1213, and 1214 was the primary focus of shipboard organic geochemical investigations employing a combination of analysis of elemental compositions, pyrolysis products, and biomarker distributions.

Remarkable amounts of organic carbon occur within the intervals corresponding to early Aptian OAE1a at Sites 1207 and 1213. Four samples possess C_{org} that exceeds 10 wt%; one is almost 35 wt% (Table T3). These values are among the highest ever recorded for Cretaceous marine sequences and attest to the extraordinary nature of the depositional conditions that led to enhanced sequestration of organic matter at this time. Moreover, this enrichment is restricted to specific intervals; other samples within the lower Aptian contain significant, but less exceptional amounts of C_{org} (1.7 and 2.9 wt% C_{org}). The highest value at Site 1214 is 1.4 wt% (Table T3). Two C_{org}-rich calcareous intervals were also recovered from the Valanginian at Site 1213 with C_{org} contents of 2.5 and 3.1 wt% (Table T3). The anomalously high C/N ratios for these samples suggest that nitrogen cycling within these intervals did not follow normal marine trends, perhaps associated with bacterial communities or hierarchies that include denitrifiers or with organic matter enriched in N-poor lipidic components, such as cyanobacterial sheaths.

Rock-Eval pyrolysis (Fig. F50) provides further measures of the abundance and character of the organic matter and of its thermal maturity. The low T_{max} values demonstrate well the immaturity of the samples with regard to petroleum generation. The lower Aptian samples from Sites 1207 and 1213 with high C_{org} contents (>3.5 wt%) plus Sample 198-1207A-44R-1, 103–104 cm (1.7 wt%), all possess high hydrogen indices (>420) and low oxygen indices (≤25; Table T3), which corresponds to type I organic matter (Tissot et al., 1974) rich in algal and bacterial debris. Their position on a modified van Krevelen diagram matches closely with an organic-rich sample (3.6 wt% C_{org}) from the interval at Site 866 that directly overlies the occurrence of a negative $\delta^{13}C$ excursion in carbonate

associated with OAE1a (Jenkyns, 1995) and with lower Aptian samples from Site 463 with >2.5 wt% C_{org} plot (Fig. F50). The apparent comparability of the organic matter associated with the early Aptian OAE1a event may reflect some uniformity in conditions exerting controls on the character of ocean production and biomass and its preservation.

The exception to this pattern at Site 1213 is Sample 198-1213B-8R-1, 96–97 cm (2.9 wt% C_{org}), which has a markedly higher oxygen index (OI) and plots closer to the type II kerogen path (Fig. F50). Its hydrogen index (HI) value is similar to that of the Valanginian organic-rich intervals, although their position on the modified van Krevelen diagram is compromised by anomalous OI values related to their high carbonate contents. Sample 198-1213B-8R-1, 96–97 cm, therefore, might be expected to contain enhanced proportions of marine organic matter compared to the other lower Aptian samples. Remarkably it is the only sample determined to contain alkenones, components only biosynthesized by haptophyte algae. The discovery of C_{37} and C_{38} alkadienones (Fig. F51) in this sample extends the record of the occurrence of these paleotemperature proxies by 15 m.y. (cf. Farrimond et al., 1986). The presence of these components in high abundance provides convincing evidence that alkatrienones are likely to have survived if they had been produced in the original depositional setting. Thus, the absence of alkatrienones may reflect warm waters (>28°C; cf. Brassell et al., 1986) or, alternatively, these sediments may predate the evolutionary development of alkatrienones.

The biomarker composition of the organic-rich intervals provides clear testimony of the extraordinary preservation of organic matter, not only in terms of its abundance, but also with regard to its unaltered character, especially at Site 1213 where the abundance of ketones significantly exceeded that of hydrocarbons. The fact that alkenones were only detected in one sample implies that contributions of organic matter from their haptophyte source were less important during deposition of the other intervals. The distribution patterns of the hydrocarbons and ketones in all of the lower Aptian samples show many similarities (Fig. F51), especially the prominence of steroidal ketones and hydrocarbons derived from eukaryotes. The same suites of compounds are also observed in the Valanginian organic-rich intervals, augmented in Sample 198-1213B-15R-1, 9–10 cm, by the presence of sterol ethers (cf. Boon and de Leeuw, 1979; Brassell et al, 1980). Thus, there appears to be a broad uniformity in the nature of the organic matter attributable to algal primary producers at Shatsky Rise. However, this observation stands in stark contrast to the restricted occurrence of critical bacterial markers, notably extended ($\geq C_{32}$) and methylhopanoids (Fig. F51). These compounds, in concert with other diagnostic components, record contributions of organic matter from cyanobacteria and from methylotrophic and methanogenic bacteria (Ourisson et al., 1979, 1987; Rohmer et al., 1989, 1992). They are prominent in several of the lower Aptian organic-rich intervals and imply a significant role for bacteria associated with processing of organic matter at higher trophic levels during OAE1a. These compounds record the development of bacterial communities, perhaps as microbial mats, in the depositional environment that may reflect the establishment of dysoxic conditions. Thus, the extraordinary sequestration of organic matter (up to 34.7%) in the lower Aptian at Shatsky Rise, even by comparison with other organic-rich intervals within the mid-Cretaceous, records a response to a radical change in the processes controlling biogeochemical cycling, which in turn reflects a perturbation of the ocean-climate system.

SUMMARY OF RESULTS

The record of 145 m.y. of sedimentation on Shatsky Rise holds clues about the nature of oceanic environments during long intervals of global warmth and the transition to colder climates of the more recent geological past. The focus of Leg 198 scientific objectives was to understand the long-term transitions into and out of the warm-climate "greenhouse," as well as transient but critical events that occurred periodically, events that involved major changes in ocean circulation, geochemical cycling, and marine biotas. The record of this shifting climate was cored during Leg 198 in a depth transect that provides a multidimensional picture of the ocean during periods of relative stability and intervening episodes of environmental perturbation. The signature of both abrupt and gradual change is graphically displayed in the lithology, biota, and geochemistry of the sediments.

The deep-sea sedimentary record of Shatsky Rise contains evidence of brief intervals of open-ocean dysoxia during the early and middle parts of the Cretaceous period. These are followed by more stable times in the Late Cretaceous and Paleocene, when the rain of calcareous skeletal material from calcareous microplankton formed almost pure biogenic ooze on the seafloor. Three highly selective extinction events interrupted these stable times, one that affected a long-ranging group of bottom-dwelling clams at ~69 Ma in the mid-Maastrichtian; another, the well-known K/T boundary event at 65 Ma that almost eradicated surface-dwelling plankton; and a third at ~55 Ma that profoundly affected benthic organisms and caused the abrupt reorganization of calcareous plankton communities. Each of these events appears to have been associated with a unique environmental perturbation. Throughout the Paleogene and the Neogene, evidence for fluctuations in climate, oceanic circulation and chemistry, and/or marine productivity forced by orbital variations are expressed in prominent lithologic cycles.

The warm mid- to Late Cretaceous and early Paleogene climate came to an end, beginning about 50 Ma, but wholesale cooling did not begin until an abrupt event at ~33.5 Ma when ice sheets developed on Antarctica and the deep oceans suddenly filled with cold water. The youngest Shatsky Rise sediments contain clear evidence of the onset and peak of Northern Hemisphere glaciation in the last 2.7 m.y. Here we present a preliminary summary of the highlights of Leg 198 beginning with the Cretaceous and moving forward in time.

A Classic Record of the Early Aptian Oceanic Anoxic Event

A major highlight of Leg 198 is the recovery of C_{org}-rich sedimentary rocks of early Aptian age at Sites 1207 and 1213 (Fig. F38). These sediments were deposited during OAE1a and provide the best truly pelagic record of this event outside of Tethys. At Site 1207 the event is found within 45 cm of finely laminated, dark brown radiolarian claystone with up to 34.7 wt% C_{org}. The Site 1213 C_{org}-rich units include olive-black to greenish black, clayey porcellanites, and radiolarian porcellanites with up to 25.2 wt% C_{org} and associated minor tuff (Site 1213). At both sites, gamma ray and uranium logs show pronounced highs, and at the same time indicate the true thickness of the critical levels and the incomplete recovery. These data suggest that at Site 1207, approximately 50% of the organic-rich unit was recovered; in the more siliceous section at Site 1213, this percentage was much lower, certainly less than 30% (Fig. F44). At Site 1214, the highest measured C_{org} content in the lower Aptian is 1.4 wt% in a black claystone, but the presence of lamination in sediments, discrete tuff layers, and a distinctive radiolarian assemblage (e.g., Erbacher and Thurow, 1997; Premoli Silva et al., 1999) suggest that the recovered sediments lie within the OAE1a interval.

Shipboard biostratigraphy indicates that the organic-rich units lie in lowermost Aptian nannofossil Zone NC6 and planktonic foraminiferal *Globigerinelloides blowi* (KS6) Zone, thus correlating to C_{org}-rich units in other localities that lie within OAE1a (e.g., Bralower et al., 1994; Erba et al., 1999; Premoli Silva et al., 1999). Rock-Eval analyses and gas chromatography-mass spectrometry (GC-MS) of extractable hydrocarbons and ketones have been used to characterize organic matter from the C_{org}-rich unit at Sites 1207 and 1213 (Figs. F50, F51). These data indicate that the organic matter is almost exclusively algal and bacterial in origin. GC-MS data, in particular, have been used to identify biomarkers that are associated with cyanobacteria in material from both sections (Fig. F51). The prevalence and character of bacterial biomarkers suggest the existence of microbial mats at the time of deposition. Compounds produced by haptopyte algae include the oldest known alkenones (Fig. F51). Organic matter of algal origin was also reported in the lower Aptian organic-rich units of Sites 463 and 866 (Dean et al., 1981; Baudin et al., 1995), suggesting that production by these organisms was widespread during OAE1a.

At Sites 1207 and 1213, the interval within and directly above and below the C_{org}-rich units lacks carbonate. Both organic-rich intervals are associated with minor amounts of tuff. The records of the two sites are different in a number of ways, however. At Site 1207 the presence of lamination in the C_{org}-rich units is clear evidence for dysoxic or anoxic deep-water conditions. Lamination is not present in the recovered, highly bioturbated C_{org}-rich units at Site 1213. This could indicate a slightly higher level of oxygenation of deep waters during deposition of the carbonaceous sediments, although conditions still must have been poorly oxygenated due to the high flux of organic matter. In fact, the exceptional preservation of organic compounds in the Site 1207 and 1213 lower Aptian samples indicates that conditions were highly dysaerobic at the time of deposition. The units at Site 1213 are more siliceous and radiolarian rich; however, this might be a result of the lack of recovery of the softer, less siliceous interbeds.

Using basement ages from Nakanishi et al. (1989), a paleodepositional depth track (based on normal crustal subsidence) from Thierstein (1979) for Site 306, and correcting for differences in the thickness of sediment between basement and the lower Aptian yields paleodepths of 1.3 km for Site 1207 on the Northern High and 2.8 km for Site 1213 on the Southern High. The true depths might have been slightly deeper given faster than normal subsidence rates, but the relative difference should be similar. These depths indicate remarkable shoaling of the CCD during OAE1a. Calcareous sediments are found directly underneath the organic-rich sediments at Site 1213, indicating that the CCD shoaled by at least 1.5 km during the event. The magnitude of the change of the CCD during OAE1a is a result of a combination of oxidation of a steady flux of organic matter over a fairly long time period (~1 m.y.) (Larson and Erba, 1999) and CO_2 outgassing (e.g., Arthur et al., 1985).

C_{org}-rich horizons of OAE1a age have been found in a number of other locations in the Pacific Ocean. These include Sites 305 on Shatsky Rise (location of Site 1211), 463 (MPM), and 866 (Resolution Guyot) (Sliter, 1989; Jenkyns, 1995). Of these, only Sites 463 and 866 have decent recovery, and both of these sites have a shallow-water influence: one is located in shallow-water carbonates (Site 866), and the other has a considerable fraction of material derived from shallow-water environments (Site 463). The only known record of OAE1a in the Atlantic Ocean, Site 641, is on the continental margin of Spain. Thus the new Shatsky Rise organic-rich units represent the most pelagic records outside of Tethys. For example, the original Selli Level in Italy is in a truly pelagic section (Coccioni et al., 1992).

The extremely high C_{org} contents of the Site 1207 and 1213 units reflect their pelagic depositional environment where dilution by clastic material was minimal. The only interval with a comparably high carbonaceous level derives from an algal mat horizon slightly above the OAE1a interval at Site 866 (Baudin et al., 1995). Maximum C_{org} values at levels that are correlative with the OAE are limited to a few Pacific Sites: 14.2 wt% at Site 866 (Jenkyns, 1995), 7.6 wt% at Site 463, and 9.3 wt% at Site 305 (Sliter, 1989) (Fig. F50). Onshore sections are much less enriched. The Selli Level in the Cismon Core from Italy contains 5 wt% C_{org} (Erba et al., 1999); and the Goguel Level in Southern France contains less than 3 wt% C_{org} (Bréhéret, 1988). C_{org}-rich lower Aptian horizons in the Santa Rosa Canyon of Mexico also contain less than 3 wt% (Bralower et al., 1999).

Early Aptian C_{org}-rich units that correlate to OAE1a have been found in a limited number of locations outside Tethys and are not as widely distributed as OAE2 (Schlanger et al., 1987). This has led to some uncertainty as to whether the OAE1a event was global in scale. Recovery of the early Aptian C_{org}-rich horizons at Sites 1207 and 1213 provides additional evidence that OAE1a was indeed a global event.

Several organic-rich levels were recovered below the lower Aptian at Site 1213. One of these levels in the upper Valanginian correlates to an anoxic event within the Tethys (Lini et al., 1992). Environments on Shatsky Rise during the deposition of this unit were not as dysoxic as during the early Aptian; organic carbon contents are considerably lower (2.5 wt%) than those of the lower Aptian horizons and the facies are clearly bioturbated. However, this is the first record of the Valanginian event outside the Tethyan region, supporting the contention that this was a widespread, even global, event that resulted in a positive $\delta^{13}C$ shift (Weissert and Lini, 1991).

There is some indirect evidence for the presence of other C_{org}-rich mid-Cretaceous levels in the unrecovered sections on Shatsky Rise. At Site 1207, a minor gamma ray peak at the Cenomanian/Turonian boundary and a subsidiary U peak signify either a thin organic-rich unit or an unconformity with an associated Fe-Mn hardground. This evidence is equivocal; however, gamma ray logs from both Sites 1207 and 1213 show background levels with a few insignificant increases throughout the Albian, suggesting that C_{org}-rich units are absent. Although the lack of recovery prohibits firm conclusions concerning the continuity of the section, the expanded nature of the Albian, especially at Site 1207 where it corresponds to 140 m of section, suggests that the sequence for most of this stage should be relatively complete. As such, the gamma ray data indicate that C_{org}-rich levels representing the Albian OAEs (OAE1b–1d) are not found on Shatsky Rise. On a regional scale, the only significant C_{org}-rich sediments (<9 wt% C_{org}) of Albian age are found within the upper Albian section (*Rotalipora appenninica* and *R. ticinenesis* Zones) at Site 465 on Hess Rise (Dean et al., 1981). Thus, the event that produced OAE1a appears to have had a more profound effect on the pelagic realm in the Pacific than did events of the Albian.

Learning from Chert on Shatsky Rise

Although chert was a significant hindrance to coring during Leg 198, it still provided significant information that fulfilled several leg objectives. The poorly recovered Berriasian to Santonian sedimentary section on Shatsky Rise is dominated by chert and associated porcellanite with minor amounts of ooze, chalk, claystone, and limestone. In the overlying Maastrichtian–Campanian interval, fewer chert horizons are found in soft nannofossil ooze. The dominant source of silica for the chert and porcellanite is thought to be radiolarians; no evidence for diatoms was found in the Cretaceous section on Shatsky Rise.

Despite poor recovery, the occurrence and character of chert and porcellanite at all Leg 198 sites show marked trends through the Cretaceous that provide important information on the nature of depositional environments on Shatsky Rise. Stratigraphic information can be obtained from FMS-sonic log data from Site 1207 and, more crudely, from drilling penetration rates at other sites. The FMS-sonic log from Hole 1207B clearly shows that chert layers have variable thickness and spacing through the stratigraphic column (Fig. F45). Changes in the spacing of chert layers also clearly affected penetration rates. These rates (Fig. F52) suggest that chert is concentrated in the upper Albian (*R. appenninica* to *R. ticinensis* Zones), near the Aptian/Albian boundary and around the lower OAE1a at Sites 1207, 1213, and 1214. Chert is also abundant in the lower Berriasian at Site 1213, and a minor peak is present in the lower Santonian at Sites 1207 and 1213. The Turonian–Coniacian interval at Site 1207 has a lower abundance of chert layers.

A more detailed record of chert occurrence was obtained from the Campanian–Maastrichtian section on the Southern High of Shatsky Rise. At Sites 1211 and 1212, the uppermost, scattered layer or nodules of chert are present in the middle part of the upper Maastrichtian (middle part of the *A. mayaorensis* foraminiferal Zone [KS31]). At Sites 1209 and 1210, the uppermost chert horizon is slightly older, occurring in the mid-Maastrichtian (*C. contusa/R.fructicosa* foraminiferal Zone [KS30]). At Site 1207 on the Northern High, the youngest chert was found in the mid-Campanian (nannofossil Zone CC20 corresponding to the middle part of the *G. ventricosa* foraminiferal Zone). The age of the shallowest chert level can be used to predict when Shatsky Rise cleared the equatorial divergence zone on its northward migration toward its current location. Thus, it appears that the Northern High was out the divergence zone about 9 m.y. earlier than the Southern High.

The color of the cherts and porcellanites is variable, ranging from very light yellow hues to black hues. A compilation of chert color for the Leg 198 sites, including data from Sites 305 and 306 (Larson, Moberly, et al., 1975), shows regional trends through time (Fig. F37). The various colors may indicate specific redox conditions; for instance, orange, red, and brown hues are indicative of deposition and diagenesis in oxidizing environments, whereas those with olive-green to black hues are indicative of more reducing conditions during deposition and burial. The color stratigraphy suggests that oxygenated conditions prevailed in the earliest Berriasian, in the late Aptian through early middle Albian, and from the late Cenomanian through the Maastrichtian. Reducing conditions within the sediment prevailed in the Berriasian through the early Aptian and in the late Albian to middle Cenomanian. Overall, similar trends were observed in all of the sites for coeval portions of the sequence, suggesting that the entire rise experienced generally similar redox conditions at bathyal depths. One possibility is that redox was a function of sedimentation rate, with higher sedimentation rates causing higher accumulation rates of organic matter.

Comparison of the color redox patterns to the inferred frequency of chert in the Cretaceous section on Shatsky Rise suggests that the higher frequency is associated with predominantly reducing conditions, at least in the Berriasian, around the OAE1a, and in the late Albian. This relationship indicates that higher siliceous production may have contributed to reducing conditions during deposition and diagenesis by increasing sedimentation rates.

Mid-Maastrichtian Event: Death on the Seafloor

An unusual record of the MME was observed in the sedimentary record at two sites on the Southern High of Shatsky Rise. At Sites 1209 and 1210, clusters of large *Inoceramus* prisms are seen in the cores for several meters (Fig. F24) but disappear abruptly. This disappearance is in the same

stratigraphic position in both holes, in the *Racemiguembelina fructicosa–Contusotruncana contusa* Zone at ~69 Ma. Furthermore, at Site 1211, *Inoceramus* prisms have been collected from core catcher samples and shells are recorded in Hole 47.2 (Fischer, Heezen, et al., 1971) within the same foraminiferal zone as at Sites 1209 and 1210. The significance of the short range of visible specimens in this open-ocean setting is not currently understood. However, the position of the event is similar to that of the *Inoceramus* extinction and the isotopic shifts that mark the MME at Site 305 and other deep sea locations (MacLeod, 1994; Frank and Arthur, 1999).

Growing evidence, however, suggests that this biotic event is distinctly diachronous in the Atlantic, Tethys, and Pacific Oceans. For example, the inoceramid extinction lies slightly higher in the Bottaccione Section (Gubbio, central Italy) within the overlying *Abathomphalus mayaroensis* Zone (Chauris et al., 1998). Moreover, the magnitude and direction of stable isotope changes are quite variable from place to place, possibly as a result of uncertainties in stratigraphic correlation or of true differences in deep-water properties. Benthic and planktonic data from Shatsky Rise will help to accurately characterize the changes in deep- and surface-water properties as well as the timing of this transition in the Pacific.

Close to the MME, the more specialized planktonic foraminifers start to decrease in diversity and more generalized groups increase, indicating a shift to less oligotrophic conditions, a trend that strongly accelerated near the end of the Maastrichtian (Premoli Silva and Sliter, 1999). This suggests changes in the structure of oceanic surface waters. Shore-based stable isotopic and foraminiferal assemblage studies will help us refine our understanding of the origin and implications of this climatic transition.

Multicore Record of the Cretaceous/Tertiary Boundary on Shatsky Rise

Although the K/T boundary was not a prime focus of investigation during Leg 198, a remarkable set of cores was taken across this critical interval. The K/T boundary was cored at four sites on the Southern High: Sites 1209, 1210, 1211 and 1212. Double and triple coring at these sites recovered a total of nine separate K/T records: three from 1211, and two each from Sites 1209, 1210, and 1212 (Fig. F53). The lithologic sequence in the K/T boundary interval is similar at all of these sites. At Sites 1209–1212, the boundary succession includes uppermost Maastrichtian (nannofossil Zone CC26) white to very pale orange, slightly indurated nannofossil ooze overlain by lowermost Paleocene (foraminiferal Zone Pα) grayish orange foraminiferal ooze (Fig. F53). The basal 8- to 12-cm-thick Paleocene layer grades into a 19- to 23-cm-thick white foraminiferal nannofossil chalk, then into a grayish-orange nannofossil ooze. The boundary between the uppermost Maastrichtian and the lowermost Paleocene is clearly bioturbated as shown by the irregular nature of the contact and the pale orange burrows that extend up to 10 cm into the white Maastrichtian ooze. The K/T boundary interval exhibits a strong magnetic susceptibility peak that allows detailed correlation among holes and sites.

The lithostratigraphy of the boundary succession is remarkably similar at all sites on Southern High, including Site 577 (near Site 1212) and to some extent Hole 47.2, although the latter section was badly disturbed by coring. The main difference between the sections is the degree of bioturbation, thickness of the bioturbated layer, and the thickness and color of the lowermost Paleocene foraminiferal ooze layer.

Preliminary biostratigraphy at all of the K/T boundary sites drilled on Leg 198 shows the well-established, abrupt change in nannofossil and planktonic foraminiferal assemblages across the

boundary (e.g., Luterbacher and Premoli Silva, 1964; Percival and Fischer, 1977; Thierstein, 1982; Monechi, 1985; Gerstel et al., 1986; Pospichal, 1991). The white nannofossil ooze yields diverse assemblages of the latest Maastrichtian *Abathomphalus mayaroensis* planktonic foraminiferal Zone and *Micula prinsii* nannofossil Zone (CC26). Sampling of the deepest sections of the burrows of Paleocene ooze within the uppermost Maastrichtian yields highly abundant, minute planktonic foraminiferal assemblages that are dominated by *Guembelitria* with rare *Hedbergella holmdelensis,* suggesting a possible Zone P0 age. The upper parts of the burrows contain foraminiferal assemblages dominated by *Guembelitria* with rare, small *Parvularugoglobigerina eugubina* that identifies the basal Paleocene (Pα) Zone, which is characterized by its unique populations of Cretaceous "survivors." Well-preserved planktonic foraminifers of Zone Pα dominate the lowermost 10 cm of the Paleocene (Fig. F23). In the overlying white foraminiferal nannofossil ooze horizon, the average size of the foraminiferal assemblage increases as the assemblages become increasingly dominated by *P. eugubina*.

Nannofossils in the basal Danian grayish orange ooze are limited to "disaster" taxa (calcispheres), survivor taxa, and reworked Cretaceous taxa. The lower part of the overlying white ooze unit is dominated by ultrafine micrite, calcispheres and the "survivor" coccolith taxa, including *Cyclagelosphaera reinhardtii* and *Markalius inversus*. Finally, the upper part of the white ooze unit contains fine micrite, small early species of the coccolith *Neobiscutum, C. reinhardtii,* and *M. inversus* (Fig. F23). This whole interval thus belongs to nannofossil Subzone CP1a. Comparable evolutionary trends in both nannoflora and planktonic foraminifers from Site 577 were described by Monechi (1985) and Gerstel et al. (1986).

A significant feature of the K/T boundaries recovered at Leg 198 sites is the widespread occurrence of light brown to amber spherules of up to 100–150 µm in diameter that are concentrated in the first few (2–3) cm of the basal Paleocene and in the shallower burrows into the uppermost Maastrichtian white nannofossil ooze. Spherules are rarely found in the overlying 30 cm of the basal Danian. These spherules show textures similar to the spherules composed of glauconite and magnetite that have been described by Smit and Romein (1985) from the K/T boundary in other locations and referred to as "microtektite-like" spherules.

The uppermost Maastrichtian planktonic foraminifers at all sites are characterized by a fair amount of etching and fragmentation. The amount of dissolution appears to be unrelated to paleodepth. The minute, thin-walled earliest Paleocene faunas, however, are well-preserved. This suggests that the lysocline and CCD over Shatsky Rise shoaled in the latest Maastrichtian, just prior to the K/T boundary, and deepened in the earliest Paleocene.

The K/T boundary sequence at Shatsky sites bears similarities to the record at other deep-sea sites. The boundary at Site 1049 in the western North Atlantic corresponds to the base of a graded spherule bed (ejecta fallout), capped by an orange-brown limonitic layer. This layer is overlain by (1) a dark, burrow-mottled clay that contains planktonic foraminifers diagnostic of Zone Pα and (2) a 5- to 15-cm-thick white foraminiferal nannofossil ooze that also correlates to Pα. The same white unit is found in varying degrees of lithification directly above the boundary at less complete sections including DSDP Site 536 (Gulf of Mexico), and ODP Sites 999 and 1001 in the Caribbean. The ultrafine micrite in this oceanwide white layer may be related to the collapse of the marine biosphere that would have caused a substantial drop in the CCD (e.g., Caldeira and Rampino, 1990).

The K/T boundaries on Shatsky Rise have been mixed by bioturbation in the interval after the boundary. Nevertheless, the substantial thickness of the uppermost Maastrichtian *M. prinsii* (CC26) Zone and the lowermost Danian *P. eugubina* (Pα) Zones indicates that the K/T boundary is paleontologically complete. The Pα Zone is either unrecovered or poorly preserved in most other

deep sea sites. Thus the sections represent some of the best-preserved and least-disrupted deep-sea records of this major extinction event as well as the subsequent biotic radiation.

Rhythmic Record of Paleogene Deep-Ocean Circulation

Sediments on Shatsky Rise show that deep ocean circulation fluctuated in a highly regular fashion in the Paleogene. The record from Sites 1209, 1210, 1211, and 1212 is strongly cyclic as a result of regular changes in the properties of the deep waters bathing Shatsky Rise. Decimeter-scale alternations in color that correspond to minor changes in clay and carbonate content are relatively faint in cores but striking in color reflectance records. Magnetic susceptibility records also show these fluctuations clearly (Fig. F46). The cycles occur in bundles that can be easily correlated between sites. The cycles are likely produced by minor changes in the dissolution of carbonate in the deep ocean. Variation in the flux of eolian material may have also played a minor role.

Preliminary biostratigraphy suggests that the frequency of cycles corresponds to orbital periodicities. The predominant frequencies appear to be short- (100 k.y.) and long- (400 k.y.) period eccentricity. However, the nature of cycles varies among sites and through time in subtle ways. The amplitude of the cycles does not appear to correlate well with paleodepth. In fact, the two shallowest sites, Sites 1209 and 1210, show the highest amplitude cycles for significant periods of time. Magnetic susceptibility and color reflectance data indicate that the two shallowest sites with the most expanded Paleogene records also have the most cycles. This suggests that the two deeper sites, Sites 1211 and 1212, have a number of condensed intervals and/or diastems.

The lack of a clear correlation of cycle amplitude with depth suggests that the cycles are not the result of a simple dissolutional scenario in which deep waters were more corrosive. If this relationship held, the deepest site should have the largest amplitude fluctuations between the dissolved and less dissolved end-members. Instead, the cycles may represent repeated shoaling and deepening of the boundary between two water masses, with the boundary lying close to the depths of the shallower two sites (Sites 1209 and 1210) at some times and in deeper waters close to Site 1211 at others. This situation would produce higher-amplitude chemical and physical fluctuations (i.e., corrosiveness, and oxygenation) at depths close to the water mass boundaries than in shallower and deeper water where conditions were less variable. Alternatively, the cycles might represent variation in surface-water productivity that produced subtle changes in chemical composition. For instance, the shallower sites might have had more variable productivity for a number of reasons. Additional compositional and isotopic data are required to shed further light on the origin of Paleogene cycles.

At this preliminary stage, the cyclic Paleogene record has helped considerably in the construction of composite sections. These composites show that multiple coring at the Southern High sites has completely sampled the Paleogene sedimentary section (see “Physical Properties, Downhole Measurements, and Core Logging” in “Specialty Syntheses”). Furthermore, with the exception of a gap close to the Oligocene/Miocene boundary, the combination of Sites 1209, 1210, 1211, and 1212 of Leg 198 has recovered a composite section from the Pleistocene down to below the K/T boundary.

A Depth Transect at the Late Paleocene Thermal Maximum

Sediments cored on Shatsky Rise show evidence of a strong deep-ocean response to warming in the LPTM. The LPTM interval was cored at four sites on the Southern High (Sites 1209, 1210, 1211, and 1212). Double and triple coring at these sites recovered a total of 10 separate LPTM records: three each from Sites 1209 and 1211, and two each from Sites 1210 and 1212 (Fig. F54). The Paleocene–

Eocene boundary interval was also recovered at Site 1208 on the Central High. The range of present depths, from 2387 m at Site 1209 to 2907 m at Site 1211 provide a 520-m depth transect to observe the sedimentary response to this abrupt warming event as a function of depth. Although the Site 1208 sequence is highly condensed and it is not currently possible to determine whether the LPTM is present, some inferences can be made from this section that extend the transect some 440 m to 960 m.

At the Southern High sites, the LPTM corresponds to an 8- to 23-cm-thick layer of clayey nannofossil ooze with a sharp base and a gradational upper contact. The clay-rich layer is generally yellowish brown in color and is often bioturbated into the underlying sediment. At several sites an extremely thin (1 mm) dark brown clay seam lies at the base of the LPTM. Carbonate contents have been measured in detail across the LPTM at Site 1210. These data show a decrease from 96 to 89 wt% $CaCO_3$ at the base of the event, a decrease that would involve a substantial increase in dissolution. Color reflectance and magnetic susceptibility data (Figs. F39, F46) allow detailed correlation between holes and sites in this time interval.

Preliminary biostratigraphic investigations show that the event lies toward the top of nannofossil Zone CP8 and planktonic foraminiferal Zone P5. At several sites, rare specimens of *Gavelinella beccariiformis,* a benthic foraminiferal species that goes extinct at the onset of the LPTM (i.e., Thomas, 1990) were found below the event. The abrupt decrease in the nannofossil *Fasciculithus* that occurs just above the LPTM in other sections (Bralower et al., 1995; Aubry et al., 1996; Monechi et al., 2000) lies near the top of the clay-rich layer. The stratigraphic level of the top of the LPTM is currently undefined, but the FO of the nannofossil *Discoaster diastypus* and the LO of the plantkonic foraminifer *Morozovella velascoensis* indicate that the record in all sections is apparently complete, with the exception of Hole 1211B. This biostratigraphy shows that the LPTM interval at Sites 1209, 1210, and 1212 are condensed compared to continental margin records from the Atlantic and Tethys (e.g., Kennett and Stott, 1991; Norris and Röhl, 1999) but somewhat expanded compared to other deep-sea sites such as Site 865 on Allison Guyot (Bralower et al., 1995) and Site 527 on Walvis Ridge (Thomas et al., 1999). At Site 1211, the LPTM interval was recovered across the break between two sections in Holes 1211A and 1211C. The clay-rich bed is more prominent and condensed than in the other records (Fig. F54). In Hole 1211B, the basal clay seam appears to be present, but the occurrence of *D. diastypus* 1–2 cm above this level and the concurrent decline in the abundance of *Fasciculithus* strongly suggests an unconformity. The LPTM in both holes at Site 1212 appears complete; however, the presence of *Globanomalina pseudomenardii* suggests a slight unconformity immediately below the event.

The LPTM interval at all of the sites contains a clear record of nannofossil and planktonic foraminiferal assemblage transformation at this time of major environmental upheaval (Fig. F22). One of the dominant nannolith genera, *Fasciculithus*, is replaced by *Zygrhablithus bijugatus,* a nannolith that is often a highly abundant or dominant component of Eocene assemblages. The genus *Discoaster* is highly abundant, likely as a result of warming or increased oligotrophy (Bralower, unpubl. data). Calcispheres, possible resting cysts produced by calcareous dinoflagellates at times of environmental instability, are also found. Planktonic foraminiferal assemblages within the clay-rich interval contain an ephemeral group of ecophenotypes or short-lived species of the genera *Acarinina* and *Morozovella* (Kelly et al., 1996). These "excursion" taxa include both end-member as well as transitional morphologies.

The depth transect strategy of Leg 198 was specifically designed to address the response of the ocean to the greenhouse forcing mechanism proposed for the LPTM. This warming is generally

thought to have resulted from input of a massive burst of methane into the ocean-atmosphere system (e.g., Dickens et al., 1997). Methane is the only agent that can explain both the warming and the rate of carbon isotopic change at the onset of the excursion. The oceanic response to this methane input is predictable but currently untested (e.g., Dickens, 2000). Regardless of how the transfer to the ocean took place, oxidation of methane would generate CO_2, which would lower the dissolved CO_3^{2-} content of seawater and cause a dramatic shoaling in the depth to the lysocline and CCD. This response should be recorded in changes in carbonate content and preservation in all marine sections. Over a depth range, shallow sections should show less change in dissolution and carbonate content than deep sections.

Nannofossil preservation below the event in all of the Southern High sites is moderate indicating that the sites were located in the broad range of the lysocline. All sites show a general deterioration in preservation at the onset of the event and abundant 10- to 20-µm-sized, needle-shaped calcite crystals that are thought to have been derived from precipitation of dissolved carbonate are found in smear slides. The detailed response of fossil preservation is complex and different from site to site, as is the absolute change in carbonate content as indicated by reflectance data.

The general changes in lithology suggest a transition from paleodepths in the shallower sites that were less sensitive to changes in carbonate solubility in the deep ocean (Sites 1209, 1210, 1212) to those that were at depth ranges highly sensitive to changes across the LPTM (Sites 1208 and 1211) (Fig. F54). The decrease in carbonate content and deterioration in nannofossil preservation are evidence for an abrupt rise in the level of the CCD and lysocline during the LPTM. Determination of the magnitude of this change awaits postcruise analysis; however, the preliminary lithostratigraphic and biostratigraphic results from the LPTM interval in the Shatsky Rise depth transect are highly consistent and thus support the expected ocean response to massive methane input.

Eocene–Oligocene Transition in the Tropical Pacific Ocean

Sediments recording the response of the tropical Pacific ocean to cooling in the Eocene–Oligocene transition were recovered across a large depth range on Shatsky Rise. The Eocene–Oligocene transition was cored at Sites 1208, 1209, 1210, and 1211 in a total of nine holes. The boundary between the two epochs is identified by the LO of the planktonic foraminiferal genus *Hantkenina* at 33.7 Ma. Preliminary nannofossil and planktonic foraminiferal biostratigraphy suggests that the boundary interval is complete. At the Southern High sites (Sites 1209, 1210, and 1211), the transition records a gradual, subtle but distinctive change, over a 4- to 7.5-m interval in the uppermost Eocene and lowermost Oligocene, from light brown to tan nannofossil ooze with clay to a light gray to white nannofossil ooze (Fig. F32). This transition is associated with marked changes in color reflectance data (Fig. F28) but fairly minor changes in percent carbonate from about 90 to 96 wt% (in Hole 1210A). Superimposed on the gradual change in color and increase in carbonate contents are marked cycles that appear to represent orbital rhythms (see "Physical Properties, Downhole Measurements, and Core Logging" in "Specialty Syntheses").

The lithologic record of the Eocene–Oligocene transition at Site 1208 on the Central Rise is markedly different from the Southern High sites. A lithologic transition from a dark brown zeolitic claystone with extremely low carbonate content to a gray-orange nannofossil ooze was observed in an identical stratigraphic position to the gradual changes observed on the Southern High. However, the Site 1208 transition is far more condensed than the other records, occurring over an interval of

1–2 cm. The Eocene/Oligocene boundary is associated with a marked increase in sedimentation rates at all of the sites.

In general, the lithologic change in all of the sites is accompanied by a general improvement in microfossil preservation; late Eocene nannofossils in most of the sections show a high degree of etching, whereas early Oligocene assemblages show less dissolution and slightly more overgrowth. Planktonic foraminifers are rare and badly fragmented in the upper Eocene, but preservation improves and abundance increases in the Oligocene. At Site 1208, the deepest site in the transect that contains the transition interval, planktonic foraminifers are largely absent from the sequence. The benthic foraminifer *Nuttallides truempyi,* the LO of which shortly precedes the Eocene/Oligocene boundary, is found below the color transition. Sparse nannofossils below the boundary are extremely etched.

The age model for the Eocene–Oligocene transition at all of the Leg 198 sites is currently preliminary, and thus the exact correlation of the change in carbonate content with the series boundary and the sharp Oi-1 cooling event (33.15–33.5 Ma) (e.g., Miller et al., 1991; Zachos et al., 1996) has yet to be determined. However, the preliminary data show that the prominent change in lithologic signature occurs just before or within the time of cooling. Moreover, because the exact location of the Oi-1 event is currently unknown, we have yet to determine whether orbital cycles can be detected within this event.

The distinctive color change in all of the Leg 198 records reflects a pronounced deepening in the CCD in the Eocene–Oligocene transition. In the latest Eocene, the CCD on Shatsky Rise was between the paleodepths of Sites 1208 and 1211, probably closer to the former site based on the sporadic occurrence of nannofossils. After the event, the depth was substantially greater than Site 1208. This significant change is observed in other ocean basins (e.g., Zachos et al., 1996) and possibly reflects an increase in mechanical and chemical weathering rates on continents associated with cooling. Alternatively, deepening of the CCD may be associated with an intensification of deep-ocean circulation and a consequent decrease in the age of deep waters. The magnitude of the change in the transition interval as shown by color reflectance data varies as a function of depth (see Fig. F28). This is consistent with the deepening of both the lysocline and CCD.

Our current understanding of the changes in climate and circulation in the Eocene–Oligocene transition is based almost entirely on records from the mid- and high-latitude Atlantic and Indian Oceans (Miller et al., 1991; Zachos et al., 1996). Changes observed across this transition in the tropical-subtropical Pacific from the Shatsky Rise depth transect have the potential to add another dimension to this understanding.

Unique Neogene Section

A surprising side note to the major Cretaceous and Paleogene objectives on Leg 198 was the recovery of two expanded late Neogene sections on the Northern High of Shatsky Rise at Site 1207 and the Central High at Site 1208. These sections could be important from both stratigraphic and paleoceanographic perspectives. The two sections have apparently complete upper middle Miocene (~12 Ma) to Holocene sections that are composed of nannofossil ooze and nannofossil clay. Both sections have a mixture of nannofossils and significant amounts of diatoms (10%–40% at Site 1207; 5%–20% at Site 1208), and minor amounts of foraminifers, radiolarians, and silicoflagellates. Numerous discrete ash horizons are found at both sites, predominantly in the Pliocene–Pleistocene interval.

Sedimentation rates at Site 1207 average 18.4 m/m.y. from the Holocene to latest Miocene. Rates at Site 1208 range between 22 and 42 m/m.y. from the Holocene to the early late Miocene (Fig. F42). These rates are far higher than typical pelagic sedimentation. The detrital clay and silt component of the sediment may have been delivered by eolian transport. However, a large component of the sediment could have been delivered by sediment drift.

Marked cyclic variations are observed in MST and color reflectance data throughout the upper Miocene to Holocene section at both sites. These variations are expressed as strong lithologic cycles that have frequencies at the decimeter to meter scale. These cycles are marked by relatively subtle to sharp color changes that are associated with variations in the amount of clay, pyrite, and different biogenic particles. The darker interbeds tend to have more abundant diatoms and clay, more dissolved nannofossil assemblages, and more abundant pyrite. The lighter interbeds contain fewer diatoms, less clay, and a better-preserved nannofossil assemblage. The cycles might represent variations in carbonate dissolution as a result of changes in the depth of the lysocline, fluctuations in biosiliceous production, or a combination of the two. Preliminary biostratigraphy indicates that these variations represent eccentricity and obliquity cycles. The section recovered at Site 1208 contains an extraordinary expanded magnetic stratigraphy extending back to Chron C5An in the late middle Miocene (Fig. F55). This section also shows great promise for establishing a paleointensity record for the North Pacific.

The Site 1207 and particularly the Site 1208 Neogene section has significant potential for establishing a high-resolution biochronology and astrochronology back to at least the late Miocene. This potential derives from the combination of siliceous and calcareous microfossil biostratigraphy, high-resolution magnetostratigraphy, a marked orbital cyclicity, numerous ash layers with potential for radiometric dating, and a potential magnetic paleointensity record. With high sedimentation rates and foraminifers found throughout the section, the sites also have significant potential for reconstructing climate and paleoceanography of the northwestern Pacific over the last 12 m.y.

Not-Quite Basement from Shatsky Rise

During Leg 198, we cored the first igneous rocks from Shatsky Rise, probing the top of the igneous pile. Coring in Hole 1213B terminated in mafic igneous rocks on the flanks of southern Shatsky Rise. In all, 46.4 m of igneous section was drilled, with 33.4 m of recovered core (72%). Six cores, 198-1213B-28R through 33R recovered mostly massive diabase and minor basalt from three subunits (IVA to IVC), with each subunit thought to be a separate sill. The igneous rocks are predominantly hypocrystalline, fine-grained diabase (97.6%) with a small amount of sparsely phyric, aphanitic basalt (2.0%) at contacts. The diabase groundmass consists mainly of euhedral to subhedral plagioclase and intervening subhedral pyroxene and olivine, with minor glass. Alteration in the igneous section ranges from minor to moderate. Plagioclase and pyroxene crystals are locally altered to clay, and in thin section, glassy groundmass has been ubiquitously devitrified and/or altered to clay minerals. Basalt occurs at subunit "chilled" contacts, symmetrically disposed around fragments of metasediment that mark the subunit boundaries. From the chilled contacts, the basalt grades toward more coarse-grained diabase in the unit centers, where the groundmass approaches medium grained.

The sills must be early Berriasian age or younger, since this is the age of the host sediment. Paleomagnetic data show two subunits that have fairly steep positive magnetic inclinations, whereas the third, basal subunit has a lower, negative inclination, implying both normal and reversed

magnetic polarities are recorded in the igneous section. This mixture indicates that the sills must have formed either before or after the Cretaceous Long Normal Superchron (i.e., the Cretaceous Quiet Period, 121–83 Ma). On the seismic profile along which Hole 1213B was drilled, the seismic "basement" has an odd character that may be related to the presence of intrusive, rather than extrusive, igneous rock at the sediment-igneous rock contact. The "basement" reflector, that being the deepest continuous seismic horizon, is weaker than elsewhere on Shatsky Rise, and other, stronger reflectors occur beneath it. These deeper reflectors were not considered "basement" because they are not continuous all along the line, as is the weaker, shallower horizon. The cored section suggests that the weak "basement" horizon denotes the top of the sills, whereas the deeper reflectors may be the top of the extrusive lava pile.

Revised Geologic History of Shatsky Rise

The stratigraphy of sites drilled on the Southern, Central, and Northern Highs during Leg 198 can be integrated to interpret the geologic history of Shatsky Rise from its formation as a LIP in the Late Jurassic and Early Cretaceous, through multiple depositional episodes and different sedimentological regimes separated by short and sometimes quite lengthy hiatuses (Fig. F42). These gaps were produced by erosion and dissolution, but distinguishing between these two processes can be difficult. Comparison of the stratigraphy of the cored sections of sites on the Northern and Central Highs shows similarities and differences with the sequence cored on the Southern High. This suggests that a combination of local and regional-scale processes controlled sedimentation. The following history is compiled from the stratigraphic data gathered during Leg 198. Although we have cored a complete record from the Southern High, drilling was terminated in the mid-Cretaceous on the other highs.

Although Leg 198 did not core "true" extrusive basement, igneous rocks intruded soon after the formation of extrusive basement were recovered at Site 1213. These sills are widespread above basement in the Pacific (e.g., Larson, Schlanger, et al., 1981; Plank, Ludden, Escutia et al., 2000) and argue for a multistage origin for the igneous foundations of Shatsky Rise. The latest Jurassic and Cretaceous history of the rise was dominated by fairly continuous deposition on the Southern and Northern Highs (Fig. F42). Unconformities found in more than one location suggest an interval of erosion on the Southern High during much of the latest Hauterivian and Barremian. The late Cenomanian to Santonian interval was also characterized by sporadic sedimentation, as noted by Sliter (1992) (Fig. F56), and widespread erosion on the Central and Southern Highs, at least in most locations (Sites 1208, 1212, and 1214). The deepest site in the depth transect (Site 1213) may have also rested below the CCD (e.g., Thierstein, 1979). The sequence on the Northern High appears to be complete in this interval. Continuous deposition resumed in the shallower sites in the Campanian and Maastrichtian whereas dissolution likely continued in deeper locations; an unconformity above the upper Campanian at Sites 1207 and 1208 was likely caused by a regional erosional episode at that time or in the early Cenozoic.

Deposition in the early Paleogene was nearly continuous at the shallow sites of the Southern High (Sites 1209–1212), but even at these sites, a lengthy hiatus in the later part of the Paleogene continued into the early Miocene in most locations. The onset of this hiatus lies in the middle Eocene at Site 1212 and in the Oligocene at the other shallower sites. At the shallower sites, this hiatus was likely a result of removal of sediment by erosion during the late Oligocene and early Miocene. Very slow sedimentation characterized the late early and early middle Miocene (except at

Sites 1213 and 1214 where no sediment from this interval was recovered), and the rate of sedimentation increased through the rest of the Neogene at most locations. Sites on the Northern and Central Highs lay in a different oceanographic regime in the late Neogene with a significant biosiliceous sediment component as well as clastic material concentrated into sediment drifts. Continuous sedimentation on the deep rise (Sites 1213 and 1214) began again in the early Pliocene.

Like other open-ocean plateaus and rises, Shatsky Rise shows many aspects of stratigraphy and sedimentation that are different from other open-ocean, abyssal settings. Open-ocean plateaus and rises are prone to erosion, and sedimentation rates are not as high as areas along the continental margins. Thus, their sedimentary sections are not as thick, and older deposits often rest at shallow burial depths. This has important implications for fossil preservation and the fidelity of paleoceanographic proxies. Because open-ocean deposits tend to be mostly biogenic and are less complex sedimentologically, their geologic record is often easier to interpret than in areas along continental margins. Vertical changes in physical and chemical oceanography can be determined using depth transects down the flanks of the rises. The cycles recovered on Shatsky Rise are a good example. Leg 198 has proven that oceanic plateaus hold some of the best records for investigating climate change through extended intervals of geologic time, particularly based on a depth transect approach.

OPERATIONS

Leg 198 officially began at 1100 hr on 27 August 2001 with passage of the first line ashore in Yokohama, Japan, ending Leg 197 approximately 19 hr early. At 0930 hr on 31 August, after four days of port call activities, the last line was released and the ship maneuvered into the harbor.

Transit from Yokohama to Site 1207

The transit to the first site was initially slowed by the presence of Typhoon Wutip, which was forecast to cross over Site 1207 about the same time as our full-speed arrival projection. To maintain a safe distance from the storm, we kept the correct course but at reduced speed for the first several days of the transit. As the typhoon increased speed and began moving to the northeast of the site, we increased our speed accordingly. Overall, the 1158-nmi, 5.2-day transit was accomplished at an average speed of 9.2 knots (kt). Upon arriving at the coordinates for the site, the thrusters and hydrophones were lowered at 1730 hr on 5 September, followed by deployment of a positioning beacon.

Site 1207

Hole 1207A

Once the vessel settled on location, an APC/XCB/motor-driven core barrel (MDCB) outer barrel assembly was assembled and the MDCB system was deck tested prior to deployment of the APC. After two unsuccessful attempts at obtaining a mudline core, a 4.82-m core was retrieved at 1225 hr on 6 September, initiating Hole 1207A. With the bit positioned at a depth of 3107 meters below rig floor (mbrf), the mudline core indicated a seafloor depth of 3111.7 mbrf, or 3000.7 meters below sea level (mbsl).

Piston coring advanced to 181.8 mbsf, with recovery averaging 103%. Cores 3H-18H were oriented. The advance-by-recovery technique was used for Cores 19H and 20H. Piston coring was terminated when these two successive cores failed to fully stroke, impeded by chert layers. We then switched to the XCB system.

The first XCB core (Core 21X) was advanced 6.7 m, with good recovery (101%) until encountering a chert layer, which destroyed a soft formation XCB cutting shoe. A second XCB core barrel was deployed, equipped with a hard formation cutting shoe; however, only minimal advancement (0.1 m) was achieved after 1 hr of rotating time, no recovery, and the destruction of the hard formation shoe. An XCB center bit was then deployed to drill through the chert, advancing to a depth of 197.9 mbsf. Three successive cores were then cut (Cores 23X through 25X); the first two recovered 100% and 99%, respectively. Core 25X advanced only 2.0 m in 75 min rotating time with no recovery. The XCB center bit was deployed for a second time to drill through the chert. Another XCB core was attempted; however, Core 26X advanced only 2.0 m, recovering only a few chert fragments (5% recovery). The center bit was deployed for a third time to drill through a chert layer to a depth of 237.3 mbsf. Core 27X advanced 6.4 m recovering a few pieces of chert (1% recovery). The center bit was deployed for a fourth time to clean up the hole and hopefully clear any remnant carbide cutters and debris from the previously used XCB cutting shoe. Prior to recovering the center bit, a 30-barrel (bbl) mud sweep was pumped to aid in flushing any debris from the hole.

We then switched to the MDCB system in attempt to increase recovery. Upon retrieval of MDCB Core 28N (5% recovery), drilling personnel observed that the core barrel had been heavily scoured. In addition to the scouring on the core barrel, the crown of the diamond bit was severely damaged. These observations suggested that either the MDCB bit had been in contact with a primary bit cone or that there was debris in the hole. Because of the doubt about the condition of the primary bit and hole, additional MDCB coring was suspended. A final XCB core was attempted with only 0.2 m advanced in 35 min. With no recovery in this core and concerns about bit and hole conditions, we decided to terminate coring in Hole 1207A at 256.6 mbsf in favor of RCB coring in Hole 1207B. Overall, the XCB was deployed for eight cores, with an average recovery of 71.1%. The drill string was retrieved, clearing the rotary table at 0015 hr on 9 September, ending Hole 1207A.

Hole 1207B

After retrieving the drill string, an RCB bottom-hole assembly (BHA) with a center bit assembly was deployed, and Hole 1207B was spudded at 1115 hr on 9 September. Approximately 4.25 hr was spent drilling the hole down to a depth of 157.0 mbsf and recovering the RCB center bit assembly. An RCB core barrel was deployed, and RCB coring advanced to a depth of 622.8 mbsf, taking 49 RCB cores. As anticipated, recovery was poor through an interval of closely spaced chert layers interbedded with ooze. Coring parameters were varied continuously in an attempt to boost recovery. In addition, several core catcher configurations were also used, including flapper core catchers. Beginning with Core 40R, a combination of flapper core catcher and no core liner was used to minimize or eliminate sources of potential jamming. Although somewhat unorthodox for coring in sedimentary strata, recovery did improve over the last 96.3 m. Improved recovery also coincided with increased lithification of the interbedded carbonate layers, so it is difficult to attribute improved recovery solely to coring without liners. Overall, recovery in Hole 1207B averaged 12.9%.

Coring was terminated when the depth objective was attained, and the hole was swept with 40 bbl of drilling mud, followed by a wiper trip to 159.9 mbsf. No overpull or drag was noted. During the

return trip to bottom, 40 m of soft fill was noted and circulated out of the hole. Another 40-bbl mud sweep was conducted, and the bit was released. The hole was then displaced with 217 bbl of logging mud, and the pipe was tripped back and positioned at 126.4 mbsf in preparation for logging.

The first logging run was made with the triple combo tool suite (see "Physical Properties, Downhole Measurements, and Core Logging" in "Specialty Syntheses" for details on the individual sensors on the logging tools), which was deployed to a depth of ~621 mbsf, or within 1.5 m of total depth. A second pass with this tool suite failed to pass ~379 mbsf.

The second logging run included two passes with the FMS-sonic tool string. Both passes with this tool suite were also halted at a depth of ~379 mbsf. The third and final logging run was made with the geologic high-resolution magnetic tool (GHMT) tool suite and reached a depth of ~367 mbsf.

After completion of the logging operations, the drill string was retrieved, clearing the seafloor at 1715 hr on 13 September, ending Site 1207. Upon recovery of the beacon and retraction of the thrusters and hydrophones, the ship began the transit to Site 1208.

Transit from Site 1207 to Site 1208

The 242-nmi transit to Site 1208 was made in 22.5 hr at an average speed of 10.8 kt. Upon arrival at the site coordinates, the ship's crew commenced lowering thrusters and hydrophones, and the ship was switched over to dynamic positioning (DP) mode, initiating operations at Site 1208 at 2315 hr on 14 September.

Site 1208

Hole 1208A

After deploying an operational beacon, an APC/XCB was assembled and lowered close to the seafloor. After one unsuccessful attempt at obtaining a mudline core, a 4.75-m core was retrieved at 0920 hr on 15 September, initiating Hole 1208A. The recovery of the mudline core indicates a seafloor depth of 3356.8 mbrf, or 3345.7 mbsl.

Piston coring advanced to 185.2 mbsf, with recovery averaging 105.3%. Cores 3H through 20H were oriented. Attempted retrieval of Core 20H resulted in overpull of ~75 kilopounds (kips), which required drilling over with the primary bit to free the core. We continued coring with the XCB, taking 22 cores (Cores 21X through 42X), extending the hole to 392.3 mbsf. Average recovery for the XCB interval was 73.5%. At Core 42X, only 0.25 m of chert was recovered; hence, the hole was terminated. The drill string was retrieved, clearing the rotary table at 1330 hr on 17 on September, ending drilling at Site 1208. After recovery of the beacon and retraction of the thrusters and hydrophones, the ship began the transit to Site 1209.

Transit from Site 1208 to Site 1209

The 210-nmi transit to Site 1209 was made in 18.4 hr at an average speed of 11.4 kt. Upon arriving on site, the thrusters and hydrophones were lowered, and the ship was switched over to DP mode, initiating Site 1209 at 0755 hr on 18 September.

Site 1209

Hole 1209A

An APC/XCB BHA was assembled, and the bit was positioned above the seafloor at 2397.0 mbrf. Hole 1209A was officially spudded at 1405 hr on 18 September, recovering 8.21 m, which established a seafloor depth of 2398.3 mbrf, or 2387.2 mbsl. APC coring continued through Core 26H to a depth of 245.7 mbsf. An incomplete stroke on Core 26H led to abandoning APC coring in favor of using the XCB. Recovery with the APC averaged 101.9%. Cores 4H through 26H were oriented. Coring with the XCB continued through Core 198-12089-28X to a depth of 259.6 mbsf. Coring was terminated after 30 min of rotating time on a hard layer, presumably chert, with no advancement. The drill string was tripped up, clearing the seafloor at 1335 hr on 19 September, officially ending drilling at Hole 1209A.

Hole 1209B

After offsetting the drill ship 15 m north, the drill string was spaced out with the bit placed 3.0 m higher than the spudding depth of Hole 1209A. Hole 1209B was spudded at 1454 hr on 19 September. Recovery on the first core measured 5.16 m, yielding a seafloor depth of 2398.4 mbrf, or 2387.4 mbsl. APC coring advanced to a depth of 297.6 mbsf through Core 32H with 98.2% recovery. Cores 4H through 32H were oriented, and Adara temperature shoe deployments were made on Cores 6H, 8H, 10H, and 12H. Three of the Adara tool measurements were good quality, but the tool deployed with Core 6H failed. Core 32H was not a complete piston stroke; hence, an XCB center bit was deployed to drill through the presumed chert layer. With 1.5 hr of rotating time and only 0.4 m advancement, we decided to terminate coring in Hole 1209B. While attempting to recover the XCB center bit, we discovered that a sub on the pulling tool had backed off. In addition, the forward wireline was damaged, which required 150 m of line to be removed. While effecting repairs, the aft wireline was used in an attempt to fish the core stub of the pulling tool. However, after two unsuccessful attempts, we had to trip the drill string back to the ship, clearing the rig floor at 0710 hr on 21 September and ending drilling at Hole 1209B.

Hole 1209C

The ship was offset 15 m east of Hole 1209A, and Hole 1209C was spudded at 1155 hr on 21 September. The hole was drilled to a depth of 98.0 mbsf, and then APC coring was initiated, continuing to a depth of 251.5 mbsf. At this depth, Core 17H contacted chert after stroking ahead only 1.5 m. An XCB center bit was deployed, drilling ahead to 252.5 mbsf. APC coring resumed (Cores 198-1209C-18H and 19H), progressing to 264.9 mbsf before encountering another chert layer. The XCB center bit was used to drill ahead to a depth of 268.4 mbsf. The next APC core barrel (Core 20H) failed to fully stroke, and shear pins in the overshot connecting the nonmagnetic sinker bars failed. This barrel was recovered after a second wireline run, and core orientation activities were suspended to avoid further complications with the nonmagnetic components. APC coring continued with Cores 21H and 22H to 296.9 mbsf, where a chert layer impeded progress. The XCB center bit was deployed and used to advance the hole through chert to 299.7 mbsf. While attempting to shoot APC Core 198-1209C-23H, the pins failed to shear and the barrel did not penetrate into the formation. Upon recovery, this barrel was inspected and seals were changed to ensure that the barrel was functioning correctly. It was redeployed, but the pins did not shear again. We then switched to

the XCB to determine if the problem was related to the APC barrel or the BHA. XCB Core 23X was advanced to 307.5 mbsf; however, despite latching properly, the barrel was recovered empty. A final APC core was attempted, but the APC barrel could not be landed correctly. Convinced that there was a mechanical problem with the bit and/or lockable float valve (LFV), coring was suspended, and the drill string was retrieved. Total recovery for Hole 1209C was 99.2%, with APC recovery averaging 103%.

At 0425 hr on 23 September, the pipe cleared the rotary table on the rig floor, ending operations at Site 1209. A subsequent inspection of the coring assembly showed that the primary bit was heavily damaged on the inner row cutters and the flapper hinge pin in the LFV was broken. Chert was found behind the flapper, likely preventing it from fully opening when the core barrels attempted to pass through. This resulted in overloading the flapper hinge, leading to the failure.

Transit from Site 1209 to Site 1210

The 29-nmi transit to Site 1210 required just 3.25 hr, at an average speed of 8.9 kt. At 0750 hr on 23 September, the ship was switched over to DP mode, initiating operations at Site 1210.

Site 1210

Hole 1210A

An APC/XCB BHA was assembled and run to near the seafloor. With the bit positioned at 2581.0 mbrf, a mudline core was recovered at 1358 hr on 23 September 5.90 m of sediment, indicating a seafloor depth of 2584.6 mbrf, or 2573.5 mbsl. APC coring continued to a depth of 233.9 mbsf without incident. Cores 4H through 26H were oriented. An incomplete stroke on Core 26H required deploying a center bit to drill through the ~1-m chert layer. APC Core 27H was deployed, but was also an incomplete stroke, resulting in a decision to terminate the hole at a depth of 242.4 mbsf. Recovery for APC coring in Hole 1210A averaged 103.3%. The drill string was tripped up to the seafloor at the pipe trip and then continued with the bit clearing the seafloor at 1415 hr on 24 September, ending drilling at Hole 1210A.

Hole 1210B

The ship was offset 15 m to the north, and the bit was positioned 3 m deeper to provide stratigraphic overlap with Hole 1210A. Hole 1210B was spudded at 1645 hr on 24 September, recovering a 9.2-m APC core, which indicated a seafloor depth of 2584.3 mbrf, or 2573.2 mbsl. APC coring advanced the hole to 267.9 mbsf. Cores 4H through 27H were oriented. An incomplete stroke on Core 29H resulted in deployment of the XCB center bit to drill through a chert layer, followed by the taking of another piston core. This technique of drilling through chert layers when encountered (a total of 11.5 m was drilled) and then redeploying the APC to core between layers continued for 13 cores to a depth of 377.0 mbsf. Because of the diminishing core quality of a few of the last cores and the time being expended to drill through the chert layers, we terminated coring after Core 42H. APC coring recovery averaged 103.0% in Hole 1210B. The drill string was retrieved and the ship secured for transit to Site 1211 by 0000 hr on 27 September.

Transit from Site 1210 to Site 1211

The 24-nmi transit to Site 1211 was completed without incident in 2.5 hr at an average speed of 9.6 kt. After arriving at the site coordinates, the thrusters and hydrophones were lowered and the ship was switched over to DP mode at 0225 hr on 27 September, initiating operations at Site 1211.

Site 1211

Hole 1211A

An APC/XCB BHA was assembled and run to near the seafloor. The bit was positioned at 2912.0 mbrf, and Hole 1211A was spudded with the APC at 0915 hr on 27 September. The mudline core contained 2.85 m of sediment, establishing a seafloor depth of 2918.7 mbrf, or 2907.5 mbsl. APC coring continued through Core 11H to 97.8 mbsf. While deploying Core 12H, the barrel dropped off the overshot and fell to the bottom. Two unsuccessful retrieval attempts and wireline trips were made before the core barrel was returned during the third run. The cause of the problem was identified as the safety tube located in the overshot, which had dislodged and resulted in the core barrel becoming jammed in the pipe. We resumed APC coring through Core 18H, which did not achieve full stroke, impeded by a chert layer. Coring was terminated at 158.9 mbsf, with an average recovery of 102.4%. The drill string was tripped up, clearing the seafloor at 0610 hr on 28 September, ending Hole 1211A.

Hole 1211B

The ship was offset 15 m to the north and the bit positioned 2 m higher than at Hole 1211A to achieve stratigraphic overlap and position critical intervals away from core breaks. Hole 1211B was spudded at 0700 hr on 28 September, recovering 6.15 m of sediment in Core 1H, indicating a seafloor depth of 2917.4 mbrf, or 2906.2 mbsl. Coring with the APC continued through Core 17H at 151.6 mbsf. An incomplete stroke on Core 17H resulted in deployment of the XCB center bit to drill 1.6 m through a chert layer. The APC was redeployed for Cores 18H and 19H. When Core 19H did not stroke completely, coring operations were suspended at 169.9 mbsf. The drill string was retrieved, with the bit clearing the seafloor at 0625 hr on 29 September, ending drilling at Hole 1211B.

Transit from Site 1211 to Site 1212

The short transit (28 nmi) to Site 1212 was completed in 3.2 hr at an average speed of 8.8 kt. At 0955 hr on 29 September, the ship was switched over to DP mode, initiating operations at Site 1212.

Site 1212

Hole 1212A

An APC/XCB BHA was run to 2689.0 mbrf, and Hole 1212A was spudded with the APC at 1540 hr on 29 September. The mudline core recovered 4.96 m of sediment, indicating a seafloor depth of 2693.6 mbrf, or 2682.5 mbsl. APC coring advanced the hole to 101.6 mbsf with 115.1% recovery. Cores 4H through 13H were oriented. After an incomplete stroke on Core 13H, we terminated coring in Hole 1212A. The drill string was recovered to the seafloor at 0255 hr on 30 September, ending operations at Hole 1212A.

Hole 1212B

The ship was offset 15 m to the north and the bit was positioned at a depth of 2689.0 mbrf. The same bit position was used in an attempt to keep critical intervals from falling at core breaks. Hole 1212B was spudded at 0345 hr on 30 September, recovering 6.74 m and establishing a seafloor depth of 2691.8 mbrf, or 2680.6 mbsl. Continuous APC coring progressed to 101.2 mbsf. Cores 4H through 12H were oriented. After an incomplete stroke on Core 12H, we adopted a strategy of deploying the XCB center bit to drill through chert layers, followed by redeployment of the APC. Ten deployments of the XCB center bit were required, including three to penetrate a layer at ~136 mbsf, drilling through 14.8 m to obtain 13 additional APC cores. Total APC recovery for Hole 1212B was 93.6%. Because of the increasing frequency of chert layers and diminishing core recovery on the last three APC cores, we terminated coring at Hole 1212B at 207.6 mbsf. The drill string was retrieved, clearing the rig floor at 2330 hr on 1 October, which concluded operations at Site 1212.

Transit from Site 1212 to Site 1213

The 56-nmi transit to Site 1213 took 6.0 hr at an average speed of 8.6 kt. Upon arriving on site, the thrusters and hydrophones were lowered, and the ship was switched over to DP mode, initiating operations at Site 1213 at 0606 hr on 2 October.

Site 1213

Hole 1213A

An RCB BHA was assembled and run to 3902.4 mbrf, and Hole 1213A was spudded at 1425 hr on 2 October. The first core recovered 8.43 m of sediment, indicating a seafloor depth of 3894.0 mbrf, or 3882.8 mbsl. RCB coring continued to 198.9 mbsf, with an average recovery for the 21 RCB cores of 21.7%. After deploying core barrel 21R, the sinker bars on the forward core line were being run in the hole when the hole packed off without warning. Before the driller could shut down the circulating pumps, the pressure built up enough to blow the sinker bars back up into the line wiper, unseating this assembly. During this event, the core line failed just above the rope socket, and the sinker bars fell to the bottom of the drill string on top of the previously deployed core barrel. The core line was repaired, and the second set of sinker bars was attached. While the repair was being made to the wireline, Core 21R was cut. The first attempt to engage the rope socket with the overshot failed, and two more wireline runs were made using a core barrel–core catcher assembly. All attempts failed to engage the rope socket, and coring had to be terminated. The drill string was retrieved after a brief loss of circulation and rotation, ending drilling at Hole 1213A at 0300 hr on 4 October.

Hole 1213B

The ship was offset 30 m to the north, and Hole 1213B was spudded with the RCB at 1155 hr on 4 October. We drilled ahead to 189.7 mbsf to provide approximately a one core overlap with Hole 1213A. Below 189.7 mbsf, RCB coring advanced the hole to 447.8 mbsf through largely a chert/chalk interval, with an average recovery of 10.5%. From 447.8 to 494.4 mbsf, RCB coring continued through diabase and basalt with good recovery (71.7%) at a slow rate ranging from 1.5 to 2.0 m/hr. Coring operations were terminated when the depth objectives were achieved (~50 m into igneous rock).

Following coring operations, the hole was prepared for logging, including a wiper trip to 90.6 mbsf and circulation of 40 bbl of drilling mud before and after the wiper trip. After releasing the bit, 165 bbl of logging mud was circulated, and the drill string tripped back and positioned at 105.4 mbsf. The first logging run with the triple combo tool string was only able to reach ~431 mbsf. While logging up from that depth several tight spots were noted, including one at ~190 mbsf that required working the tool for ~30 min. The tool had to be turned off during this process, so no logs were obtained between 190 mbsf and the base of the pipe.

We did not deploy the second tool string, the FMS-sonic, because of the questionable hole conditions and the approach of severe tropical storm Krosa into the operational area. With the storm forecast to come within 150 nmi of the location, it was necessary that the drill string be recovered and the drill collars stowed before conditions worsened. After rigging down the logging equipment, the drill string was retrieved, clearing the rig floor at 1900 hr on 9 October, concluding operations at Site 1213. After securing the ship for transit, we departed on a southerly heading to avoid the approaching storm.

Transit from Site 1213 to Site 1211

After departing Site 1213, we proceeded due south to distance ourselves from the forecast center of severe tropical depression Krosa. During the night, the storm accelerated to 40 kt and moved rapidly to the northeast, passing north of the operational location. After passage of the storm, we reversed course and proceeded back to Site 1211. A total of 116 nmi were covered during the 22.7-hr transit at an average speed of 5.1 kt. At 1742 hr on 10 October, the ship was switched over to DP mode, recommencing operations at Site 1211.

Return to Site 1211

Hole 1211C

An APC/XCB BHA was assembled and run to 2916.0 mbrf, near the seafloor. Hole 1211C was spudded with the APC at 0545 hr on 11 October. The mudline recovered 7.30 m of sediment, indicating a seafloor depth of 2918.2 mbrf, or 2906.9 mbsl. APC coring continued to a depth of 138.3 mbsf, after which coring was terminated when the objective was achieved. Cores 4H through 15H were oriented, and APC coring averaged 101.9% recovery. The drill string was retrieved clearing the rig floor at 0125 hr on 12 October, concluding operations at Site 1121.

Transit from Site 1211 to Site 1214

The 22-nmi transit to Site 1214 took 2.5 hr at an average speed of 8.8 kt. At 0420 hr on 12 October, the ship was switched over to DP mode, initiating operations at Site 1214.

Site 1214

Hole 1214A

An RCB BHA was tripped to the seafloor, and the bit tagged bottom at 3413.0 mbrf, or 3402 mbsl. RCB coring advanced the hole from the seafloor to 235.9 mbsf before coring time expired for the leg. Chert was encountered in drilling the first core and continued throughout the hole, which is reflected in the poor overall recovery (7%). The drill string was retrieved while the usual end-of-leg

maintenance and inspections were performed. At 0025 hr on 15 October, the bit cleared the rig floor, ending operations at Site 1214.

Transit from Site 1214 to Honolulu, Hawaii

After securing the ship for transit, we departed Site 1214 for port at 0030 hr on 15 October. The 2500 nmi transit to Honolulu, Hawaii took 9.85 days at an average speed of 10.75 kt. At 2100 hr on 23 October, the first line was ashore, officially ending Leg 198.

REFERENCES

Arthur, M.A., and Dean, W.E., 1986. Cretaceous paleoceanography. *In* Tucholke, B.E., and Vogt, P.R. (Eds.), *Decade of North American Geology, Western North Atlantic Basin Synthesis Volume,* Geol. Soc. Am., 617–630.

Arthur, M.A., Dean, W.E., Schlanger, S.O., 1985. Variations in the global carbon cycle during the Cretaceous related to climate, volcanism, and changes in atmospheric CO_2. *In* Sundquist, E.T., and Broecker, W.S. (Eds.), *The Carbon Cycle and Atmospheric CO_2: Natural Variations Archean to Present.* Geophys. Monogr., Am. Geophys. Union, 32:504–529.

Arthur, M.A., Dean, W.E., and Stow, D.A.V., 1984. Models for the deposition of Mesozoic-Cenozoic fine-grained, organic-carbon–rich sediment in the deep-sea. *In* Stow, D.A.V., and Piper, D.J.W (Eds.), *Fine-Grained Sediments: Deep-Water Processes and Facies.* Spec. Publ.—Geol. Soc. London, 15:527–560.

Arthur, M.A., Jenkyns, H.C., Brumsack, H., and Schlanger, S.O., 1990. Stratigraphy, geochemistry, and paleo-oceanography of organic carbon-rich Cretaceous sequences. *In* Ginsburg, R.N., and Beaudoin, B. (Eds.), *Cretaceous Resources, Events and Rhythms.* NATO ASI Ser., 304:75–119.

Arthur, M.A., Kump, L., Dean, W., and Larson, R., 1991. Superplume? Supergreenhouse? *Eos,* 2:301.

Arthur, M.A., and Premoli-Silva, I., 1982. Development of widespread organic carbon-rich strata in the Mediterranean Tethys. *In* Schlanger, S.O., and Cita, M.B. (Eds.), *Nature and Origin of Cretaceous Carbon-Rich Facies:* London (Academic Press), 7–54.

Aubry, M.-P., Berggren, W.A., Stott, L., and Sinha, A., 1996. The upper Paleocene–lower Eocene stratigraphic record and the Paleocene/Eocene boundary carbon isotope excursion: implications for geochronology. *In* Knox, R.W.O'B., Corfield, R.M., and Dunay, R.E. (Eds.), *Correlation of the Early Paleogene in Northwestern Europe.* Spec. Publ.—Geol. Soc. Am., 101:353–380.

Aubry, M.-P., Lucas, S., and Berggren, W.A. (Eds.), 1998. *Late Paleocene and Early Eocene Climatic and Biotic Evolution:* New York (Columbia Univ. Press).

Bains, S., Corfield, R.M., and Norris, R.D., 1999. Mechanisms of climate warming at the end of the Paleocene. *Science,* 285:724–727.

Baker, P.A., Gieskes, J.M., and Elderfield, H., 1982. Diagenesis of carbonates in deep-sea sediments: evidence from Sr^{2+}/Ca^{2+} ratios and interstitial dissolved Sr^{2+} data. *J. Sediment. Petrol.,* 52:71–82.

Barrera, E., 1994. Global environmental changes preceding the Cretaceous-Tertiary boundary: early-late Maastrichtian transition. *Geology,* 22:877–880.

Barrera, E., and Huber, B.T., 1990. Evolution of Antarctic waters during the Maestrichtian: foraminifer oxygen and carbon isotope ratios, Leg 113. *In* Barker, P.F., Kennett, J.P., et al., *Proc. ODP, Sci. Results,* 113: College Station, TX (Ocean Drilling Program), 813–827.

Barrera, E., and Savin, S.M., 1999. Evolution of Campanian–Maastrichtian marine climates and oceans. *In* Barrera, E., and Johnson, C.C. (Eds.), *Evolution*

of the Cretaceous Ocean-Climate System, Spec. Pap.—Geol. Soc. Am., 332:245–282.

Barrera, E., Savin, S.M., Thomas, E., and Jones, C.E., 1997. Evidence for thermohaline-circulation reversals controlled by sea level change in the latest Cretaceous. *Geology,* 25:715–718.

Barron, J.A., Basov, I.A., Beaufort, L., Dubuisson, G., Gladenkov, A.Y., Morley, J.J., Okada, M., Ólafsson, D.K., Pak, D.K., Roberts, A.P., Shilov, V.V., and Weeks, R.J., 1995. Biostratigraphic and magnetostratigraphic summary. *In* Rea, D.K., Basov, I.A., Scholl, D.W., and Allan, J.F. (Eds.), *Proc. ODP, Sci. Results,* 145: College Station, TX (Ocean Drilling Program), 559–575.

Barron, E.J., and Peterson, W.H., 1991. The Cenozoic ocean circulation based on ocean General Circulation Model results. *Palaeogeogr., Palaeoclimatol., Palaeoecol.,* 83:1–28.

Baudin, F., Deconinck, J.-F., Sachsenhofer, R.F., Strasser, A., and Arnaud, H., 1995. Organic geochemistry and clay mineralogy of Lower Cretaceous sediments from Allison and Resolution guyots (Sites 865 and 866), Mid-Pacific Mountains. *In* Winterer, E.L., Sager, W.W., Firth, J.V., and Sinton, J.M. (Eds.), *Proc. ODP, Sci. Results,* 143: College Station, TX (Ocean Drilling Program), 173–196.

Berger, W.H., Kroenke, L.W., Mayer, L.A., and Shipboard Scientific Party, 1991. Ontong Java Plateau, Leg 130: synopsis of major drilling results. *In* Kroenke, L.W., Berger, W.H., Janecek, T.R., et al., *Proc. ODP, Init. Repts.,* 130: College Station, TX (Ocean Drilling Program), 497–537.

Berggren, W.A., Kent, D.V., Swisher, C.C., III, and Aubry, M.-P., 1995. A revised Cenozoic geochronology and chronostratigraphy. *In* Berggren, W.A., Kent, D.V., Aubry, M.-P., and Hardenbol, J. (Eds.), *Geochronology, Time Scales and Global Stratigraphic Correlation.* Spec. Publ.–Soc. Econ. Paleontol. Mineral. (Soc. Sediment. Geol.), 54:129–212.

Boon, J.J., and de Leeuw, J.W., 1979. The analysis of wax esters, very long mid-chain ketones and sterol ethers isolated from Walvis Bay diatomaceous ooze. *Mar. Chem.,* 7:117–132.

Bralower, T.J., Arthur, M.A., Leckie, R.M., Sliter, W.V., Allard, D.J., and Schlanger, S.O., 1994. Timing and paleoceanography of oceanic dysoxia/anoxia in the Late Barremian to Early Aptian. *Palaios,* 9:335–369.

Bralower, T.J., CoBabe, E., Clement, B., Sliter, W.V., Osburne, C., and Longoria, J., 1999. The record of global change in mid-Cretaceous (Barremian–Albian) sections from the Sierra Madre, northeastern Mexico. *In* Huber, B.T., Bralower, T.J., and Leckie, R.M. (Eds.), *J. Foraminiferal Res.,* 29:418–437.

Bralower, T.J., Fullagar, P.D., Paull, C.K., Dwyer, G.S., and Leckie, R.M., 1997a. Mid-Cretaceous strontium-isotope stratigraphy of deep-sea sections. *Geol. Soc. Am. Bull.,* 109:1421–1442.

Bralower, T.J., Monechi, S., and Thierstein, H.R., 1989. Calcareous nannofossil zonation of the Jurassic-Cretaceous boundary interval and correlation with the geomagnetic polarity timescale. *Mar. Micropaleontol.,* 14:153–235.

Bralower, T.J., Sliter, W.V., Arthur, M.A., Leckie, R.M., Allard, D.J., and Schlanger, S.O., 1993. Dysoxic/anoxic episodes in the Aptian-Albian (Early Cretaceous). *In* Pringle, M.S., Sager, W.W., Sliter, M.V., and Stein, S. (Eds.), *The Mesozoic Pacific: Geology, Tectonics, and Volcanism*. Geophys. Monogr., Am. Geophys. Union, 77:5–37.

Bralower, T.J., Thomas, D.J., Zachos, J.C., Hirschmann, M.M., Röhl, U., Sigurdsson, H., Thomas, E., and Whitney, D.L., 1997b. High-resolution records of the late Paleocene thermal maximum and circum-Caribbean volcanism: is there a causal link? *Geology,* 25:963–966.

Bralower, T.J., Zachos, J.C., Thomas, E., Parrow, M., Paull, C.K., Kelly, D.C., Premoli Silva, I., Sliter, W.V., and Lohmann, K.C., 1995. Late Paleocene to Eocene paleoceanography of the equatorial Pacific Ocean: stable isotopes recorded at Ocean Drilling Program Site 865, Allison Guyot. *Paleoceanography,* 10:841–865.

Brass, G.W., Southam, J.R., and Peterson, W.H., 1982. Warm saline bottom water in the ancient ocean. *Nature,* 296:620–623.

Brassell, S.C., Comet, P.A., Eglinton, G., Isaacson, P.J., McEvoy, J., Maxwell, J.R., Thomson, I.D., Tibbetts, P.J., and Volkman, J.K., 1980. The origin and fate of lipids in the Japan Trench. *In* Douglas, A.G., and Maxwell, J.R. (Eds.), *Advances in Organic Geochemistry 1979:* Oxford (Pergamon Press), 375–392.

Brassell, S.C., Eglinton, G., Marlowe, I.T., Pflaumann, U., and Sarnthein, M., 1986. Molecular stratigraphy: a new tool for climatic assessment. *Nature,* 320:129–133.

Bréhéret, J.G., 1988. Episodes de sédimentation riches en matière organique dans les marnes bleues d'âge Aptien et Albien de la partie pélagique du bassin vocontien. *Bull. Geol. Soc. Fr.,* 8:349–356.

Browning, J.V., Miller, K.G., and Pak, D.K., 1996. Global implications of lower to middle Eocene sequence boundaries on the New Jersey Coastal Plain—the Icehouse cometh. *Geology,* 24:639–642.

Busson, G., and Noël, D., 1972. Les coccolithophoridées fossiles ne peuvent plus être considérées comme caractéristiques du seul environnement pélagique. *Bull. Soc. Geol. Fr.,* 164:493–502.

Busson, G., and Noël, D., 1991. Les Nannoconides, indicateurs environnementaux des oceans et mers epicontinentales du Jurassique terminal et du Cretace inferieur. *Oceanol. Acta,* 14:333–356.

Caldeira, K., and Rampino, M.R., 1990. Carbon dioxide emissions from Deccan volcanism and the K/T boundary greenhouse effect. *Geophys. Res. Lett.,* 17:1299–1302.

Cande, S.C., and Kent, D.V., 1995. Revised calibration of the geomagnetic polarity timescale for the Late Cretaceous and Cenozoic. *J. Geophys. Res.,* 100:6093–6095.

Chauris, H., LeRousseau, J., Beaudoin, B., Propson, S., and Montanari, A., 1998. Inoceramid extinction in the Gubbio Basin (northeastern Apennines of Italy) and relations with mid-Maastrichtian environmental changes. *Palaeogeogr., Palaeoclimatol., Palaeoecol.* 139:177–193.

Chepstow-Lusty, A., Backman, J., and Shackleton, N.J., 1989. Comparison of upper Pliocene *Discoaster* abundance variations from North Atlantic Sites 552, 607, 658, 659 and 662: further evidence for marine plankton responding to orbital forcing. *In* Ruddiman, W.F., Sarnthein, M., et al., *Proc. ODP, Sci. Results,* 108: College Station, TX (Ocean Drilling Program), 121–141.

Clarke, L.J., and H.C. Jenkyns, 1999. New oxygen isotope evidence for long-term Cretaceous climatic change in the Southern Hemisphere. *Geology,* 27:699–702.

Coccioni, A., Nesci, O., Tramontana, M., Wezel, F.C., and Moretti, E., 1987. Descrizione di un livello-guida "radiolaritico-bituminoso-ittiolitico" alla base delle marne a fucoidi nell'Apennino umbro-marchigiano. *Boll. Soc. Geol. Ital.,* 106:183–192.

Coccioni, R., Erba, E., and Premoli Silva, I., 1992. Barremian-Aptian calcareous plankton biostratigraphy from the Gorgo Cerbara section (Marche, central Italy) and implications for plankton evolution. *Cretaceous Res.,* 13:517–537.

Coccioni, R., and Premoli Silva, I., 1994. Planktonic foraminifera from the Lower Cretaceous of Rio Argos sections (southern Spain) and biostratigraphic implications. *Cretaceous Res.,* 15:645-687.

Coffin, M.F., and Eldholm, O., 1994. Large igneous provinces: crustal structure, dimensions, and external consequences. *Rev. Geophys.,* 32:1–36.

Corfield, R.M., Cartlidge, J.E., Premoli Silva, I., and Housley, R.A., 1991. Oxygen and carbon isotope stratigraphy of the Palaeogene and Cretaceous limestones in the Bottaccione Gorge and the Contessa Highway sections, Umbria, Italy. *Terra Nova,* 3:414–422.

Dean, W.E., Claypool, G.E., and Thiede, J., 1981. Origin of organic-carbon–rich Mid-Cretaceous limestones, Mid-Pacific Mountains and southern Hess Rise. *In* Thiede, J., Vallier, T.L., et al., *Init. Repts. DSDP,* 62: Washington (U.S. Govt. Printing Office), 877–890.

Dean, W.E., and Gardner, J.W., 1982. Origin and geochemistry of redox cycles of Jurassic to Eocene age, Cape Verde Basin (DSDP Site 367), Continental Margin of North-West Africa. *In* Schlanger, S.O., and Cita, M.B. (Eds.), *Nature and Origin of Cretaceous Carbon-Rich Facies:* London (Academic Press), 55–78.

D'Hondt, S., and Arthur, M.A., 1996. Late Cretaceous oceans and the cool tropic paradox. *Science,* 271:1838–1841.

Dickens, G.R., 2000. Methane oxidation during the Late Palaeocene Thermal Maximum. *Bull. Soc. Geol. Fr.,* 171:37–49.

Dickens, G.R., Castillo, M.M., and Walker, J.G.C., 1997. A blast of gas in the latest Paleocene: simulating first-order effects of massive dissociation of oceanic methane hydrate. *Geology,* 25:259–262.

Dickens, G.R., O'Neil, J.R., Rea, D.K., and Owen, R.M., 1995. Dissociation of oceanic methane hydrate as a cause of the carbon isotope excursion at the end of the Paleocene. *Paleoceanography,* 10:965–971.

Douglas, R.G., 1971. Cretaceous foraminifera from the northwestern Pacific Ocean: Leg 6, Deep Sea Drilling Project. *In* Fischer, A.G., Heezen, B.C., et al., *Init. Repts. DSDP,* 6: Washington (U.S. Govt. Printing Office), 1027–1053.

Douglas, R.G., and Savin, S.M., 1971. Isotopic analyses of planktonic foraminifers from the Cenozoic of the northwest Pacific, Leg 6. *In* Fischer, A.G., Heezen, B.C., et al., *Init. Repts. DSDP,* 6: Washington (U.S. Govt. Printing Office), 1123–1127.

Douglas, R.G., and Savin, S.M., 1975. Oxygen and carbon isotope analyses of Tertiary and Cretaceous microfossils from Shatsky Rise and other sites in the North Pacific Ocean. *In* Larson, R.L., Moberly, R., et al., *Init. Repts. DSDP,* 32: Washington (U.S. Govt. Printing Office), 509–520.

Duncan, R.A., and Richards, M.A., 1991. Hotspots, mantle plumes, flood basalts, and true polar wander. *Rev. Geophys., 29*:31–50.

Erba, E., 1994. Nannofossils and superplumes: the early Aptian "nannoconids crisis." *Paleoceanography,* 9:483–501.

Erba, E., Channell, J.E.T., Claps, M., Jones, C., Larson, R., Opdyke, B., Premoli-Silva, I., Riva, A., Salvini, G., and Torricelli, S., 1999. Integrated stratigraphy of the Cismon APTICORE (southern Alps, Italy): a "reference section" for the Barremian–Aptian interval at low latitudes. *J. Foraminiferal Res., 29*:371–391.

Erba, E., and Larson, R.L., 1991. Nannofossils and superplumes. *Eos, Transactions, Am. Geophys. Union,* 72:301. (Abstract).

Erbacher, J., Huber, B.T., Norris, R.D., and Markey, M., 2001. Intensified thermohaline stratification as a possible cause for an ocean anoxic event in the Cretaceous period. *Nature,* 409:325–327.

Erbacher, J., and Thurow, J., 1997. Influence of oceanic anoxic events on the evolution of mid-Cretaceous radiolaria in the North Atlantic and western Tethys. *Mar. Micropalaeontol.,* 30:139–158.

Erbacher, J., Thurow, J., and Littke, R., 1996. Evolution patterns of radiolaria and organic matter variations: a new approach to identify sea-level changes in mid-Cretaceous pelagic environments. *Geology,* 24:499–502.

Ewing, M., Saito, T., Ewing, J.I., and Burckle, L.M., 1966. Lower Cretaceous sediments from the Northwestern Pacific. *Science,* 152:751–755.

Farrell, J.W., and Prell, W.L., 1991. Pacific $CaCO_3$ preservation and $\delta^{18}O$ since 4 Ma: paleoceanic and paleoclimatic implications. *Paleoceanography,* 6:485–498.

Farrimond, P., Eglinton, G., and Brassell, S.C., 1986. Alkenones in Cretaceous black shales, Blake-Bahama Basin, western North Atlantic. *In* Leythaeuser, D., and Rullkötter, J. (Eds.), *Advances in Organic Geochemistry, 1985.* Org. Geochem., 10:897–903.

Fassell, M.L., and Bralower, T.J., 1999. Warm, equable mid-Cretaceous: stable isotope evidence. In Barrera, E., and Johnson, C.C. (Eds.), *The Evolution of the Cretaceous Ocean Climate System,* Spec. Pap.—Geol. Soc. Am., 332:121–142.

Fischer, A.G., Heezen, B.C., et al., 1971. *Init. Repts. DSDP,* 6: Washington (U.S. Govt. Printing Office).

Frank, T.D., and Arthur, M.A., 1999. Tectonic forcings of Maastrichtian ocean-climate evolution. *Paleoceanography,* 14:103–117.

Gerstel, J., Thunell, R.C., Zachos, J.C., and Arthur, M.A., 1986. The Cretaceous/Tertiary boundary event in the North Pacific: planktonic foraminiferal results from Deep Sea Drilling Project Site 577, Shatsky Rise. *Paleoceanography,* 1:97–117.

Gibson, T.G., Bybell, L.M., and Owens, J.P., 1993. Latest Paleocene lithologic and biotic events in neritic deposits of southwestern New Jersey. *Paleoceanography,* 8:495–514.

Gradstein, F.M., Agterberg, F.P., Ogg, J.G., Hardenbol, J., van Veen, P., Thierry, J., and Huang, Z., 1994. A Mesozoic time scale. *J. Geophys. Res.,* 99:24051–24074.

Gröcke, D.R., Hesselbo, S.P., and Jenkyns, H.C., 1999. Carbon-isotope composition of Lower Cretaceous fossil wood: ocean-atmosphere chemistry and relation to sea-level change. *Geology,* 27: 155–158.

Haq, B.U., Hardenbol, J., and Vail, P.R., 1988. Mesozoic and Cenozoic chronostratigraphy and cycles of sea-level change. *In* Wilgus, C.K., Hastings, B.S., Kendall, C.G.St.C., Posamentier, H.W., Ross, C.A., and Van Wagoner, J.C. (Eds.), *Sea-Level Changes—An Integrated Approach*. Spec. Publ.—Soc. Econ. Paleontol. Mineral., 42:72–108.

Harland, W.B., Armstrong, R.L., Cox, A.V., Craig, L.E., Smith, A.G., and Smith, D.G., 1990. *A Geologic Time Scale 1989:* Cambridge (Cambridge Univ. Press).

Haug, G.H., Maslin, M.A., Sarnthein, M., Stax, R., and Tiedemann, R., 1995. Evolution of northwest Pacific sedimentation patterns since 6 Ma (Site 882). *In* Rea, D.K., Basov, I.A., Scholl, D.W., and Allan, J.F. (Eds.), *Proc. ODP, Sci. Results,* 145: College Station, TX (Ocean Drilling Program), 293–314.

Hays, J.D., and Pitman, W.C., III, 1973. Lithospheric plate motion, sea level changes, and climatic and ecological consequences. *Nature,* 246:18–22.

Heath, G.R., Burkle, L.H., et al., 1985. *Init Repts., DSDP,* 86: Washington (U.S. Govt. Printing Office).

Hilde, T.W.C., Isezaki, N., and Wageman, J.M., 1976. Mesozoic sea-floor spreading in the North Pacific. *In* Woolard, G.P., Sutton, G.H., Manghnani, M.H., and Moberly, R. (Eds.), *The Geophysics of the Pacific Ocean Basin and its Margins*. Geophys. Monogr., Am. Geophys. Union, 19:205–226.

Huber, B.T., Hodell, D.A., and Hamilton, C.P., 1995. Mid- to Late Cretaceous climate of the southern high latitudes: stable isotopic evidence for minimal equator-to-pole thermal gradients. *Geol. Soc. Am. Bull.,* 107:1164–1191.

Huber, M., and Sloan, L.C., 2000. Climatic response to tropical sea surface temperature changes on a "greenhouse" Earth. *Paleoceanography,* 15:443–450.

Jahren, A.H., and Arens, N.C., 1998. Methane hydrate dissociation implicated in Aptian OAE events. *Abstracts with Programs*. Geol. Soc. Am., 30:52. (Abstract).

Jahren, A.H., Arens, N.C., Sarmiento, G., Guerrero, J., and Amundson, R., 2001. Terrestrial record of methane hydrate dissociation in the Early Cretaceous. *Geology,* 29:159–162.

Jenkyns, H.C., 1980. Cretaceous anoxic events: from continents to oceans. *J. Geol. Soc. London,* 137:171–188.

Jenkyns, H.C., 1995. Carbon-isotope stratigraphy and paleoceanographic significance of the Lower Cretaceous shallow-water carbonates of Resolution Guyot, Mid-Pacific Mountains. *In* Winterer, E.L., Sager, W.W., Firth, J.V., and Sinton, J.M. (Eds.), *Proc. ODP, Sci. Results,* 143: College Station, TX (Ocean Drilling Program), 99–104.

Jenkyns, H.C., Gale, A.S., and Corfield, R.M., 1994. Carbon- and oxygen-isotope stratigraphy of the English Chalk and Italian Scaglia and its palaeoclimatic significance. *Geol. Mag.,* 131:1–34.

Jenkyns, H.C., Paull, C.K., Cummins, D.I., and Fullagar, P.D., 1995. Strontium-isotope stratigraphy of Lower Cretaceous atoll carbonates in the Mid-Pacific Mountains. *In* Winterer, E.L., Sager, W.W., Firth, J.V., and Sinton, J.M. (Eds.), *Proc. ODP, Sci. Results,* 143: College Station, TX (Ocean Drilling Program), 89–97.

Johnson, C.C., Barron, E.J., Kauffman, E.G., Arthur, M.A., Fawcett, P.J., and Yasuda, M.K., 1996. Middle Cretaceous reef collapse linked to ocean heat transport. *Geology,* 24:376–380.

Keller, G., and Barron, J.A., 1987. Paleodepth distribution of Neogene deep-sea hiatuses. *Paleoceanography,* 2:697–713.

Kelly, D.C., Bralower, T.J., Zachos, J.C., Premoli Silva, I., and Thomas, E., 1996. Rapid diversification of planktonic foraminifera in the tropical Pacific (ODP Site 865) during the late Paleocene thermal maximum. *Geology,* 24:423–426.

Kennett, J.P., 1977. Cenozoic evolution of Antarctic glaciation, the circum-Antarctic Ocean, and their impact on global paleoceanography. *J. Geophys. Res.,* 82:3843–3860.

Kennett, J.P., Keller, G., and Srinivasan, M.S., 1985. Miocene planktonic foraminiferal biogeography and paleoceanographic development of the Indo-Pacific region. *In* Kennett, J.P. (Ed.), *The Miocene Ocean: Paleoceanography and Biogeography.* Mem.—Geol. Soc. Am., 163:197–236.

Kennett, J.P., and Shackleton, N.J., 1976. Oxygen isotopic evidence for the development of the psychrosphere 38 Myr ago. *Nature,* 260:513–515.

Kennett, J.P., and Stott, L.D., 1991. Abrupt deep-sea warming, paleoceanographic changes and benthic extinctions at the end of the Palaeocene. *Nature,* 353:225–229.

Koizumi, I., 1975. Neogene diatoms from the northwestern Pacific Ocean, Deep Sea Drilling Project. *In* Larson, R.L., Moberly, R., et al., *Init. Repts. DSDP,* 32: Washington (U.S. Govt. Printing Office), 865–889.

Koizumi, I., 1985. Late Neogene paleoceanography in the western north Pacific. *In* Heath, G.R., Burckle, L.H., et al., *Init. Repts. DSDP,* 86: Washington (U.S. Govt. Printing Office), 429–438.

Koizumi, I., and Tanimura, Y., 1985. Neogene diatom biostratigraphy of the middle latitude western North Pacific, Deep Sea Drilling Project Leg 86. *In* Heath, G.R., Burckle, L.H., et al., *Init. Repts. DSDP,* 86: Washington (U.S. Govt. Printing Office), 269–300.

Larson, R.L., 1991a. Geological consequences of superplumes. *Geology,* 19:963–966.

Larson, R.L., 1991b. The latest pulse of Earth: evidence for a mid-Cretaceous superplume. *Geology,* 19:547–550.

Larson, R.L., and Chase, C.G., 1972. Late Mesozoic evolution of the western Pacific Ocean. *Geol. Soc. Am. Bull.,* 83:3627–3643.

Larson, R.L., and Erba, E., 1999. Onset of the Mid-Cretaceous greenhouse in the Barremian–Aptian: igneous events and the biological, sedimentary and geochemical responses. *Paleoceanography,* 14:663–678.

Larson, R.L., Moberly, R., et al., 1975. *Init. Repts. DSDP,* 32: Washington (U.S. Govt. Printing Office).

Larson, R.L., Schlanger, S.O., et al., 1981. *Init. Repts. DSDP,* 61: Washington (U.S. Govt. Printing Office).

Larson, R.L., Steiner, M.B., Erba, E., and Lancelot, Y., 1992. Paleolatitudes and tectonic reconstructions of the oldest portion of the Pacific plate: a comparative study. *In* Larson, R.L., Lancelot, Y., et al., *Proc. ODP, Sci. Results,* 129: College Station, TX (Ocean Drilling Program), 615–631.

Laskar, J., 1990. The chaotic motion of the solar system: a numerical estimate of the size of the chaotic zones. *Icarus,* 88:266–291.

Leckie, R.M., 1989. A paleoceanographic model for the early evolutionary history of planktonic foraminifera. *Palaeogeogr., Palaeoclimatol., Palaeoecol.,* 73:107–138.

Leckie, R.M., Bralower, T.J., and Cashman, R., in press. Oceanic Anoxic Events and Plankton Evolution: Exploring Biocomplexity in the Mid-Cretaceous, *Paleoceanography.*

Lini, A., Weissert, H., and Erba, E., 1992. The Valanginian carbon isotope event: a first episode of greenhouse climate conditions during the Cretaceous. *Terra Nova,* 4:374–384.

Loutit, T.S., Hardenbol, J., Vail, P.R. and Baum, G.R., 1988. Condensed sections: the key to age determination and correlation of continental margin sequences. *In* Wilgus, C.K., Hastings, B.S., Ross, C.A., Posamentier, H.W., Van Wagoner, J., and Kendall, C.G.St.C. (Eds.), *Sea-Level Changes: An Integrated Approach.* Spec. Publ.—Soc. Econ. Paleontol. Mineral., 42:183–213.

Luterbacher, H.P., 1975. Early Cretaceous foraminifera from the northwestern Pacific, Leg 32, Deep Sea Drilling Project. *In* Larson, R.L., Moberly, R., et al., *Init. Repts. DSDP,* 32: Washington (U.S. Govt. Printing Office), 703–718.

Luterbacher, H.P., and Premoli Silva, I., 1964. Biostratigrafia del limite Cretaceo-terziario nell' Appennino centrale. *Riv. Ital. Paleontol.,* 70:67–117.

MacLeod, K.G., 1994. Bioturbation, inoceramid extinction, and mid-Maastrichtian ecological change. *Geology,* 22:139–142.

MacLeod, K.G., and Huber, B.T., 1996. Reorganization of deep ocean circulation accompanying a Late Cretaceous extinction event. *Nature,* 380:422–425.

MacLeod, K.G., Huber, B.T., and Ward, P.D., 1996. The biostratigraphy and paleobiogeography of Maastrichtian inoceramids. *In* Ryder, G., Fastowsky, D., and Gartner, S. (Eds.), *The Cretaceous–Tertiary Event and Other Catastrophes in Earth History.* Spec. Publ.–Geol. Soc. Am., 307: 361–373.

Magniez-Jannin, F., 1998. L'élongation des loges chez les foraminifères panctoniques du Crétacé inférieur: une adaptation à la sous-oxygénation des eaux?. *Comptes Rendues de l'Académie des Sciences* (Serie II): *Sciences de la Terre et des Planetes:* Montrouge (Gauthier-Villars), 207–213.

Maslin, M.A., Haug, G.H., Sarnthein, M., Tiedemann, R., Erlenkeuser, H., and Stax, R., 1995. Northwest Pacific Site 882: the initiation of Northern Hemisphere glaciation. *In* Rea, D.K., Basov, I.A., Scholl, D.W., and Allan, J.F.

(Eds.), *Proc. ODP, Sci. Results,* 145: College Station, TX (Ocean Drilling Program), 315–329.

Matter, A., Douglas, R.G., and Perch-Nielsen, K., 1975. Fossil preservation, geochemistry and diagenesis of pelagic carbonates from the Shatsky Rise, northwest Pacific. *In* Larson, R.L., Moberly, R., et al., *Init. Repts. DSDP,* 32: Washington (U.S. Govt. Printing Office), 891–921.

McNutt, M.K., and Fischer, K.M., 1987. The South Pacific superswell. *In* Keating, B.H., Fryer, P., Batiza, R., and Boehlert, G.W. (Eds.), *Seamounts, Islands, and Atolls*. Geophys. Monogr., Am. Geophys. Union, 43:25–34.

Mélières, F., Deroo, G., and Herbin, J.-P., 1981. Organic-matter-rich and hypersiliceous Aptian sediments from western Mid-Pacific Mountains, Deep Sea Drilling Project Leg 62. *In* Thiede, J., Vallier, T.L., et al., *Init. Repts. DSDP,* 62: Washington (U.S. Govt. Printing Office), 903–915.

Menegatti, A.P., Weissert, H., Brown, R.S., Tyson, R.V., Farrimond, P., Strasser, A., and Caron, M., 1998. High resolution $\delta^{13}C$ stratigraphy through the early Aptian "Livello Selli" of the Alpine Tethys. *Paleoceanography,* 13:530–545.

Miller, K.G., and Fairbanks, R.G., 1985. Oligocene to Miocene carbon isotope cycles and abyssal circulation changes. *In* Sundquist, E.J., and Broecker, W.S. (Eds.), *The Carbon Cycle and Atmospheric CO_2: Natural Variations Archean to Present*. Geophys. Monogr., Am. Geophys. Union, 32:469–486.

Miller, K.G., Fairbanks, R.G., and Thomas, E., 1987a. Benthic foraminiferal carbon isotopic records and the development of abyssal circulation in the eastern North Atlantic. *In* Ruddiman, W.F., Kidd, R.B., and Thomas, E., et al., *Init. Repts. DSDP,* 94: Washington (U.S. Govt. Printing Office), 981–996.

Miller, K.G., Janecek, T.R., Katz, M.E., and Keil, D.J., 1987b. Abyssal circulation and benthic foraminiferal changes near the Paleocene/Eocene boundary. *Paleoceanography,* 2:741–761.

Miller, K.G., and Thomas, E., 1985. Late Eocene to Oligocene benthic foraminiferal isotopic record, Site 574, equatorial Pacific. *In* Mayer, L., Theyer, F., Thomas, E., et al., *Init. Repts. DSDP,* 85: Washington (U.S. Govt. Printing Office), 771–777.

Miller, K.G., Wright, J.D., and Fairbanks, R.G., 1991. Unlocking the Ice House: Oligocene-Miocene oxygen isotopes, eustasy, and margin erosion. *J. Geophys. Res.,* 96:6829–6848.

Monechi, S., 1985. Campanian to Pleistocene calcareous nannofossil stratigraphy from the northwest Pacific Ocean, Deep Sea Drilling Project Leg 86. *In* Heath, G.R., Burckle, L.H., et al., *Init. Repts. DSDP,* 86: Washington (U.S. Govt. Printing Office), 301–336.

Monechi, S., Angori, E., and von Salis, K., 2000. Calcareous nannofossil turnover around the Paleocene/Eocene transition at Alamedilla (southern Spain). *Bull. Soc. Geol. Fr.,* 171:477–489.

Nakanishi, M., Sager, W.W., and Klaus, A., 1999. Magnetic lineations within Shatsky Rise, northwest Pacific Ocean: implications for hot spot–triple junction interaction and oceanic plateau formation. *J. Geophys. Res.,* 104:7539–7556.

Nakanishi, M., Tamaki, K., and Kobayashi, K., 1989. Mesozoic magnetic anomaly lineations and seafloor spreading history of the Northwestern Pacific. *J. Geophys. Res.,* 94:15437–15462.

Nakanishi, M., Tamaki, K., and Kobayashi, K., 1992. Magnetic anomaly lineations from Late Jurassic to Early Cretaceous in the west-central Pacific Ocean. *Geophys. J. Int.,* 109:701–719.

Norris, R.D., and Röhl, U., 1999. Carbon cycling and chronology of climate warming during the Palaeocene/Eocene transition. *Nature,* 401:775–778.

Norris, R.D., and Wilson, P.A., 1998. Low-latitude sea-surface temperatures for the mid-Cretaceous and the evolution of planktic foraminifera. *Geology,* 26:823–826.

Opdyke, B.N., Erba, E., and Larson, R.L., 1999. Hot LIPs, methane, and the carbon record of the Apticore. *Eos, Transactions, Am. Geophys. Union.* 80:486–487.

Ourisson, G., Albrecht, P., and Rohmer, M., 1979. The hopanoids: paleochemistry and biochemistry of a group of natural products. *Pure Appl. Chem.,* 51:709–729.

Ourisson, G., Rohmer, M., and Poralla, K., 1987. Microbial lipids betrayed by their fossils. *Microbiol. Sci.,* 4:52–57.

Ozima, M., Kaneoka, I., and Aramaki, S., 1970. K-Ar ages of submarine basalts dredged from seamounts in the western Pacific area and discussion of oceanic crust. *Earth Planet. Sci. Lett.,* 8:237–249.

Pak, D.K., and Miller, K.G., 1992. Paleocene to Eocene benthic foraminiferal isotopes and assemblages: implications for deepwater circulation. *Paleoceanography,* 7:405–422.

Parrish, J.T., and Curtis, R.L., 1982. Atmospheric circulation, upwelling, and organic-rich rocks in the Mesozoic and Cenozoic eras. *Palaeogeogr., Palaeoclimatol., Palaeoecol.,* 40:31–66.

Pearson, P.N., Ditchfield, P.W., Singano, J., Harcourt-Brown, K.G., Nicholas, C.J., Olsson, R.K., Shackleton, N.J., and Hall, M.A., 2001. Warm tropical sea surface temperatures in the Late Cretaceous and Eocene epochs. *Nature,* 413:481–487.

Pedersen, T.F., and Calvert, S.E., 1991. Anoxia vs. productivity: what controls the formation of organic-carbon–rich sediments and sedimentary rocks? *AAPG Bull.,* 74:454–466.

Perch-Nielsen, K., 1985. Cenozoic calcareous nannofossils. *In* Bolli, H.M., Saunders, J.B., and Perch-Nielsen, K. (Eds.), *Plankton Stratigraphy:* Cambridge (Cambridge Univ. Press), 427–554.

Percival, S.F., Jr., and Fischer, A.G., 1977. Changes in calcareous nannoplankton in the Cretaceous–Tertiary biotic crisis at Zumaya, Spain. *Evol. Theory,* 2:1–35.

Plank, T., Ludden, J.N., Escutia, C., et al., 2000. *Proc. ODP, Init. Repts.,* 185 [CD-ROM]. Available from: Ocean Drilling Program, Texas A&M University, College Station TX 77845-9547, USA.

Pospichal, J.J., 1991. Calcareous nannofossils across Cretaceous/Tertiary boundary at Site 752, eastern Indian Ocean. *In* Weissel, J., Peirce, J., Taylor, E.,

Alt, J., et al., *Proc. ODP, Sci. Results,* 121: College Station, TX (Ocean Drilling Program), 395–414.

Premoli Silva, I., Castradori, D., and Spezzaferri, S., 1993. Calcareous nannofossil and planktonic foraminifer biostratigraphy of Hole 810C (Shatsky Rise, northwestern Pacific). *In* Natland, J.H., Storms, M.A., et al., *Proc. ODP, Sci. Results,* 132: College Station, TX (Ocean Drilling Program), 15–36.

Premoli Silva, I., Erba, E., Salvini, G., Locatelli, C., and Verga, D., 1999. Biotic changes in Cretaceous oceanic anoxic events of the Tethys. *J. Foraminiferal Res.,* 29:352–370.

Premoli Silva, I., and Sliter, W.V., 1999. Cretaceous paleoceanography: evidence from planktonic foraminiferal evolution. *In* Barrera, E., and Johnson, C.C. (Eds.), *The Evolution of Cretaceous Ocean-Climatic System.* Spec. Pap.–Geol. Soc. Am., 332:301–328.

Rea, D.K., Basov, I.A., Krissek, L.A., and the Leg 145 Scientific Party, 1995. Scientific results of drilling the North Pacific transect. *In* Rea, D.K., Basov, I.A., Scholl, D.W., and Allan, J.F. (Eds.), *Proc. ODP, Sci. Results,* 145: College Station, TX (Ocean Drilling Program), 577–596.

Robert, C., and Kennett, J.P., 1994. Antarctic subtropical humid episode at the Paleocene-Eocene boundary: clay mineral evidence. *Geology,* 22:211–214.

Rohmer, M., Bisseret, P., and Neunlist, S., 1992. The hopanoids, prokaryotic triterpenoids and precursors of ubiquitous molecular fossils. *In* Moldowan, J.M., Albrecht, P., and Philp, R.P., *Biological Markers in Sediments and Petroleum:* Englewood Cliffs, NJ (Prentice Hall), 1–17.

Rohmer, M., Boivier-Nave, P., and Ourisson, G., 1989. Distribution of hopanoid triterpenes in prokaryotes. *J. Genetic Microbiol.,* 130:1137–1150.

Romine, K., and Lombari, G., 1985. Evolution of Pacific circulation in the Miocene: radiolarian evidence from DSDP Site 289. *In* Kennett, J.P. (Ed.), *The Miocene Ocean: Paleoceanography and Biogeography.* Mem.—Geol. Soc. Am., 163:273–290.

Roth, P.H., 1973. Calcareous nannofossils—Leg 17, Deep Sea Drilling Project. *In* Winterer, E.L., Ewing, J.I., et al., *Init. Repts. DSDP,* 17: Washington (U.S. Govt. Printing Office), 695–795.

Roth, P.H., 1987. Mesozoic calcareous nannofossil evolution: relation to paleoceanographic events. *Paleoceanography,* 2:601–612.

Roth, P.H., and Bowdler, J., 1981. Middle Cretaceous calcareous nannoplankton biogeography and oceanography of the Atlantic Ocean. *In* Warme, J.E., Douglas, R.G., and Winterer, E.L. (Eds.), *The Deep Sea Drilling Project: A Decade of Progress*. Spec. Publ.—Soc. Econ. Paleontol. Mineral., 32:517–546.

Roth, P.H., and Krumbach, K.R., 1986. Middle Cretaceous calcareous nannofossil biogeography and preservation in the Atlantic and Indian Oceans: implications for paleoceanography. *Mar. Micropaleontol.,* 10:235–266.

Ryan, W.B.F., and Cita, M.B., 1977. Ignorance concerning episodes of ocean-wide stagnation. *Mar. Geol.,* 23:197–215.

Sager, W.W., and Han, H.-C., 1993. Rapid formation of the Shatsky Rise oceanic plateau inferred from its magnetic anomaly. *Nature,* 364:610–613.

Sager, W.W., Handschumacher, D.W., Hilde, T.W.C., and Bracey, D.R., 1988. Tectonic evolution of the northern Pacific Plate and Pacific-Farallon-Izanagi triple junction in the Late Jurassic and Early Cretaceous (M21-M10). *Tectonophysics,* 155:345–364.

Sager, W.W., Kim, J., Klaus, A., Nakanishi, M., and Khankishieva, L.M., 1999. Bathymetry of Shatsky Rise, northwest Pacific Ocean: implications for ocean plateau development at a triple junction. *J. Geophys. Res.,* 104:7557–7576.

Savin, S.M., 1977. The history of the Earth's surface temperature during the past 100 million years. *Annu. Rev. Earth Planet. Sci.,* 5:319–355.

Schaaf, A., 1981. Late Early Cretaceous radiolarians from Deep Sea Drilling Project Leg 62. *In* Thiede, J., Vallier, T.L., et al., *Init. Repts. DSDP,* 62: Washington (U.S. Govt. Printing Office), 419–470.

Schlanger, S.O., Arthur, M.A., Jenkyns, H.C., and Scholle, P.A., 1987. The Cenomanian–Turonian oceanic anoxic event, I. Stratigraphy and distribution of organic carbon-rich beds and the marine $\delta^{13}C$ excursion. *In* Brooks, J., and Fleet, A.J. (Eds.), *Marine Petroleum Source Rocks*. Spec. Publ.—Geol. Soc. London, 26:371–399.

Schlanger, S.O., and Douglas, R.G., 1974. The pelagic ooze-chalk-limestone transition and its implication for marine stratigraphy. *In* Hsü, K.J., and Jenkyns, H.C. (Eds.), *Pelagic Sediments: On Land and Under the Sea.* Spec. Publ.—Int. Assoc. Sedimentol., 1:117–148.

Schlanger, S.O., and Jenkyns, H.C., 1976. Cretaceous oceanic anoxic events: causes and consequences. *Geol. Mijnbouw,* 55:179–184.

Schlanger, S.O., Jenkyns, H.C., and Premoli-Silva, I., 1981. Volcanism and vertical tectonics in the Pacific Basin related to global Cretaceous transgressions. *Earth Planet. Sci. Lett.,* 52:435–449.

Scholle, P.A., and Arthur, M.A., 1980. Carbon isotope fluctuations in Cretaceous pelagic limestones: potential stratigraphic and petroleum exploration tool. *AAPG Bull.,* 64:67–87.

Shackleton, N.J., 1986. Paleogene stable isotope events. *Palaeogeogr., Palaeoclimatol., Palaeoecol.,* 57:91–102.

Sliter, W.V., 1984. Foraminifers from Cretaceous limestone of the Franciscan Complex, northern California. *In* Blake, C., Jr. (Ed.), *Franciscan Geology of Northern California*. SEPM Pacific Sect., 43:149–162.

Sliter, W.V., 1989. Aptian anoxia in the Pacific Basin. *Geology,* 17:909–912.

Sliter, W.V., 1992. Cretaceous planktonic foraminiferal biostratigraphy and paleoceanographic events in the Pacific Ocean with emphasis on indurated sediment. *In* Ishizaki, K., and Saito, T. (Eds.), *Centenary of Japanese Micropaleontology:* Tokyo (Terra Sci.), 281–299.

Sliter, W.V., and Brown, G.R., 1993. Shatsky Rise: seismic stratigraphy and sedimentary record of Pacific paleoceanography since the Early Cretaceous. *In* Natland, J.H., Storms, M.A., et al., *Proc. ODP, Sci. Results,* 132: College Station, TX (Ocean Drilling Program), 3–13.

Sliter, W.V., van Waasbergen, R.J., Brown, G.R., and ODP Leg 132 Scientific Party, 1990. Tectonic and stratigraphic evolution of Shatsky Rise. *Eos,* 71:1673.

Sloan, L.C., and Thomas, E., 1998. Global climate of the late Paleocene epoch: modeling the circumstances associated with a climatic "event." *In* Aubry, M.P., Lucas, S.G., Berggren, W.A. (Eds.), *Late Paleocene–Early Eocene Climatic and Biotic Events in the Marine and Terrestrial Records:* New York (Columbia Univ. Press), 138–157.

Smit, J., and Romein, A.J.T., 1985. A sequence of events across the Cretaceous-Tertiary boundary. *Earth Planet. Sci. Lett.,* 74:155–170.

Stein, R., Rullkötter, J., and Welte, D.H., 1986. Accumulation of organic-carbon–rich sediments in the late Jurassic and Cretaceous Atlantic Ocean—a synthesis. *Chem. Geol.,* 56:1–32.

Stoll, H.M., and Schrag, D.P., 1996. Evidence for glacial control of rapid sea level changes in the Early Cretaceous. *Science,* 272:1771–1774.

Storms, M.A., Natland, J.H., et al., 1991. *Proc. ODP, Init. Repts.,* 132: College Station, TX (Ocean Drilling Program).

Stott, L.D., 1992. Higher temperatures and lower pCO_2: A climate enigma at the end of the Paleocene Epoch. *Paleoceanography,* 7: 395–404.

Stott, L.D., and Kennett, J.P., 1990. The paleoceanographic and paleoclimatic signature of the Cretaceous/Paleogene boundary in the Antarctic: stable isotopic results from ODP Leg 113. *In* Barker, P.F., Kennett, J.P., et al., *Proc. ODP, Sci. Results,* 113: College Station, TX (Ocean Drilling Program), 829–848.

Stott, L.D., Kennett, J.P., Shackleton, N.J., and Corfield, R.M., 1990. The evolution of Antarctic surface waters during the Paleogene: inferences from the stable isotopic composition of planktonic foraminifers, ODP Leg 113. *In* Barker, P.F., Kennett, J.P., et al., *Proc. ODP, Sci. Results,* 113: College Station, TX (Ocean Drilling Program), 849–863.

Tarduno, J.A., Sliter, W.V., Kroenke, L., Leckie, M., Mayer, H., Mahoney, J.J., Musgrave, R., Storey, M., and Winterer, E.L., 1991. Rapid formation of Ontong Java Plateau by Aptian mantle plume volcanism. *Science,* 254:399–403.

Tatsumi, Y., Shinjoe, H., Ishizuka, H., Sager, W.W., and Klaus, A., 1998. Geochemical evidence for a mid-Cretaceous superplume. *Geology,* 26:151–154.

Thiede, J., Dean, W.E., and Claypool, G.E., 1982. Oxygen deficient depositional environments in the mid-Cretaceous tropical and subtropical Pacific Ocean. *In* Schlanger, S.O., and Cita, M.B. (Eds.), *Nature and Origin of Cretaceous Carbon-rich Facies:* London (Academic Press), 79–100.

Thierstein, H.R., 1979. Paleoceanographic implications of organic carbon and carbonate distribution in Mesozoic deep sea sediments. *In* Talwani, M., Hay, W., and Ryan, W.B.F. (Eds.), *Deep Drilling Results in the Atlantic Ocean.* Am. Geophys. Union, Maurice Ewing Ser., 3:249–274.

Thierstein, H.R., 1982. Terminal Cretaceous plankton extinctions: a critical assessment. *In* Silver, L.T., and Schultz, P.H. (Eds.), *Geological Implications of*

Impacts of Large Asteroids and Comets on the Earth. Spec. Pap.–Geol. Soc. Am., 190:385–399.

Thierstein, H.R., and Berger, W.H., 1978. Injection events in ocean history. *Nature,* 276:461–466.

Thomas, D.J., Bralower, T.J., and Zachos, J.C., 1999. New evidence for subtropical warming during the late Paleocene thermal maximum: stable isotopes from Deep Sea Drilling Project Site 527, Walvis Ridge. *Paleoceanography,* 14:561–570.

Thomas, E., 1990. Late Cretaceous–early Eocene mass extinctions in the deep sea. *In* Sharpton, V.L., and Ward, P.D. (Eds.), *Global Catastrophes in Earth History: An Interdisciplinary Conference on Impacts, Volcanism, and Mass Mortality*. Spec. Pap.—Geol. Soc. Am., 247:481–495.

Thomas, E., 1998. Biogeography of the late Paleocene benthic foraminiferal extinction. *In* Aubry, M.-P., Lucas, S.G., and Berggren, W.A. (Eds.), *Late Paleocene-Early Eocene: Climatic and Biotic Events in the Marine and Terrestrial Records:* New York (Columbia Univ. Press), 214–235.

Thomas, E., and Shackleton, N., 1996. The Palaeocene-Eocene benthic foraminiferal extinction and stable isotope anomalies. *In* Knox, R.W.O'B., Corfield, R.M., and Dunay, R.E. (Eds.), *Correlation of the Early Paleogene in Northwest Europe*. Spec. Publ.—Geol. Soc. London, 101:401–441.

Thomas, E., and Zachos, J.C., 1999. Deep-sea faunas during the late Paleocene–early Eocene climate optimum: boredom or boredom with short periods of terror. *Abstracts with Programs*. Geol. Soc. Am., 31:122.

Thomas, E., Zachos, J.C., and Bralower, T.J., 2000. Ice-free to glacial world transition as recorded by benthic foraminifera. *In* Huber, B.T., MacLeod, K.G., and Wing, S.L. (Eds.), *Warm Climates in Earth History:* Cambridge (Cambridge Univ. Press), 132–160.

Tissot, B., Durand, B., Espitalié, J., and Combaz, A., 1974. Influence of the nature and diagenesis of organic matter in the formation of petroleum. *AAPG Bull.,* 58:499–506.

Tremolada, F., and Erba, E., in press. Morphometric analysis of Aptian *Assipetra infracretacea* and Rucinolithus terebrodentarius nannoliths: implications for taxonomy, biostratigraphy, and paleoceanography. *Mar. Micropaleo*.

van Andel, T.H., 1975. Mesozoic/Cenozoic calcite compensation depth and the global distribution of calcareous sediments. *Earth Planet. Sci. Lett.,* 26:187–194.

Walter, L.M. and Morse, J.M., 1984. Reactive surface area of skeletal carbonates during dissolution: effect of grain size. *J. Sediment. Petrol.* 54:1081–1090.

Weissert, H., 1989. C-isotope stratigraphy, a monitor of paleoenvironmental change: a case study from the Early Cretaceous. *Surv. Geophys.,* 10:1–61.

Weissert, H., and Lini, A., 1991. Ice age interludes during the time of Cretaceous greenhouse climate? *In* Müller, D.W., McKenzie, J.A., and Weissert, H. (Eds.), *Controversies in Modern Geology: Evolution of Geological Theories in Sedimentology, Earth History and Tectonics:* New York (Academic Press), 173–191.

Wilson, P.A., and Norris, R.D., 2001. Warm tropical ocean surface and global anoxia during the mid-Cretaceous period. *Nature,* 412:425-429.

Wilson, P.A., and Opdyke, B.N., 1996. Equatorial sea-surface temperatures for the Maastrichtian revealed through remarkable preservation of metastable carbonate. *Geology,* 24:555–558.

Wright, A.A., Bleil, U., Monechi, S., Michel, H.V., Shackleton, N.J., Simoneit, B.R.T., and Zachos, J.C., 1985. Summary of Cretaceous/Tertiary boundary studies, Deep Sea Drilling Project Site 577, Shatsky Rise. *In* Heath, G.R., Burckle, L.H., et al., *Init. Repts. DSDP,* 86: Washington (U.S. Govt. Printing Office), 799–804.

Wright, J.D., and Miller, K.G., 1993. Southern Ocean influences on Late Eocene to Miocene deep-water circulation. *In* Kennett, J.P., and Warnke, D.A. (Eds.), *The Antarctic Paleoenvironment: A Perspective on Global Change.* Antarct. Res. Ser., 60:1–25.

Zachos, J.C., and Arthur, M.A., 1986. Paleoceanography of the Cretaceous/Tertiary boundary event: inferences from stable isotopic and other data. *Paleoceanography,* 1:5–26.

Zachos, J.C., Arthur, M.A., and Dean, W.E., 1989. Geochemical evidence for suppression of pelagic marine productivity at the Cretaceous/Tertiary boundary. *Nature,* 337:61–64.

Zachos, J.C., Breza, J.R., and Wise, S.W., 1992a. Early Oligocene ice-sheet expansion on Antarctica: stable isotope and sedimentological evidence from Kerguelen Plateau, southern Indian Ocean. *Geology,* 20:569–573.

Zachos, J.C., Lohmann, K.C., Walker, J.C.G., and Wise, S.W., Jr., 1993. Abrupt climate changes and transient climates during the Paleogene: a marine perspective. *J. Geol.,* 101:191–213.

Zachos, J.C., Quinn, R.M., and Salamy, K., 1996. High resolution (10^4 yr) deep-sea foraminiferal stable isotope records of the Eocene-Oligocene climate transition. *Paleoceanography,* 11:251–266.

Zachos, J.C., Rea, D.K., Seto, K., Niitsuma, N., and Nomura, R., 1992b. Paleogene and early Neogene deep water history of the Indian Ocean: inferences from stable isotopic records. *In* Duncan, R.A., Rea, D.K., Kidd, R.B., von Rad, U., and Weissel, J.K. (Eds.), *Synthesis of Results from Scientific Drilling in the Indian Ocean.* Geophys. Monogr., Am. Geophys. Union, 70:351–386.

Zachos, J.C., Stott, L.D., and Lohmann, K.C., 1994. Evolution of early Cenozoic marine temperatures. *Paleoceanography,* 9:353–387.

Zahn, R., Rushdi, A., Pisias, N.G., Bornhold, B.D., Blaise, B., and Karlin, R., 1991. Carbonate deposition and benthic $\delta^{13}C$ in the subarctic Pacific: implications for changes of the oceanic carbonate system during the past 750,000 years. *Earth Planet. Sci. Lett.,* 103:116–132.

TABLE CAPTIONS

Table T1. Leg 198 operations summary.

Table T2. Locations, depths, maximum ages, and ages of major unconformities at Shatsky Rise sites.

Table T3. Elemental compositions, carbonate contents, and results from Rock-Eval pyrolysis of organic-rich horizons from Shatsky Rise.

FIGURE CAPTIONS

Figure F1. Location of topographic highs in the Western Pacific Basin.

Figure F2. Relief map of Shatsky Rise showing location of Leg 198 sites. Site 1207 is located on the Northern High, Site 1208 is on the Central High, and Sites 1209–1214 are on the Southern High.

Figure F3. Magnetic lineations across Shatsky Rise and trace of the hotspot from Nakanishi et al. (1989), showing previously drilled DSDP and ODP sites on the southern plateau.

Figure F4. Reconstruction of position of Shatsky Rise across the Pacific. After McNutt and Fischer (1987) and R.L. Larson (pers. comm., 2000).

Figure F5. Lithologic columns from previous DSDP and ODP sites on Shatsky Rise showing age, lithology, and prominent unconformities (after Sliter and Brown, 1993). Water depths for each site are listed beneath the site number. Bk = black.

Figure F6. Compilation of benthic foraminiferal oxygen isotopic composition from 34 DSDP and ODP sites plotted vs. age (from Zachos et al., 1993; J. Zachos et al., unpubl. data). MME = mid-Maastrichtian event, LPTM = late Paleocene thermal maximum, OAE = oceanic anoxic event.

Figure F7. Carbon and oxygen isotope values of planktonic and benthic foraminifers from the upper Paleocene of Sites 527 (closed squares), 690 (open circles, open diamonds), and 865 (closed circles, closed diamonds, crosses) (Kennett and Stott, 1991; Bralower et al., 1995; Thomas and Shackleton, 1996; J. Zachos and D. Rea, unpubl. data) plotted vs. age.

Figure F8. Compilation of DSDP/ODP isotope data from Albian to Maastrichtian (from Huber et al., 1995; Fassell and Bralower, 1999; Stott and Kennett, 1990; Barrera and Huber, 1990; Barrera, 1994; Barrera and Savin, 1999). Dashed lines connecting benthic foraminiferal data represent unconformities. CTBI = Cenomanian/Turonian boundary interval.

Figure F9. Mid-Cretaceous record of black shales and oceanic anoxic events (OAEs) in the context of the carbon isotopic record (Erbacher et al., 1996; Bralower et al., 1999), changing global sea level (Haq et al., 1988), seawater $^{87}Sr/^{86}Sr$ (Bralower et al., 1997a), LIP emplacement (Larson, 1991a), plankton evolution (Erbacher and Thurow, 1997; R.M. Leckie, et al., unpubl. data), and platform drowning (R.M. Leckie, et al., unpubl. data).

Figure F10. Worldwide volume of oceanic plateaus, seamount chains and continental flood basalts plotted as a function of geologic time according to Harland et al. (1990) (after Larson, 1991b).

Figure F11. Interpretation of seismic reflection profile across Site 1207. Mustard unit = middle Miocene to Holocene, light green = Campanian–Turonian, medium green = Cenomanian to Aptian, and dark green is Barremian to Valanginian. Eroded or slumped layers are seen on north and south ends of the Campanian–Turonian unit. Numbers across the figures are shotpoints. R = reflector.

Figure F12. Summary diagram of coring results for Hole 1207A plotted on the meters below seafloor (mbsf) scale. Maximum penetration measured with the drill pipe was 256.6 mbsf. The core recovery column is a graphic representation of the cored and recovered intervals for this hole. Large gaps in core recovery (<100% nominal recovery) near the base of the hole are primarily the result of coring problems that arose when chert was encountered. The graphic lithology column presents the major sediment types and defined lithologic units. The depth-age model is represented by calcareous nannofossil (red diamonds) and planktonic foraminiferal (black crosses) datum levels; dashed lines represent the boundaries between the Cretaceous/Paleocene and Oligocene/Miocene. Mass accumulation rates were calculated for total sediment (green open circles) and carbonate only (blue triangles). The color reflectance lightness parameter (L*) (purple points) was measured every 2.5 cm, and the percentage calcium carbonate ($CaCO_3$) values are shown for comparison. Multisensor track (MST) magnetic susceptibility (brown points) and GRA wet bulk density (dark blue points) were measured every 2.5 cm, and index properties wet bulk density measurements (red circles) were completed on average once per section. MST *P*-wave velocity (light blue points) was determined every 2.5 cm, and discrete *P*-wave measurements (green circles) averaged at least one per section for comparison. Index properties determinations of porosity (blue squares) and percentage water content (red circles) were completed once per section on average.

Figure F13. Changes in ocean circulation that led to cycles in upper Miocene to Holocene section. **A.** Circulation during warm/light cycle member. **B.** Circulation during cold/dark cycle member.

Figure F14. Hypothesized sequence of events that produced major Campanian–Miocene unconformity on the Northern High of Shatsky Rise.

Figure F15. Interpretation of seismic reflection profile across Site 1208. Mustard unit = middle Miocene to Holocene, light brown = lower Miocene and Paleogene, light green = Campanian, and medium green = Albian.

Figure F16. Summary diagram of coring results for Hole 1208A plotted on the meters below seafloor (mbsf) scale. The maximum penetration measured with the drill pipe was 392.3 mbsf. For details about figure symbols and descriptions see Figure F12.

Figure F17. Change in circulation in North Pacific associated with the closure of the Indonesian Seaway. The size of arrows indicates intensity of currents (after Kennett et al., 1985).

Figure F18. Interpretation of the evolution of stratigraphic section at Site 1208 based on drilling results and seismic section.

Figure F19. Interpretation of seismic reflection profile across Site 1209. Mustard unit = Miocene to Holocene, light brown = Paleogene, and light green = Maastrichtian.

Figure F20. Summary diagram of coring results at Site 1209 plotted on the meters composite depth (mcd) scale. Maximum penetration measured with the drill pipe was 307.5 mbsf. Small gaps (typically 0.5–2.0 m) in core recovery, revealed by hole-to-hole correlation, occur even when nominal core recovery is 100% or more. For details about figure symbols and descriptions see Figure F12.

Figure F21. Summary of stratigraphy and lithological succession from Sites 1207 to 1214. Lithology is plotted against time to show duration of periods of deposition and location of unconformities. Southern High Sites 1211 through 1214 are ordered by present-day water depth.

Figure F22. Paleontological summary of the LPTM interval in Section 198-1209B-22H-1. The LO of *Morozovella velascoensis,* which defines the boundary between Zone P5 and Subzone P6a, lies between Samples 198-1209B-22H-1, 74–75 cm and 9–10 cm, probably close to the latter sample. Depths listed along the lithology column are in meters below seafloor (mbsf). FO = first occurrence.

Figure F23. Paleontological summary of the Cretaceous/Paleocene boundary in Holes 1209A and 1209C. Samples described include planktonic foraminifers (F) and nannofossils (N).

Figure F24. Cores that contain the appearance and sudden disappearance of prisms of *Inoceramus*. In Sections 198-1209C-21H-1 through 198-1209C-21H-21H-3, and 198-1210B-28H-5 and 1209B-28H-6. The interval shown lies in the same biostratigraphic interval as the extinction in the deep sea. The small arrows indicate positions of prisms in cores, and large arrows show the disappearance level.

Figure F25. Interpretation of seismic reflection profile across Site 1210. Mustard unit = Miocene to Holocene, light brown = Paleogene, light green = Maastrichtian. CPD = common depth point.

Figure F26. Summary diagram of coring results at Site 1210 plotted on the meters composite depth (mcd) scale. The maximum penetration measured with the drill pipe was 377.0 mbsf. Multisensor track (MST) magnetic susceptibility (brown points) and GRA wet bulk density (dark blue points) were measured every 3.0 cm. For details about figure symbols and descriptions see Figure F12.

Figure F27. Comparison of magnetic susceptibility records for Holes 1210A (black) and 1210B (blue). The data show the location of critical events (LPTM = late Paleocene thermal maximum, E/O = Eocene/Oligocene boundary, and K/T = Cretaceous/Tertiary boundary) as well as significant gaps in the records of individual holes.

Figure F28. Total reflectance (L*) records for the Eocene/Oligocene (E/O) boundary interval at four sites (Holes 1209A, 1210A, 1211A and 1208A) in a depth transect across Shatsky Rise. Reflectance (L*) is a rough indicator of $CaCO_3$ content as demonstrated in the Hole 1210A plot where $CaCO_3$ is plotted as well. These records suggest that $CaCO_3$ increased across the Eocene–Oligocene transition, possibly because of a deepening of the lysocline and calcite compensation depth (CCD). Note that the deepest record (Site 1208) has the lowest L* values and highest amplitude of variation of all, probably because it is near the lysocline depth. Water depths are indicated at the bottom of each plot.

Figure F29. Interpretation of seismic reflection profile across Site 1211 based on coring results as well as results of Sliter (1992) and Sliter and Brown (1993). Mustard unit = Miocene to Holocene, light brown = Paleogene, light green = Maastrichtian–Campanian, medium green = Cenomanian through Aptian; dark green is Neocomian. CDP = common depth point.

Figure F30. Summary diagram of coring results at Site 1211 plotted on the meters composite depth (mcd) scale. The maximum penetration measured with the drill pipe was 169.9 mbsf. Multisensor track (MST) magnetic susceptibility (brown points) and GRA wet bulk density (dark blue points) were measured every 3.0 cm. For details about figure symbols and descriptions see Figure F12.

Figure F31. Age-depth curves for Sites 1209, 1210, 1211, and 1212 based on shipboard biostratigraphy. Circles = planktonic foraminiferal datums, squares = nannofossil datums, P. = Pleistocene, Pl. = Pliocene.

Figure F32. Lithology of the Eocene/Oligocene boundary interval in Core 198-1211C-9H. Arrow points to the last observed occurrence of *Hantkenina* sp., the planktonic foraminiferal datum that defines the boundary.

Figure F33. Correlation of LPTM sections recovered in Holes 1211A, 1211B, and 1211C.

Figure F34. Summary diagram of coring results at Site 1212 plotted on the meters composite depth (mcd) scale. The maximum penetration measured with the drill pipe was 207.6 mbsf. Multisensor track (MST) magnetic susceptibility (brown points) and GRA wet bulk density (dark blue points) were measured every 3.0 cm. For details about figure symbols and descriptions see Figure F12.

Figure F35. Interpretation of seismic reflection profile across Site 1213 based on coring results. Mustard unit = Pliocene to Holocene, medium green = Albian through Aptian, dark green = Neocomian, and brown = igneous sill unit (Unit IV) and basement. Lithologic units and subunits and depths (in meters below seafloor [mbsf]) are indicated.

Figure F36. Summary of lithostratigraphy for Sites 1207–1214. TD = total depth.

Figure F37. Summary of generalized chert color by age for the Cretaceous at ODP Leg 198 and DSDP Leg 32 sites on Shatsky Rise. Red represents oxidized hues of brown, orange, red and pink, whereas black represents reduced hues of olive-green, gray and black. Note the similar regional temporal trends in chert color.

Figure F38. Lithology and carbonate, organic carbon and pyrolysis hydrogen indices for lower Aptian sedimentary rocks recovered at Sites 1207, 1213, and 1214 on Shatsky Rise. Note that Sites 1207 and 1213 recovered very organic C_{org}-rich intervals representing OAE1a. Homog. clayst. = homogeneous claystone.

Figure F39. Total reflectance (L*) records for the Paleocene/Eocene boundary interval at four sites (Holes 1209C, 1210A, 1212A, and 1211A) in a depth transect across Shatsky Rise. Reflectance (L*) is a rough indicator of $CaCO_3$ content as demonstrated in the Hole 1210A plot where $CaCO_3$ is plotted as well. The abrupt decrease in L* denoted between the ages of 58.95 and 54.83 Ma represents an hypothesized shoaling of the lysocline associated with the LPTM event. Water depths are indicated at the bottom of each plot.

Figure F40. Percentage estimates of biosiliceous material of late Neogene to Quaternary sediments from smear slides plotted vs. depth in meters below seafloor (mbsf) for Sites 1207–1213. Site 1214 has been excluded on the basis that only 1.32 m of late Neogene–Quaternary sediments were recovered. This figure illustrates that biosiliceous material is more abundant within the late Neogene–Quaternary sections on the Northern and Central High than on the Southern High of Shatsky Rise. The expanded Pleistocene to Miocene sedimentary sections at Sites 1207 and 1208 can partly be attributed to relatively high sea-surface productivity inferred from the higher occurrence of diatoms, radiolarians, and silicoflagellates relative to the other sites further south. The trends in biogenic silica abundance correlate strongly with sedimentation rate, as the more southerly Sites 1209 through 1212 were characterized by lower sedimentation rates.

Figure F41. Photomicrographs from sediment containing diagenetic "green bands." (**A**) Plane-polarized light and (**B**) cross-polarized light images of clayey nannofossil ooze with foraminiferal tests (arrow) containing authigenic smectite clays (note that black dendritic areas are epoxy used to impregnate the soft sediment); the bottom half of each image is within a "green band." (**C**) plane and (**D**) polarized light photomicrograph of a burrow in clayey nannofossil ooze filled with volcanic glass. Burrow (arrow; glass is isotropic) shows authigenic smectite (saponite) filling pore spaces and part of foraminifer test.

Figure F42. Age-depth plots for Sites 1207–1214 based on calcareous nannofossil and planktonic foraminiferal datums. Horizontal lines represent unconformities in the sections. Critical events are marked by thin gray vertical bands. Widespread unconformities are indicated by the wide blue vertical bands.

Figure F43. Mass accumulation rates for bulk sediment and carbonate fraction for Sites 1207–1212. Mass accumulation rates were determined using dry bulk density and carbonate content data through linear sedimentation rate segments. No rates were determined at Sites 1213 and 1214.

Figure F44. Downhole gamma radiation and resistivity logs from Holes 1207B and 1213B illustrating the form and setting of the OAE1a black shale.

Figure F45. Chert layers in Hole 1207B as observed in FMS resistivity images.

Figure F46. Magnetic susceptibility data for the uppermost Cretaceous to lower Eocene interval at Sites 1209–1212 showing the position of critical events as well as cycles. LPTM = late Paleocene thermal maximum, K/T = Cretaceous/Tertiary boundary.

Figure F47. Spliced magnetic susceptibility data covering the Eocene/Oligocene boundary and Eocene interval of Sites 1211, 1210, and 1209 vs. meters composite depth (mcd). Systematic changes in cycle amplitude and frequency are consistent from site to site suggesting that these changes reflect regional paleoceanographic processes. The cycle packages are distinct enough to allow for detailed correlation between sites.

Figure F48. Total color reflectance data on a timescale for Holes 1208A and 1209A plotted along with orbital obliquity and eccentricity for the (**A**) 0- to 2-Ma and (**B**) 3- to 5-Ma time intervals. These data suggest that the dominant cycle frequency over the last 0.7 m.y. is near that of the 100-k.y. eccentricity cycle. From 0.7 to 2.6 Ma, the dominant period shifts toward a higher frequency close to that associated with the 40-k.y. obliquity cycle. A long wavelength oscillation with a period of roughly 1.0 to 1.25 m.y. appears in the total color reflectance record from Site 1209 over the period 3 to 5 Ma. Comparison with the orbital curves suggest that this cycle may be in phase with the long period 1.25-m.y. cycle of obliquity.

Figure F49. Relationship between (**A**) sedimentation rate, (**B**) mass accumulation rate (MAR), (**C**) SO_4^{2-} reduction, (**D**) NH_4^+ production, and (**E**) CH_4 generation on Shatsky Rise.

Figure F50. Oxygen and hydrogen indices for samples from lower Aptian organic-rich horizons (OAE1a; Table T3) plotted on a modified van Krevelen diagram. The characteristics of organic-rich samples from Holes 1207B and 1213B, and from the Aptian at Holes 463 and 866A in the mid-Pacific are also shown. Data for Sites 463 and 866A are compiled from Dean et al. (1981), Mélières et al. (1981), and Baudin et al. (1995). The size of the data points is proportional to organic carbon contents. The lines designated I, II and III represent the evolutionary trends with thermal maturation of the three major kerogen types (Tissot et al., 1974). OI = oxygen index.

Figure F51. GC-MS traces of aliphatic hydrocarbons and ketones for representative samples from Holes 1207B, 1213B and 1214A. For the aliphatic hydrocarbon traces, the numbers refer to *n*-alkanes; other peak assignments and identities are given in the lists.

Figure F52. Plots of coring rate vs. depth for three Cretaceous sections on Shatsky Rise. Coring rate may be a function of the frequency of hard chert layers in the section.

Figure F53. Cretaceous/Tertiary boundary on Shatsky Rise in Sections 198-1209A-25H-6, 198-1209C-15H-3, 198-1210A-24H-4, 198-1210B-24H-1, 198-1211A-15H-4, 198-1211B-15H-3, 198-1211C-15H-3, 198-1212A-12H-7, and 198-1212B-11H-7.

Figure F54. LPTM on Shatsky Rise in Sections 198-1209A-21H-7, 198-1209B-22H-1, 198-1209C-11H-3, 198-1210A-20H-6, 198-1210B-20H-3, 198-1211A-13H-6, and 198-1211A-13H-5, 198-1211B-13H-4 (unconformity above clay-rich seam), 198-1211C-13H-2, and 198-1211C-13H-3, 198-1212A-10H-1, 198-1212B-9H-5.

Figure F55. Age vs. depth plots for Leg 198 sites constructed from magnetic stratigraphy using the timescale of Cande and Kent (1995). Only Neogene sediment cores produced an interpretable magnetic stratigraphy.

Figure F56. Stratigraphy of Cretaceous sections on Shatsky Rise showing recovered intervals in blue and nonrecovered intervals in white. Purple intervals indicate widespread unconformities on Shatsky Rise. Water depths are listed in parentheses for each site. KS = zonation of Sliter (1992).

Table T1. Leg 198 operations summary.

Hole	Latitude	Longitude	Water depth (mbsf)	Number of cores	Length cored (m)	Length recovered (m)	Recovery (%)	Interval drilled (m)	Total penetration (mbsf)	Time on site (hr)	Time on site (days)
1207A	37°47.4287′N	162°45.0530′E	3100.6	29	223.0	213.62	95.8	33.6	256.6	77.00	3.21
1207B	37°47.4370′N	162°45.0534′E	3100.8	49	465.8	60.22	12.9	157.0	622.8	119.25	4.97
			Site 1207 totals:	78	688.8	273.84	39.8	190.6	879.4	196.25	8.18
1208A	36°7.6301′N	158°12.0952′E	3345.7	42	392.3	345.89	88.2	0.0	392.3	62.25	2.59
			Site 1208 totals:	42	392.3	345.89	88.2	0.0	392.3	62.25	2.59
1209A	32°39.1001′N	158°30.3560′E	2387.2	28	259.6	262.27	101.0	0.0	259.6	29.50	1.23
1209B	32°39.1081′N	158°30.3564′E	2387.4	32	297.6	303.20	101.9	0.4	298.0	41.75	1.74
1209C	32°39.0995′N	158°30.3653′E	2387.3	23	202.2	200.60	99.2	105.3	307.5	45.25	1.89
			Site 1209 totals:	83	759.4	766.07	100.9	105.7	865.1	116.50	4.85
1210A	32°13.4123′N	158°15.5618′E	2573.6	27	241.4	249.30	103.3	1.0	242.4	30.50	1.27
1210B	32°13.4203′N	158°15.5623′E	2573.2	42	365.5	376.36	103.0	11.5	377.0	57.75	2.41
			Site 1210 totals:	69	606.9	625.66	103.1	12.5	619.4	88.25	3.68
1211A	32°0.1300′N	157°50.9999′E	2907.5	18	158.9	162.72	102.4	0.0	158.9	27.75	1.16
1211B	32°0.1391′N	157°51.0002′E	2906.2	19	168.3	181.90	108.1	1.6	169.9	24.25	1.01
1211C	32°0.1224′N	157°51.0002′E	2906.9	15	138.3	140.87	101.9	0.0	138.3	31.75	1.32
			Site 1211 totals:	52	465.5	485.49	104.3	1.6	467.1	83.75	3.49
1212A	32°26.9000′N	157°42.7016′E	2682.5	13	101.6	116.94	115.1	0.0	101.6	29.00	1.21
1212B	32°26.9070′N	157°42.7002′E	2680.6	27	192.8	180.50	93.6	14.8	207.6	32.50	1.35
			Site 1212 totals:	40	294.4	297.44	101.0	14.8	309.2	61.50	2.56
1213A	31°34.6402′N	157°17.8605′E	3882.8	21	198.9	43.09	21.7	0.0	198.9	45.00	1.88
1213B	31°34.6576′N	157°17.8621′E	3882.8	33	304.7	60.46	19.8	189.7	494.4	136.00	5.67
			Site 1213 totals:	54	503.6	103.55	20.6	189.7	693.3	181.00	7.54
1214A	31°52.0254′N	157°28.7178′E	3401.6	25	235.5	16.49	7.0	0.0	235.5	68.25	2.84
			Site 1214 totals:	25	235.5	16.49	7.0	0.0	235.5	68.25	2.84
			Leg 198 totals:	443	3946.4	2914.43	73.9	514.9	4461.3	857.75	35.74

Table T2. Locations, depths, maximum ages, and ages of major unconformities at Shatsky Rise sites.

Site	Latitude (N)	Longitude (E)	Water depth (mbsf)	Penetration (m)	Maximum age	Major unconformities
47	32°26.9′	157°42.7′	2689	129	Maastrichtian	Eocene/Miocene
48	32°24.5′	158°1.3′	2619	72	Maastrichtian	Miocene/Maastrichtian
49	32°24.1′	156°36.0′	4282	20	Tithonian	Pleistocene/Tithonian
50	32°24.2′	156°34.3′	4487	45	Tithonian	Pleistocene/Tithonian
305	32°00.13′	157°51.00′	2903	631	Valanginian	Mio./Oligo., Paleoc./Eoc.
306	31°52.02′	157°28.71′	3399	381	Berriasian	Pleistocene/Albian
577	32°26.51′	157°43.40′	2675	123	Maastrichtian	Pliocene/Eocene
810	32°25.40′	157°50.73′	2634	136	Maastrichtian	Mio./Eoc./Paleoc./Maast.
1207	37°47.43′	162°45.05′	3123	623	Barremian	Miocene/Campanian

Table T3. Elemental compositions, carbonate contents, and results from Rock-Eval pyrolysis of organic-rich horizons from Shatsky Rise.

Core, section, interval (cm)	Elemental composition					Rock-Eval					
	C_{org} (%)	Nitrogen (%)	Sulfur (%)	C/N (atomic)	Carbonate (%)	S_1 (mg/g)	S_2 (mg/g)	S_3 (mg/g)	T_{max} (C)	HI (mg HC/ g TOC)	OI (mg CO_2/ g TOC)
198-1207B-											
44R-1, 60-61	34.74	1.19	10.56	25.00	0.01	13.99	147.12	7.64	401	423	21
44R-1, 76-77	10.40	0.40	1.92	22.30	0.00	3.24	54.46	2.69	403	523	25
44R-1, 103-104	1.70	0.09	1.30	16.20	0.00	0.49	7.45	0.94	417	438	55
198-1213B-											
8R-1, 47-48	10.23	0.37	2.00	23.60	0.50	2.54	51.30	2.14	418	501	20
8R-1, 63-64	25.20	0.83	4.36	25.90	0.75	6.97	127.59	5.87	404	506	23
8R-1, 96-97	2.87	0.14	0.76	17.20	0.42	0.39	10.49	6.08	422	365	211
15R-1, 9-10	2.54	0.12	2.86	17.90	49.06	0.19	10.30	12.13	424	405	477*
19R-1, 112-113	3.13	0.18	5.18	14.90	60.56	0.15	12.62	13.96	426	403	446*
198-1214A-											
23R-1, 5-7	1.38	0.08	0.23	14.80	0.75	ND	ND	ND	ND	ND	ND

Notes: HC = hydrocarbon, TOC = total organic carbon. S_1 and S_2 are peaks corresponding to free and kerogen-bound HC (respectively generated by Rock-Eval pyrolysis), S_3 is the amount of CO_2 released by thermal cracking of kerogen, T_{max} is the peak temperature of kerogen breakdown. HI = hydrogen index, OI = oxygen index. * = values enhanced by carbonate contents. ND = not determined.

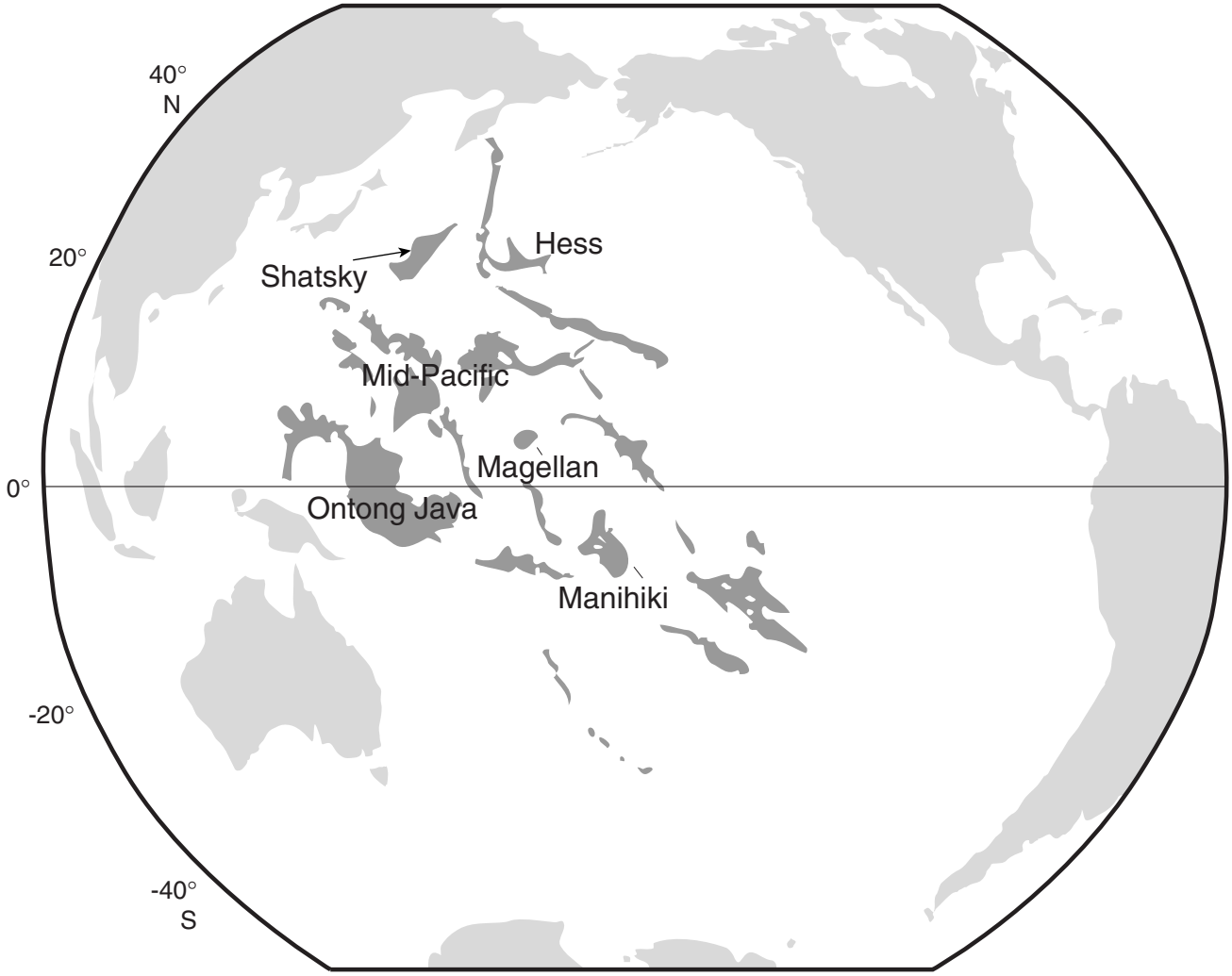
40°
N
20°
0°
-20°
-40°
S
Shatsky
Hess
Mid-Pacific
Magellan
Ontong Java
Manihiki

Figure F1

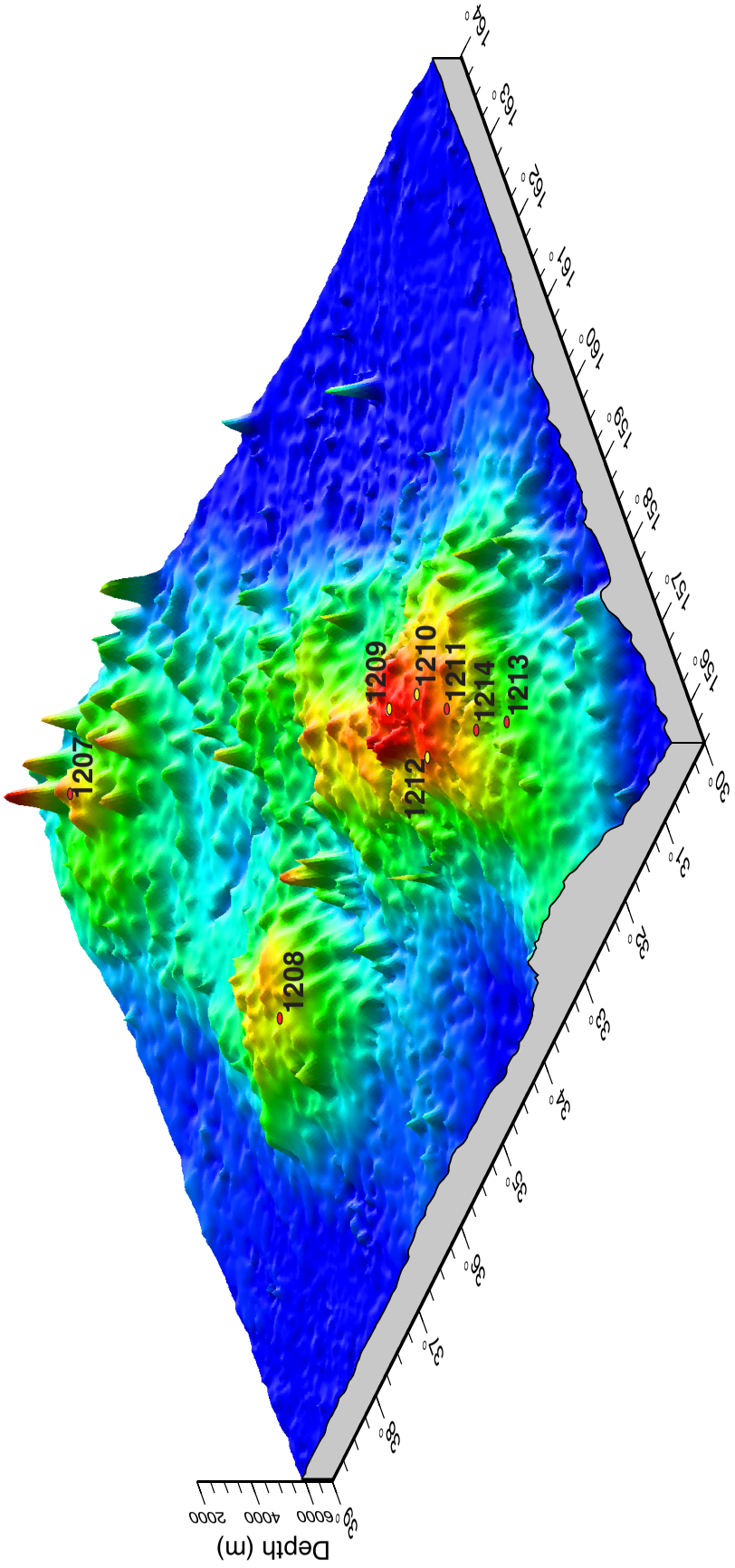
1207
1208
1209
1210
1211
1212
1213
1214
Depth (m)
2000
4000
6000
30°
31°
32°
33°
34°
35°
36°
37°
38°
39°
130°
131°
132°
133°
134°
135°
136°
137°
138°
139°
140°
141°
142°

Figure F2

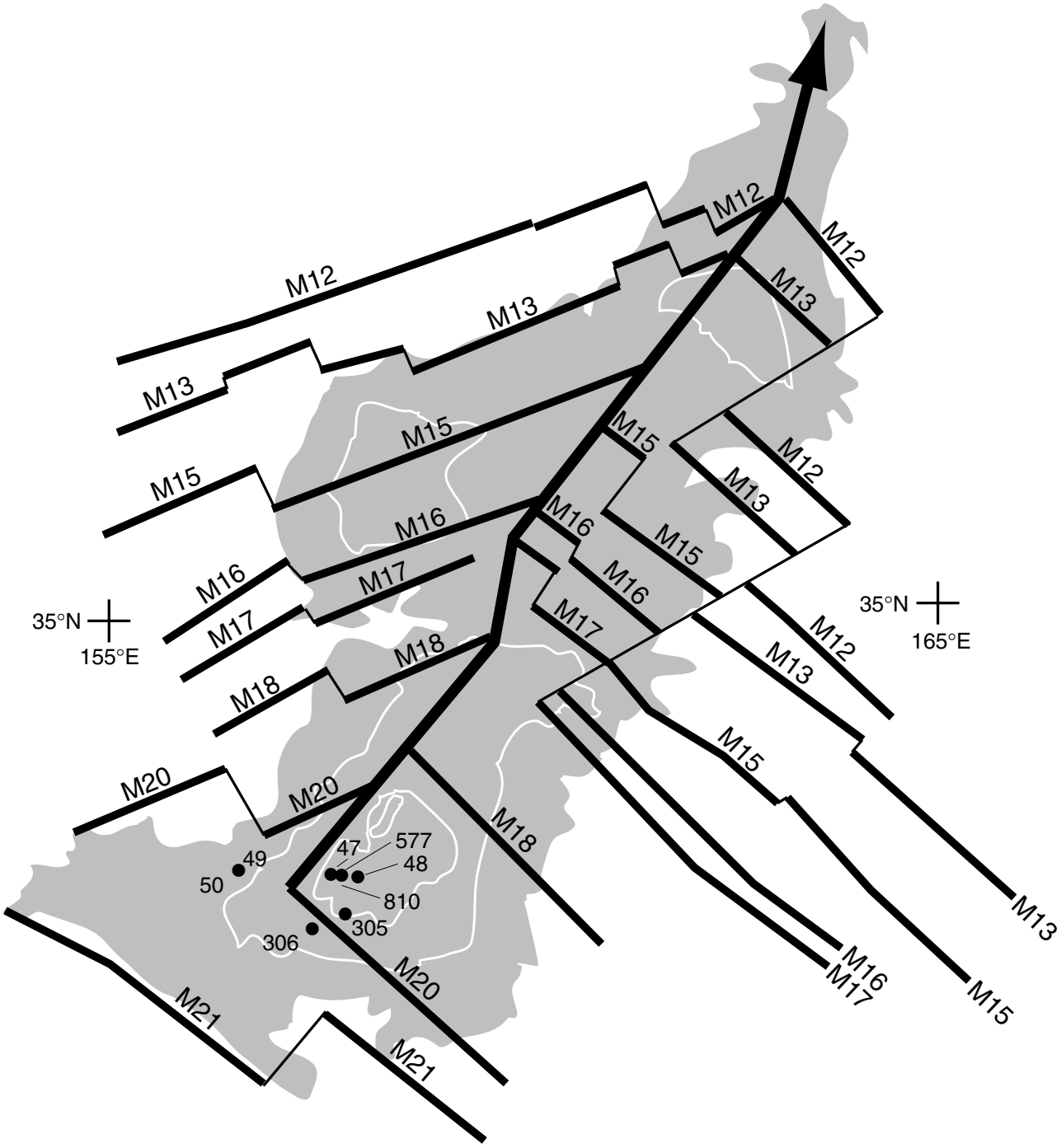
M12
M12
M12
M13
M13
M13
M15
M15
M15
M15
M12
M13
M16
M16
M16
M15
M16
M17
M17
M17
M18
M18
M18
M12
M13
M15
M20
M20
M21
M21
M16
M17
M15
M13
35°N
155°E
35°N
165°E
49
50
47
577
48
810
305
306

Figure F3

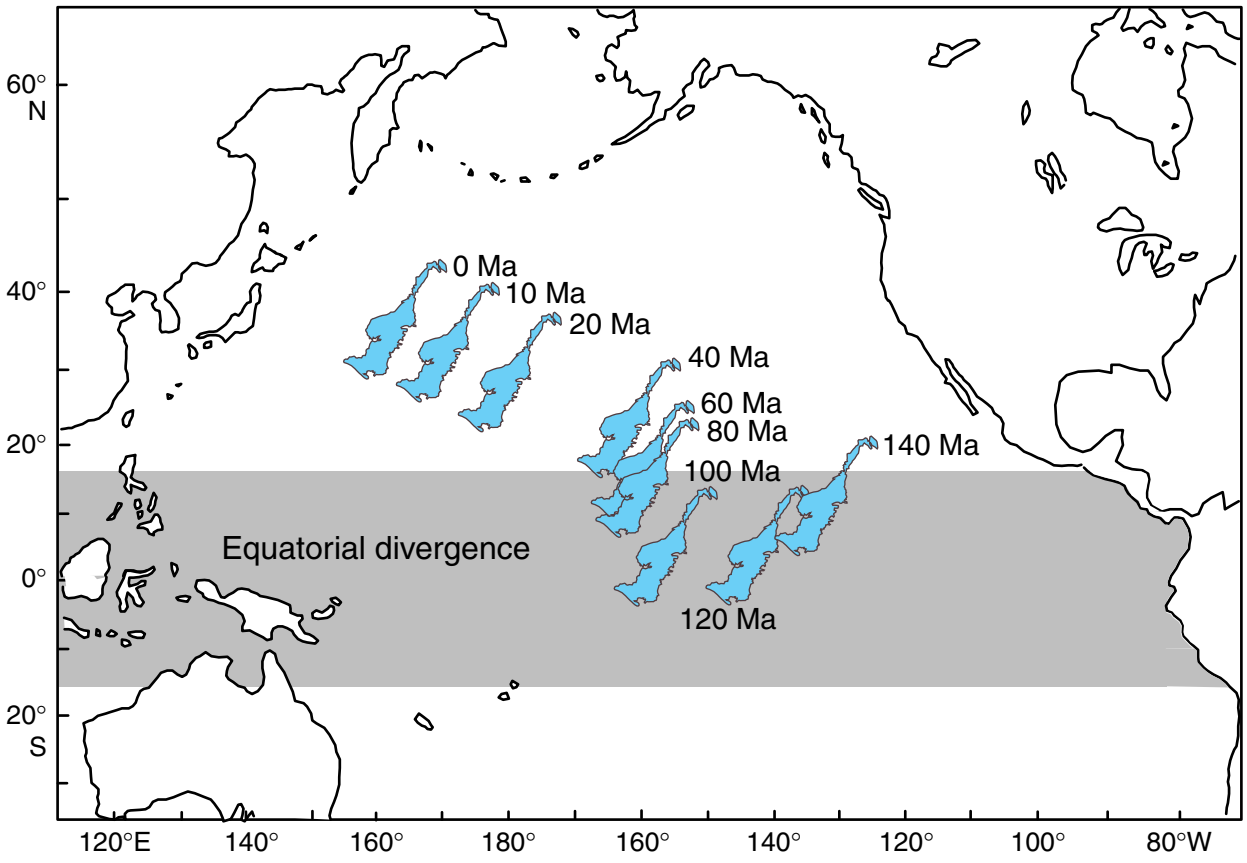
60° N
40°
20°
0°
20° S
120°E
140°
160°
180°
160°
140°
120°
100°
80°W
0 Ma
10 Ma
20 Ma
40 Ma
60 Ma
80 Ma
100 Ma
120 Ma
140 Ma
Equatorial divergence

Figure F4

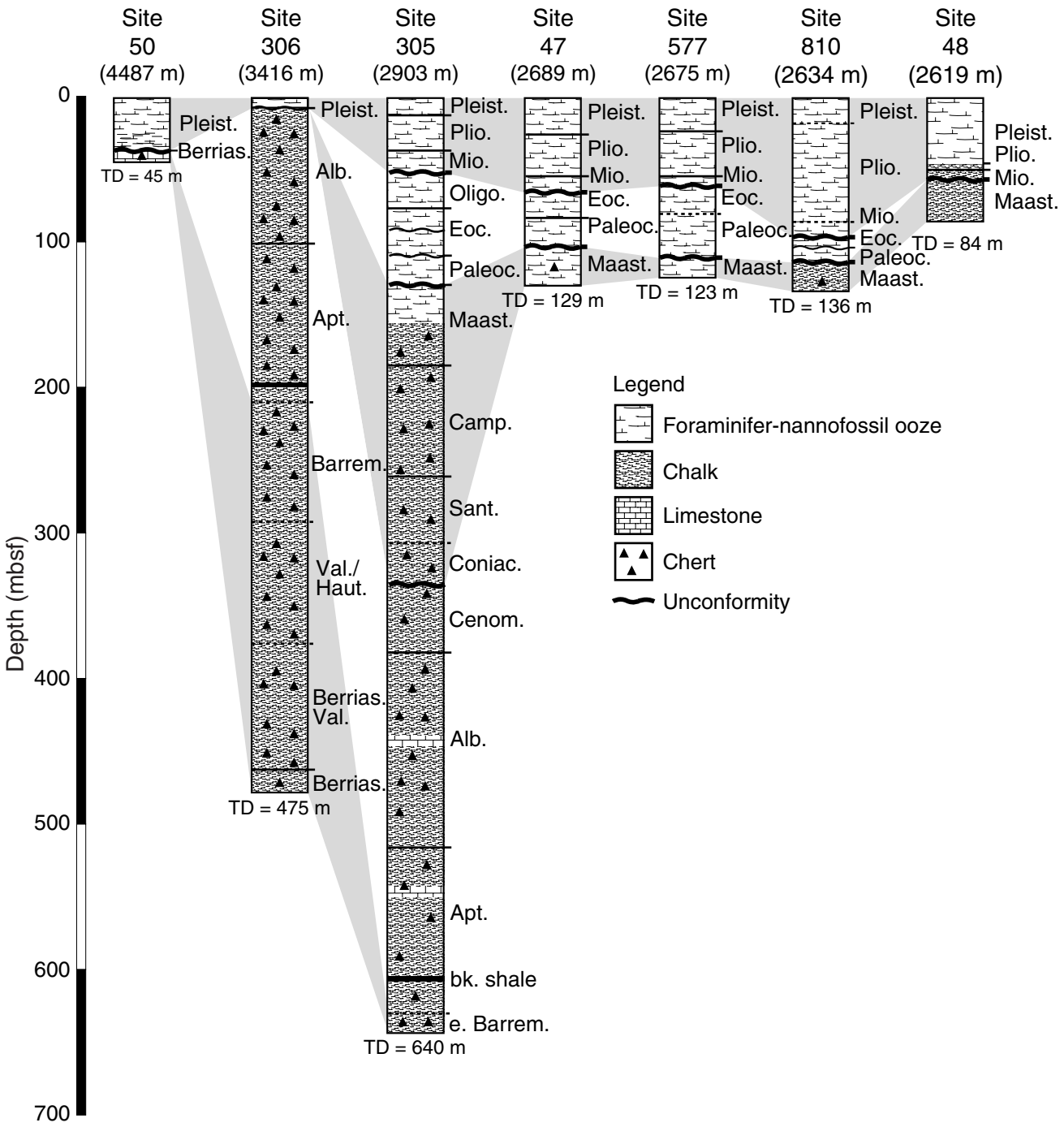
Site 50 (4487 m)
Site 306 (3416 m)
Site 305 (2903 m)
Site 47 (2689 m)
Site 577 (2675 m)
Site 810 (2634 m)
Site 48 (2619 m)
Depth (mbsf)
0
100
200
300
400
500
600
700
Pleist.
Berrias.
TD = 45 m
Alb.
Apt.
Barrem.
Val./ Haut.
Berrias. Val.
Berrias.
TD = 475 m
Plio.
Mio.
Oligo.
Eoc.
Paleoc.
Maast.
Camp.
Sant.
Coniac.
Cenom.
Alb.
Apt.
bk. shale
e. Barrem.
TD = 640 m
TD = 129 m
TD = 123 m
TD = 136 m
TD = 84 m
Legend
Foraminifer-nannofossil ooze
Chalk
Limestone
Chert
Unconformity

Figure F5

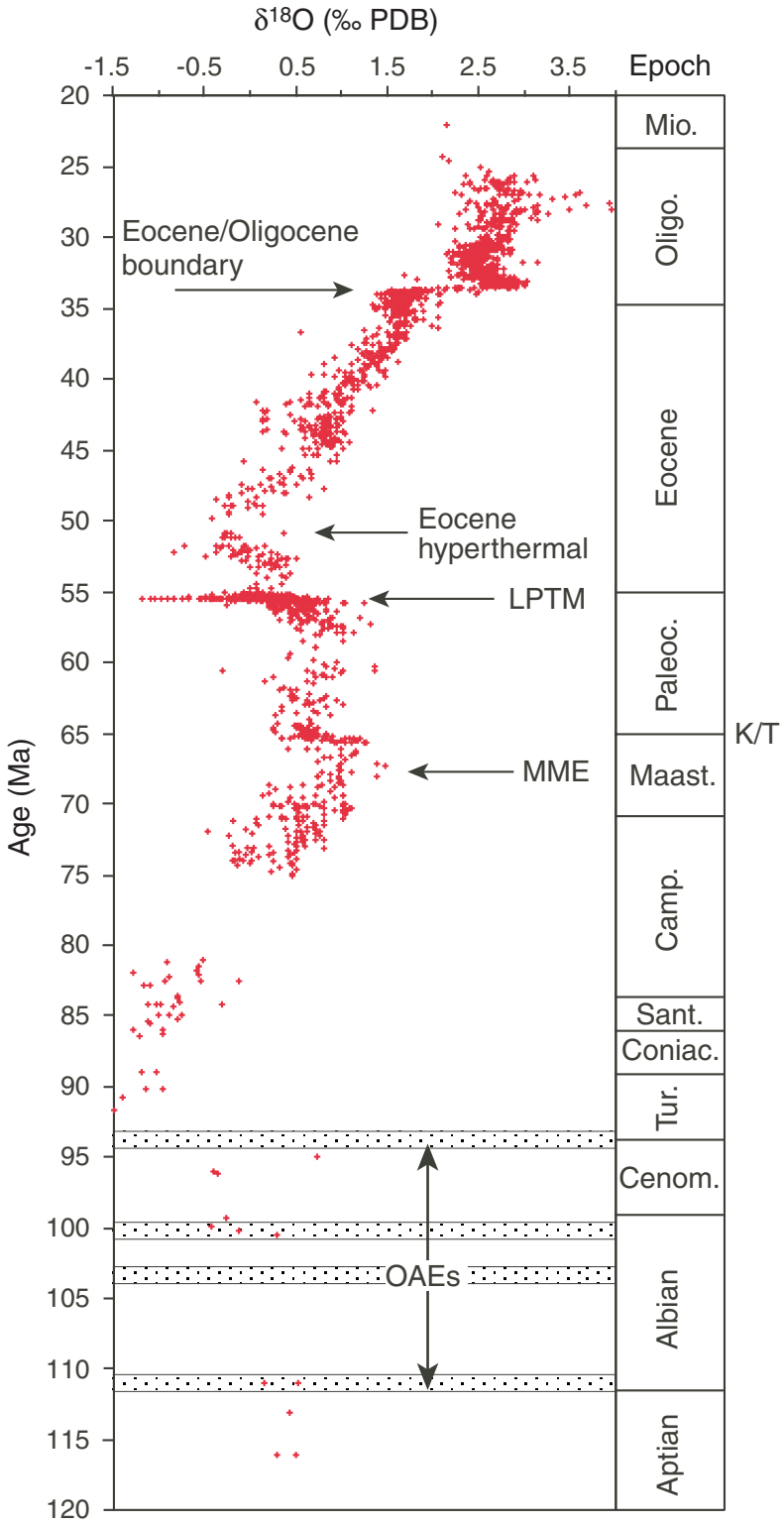
δ18O (‰ PDB)
-1.5
-0.5
0.5
1.5
2.5
3.5
Epoch
Age (Ma)
20
25
30
35
40
45
50
55
60
65
70
75
80
85
90
95
100
105
110
115
120
Eocene/Oligocene boundary
Eocene hyperthermal
LPTM
MME
OAEs
Mio.
Oligo.
Eocene
Paleoc.
Maast.
Camp.
Sant.
Coniac.
Tur.
Cenom.
Albian
Aptian
K/T

Figure F6

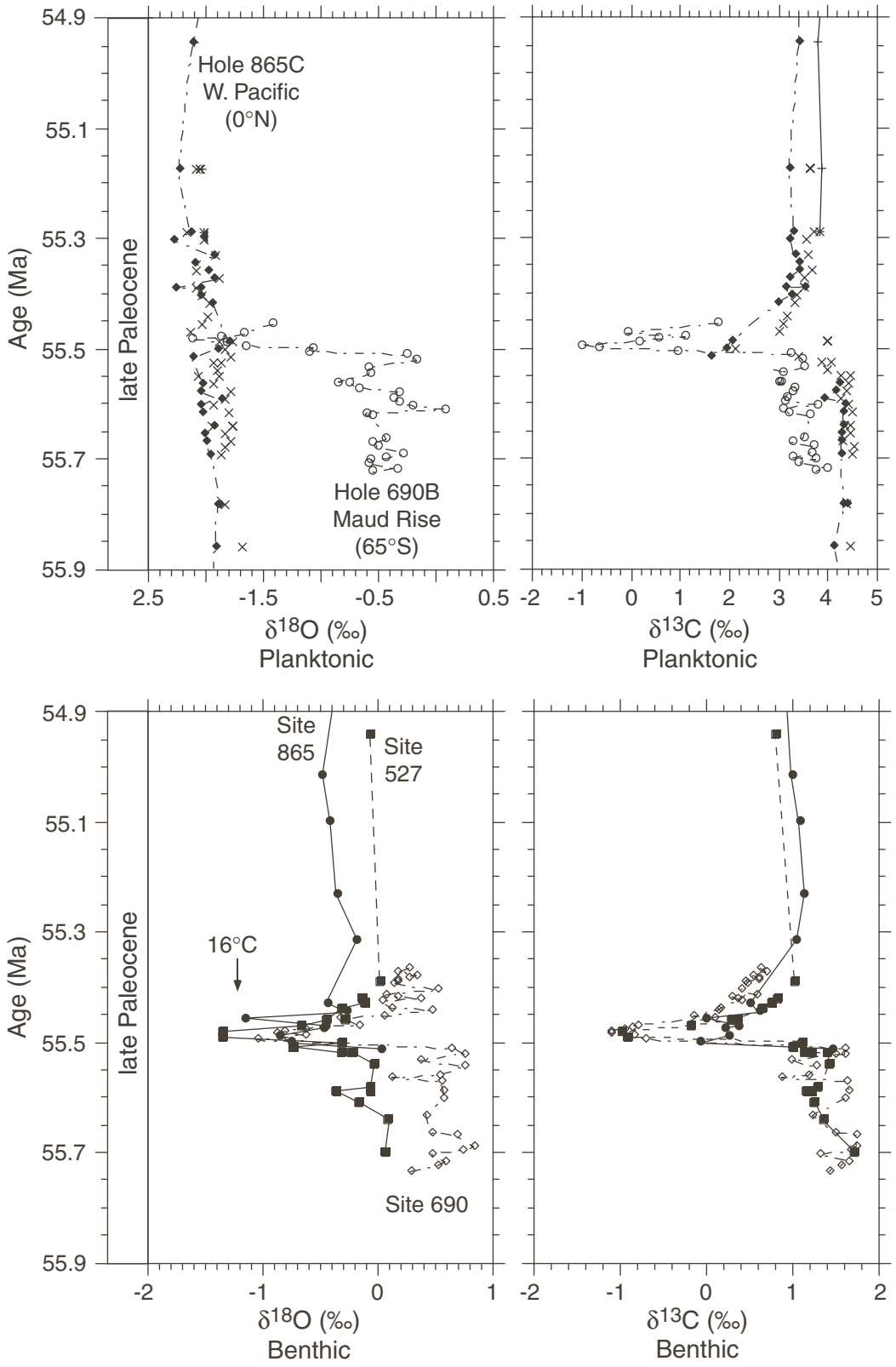
54.9
55.1
55.3
55.5
55.7
55.9
Age (Ma)
late Paleocene
Hole 865C
W. Pacific
(0°N)
Hole 690B
Maud Rise
(65°S)
2.5
-1.5
-0.5
0.5
δ18O (‰)
Planktonic
-2
-1
0
1
2
3
4
5
δ13C (‰)
Planktonic
Site
865
Site
527
16°C
Site 690
-2
-1
0
1
δ18O (‰)
Benthic
-2
-1
0
1
2
δ13C (‰)
Benthic

Figure F7

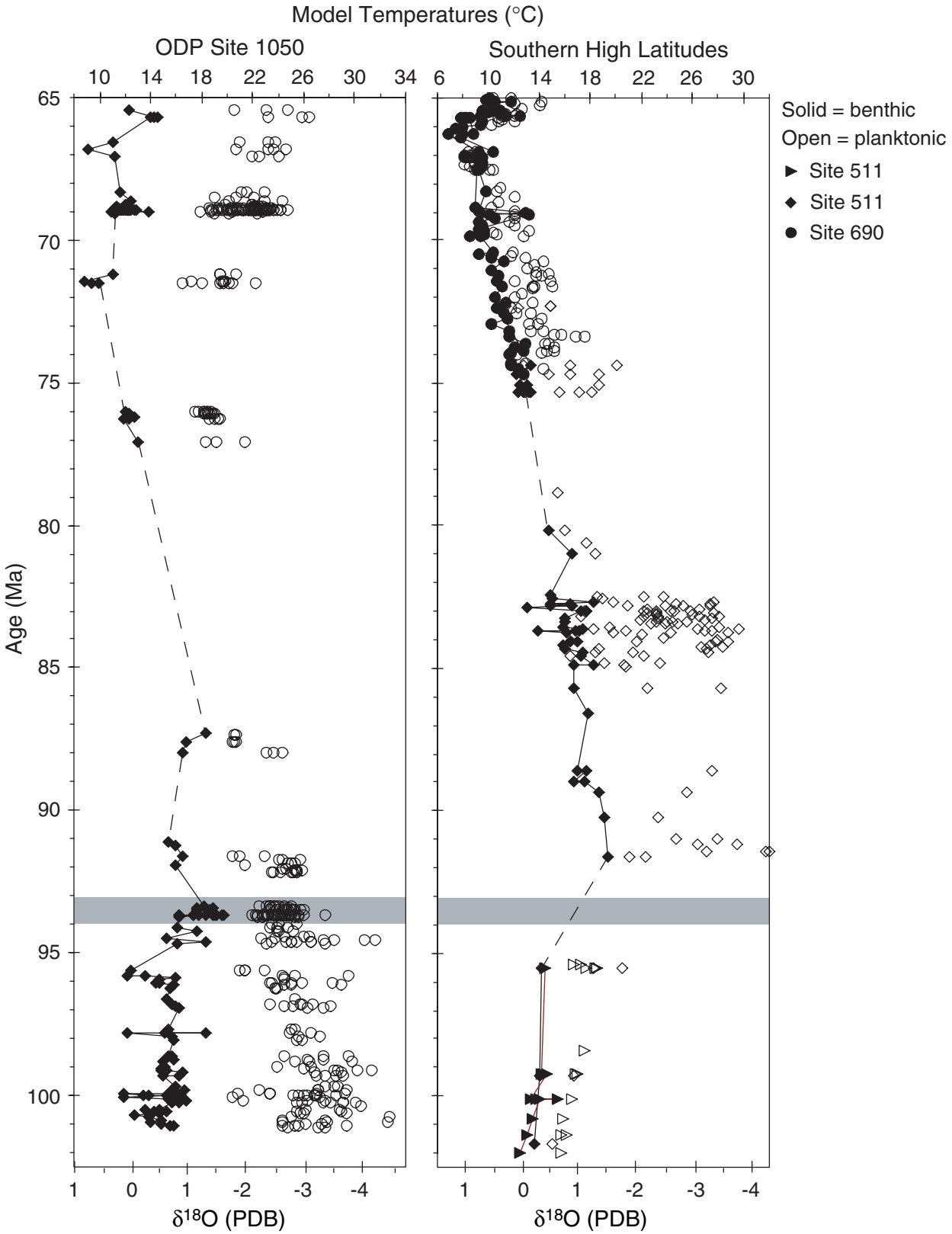
Model Temperatures (°C)
ODP Site 1050
Southern High Latitudes
10 14 18 22 26 30 34
6 10 14 18 22 26 30
Solid = benthic
Open = planktonic
Site 511
Site 511
Site 690
Age (Ma)
65
70
75
80
85
90
95
100
1 0 1 -2 -3 -4
δ18O (PDB)

Figure F8

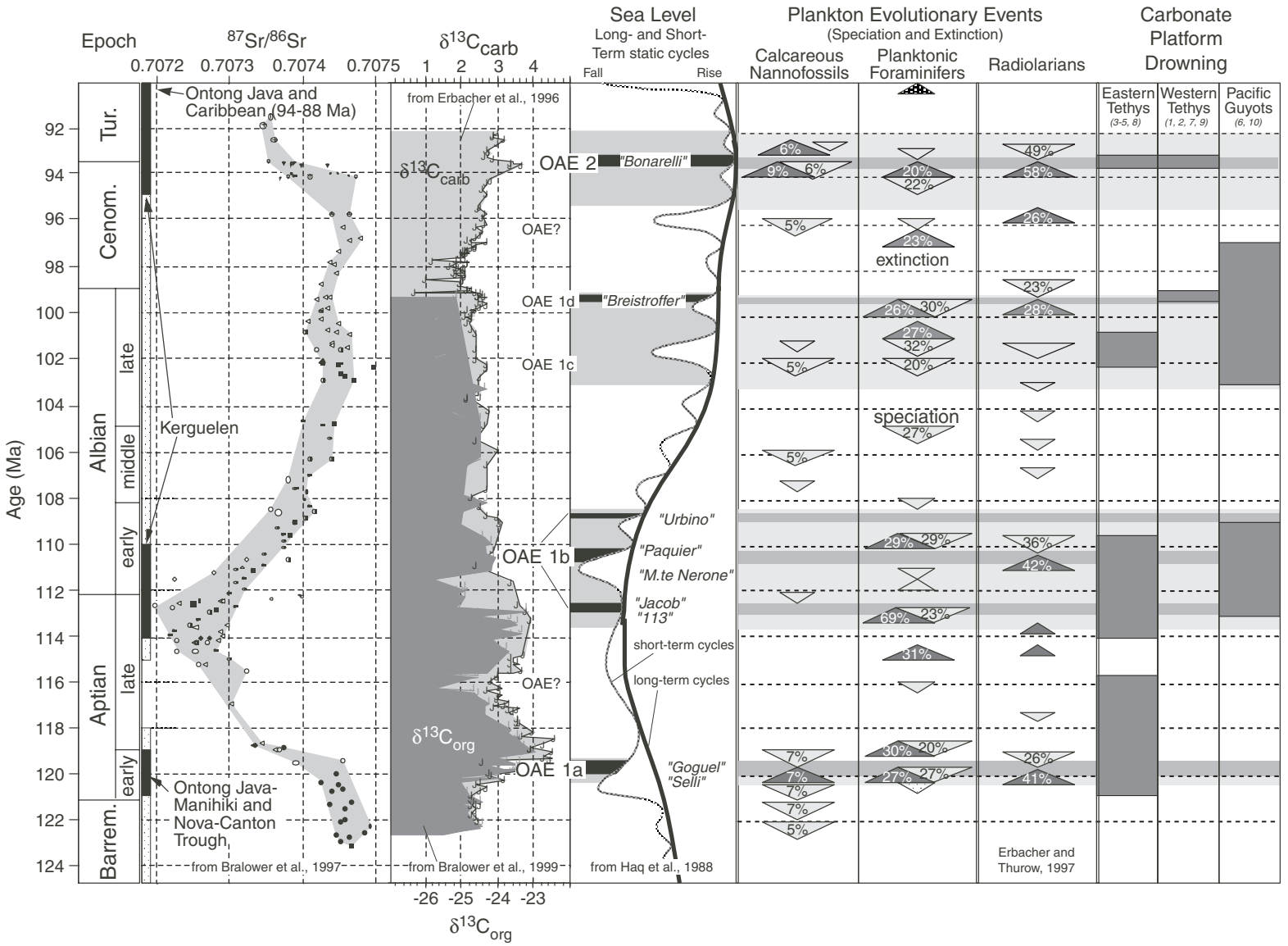
Epoch
87Sr/86Sr
0.7072 0.7073 0.7074 0.7075
δ13Ccarb
1 2 3 4
Sea Level
Long- and Short-Term static cycles
Fall Rise
Plankton Evolutionary Events
(Speciation and Extinction)
Calcareous Nannofossils
Planktonic Foraminifers
Radiolarians
Carbonate Platform Drowning
Eastern Tethys (3-5, 8)
Western Tethys (1, 2, 7, 9)
Pacific Guyots (6, 10)
Age (Ma)
Tur.
Cenom.
Albian
late
middle
early
Aptian
late
early
Barrem.
92
94
96
98
100
102
104
106
108
110
112
114
116
118
120
122
124
Ontong Java and Caribbean (94-88 Ma)
Kerguelen
Ontong Java-Manihiki and Nova-Canton Trough
from Bralower et al., 1997
from Erbacher et al., 1996
δ13Ccarb
δ13Corg
from Bralower et al., 1999
OAE 2
"Bonarelli"
OAE?
OAE 1d
"Breistroffer"
OAE 1c
OAE 1b
"Urbino"
"Paquier"
"M.te Nerone"
"Jacob"
"113"
short-term cycles
long-term cycles
OAE?
OAE 1a
"Goguel"
"Selli"
from Haq et al., 1988
6%
9% 6%
5%
49%
58%
20%
22%
26%
23%
extinction
23%
26% 30%
28%
27%
32%
5%
20%
speciation
27%
5%
29% 29%
36%
42%
69% 23%
31%
7%
7%
7%
7%
5%
30% 20%
27% 27%
26%
41%
Erbacher and Thurow, 1997
-26 -25 -24 -23
δ13Corg

Figure F9

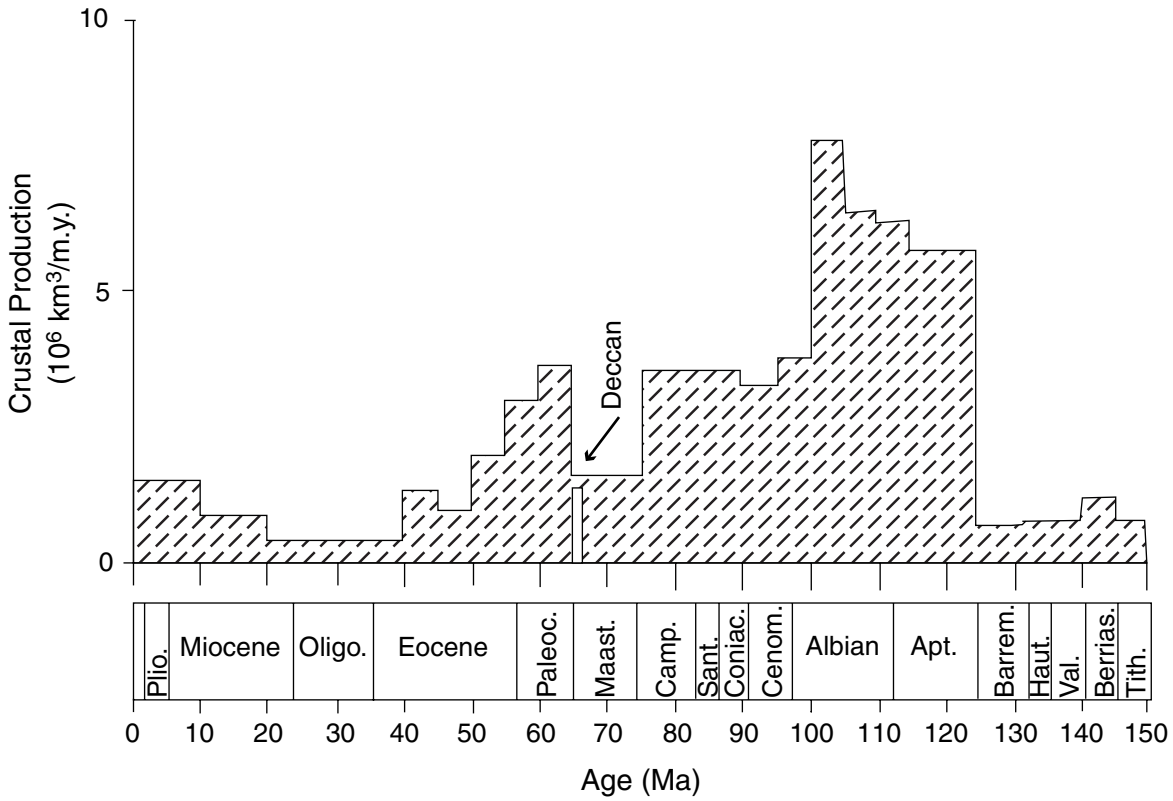
10
5
0
Crustal Production
(10⁶ km³/m.y.)
Deccan
Plio.
Miocene
Oligo.
Eocene
Paleoc.
Maast.
Camp.
Sant.
Coniac.
Cenom.
Albian
Apt.
Barrem.
Haut.
Val.
Berrias.
Tith.
0 10 20 30 40 50 60 70 80 90 100 110 120 130 140 150
Age (Ma)

Figure F10

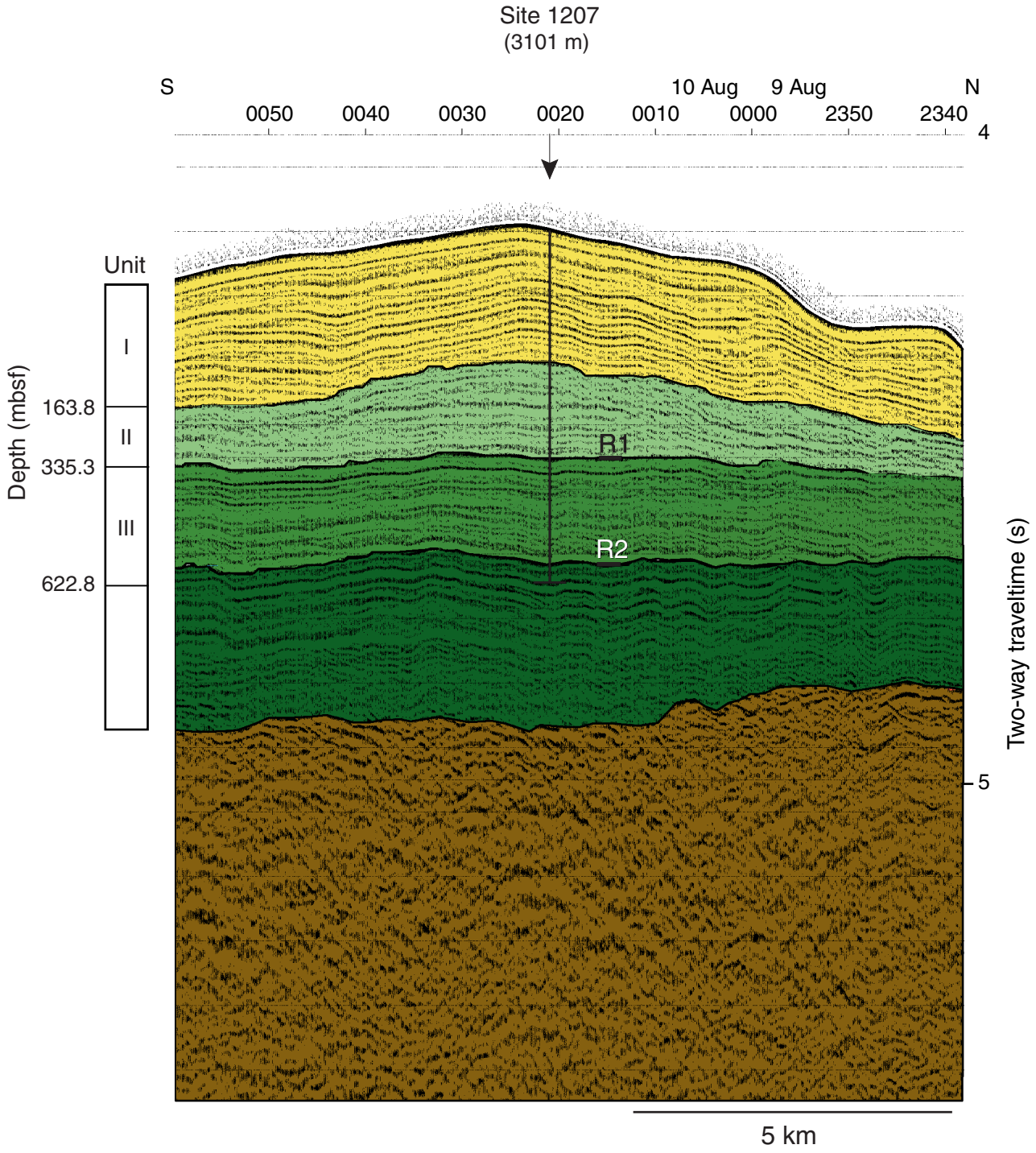
Site 1207
(3101 m)
S
N
10 Aug
9 Aug
0050
0040
0030
0020
0010
0000
2350
2340
4
5
Unit
I
II
III
163.8
335.3
622.8
Depth (mbsf)
R1
R2
Two-way traveltime (s)
5 km

Figure F11

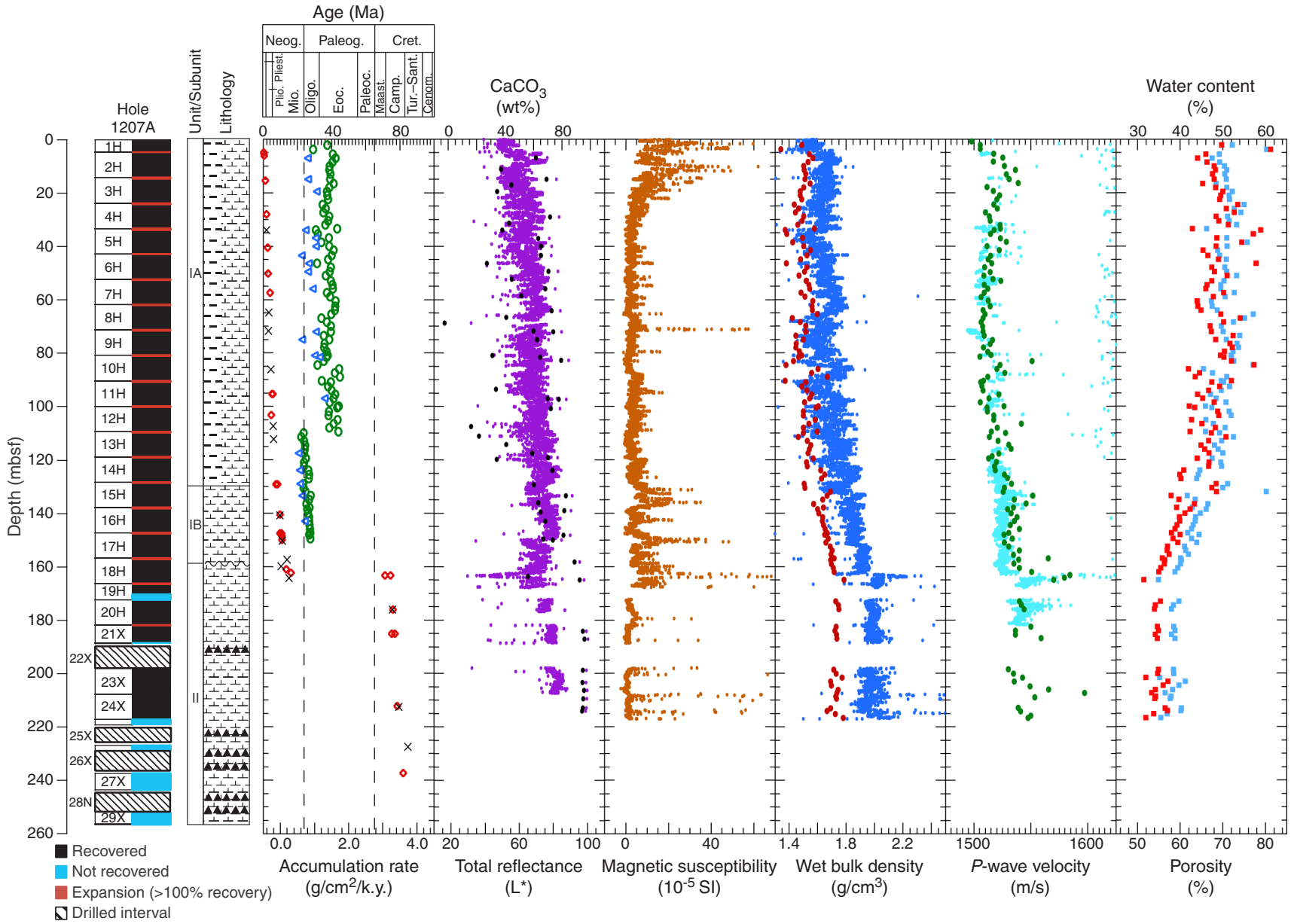
Age (Ma)
Neog.
Paleog.
Cret.
Plio.
Pliest.
Mio.
Oligo.
Eoc.
Paleoc.
Maast.
Camp.
Tur.–Sant.
Canom.
Hole 1207A
Unit/Subunit
Lithology
IA
IB
II
Depth (mbsf)
1H
2H
3H
4H
5H
6H
7H
8H
9H
10H
11H
12H
13H
14H
15H
16H
17H
18H
19H
20H
21X
22X
23X
24X
25X
26X
27X
28N
29X
Recovered
Not recovered
Expansion (>100% recovery)
Drilled interval
Accumulation rate (g/cm²/k.y.)
CaCO3 (wt%)
Total reflectance (L*)
Magnetic susceptibility (10⁻⁵ SI)
Wet bulk density (g/cm³)
P-wave velocity (m/s)
Water content (%)
Porosity (%)

Figure F12

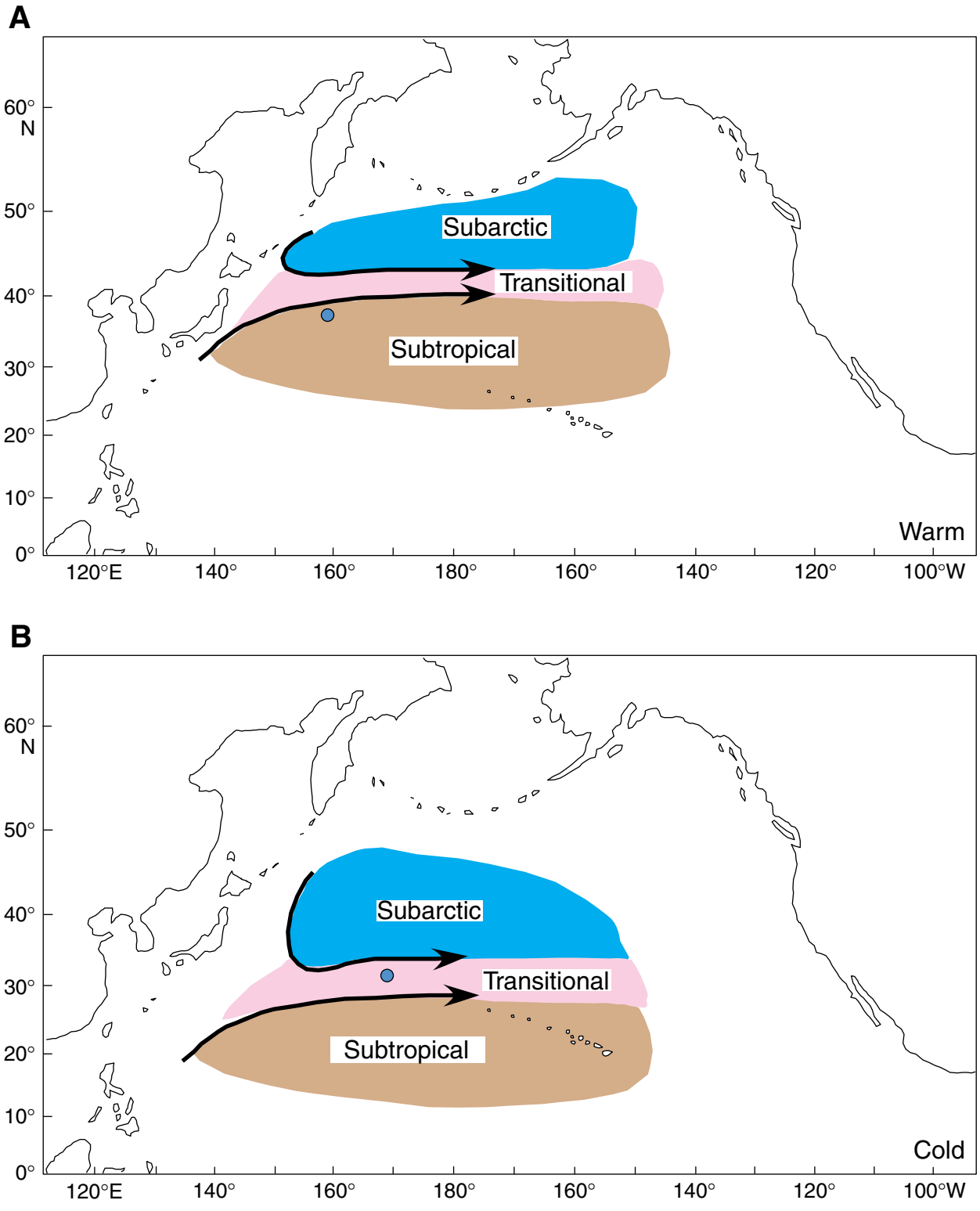
A
60° N
50°
40°
30°
20°
10°
0°
Subarctic
Transitional
Subtropical
Warm
120°E
140°
160°
180°
160°
140°
120°
100°W
B
60° N
50°
40°
30°
20°
10°
0°
Subarctic
Transitional
Subtropical
Cold
120°E
140°
160°
180°
160°
140°
120°
100°W

Figure F13

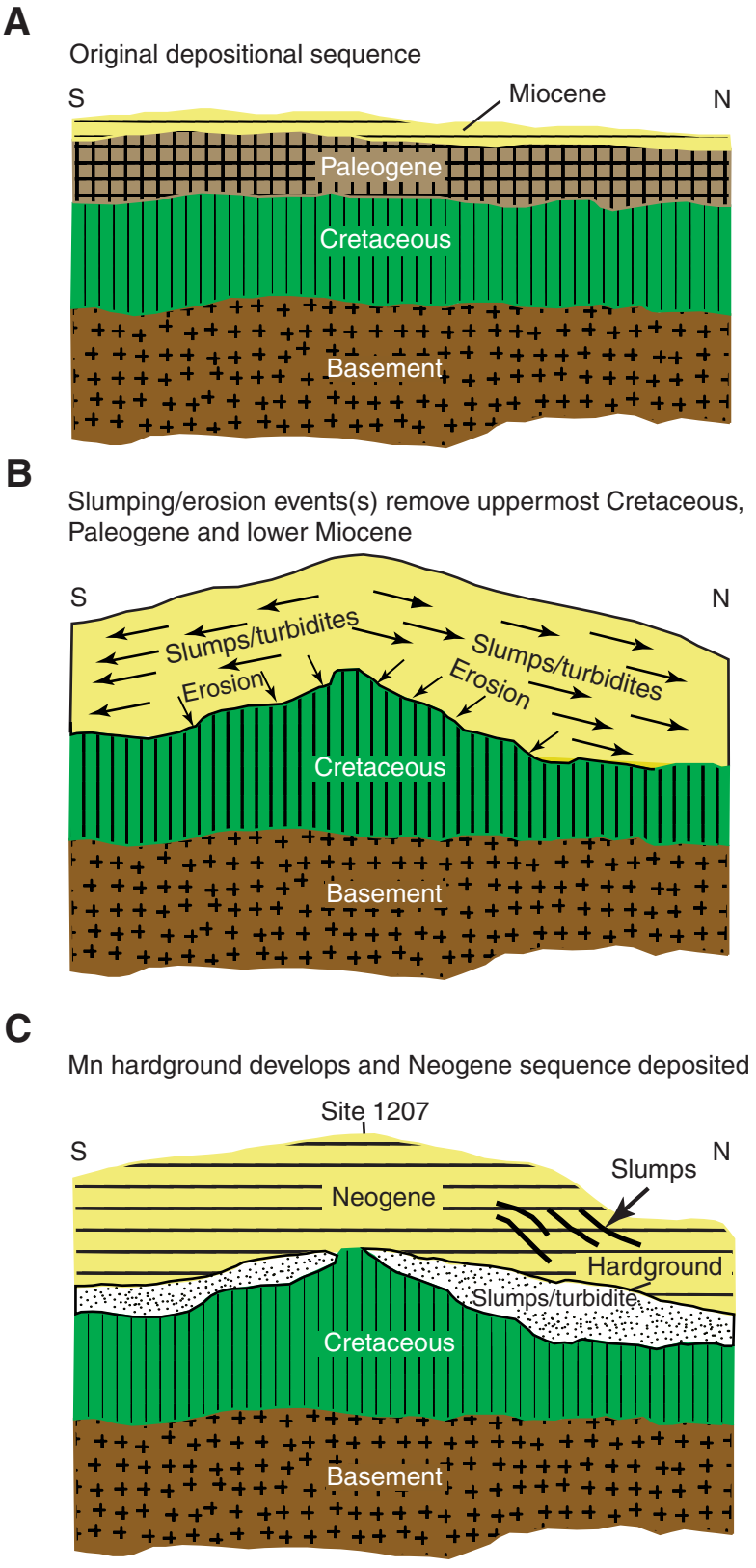
A
Original depositional sequence
S
Miocene
N
Paleogene
Cretaceous
Basement
B
Slumping/erosion events(s) remove uppermost Cretaceous, Paleogene and lower Miocene
S
N
Slumps/turbidites
Erosion
Slumps/turbidites
Erosion
Cretaceous
Basement
C
Mn hardground develops and Neogene sequence deposited
Site 1207
S
N
Slumps
Neogene
Hardground
Slumps/turbidite
Cretaceous
Basement

Figure F14

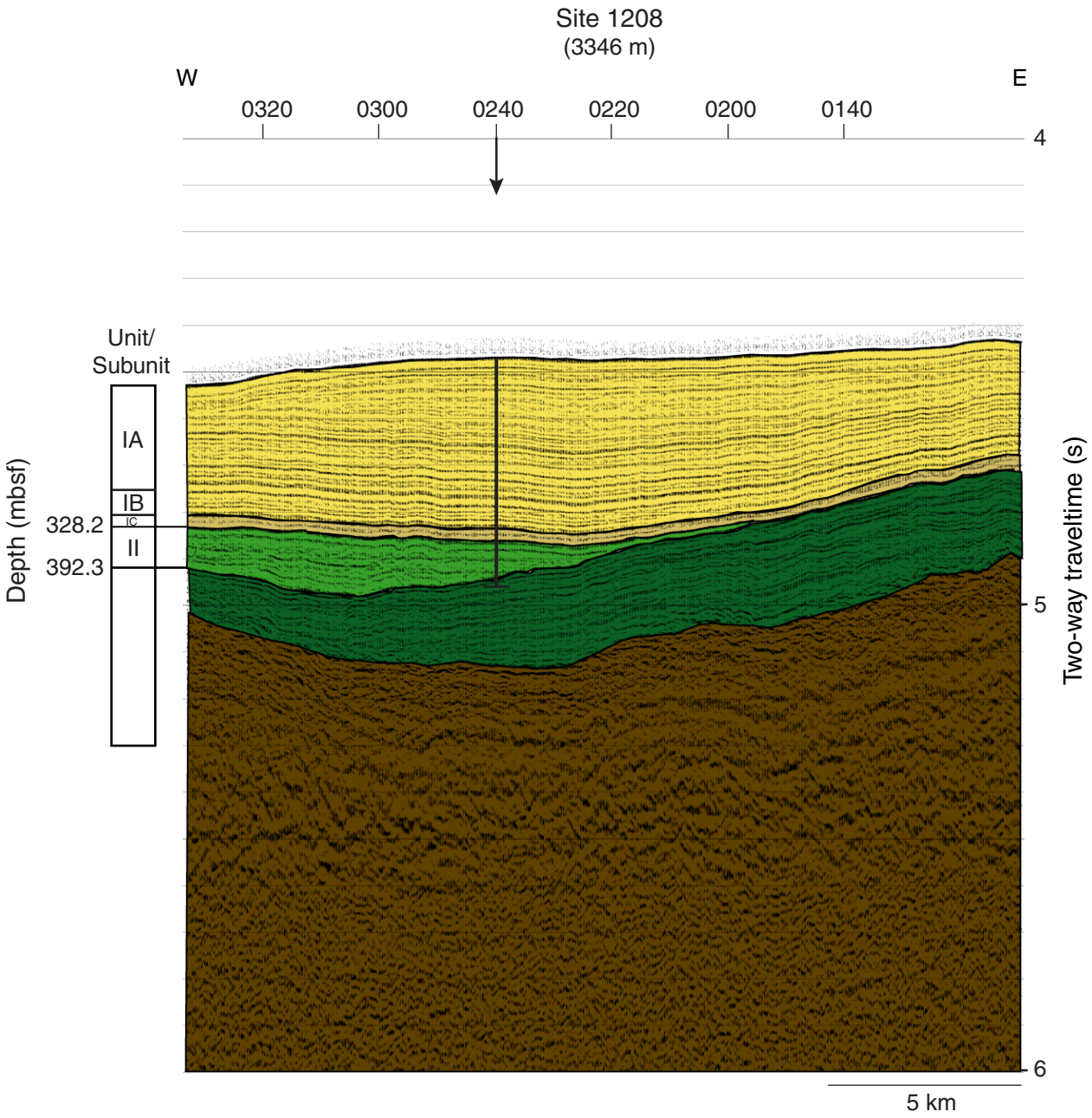
Site 1208
(3346 m)
W
E
0320
0300
0240
0220
0200
0140
4
Unit/
Subunit
IA
IB
IC
II
328.2
392.3
Depth (mbsf)
5
6
Two-way traveltime (s)
5 km

Figure F15

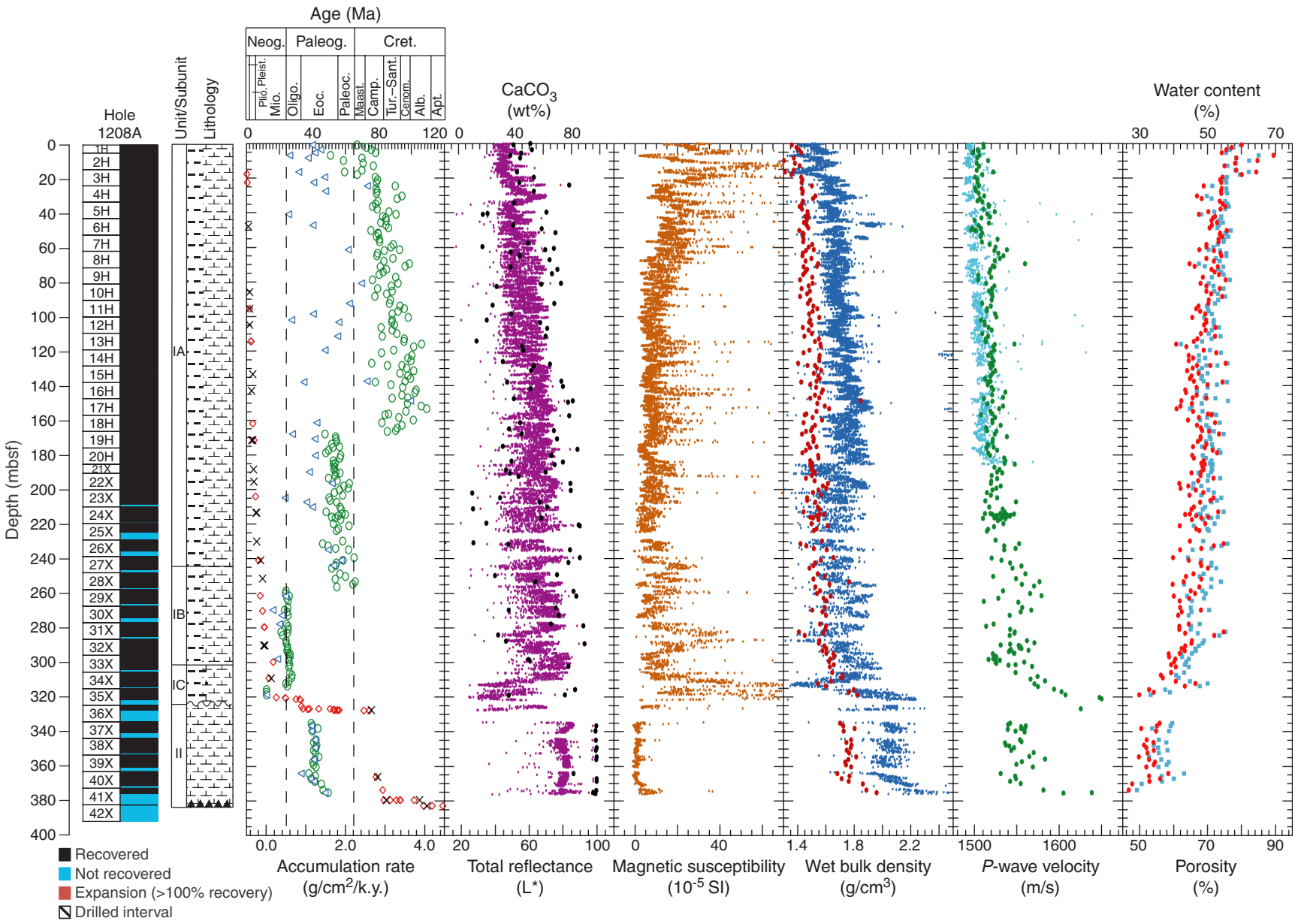
Age (Ma)
Neog.
Paleog.
Cret.
Plio.
Pleist.
Mio.
Oligo.
Eoc.
Paleoc.
Maast.
Camp.
Tur.–Sant.
Cenom.
Alb.
Apt.
Hole 1208A
Unit/Subunit
Lithology
IA
IB
IC
II
Depth (mbsf)
CaCO3 (wt%)
Water content (%)
Accumulation rate (g/cm2/k.y.)
Total reflectance (L*)
Magnetic susceptibility (10-5 SI)
Wet bulk density (g/cm3)
P-wave velocity (m/s)
Porosity (%)
Recovered
Not recovered
Expansion (>100% recovery)
Drilled interval

Figure F16

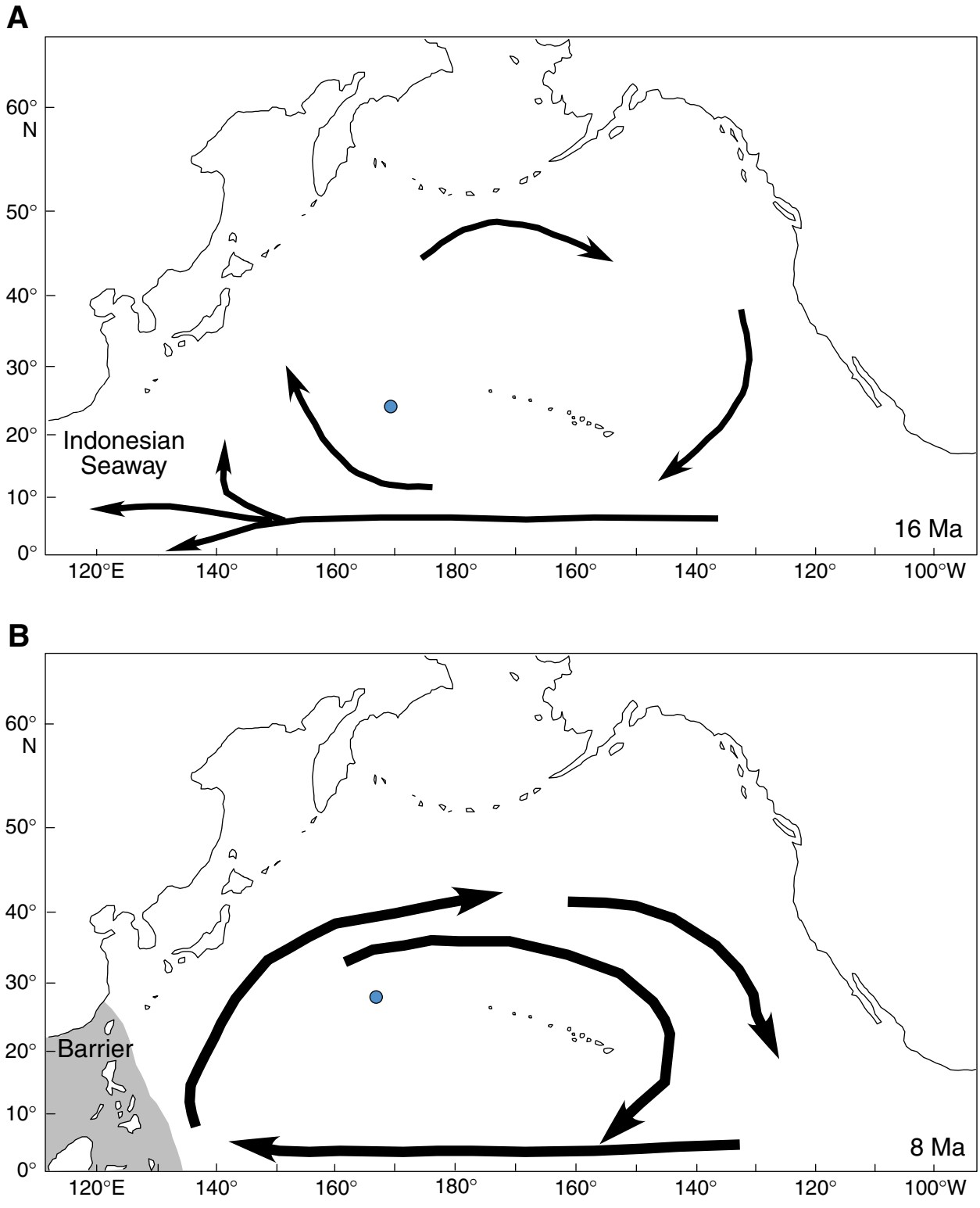
A
60° N
50°
40°
30°
20°
10°
0°
Indonesian Seaway
16 Ma
120°E
140°
160°
180°
160°
140°
120°
100°W
B
60° N
50°
40°
30°
20°
10°
0°
Barrier
8 Ma
120°E
140°
160°
180°
160°
140°
120°
100°W

Figure F17

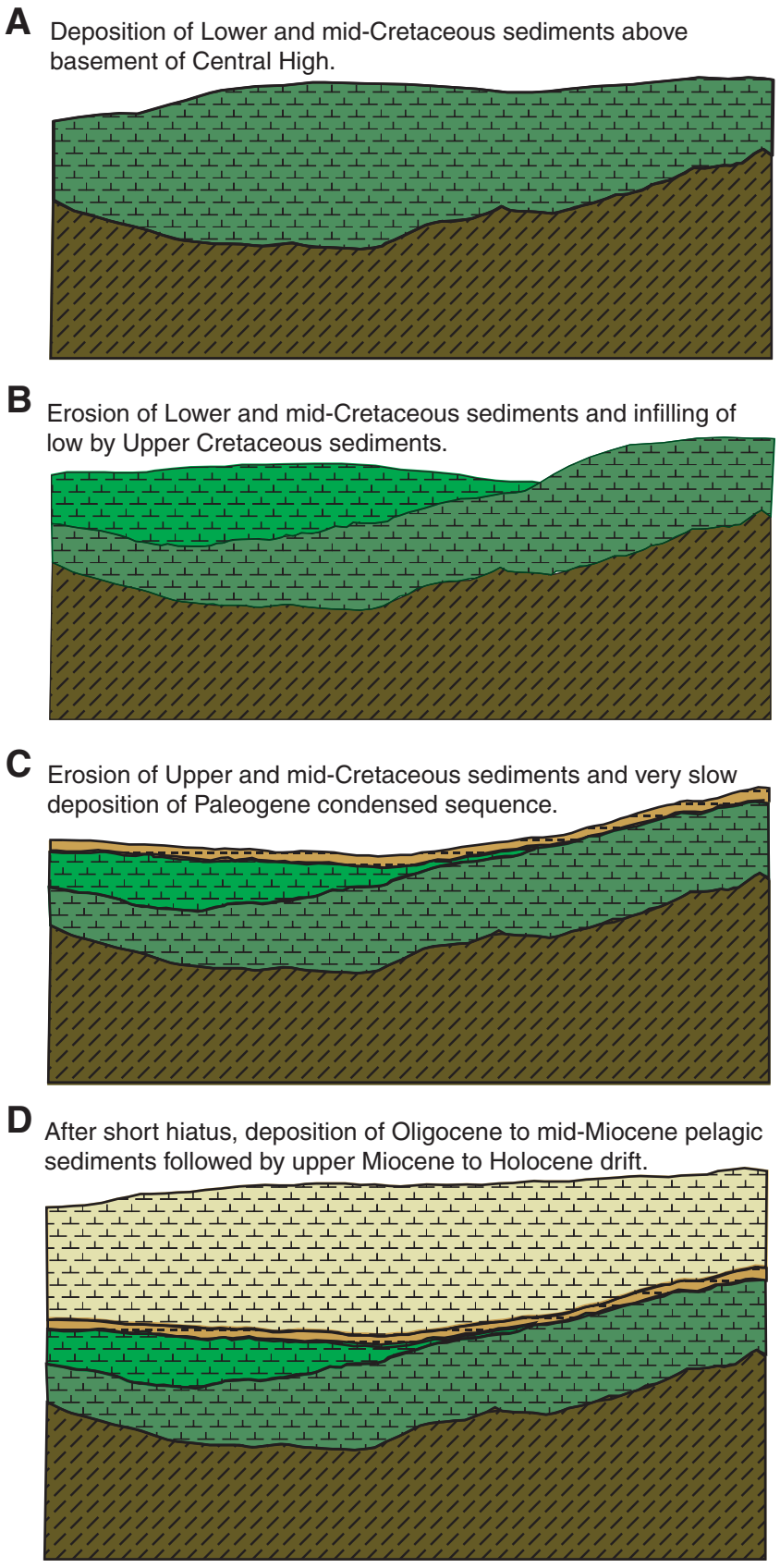
A
Deposition of Lower and mid-Cretaceous sediments above basement of Central High.
B
Erosion of Lower and mid-Cretaceous sediments and infilling of low by Upper Cretaceous sediments.
C
Erosion of Upper and mid-Cretaceous sediments and very slow deposition of Paleogene condensed sequence.
D
After short hiatus, deposition of Oligocene to mid-Miocene pelagic sediments followed by upper Miocene to Holocene drift.

Figure F18

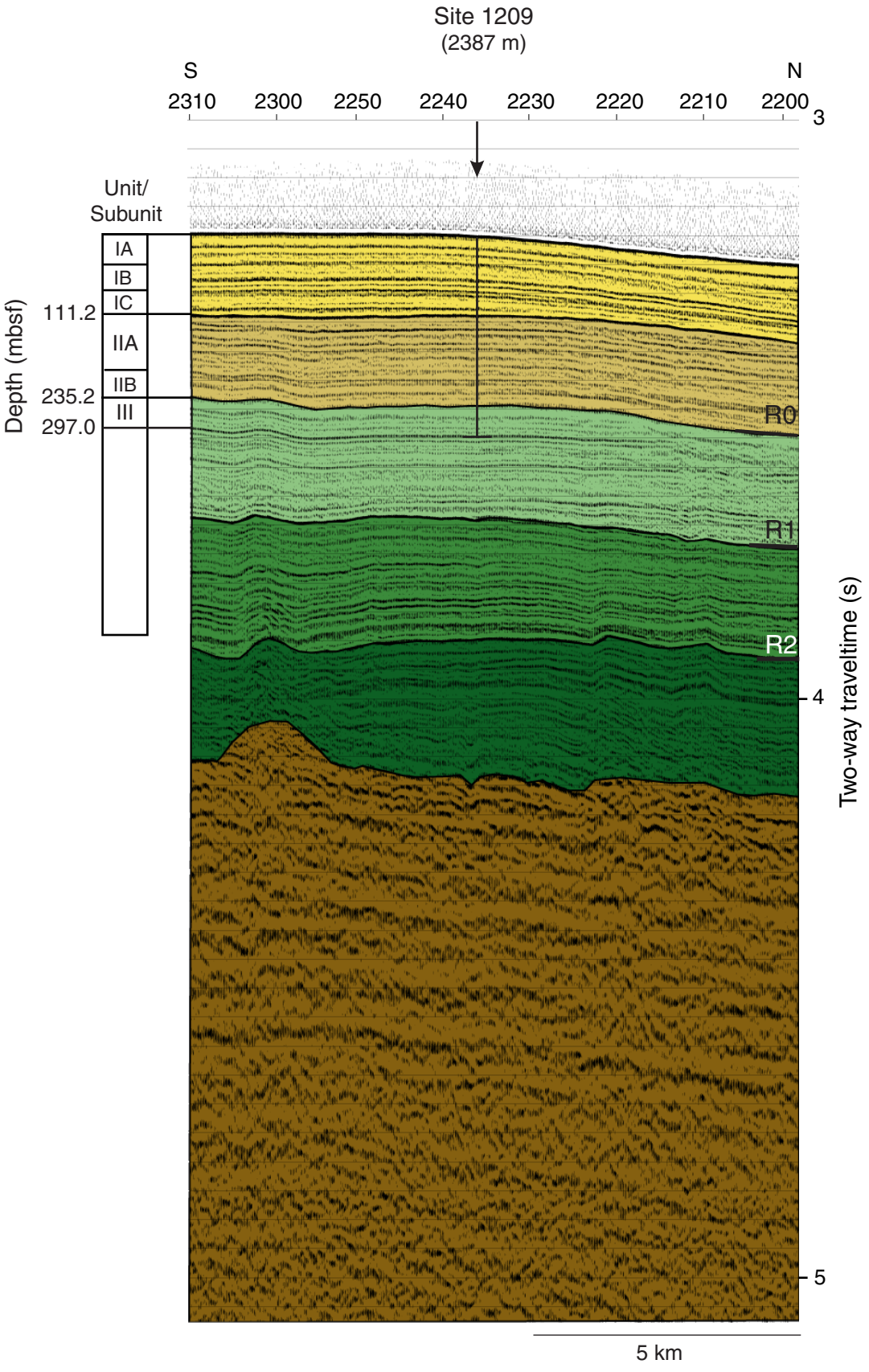
Site 1209
(2387 m)
S
N
2310
2300
2250
2240
2230
2220
2210
2200
3
Unit/
Subunit
IA
IB
IC
IIA
IIB
III
111.2
235.2
297.0
Depth (mbsf)
R0
R1
R2
4
5
Two-way traveltime (s)
5 km

Figure F19

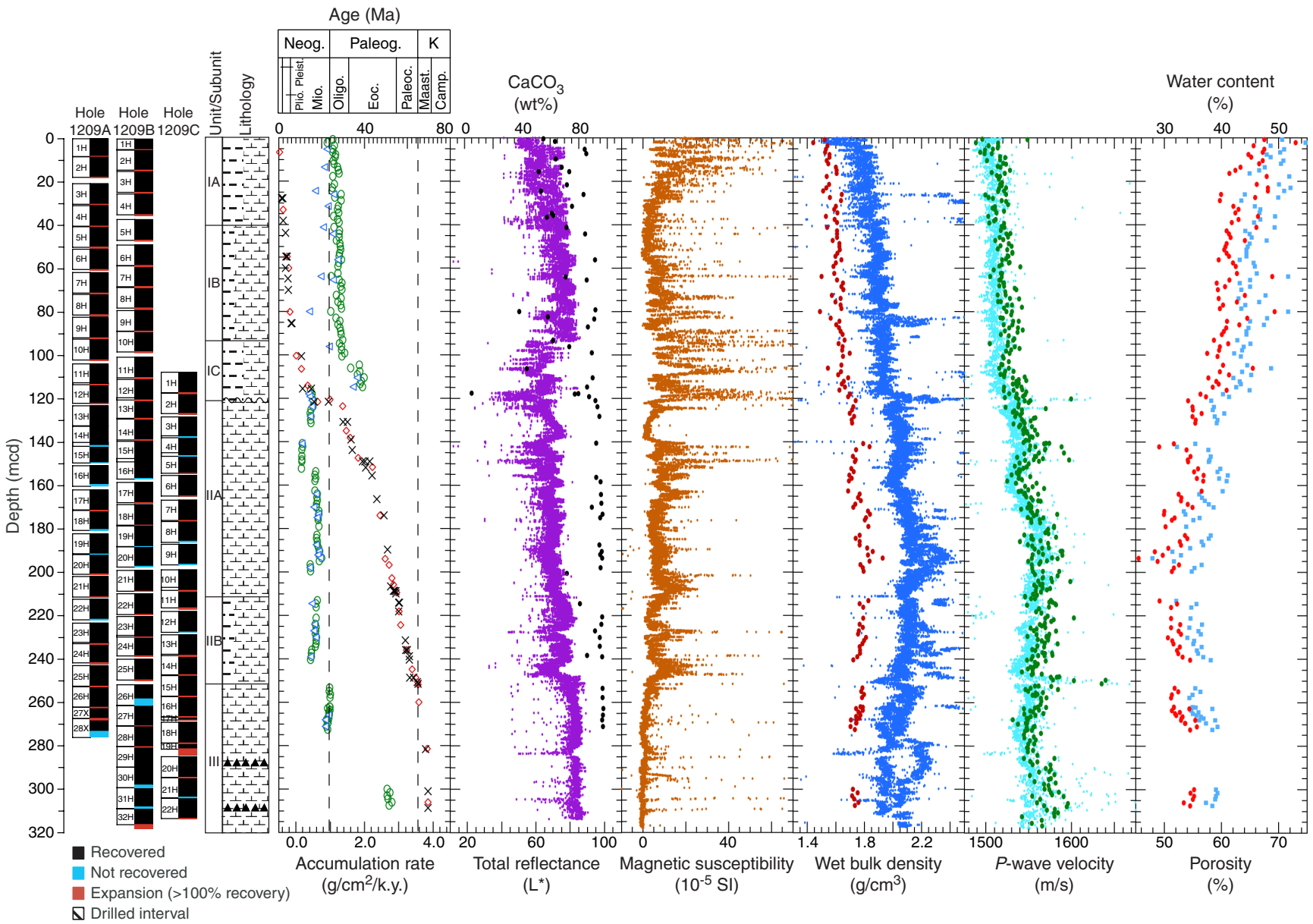
Age (Ma)
Neog.
Paleog.
K
Plio.
Pleist.
Mio.
Oligo.
Eoc.
Paleoc.
Maast.
Camp.
Hole 1209A
Hole 1209B
Hole 1209C
Unit/Subunit
Lithology
IA
IB
IC
IIA
IIB
III
Depth (mcd)
CaCO3 (wt%)
Water content (%)
Accumulation rate (g/cm2/k.y.)
Total reflectance (L*)
Magnetic susceptibility (10-5 SI)
Wet bulk density (g/cm3)
P-wave velocity (m/s)
Porosity (%)
Recovered
Not recovered
Expansion (>100% recovery)
Drilled interval

Figure F20

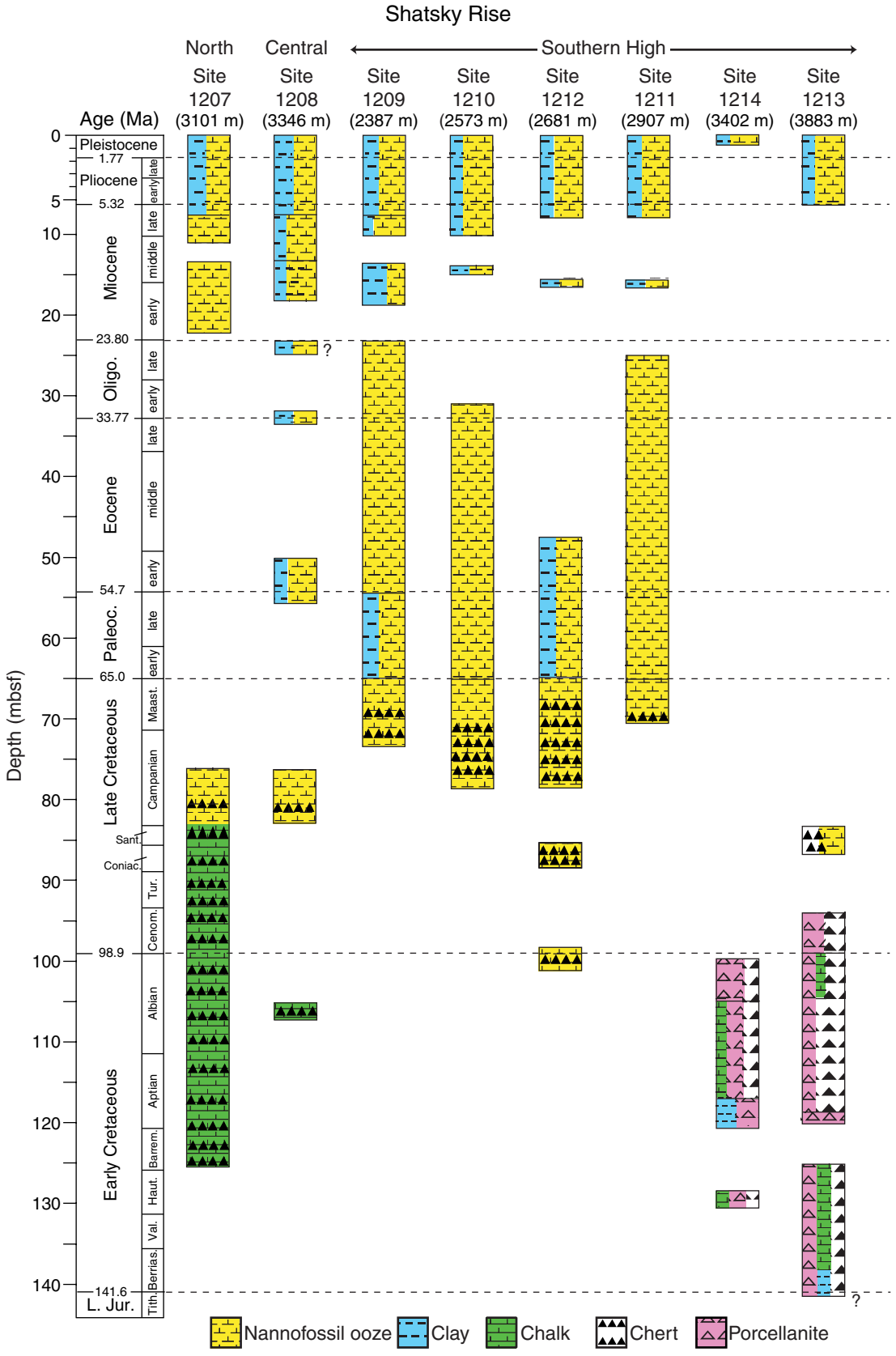
Shatsky Rise
North
Central
Southern High
Site 1207 (3101 m)
Site 1208 (3346 m)
Site 1209 (2387 m)
Site 1210 (2573 m)
Site 1212 (2681 m)
Site 1211 (2907 m)
Site 1214 (3402 m)
Site 1213 (3883 m)
Age (Ma)
Depth (mbsf)
Pleistocene
Pliocene
Miocene
Oligo.
Eocene
Paleoc.
Late Cretaceous
Early Cretaceous
L. Jur.
1.77
5.32
23.80
33.77
54.7
65.0
98.9
141.6
Sant.
Coniac.
Nannofossil ooze
Clay
Chalk
Chert
Porcellanite

Figure F21

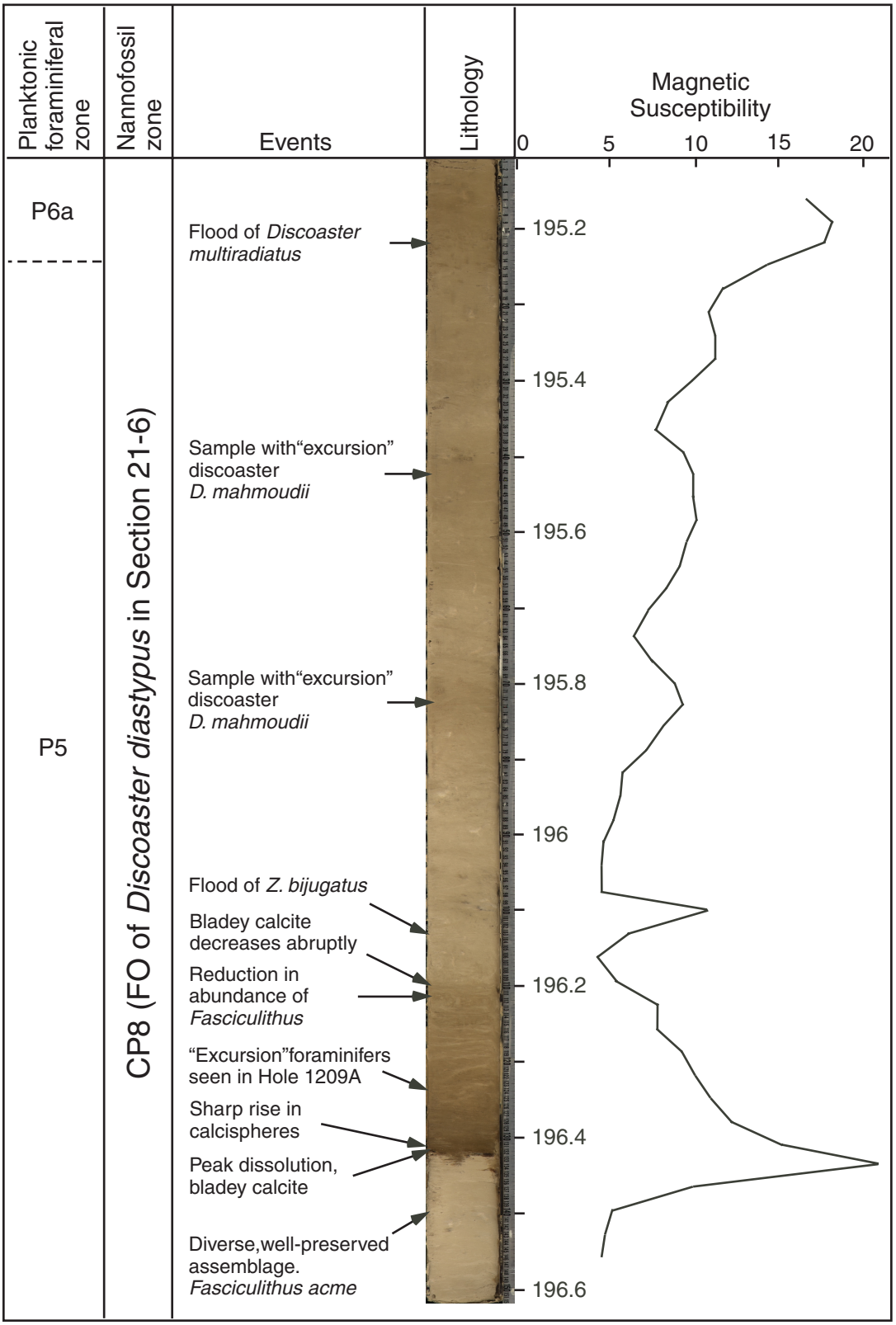
Planktonic foraminiferal zone
Nannofossil zone
Events
Lithology
Magnetic Susceptibility
0
5
10
15
20
P6a
P5
CP8 (FO of Discoaster diastypus in Section 21-6)
Flood of Discoaster multiradiatus
Sample with"excursion" discoaster D. mahmoudii
Sample with"excursion" discoaster D. mahmoudii
Flood of Z. bijugatus
Bladey calcite decreases abruptly
Reduction in abundance of Fasciculithus
"Excursion"foraminifers seen in Hole 1209A
Sharp rise in calcispheres
Peak dissolution, bladey calcite
Diverse,well-preserved assemblage. Fasciculithus acme
195.2
195.4
195.6
195.8
196
196.2
196.4
196.6

Figure F22

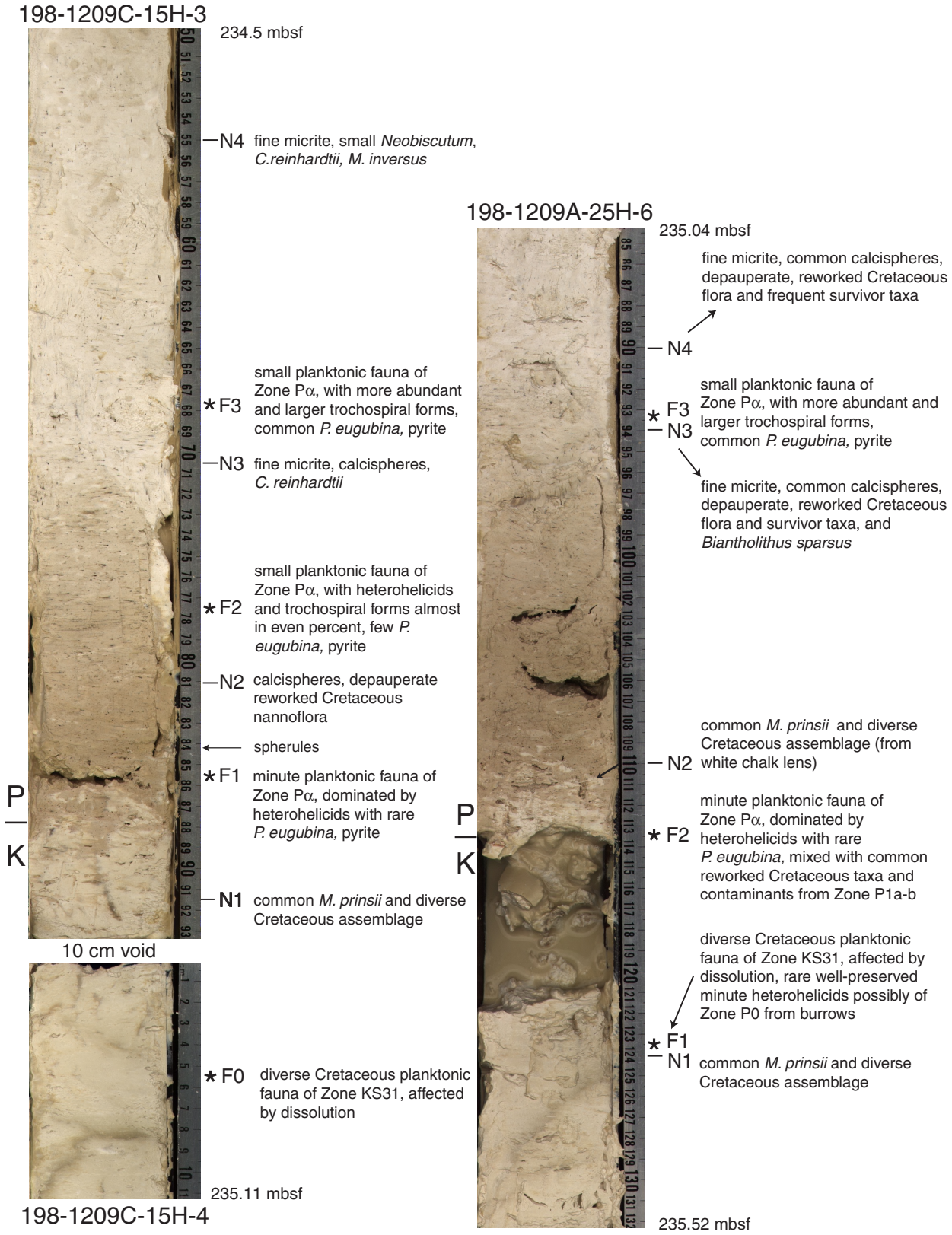
198-1209C-15H-3
234.5 mbsf
N4
fine micrite, small Neobiscutum, C.reinhardtii, M. inversus
*F3
small planktonic fauna of Zone Pα, with more abundant and larger trochospiral forms, common P. eugubina, pyrite
N3
fine micrite, calcispheres, C. reinhardtii
*F2
small planktonic fauna of Zone Pα, with heterohelicids and trochospiral forms almost in even percent, few P. eugubina, pyrite
N2
calcispheres, depauperate reworked Cretaceous nannoflora
spherules
*F1
minute planktonic fauna of Zone Pα, dominated by heterohelicids with rare P. eugubina, pyrite
P
K
N1
common M. prinsii and diverse Cretaceous assemblage
10 cm void
*F0
diverse Cretaceous planktonic fauna of Zone KS31, affected by dissolution
235.11 mbsf
198-1209C-15H-4
198-1209A-25H-6
235.04 mbsf
fine micrite, common calcispheres, depauperate, reworked Cretaceous flora and frequent survivor taxa
N4
*F3
N3
small planktonic fauna of Zone Pα, with more abundant and larger trochospiral forms, common P. eugubina, pyrite
fine micrite, common calcispheres, depauperate, reworked Cretaceous flora and survivor taxa, and Biantholithus sparsus
common M. prinsii and diverse Cretaceous assemblage (from white chalk lens)
N2
P
K
*F2
minute planktonic fauna of Zone Pα, dominated by heterohelicids with rare P. eugubina, mixed with common reworked Cretaceous taxa and contaminants from Zone P1a-b
diverse Cretaceous planktonic fauna of Zone KS31, affected by dissolution, rare well-preserved minute heterohelicids possibly of Zone P0 from burrows
*F1
N1
common M. prinsii and diverse Cretaceous assemblage
235.52 mbsf

Figure F23

The mid-Maastrichtian event on Shatsky Rise

Figure F24

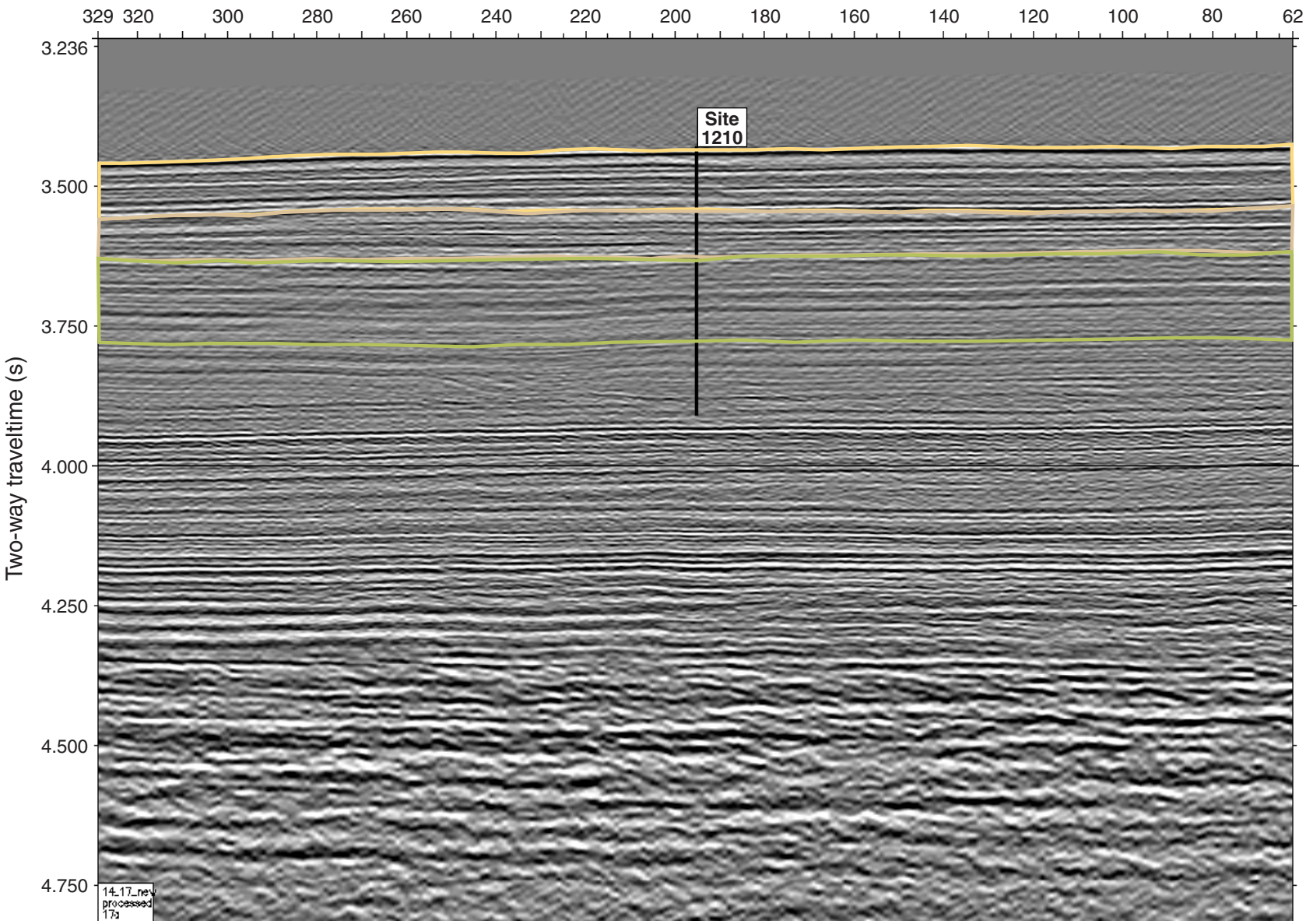
329 320 300 280 260 240 220 200 180 160 140 120 100 80 62
3.236
3.500
3.750
4.000
4.250
4.500
4.750
Two-way traveltime (s)
Site
1210
14_17_new
processed
17a

Figure F25

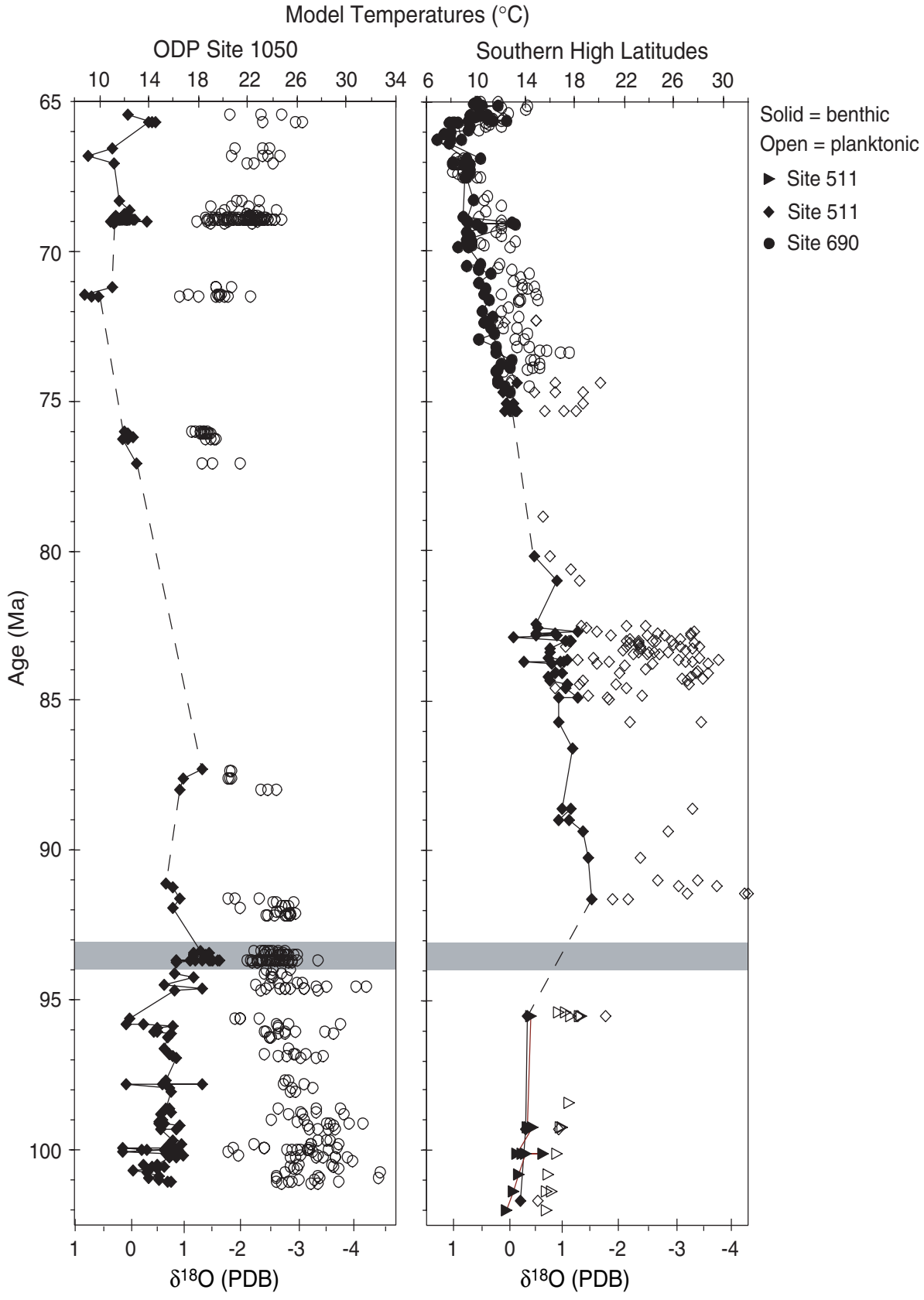
Model Temperatures (°C)
ODP Site 1050
Southern High Latitudes
10 14 18 22 26 30 34
6 10 14 18 22 26 30
Solid = benthic
Open = planktonic
Site 511
Site 511
Site 690
Age (Ma)
65 70 75 80 85 90 95 100
1 0 1 -2 -3 -4
δ18O (PDB)

Figure F26

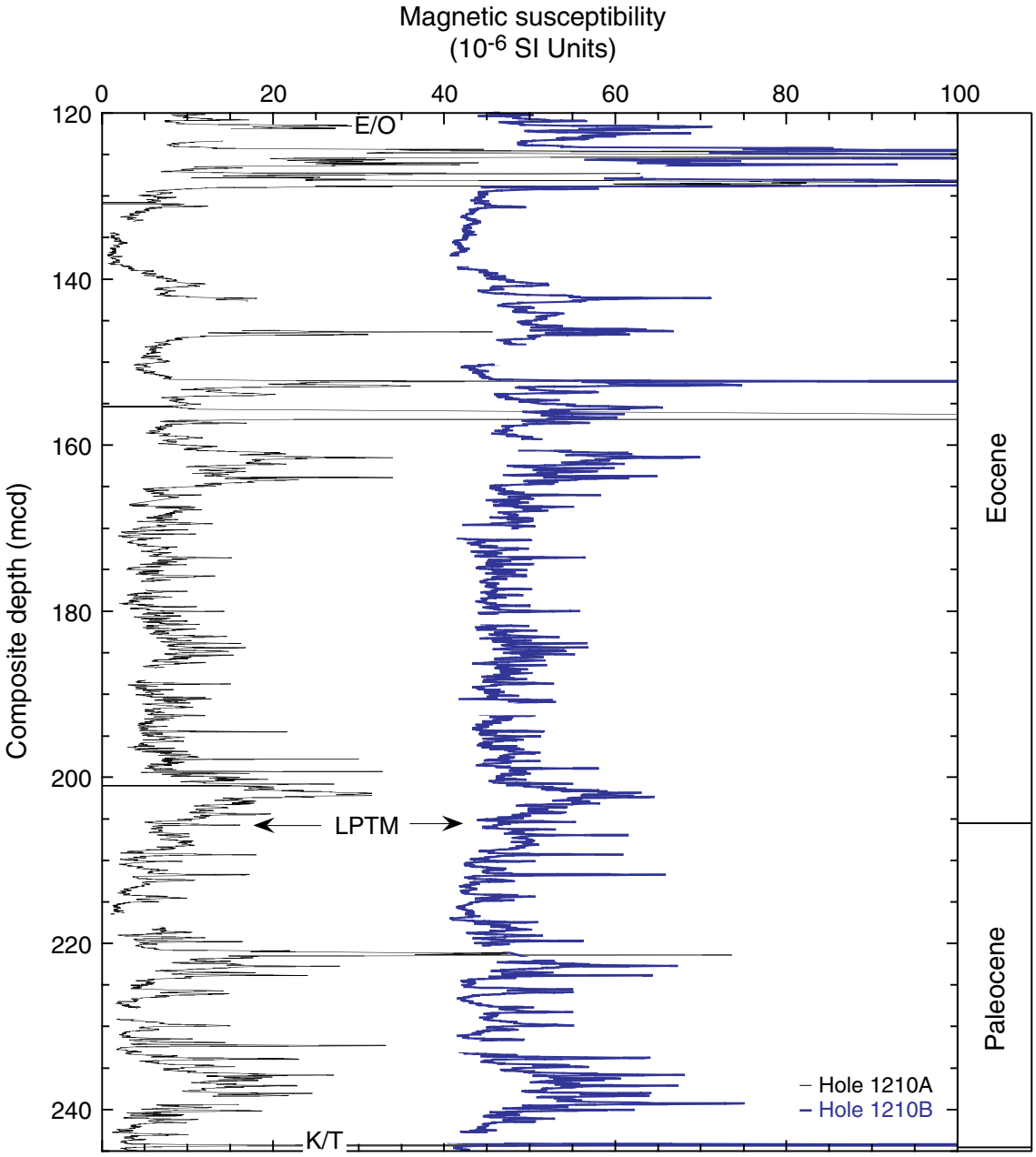
Magnetic susceptibility
(10-6 SI Units)
0
20
40
60
80
100
120
140
160
180
200
220
240
Composite depth (mcd)
E/O
LPTM
K/T
Eocene
Paleocene
Hole 1210A
Hole 1210B

Figure F27

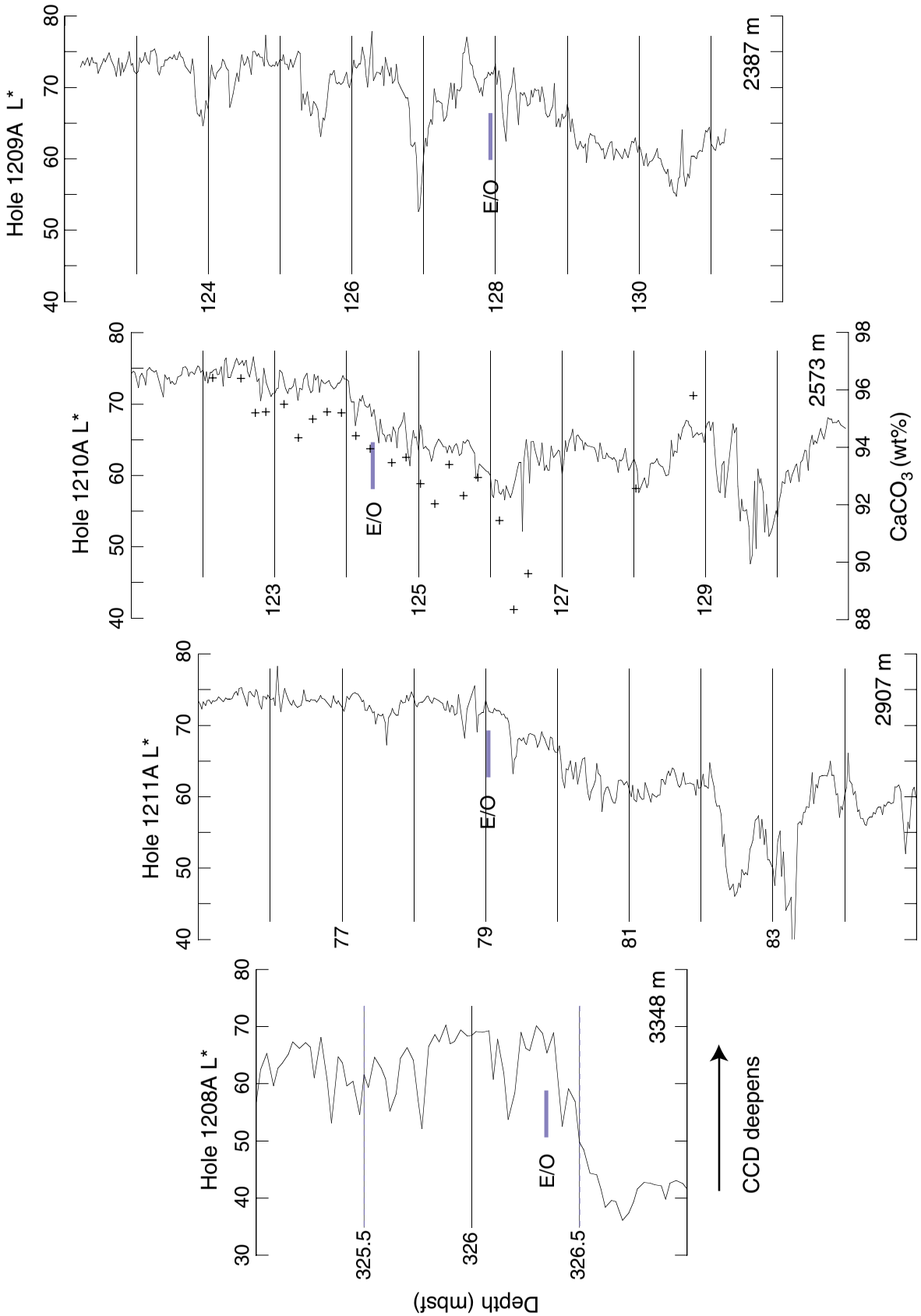
Hole 1209A L*
Hole 1210A L*
Hole 1211A L*
Hole 1208A L*
E/O
2387 m
2573 m
2907 m
3348 m
CaCO3 (wt%)
Depth (mbsf)
CCD deepens

Figure F28

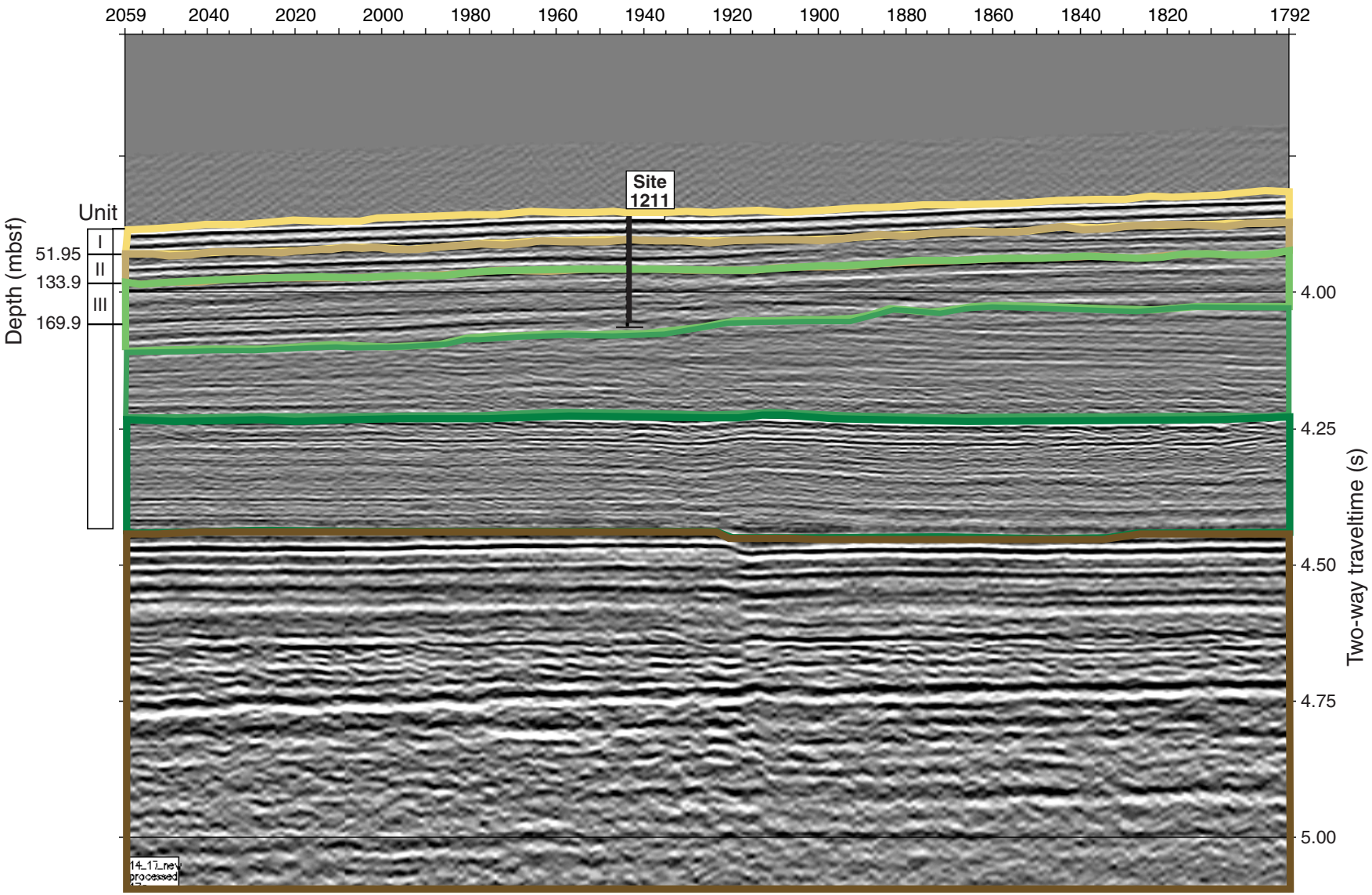
2059
2040
2020
2000
1980
1960
1940
1920
1900
1880
1860
1840
1820
1792
Site
1211
Unit
I
II
III
51.95
133.9
169.9
Depth (mbsf)
4.00
4.25
4.50
4.75
5.00
Two-way traveltime (s)

Figure F29

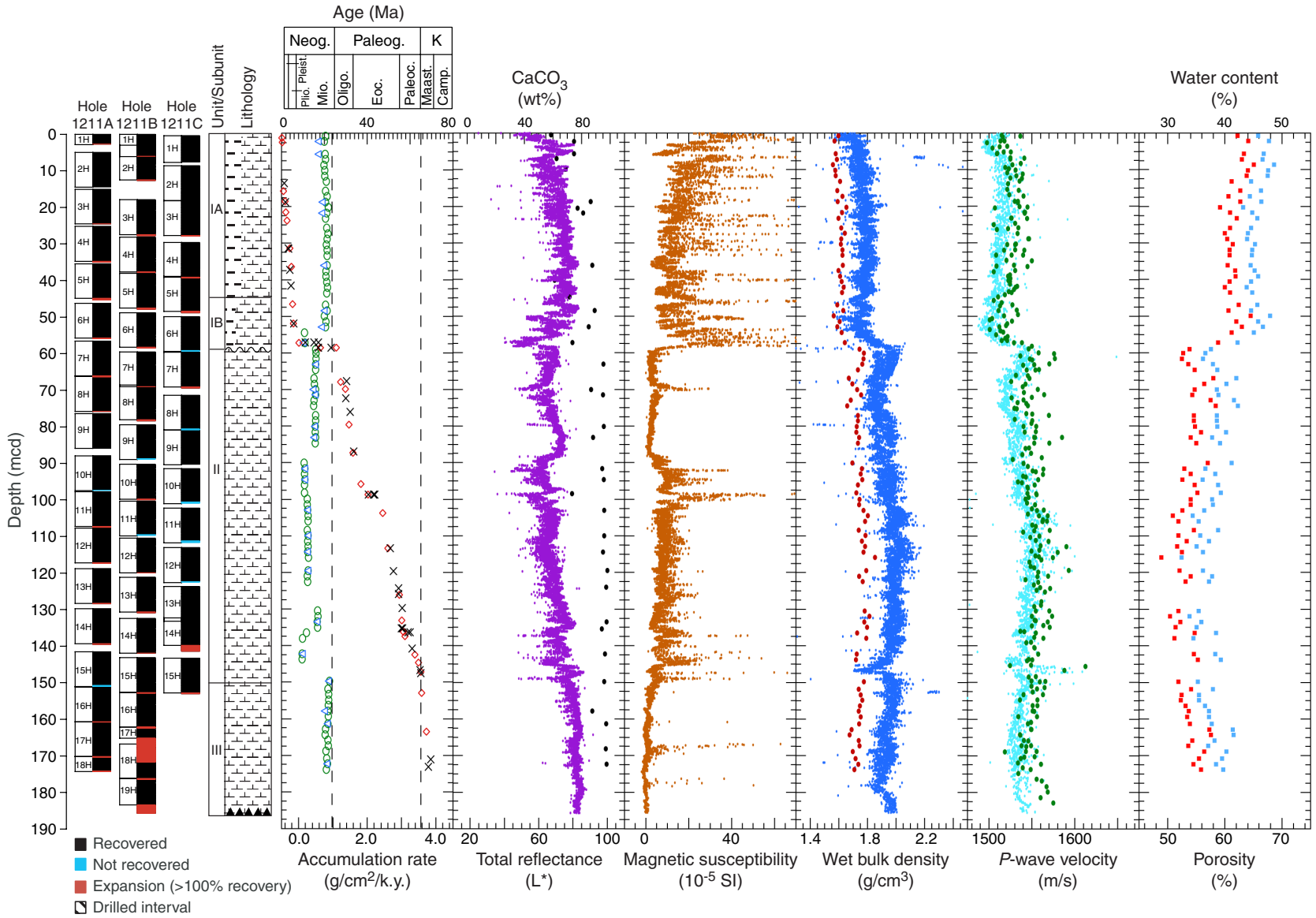
Age (Ma)
Neog.
Paleog.
K
Plio.
Pleist.
Mio.
Oligo.
Eoc.
Paleoc.
Maast.
Camp.
Hole 1211A
Hole 1211B
Hole 1211C
Unit/Subunit
Lithology
IA
IB
II
III
Depth (mcd)
CaCO3 (wt%)
Water content (%)
Recovered
Not recovered
Expansion (>100% recovery)
Drilled interval
Accumulation rate (g/cm2/k.y.)
Total reflectance (L*)
Magnetic susceptibility (10-5 SI)
Wet bulk density (g/cm3)
P-wave velocity (m/s)
Porosity (%)

Figure F30

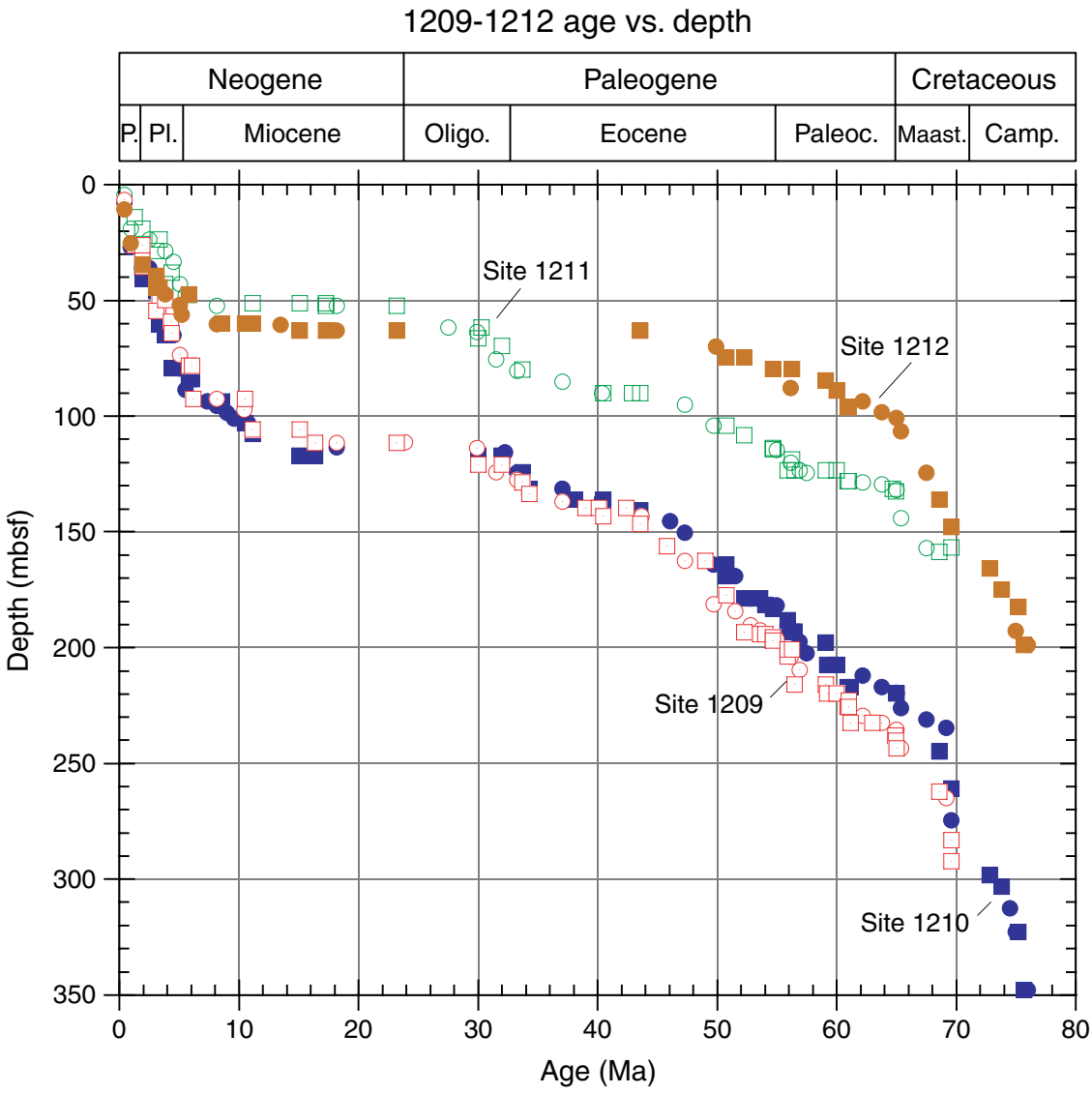
1209-1212 age vs. depth
Neogene
Paleogene
Cretaceous
P.
Pl.
Miocene
Oligo.
Eocene
Paleoc.
Maast.
Camp.
Site 1211
Site 1212
Site 1209
Site 1210
Depth (mbsf)
Age (Ma)
0
50
100
150
200
250
300
350
0
10
20
30
40
50
60
70
80

Figure F31

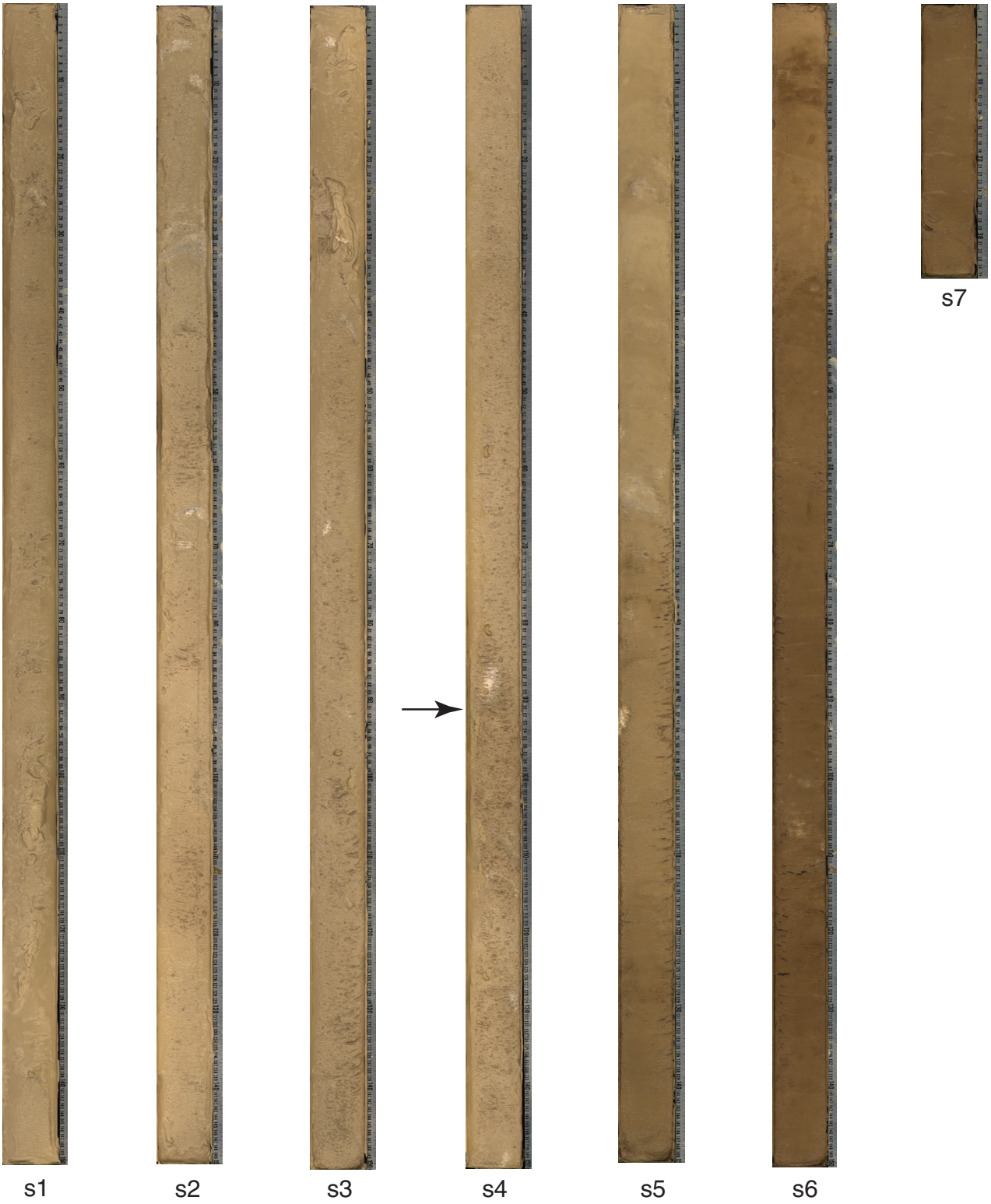

Figure F32

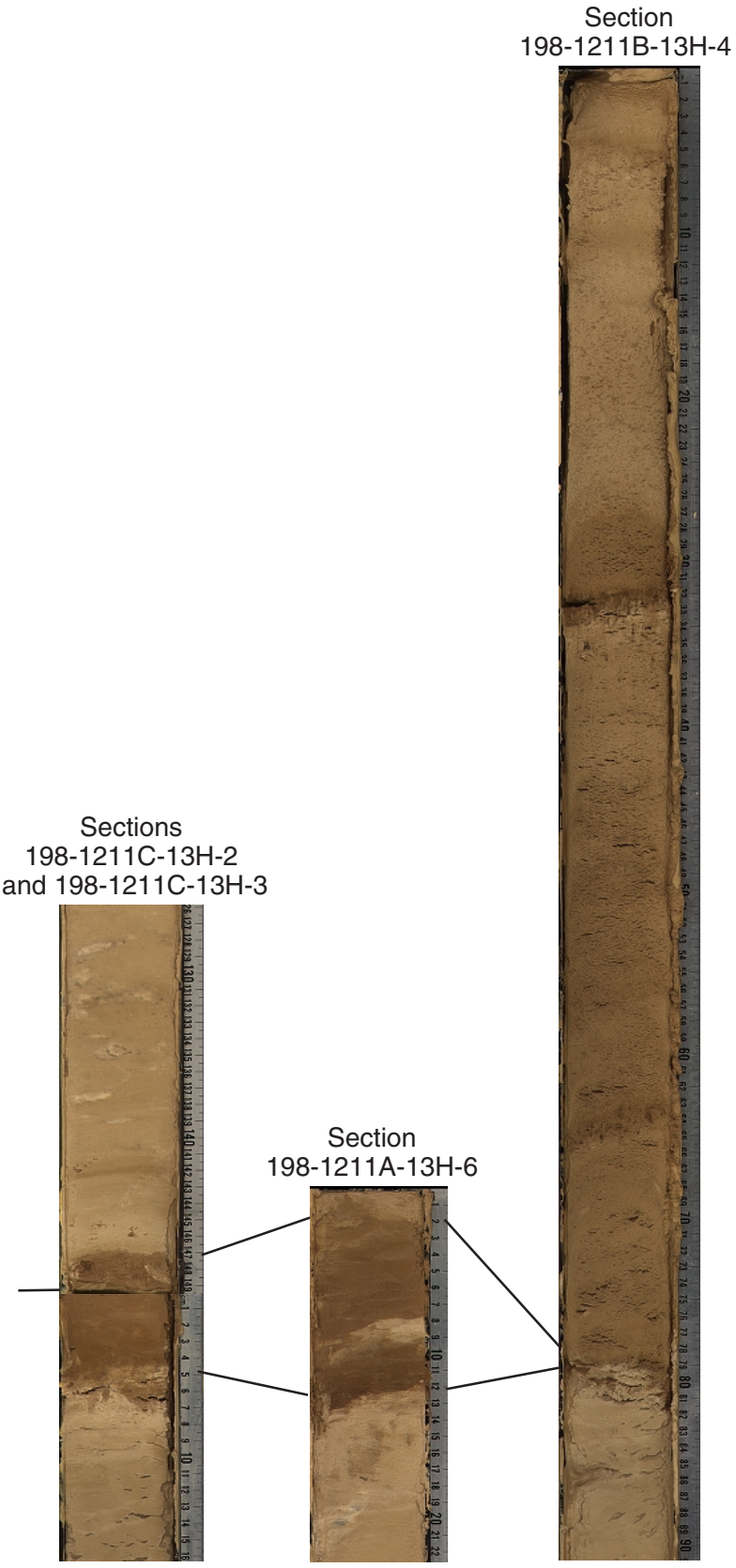
Section
198-1211B-13H-4
Sections
198-1211C-13H-2
and 198-1211C-13H-3
Section
198-1211A-13H-6

Figure F33

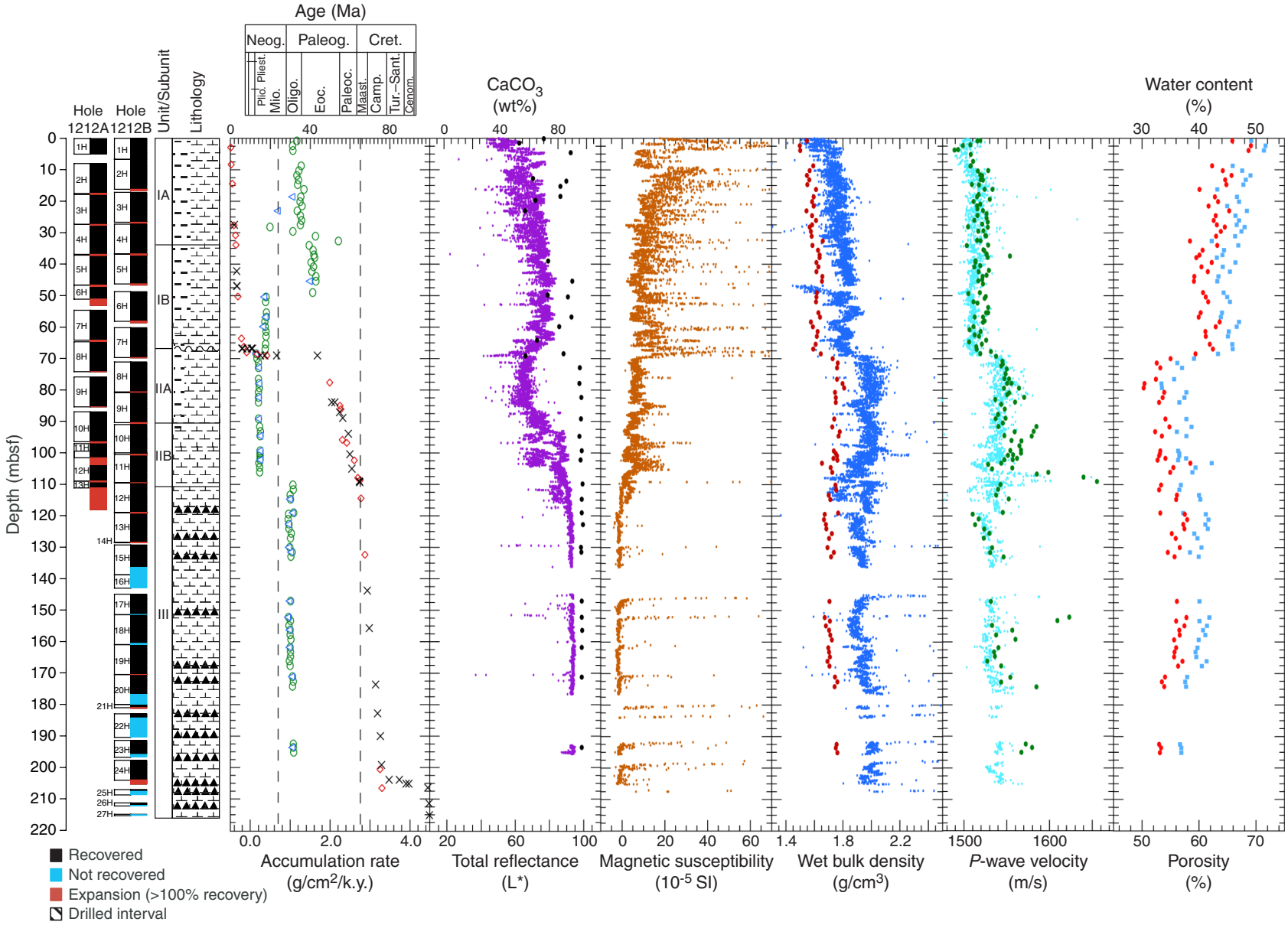
Age (Ma)
Neog.
Paleog.
Cret.
Plio.
Pliest.
Mio.
Oligo.
Eoc.
Paleoc.
Maast.
Camp.
Tur.–Sant.
Cenom.
Hole 1212A
Hole 1212B
Unit/Subunit
Lithology
IA
IB
IIA
IIB
III
Depth (mbsf)
CaCO3 (wt%)
Water content (%)
Accumulation rate (g/cm2/k.y.)
Total reflectance (L*)
Magnetic susceptibility (10-5 SI)
Wet bulk density (g/cm3)
P-wave velocity (m/s)
Porosity (%)
Recovered
Not recovered
Expansion (>100% recovery)
Drilled interval

Figure F34

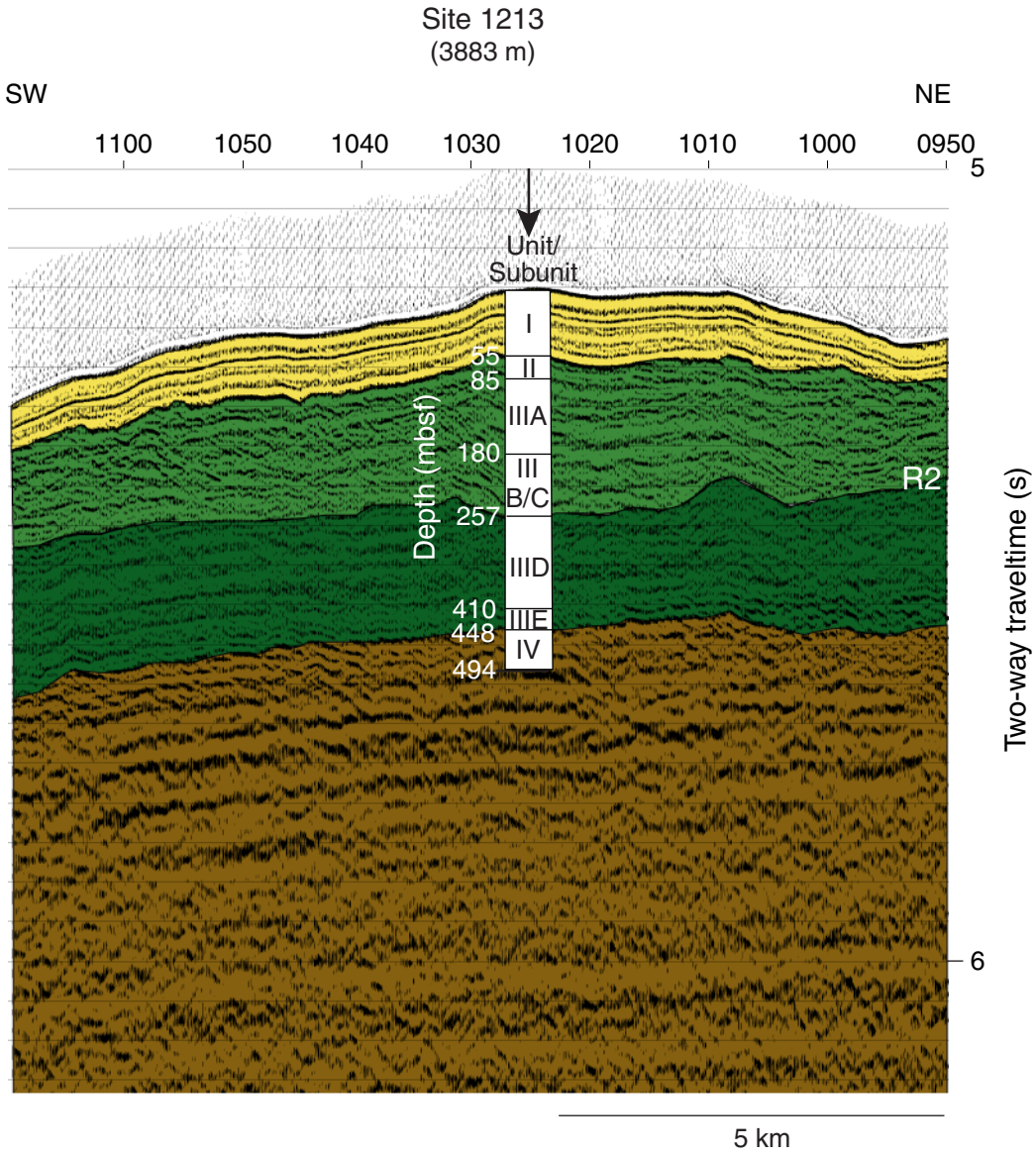
Site 1213
(3883 m)
SW
NE
1100
1050
1040
1030
1020
1010
1000
0950
5
Unit/
Subunit
I
II
IIIA
III
B/C
IIID
IIIE
IV
55
85
180
257
410
448
494
Depth (mbsf)
R2
Two-way traveltime (s)
6
5 km

Figure F35

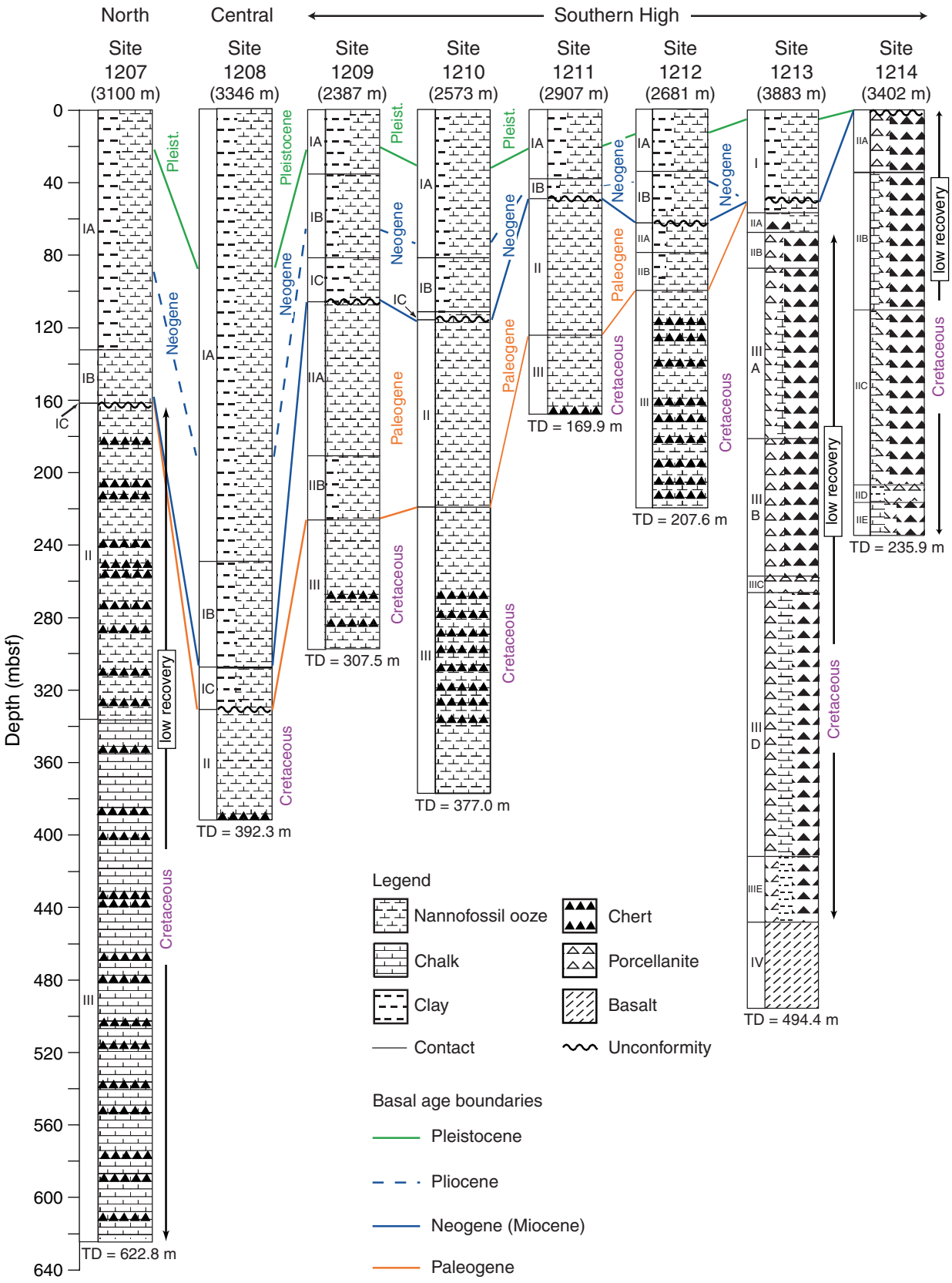
North
Central
Southern High
Site 1207 (3100 m)
Site 1208 (3346 m)
Site 1209 (2387 m)
Site 1210 (2573 m)
Site 1211 (2907 m)
Site 1212 (2681 m)
Site 1213 (3883 m)
Site 1214 (3402 m)
Depth (mbsf)
0
40
80
120
160
200
240
280
320
360
400
440
480
520
560
600
640
Pleist.
Pleistocene
Neogene
Paleogene
Cretaceous
low recovery
TD = 622.8 m
TD = 392.3 m
TD = 307.5 m
TD = 377.0 m
TD = 169.9 m
TD = 207.6 m
TD = 494.4 m
TD = 235.9 m
Legend
Nannofossil ooze
Chalk
Clay
Contact
Chert
Porcellanite
Basalt
Unconformity
Basal age boundaries
Pleistocene
Pliocene
Neogene (Miocene)
Paleogene

Figure F36

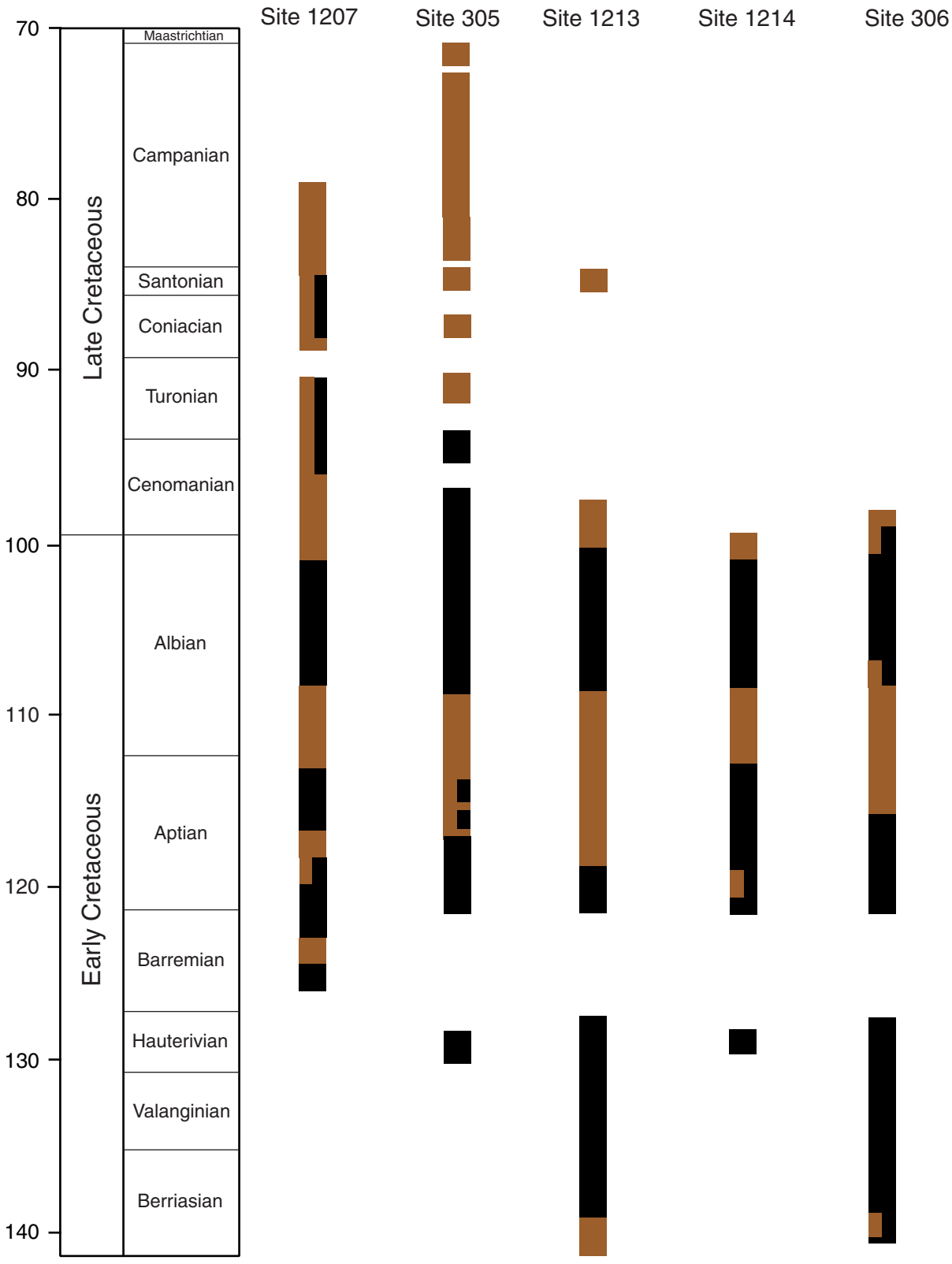
Site 1207
Site 305
Site 1213
Site 1214
Site 306
70
80
90
100
110
120
130
140
Late Cretaceous
Early Cretaceous
Maastrichtian
Campanian
Santonian
Coniacian
Turonian
Cenomanian
Albian
Aptian
Barremian
Hauterivian
Valanginian
Berriasian

Figure F37

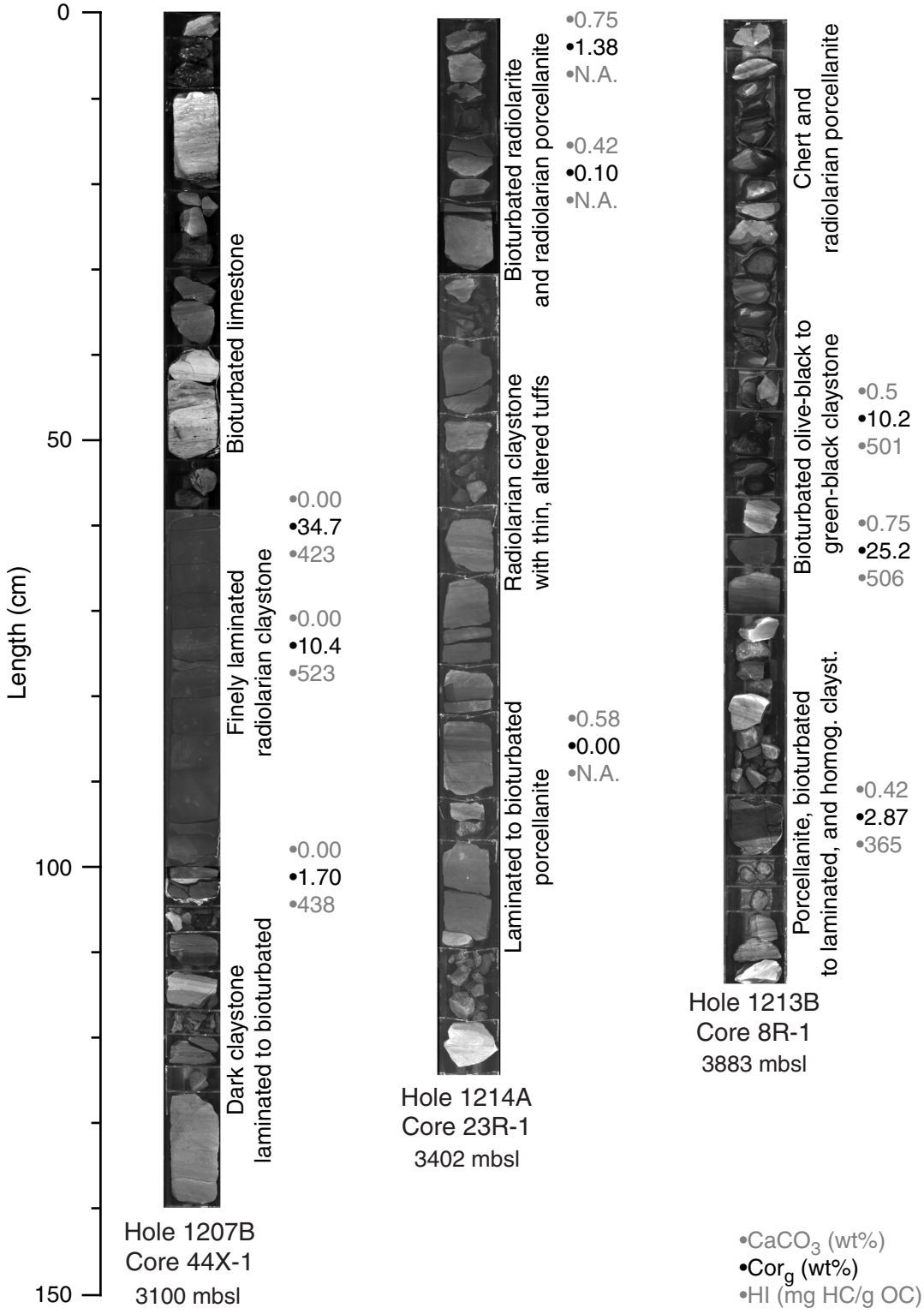
0
50
100
150
Length (cm)
Bioturbated limestone
Finely laminated radiolarian claystone
Dark claystone laminated to bioturbated
•0.00
•34.7
•423
•0.00
•10.4
•523
•0.00
•1.70
•438
Hole 1207B
Core 44X-1
3100 mbsl
Bioturbated radiolarite and radiolarian porcellanite
Radiolarian claystone with thin, altered tuffs
Laminated to bioturbated porcellanite
•0.75
•1.38
•N.A.
•0.42
•0.10
•N.A.
•0.58
•0.00
•N.A.
Hole 1214A
Core 23R-1
3402 mbsl
Chert and radiolarian porcellanite
Bioturbated olive-black to green-black claystone
Porcellanite, bioturbated to laminated, and homog. clayst.
•0.5
•10.2
•501
•0.75
•25.2
•506
•0.42
•2.87
•365
Hole 1213B
Core 8R-1
3883 mbsl
•CaCO3 (wt%)
•Corg (wt%)
•HI (mg HC/g OC)

Figure F38

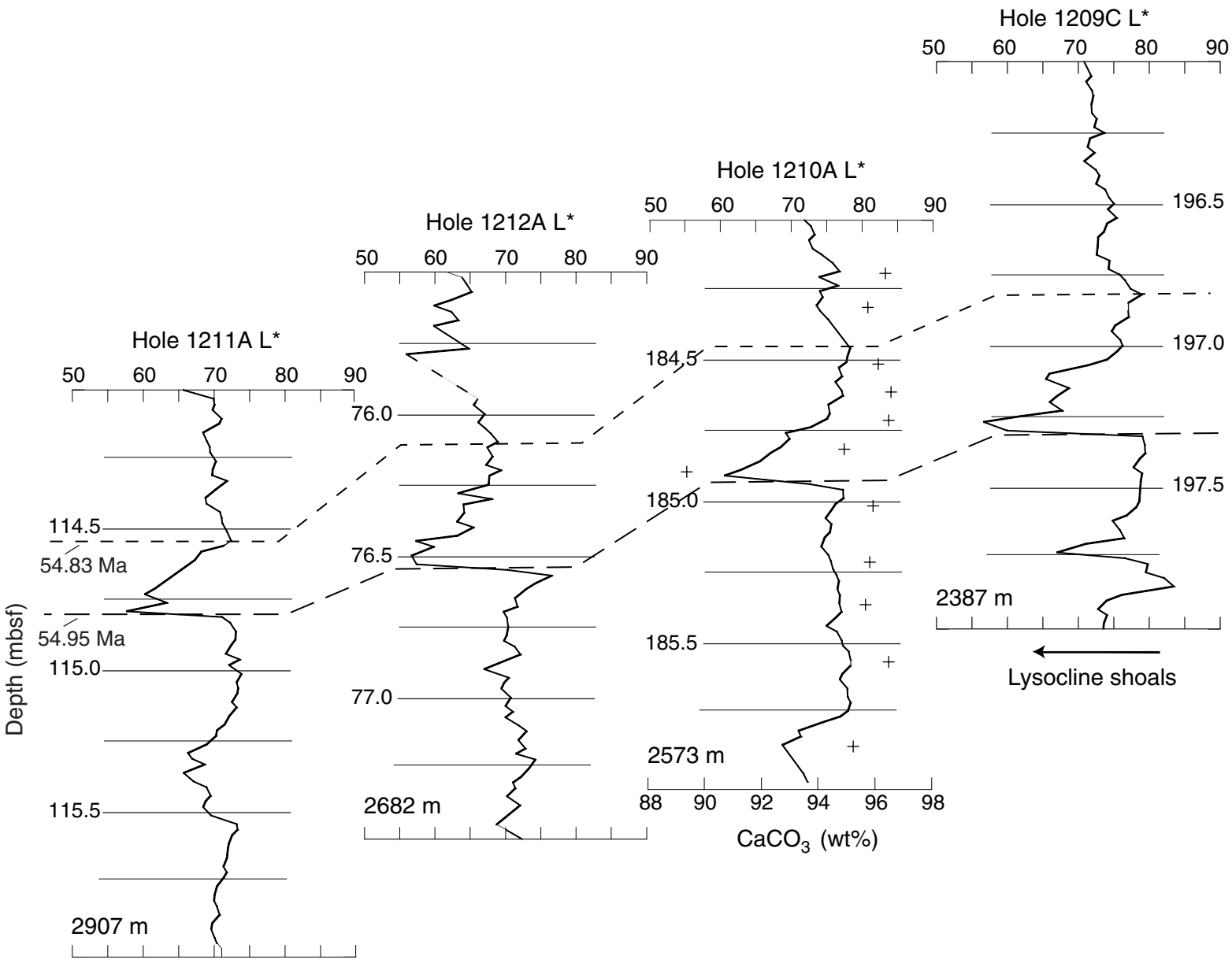
Hole 1209C L*
50 60 70 80 90
196.5
197.0
197.5
2387 m
Lysocline shoals
Hole 1210A L*
50 60 70 80 90
184.5
185.0
185.5
2573 m
88 90 92 94 96 98
CaCO3 (wt%)
Hole 1212A L*
50 60 70 80 90
76.0
76.5
77.0
2682 m
Hole 1211A L*
50 60 70 80 90
114.5
54.83 Ma
54.95 Ma
115.0
115.5
2907 m
Depth (mbsf)

Figure F39

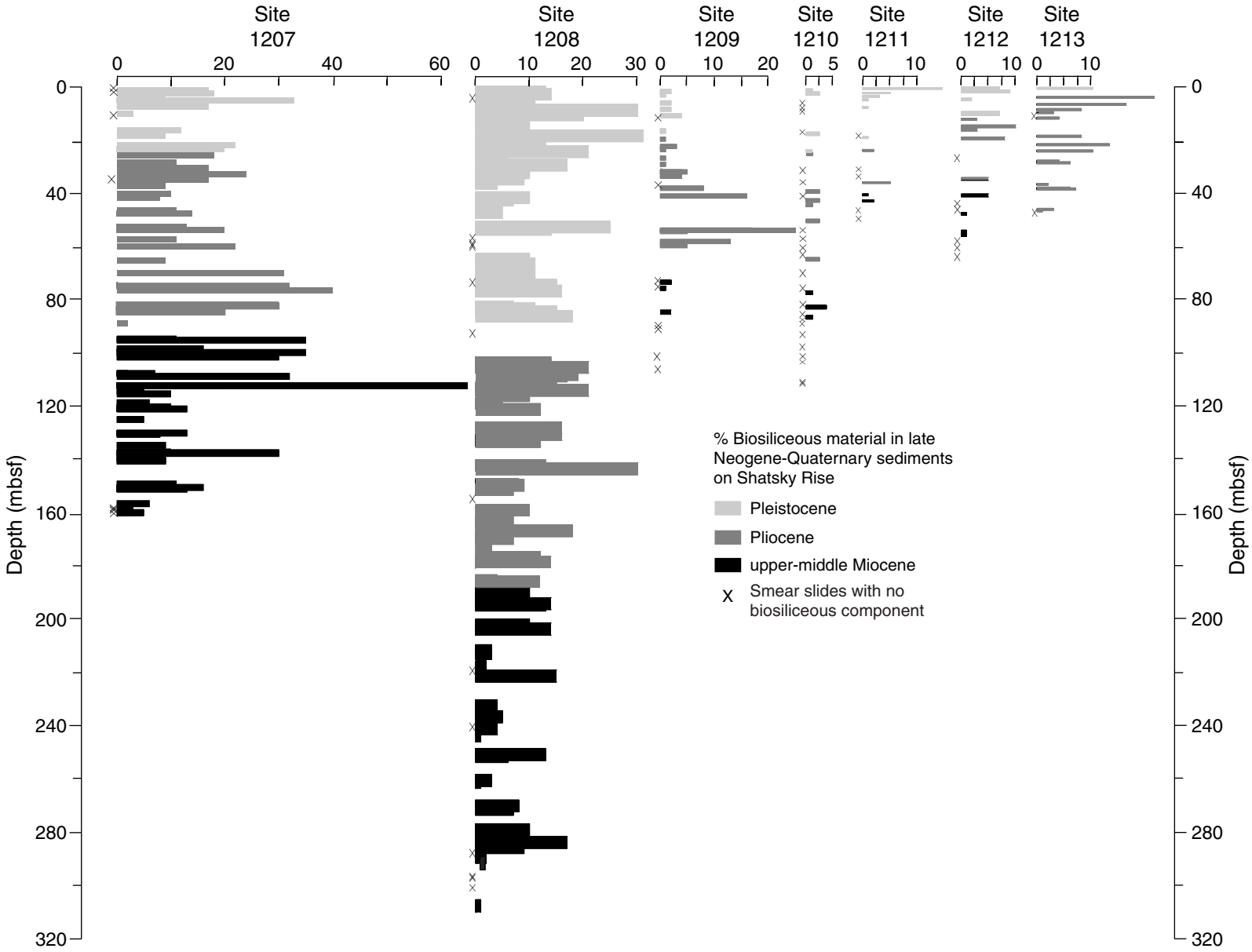
Site 1207
Site 1208
Site 1209
Site 1210
Site 1211
Site 1212
Site 1213
Depth (mbsf)
% Biosiliceous material in late Neogene-Quaternary sediments on Shatsky Rise
Pleistocene
Pliocene
upper-middle Miocene
X Smear slides with no biosiliceous component

Figure F40

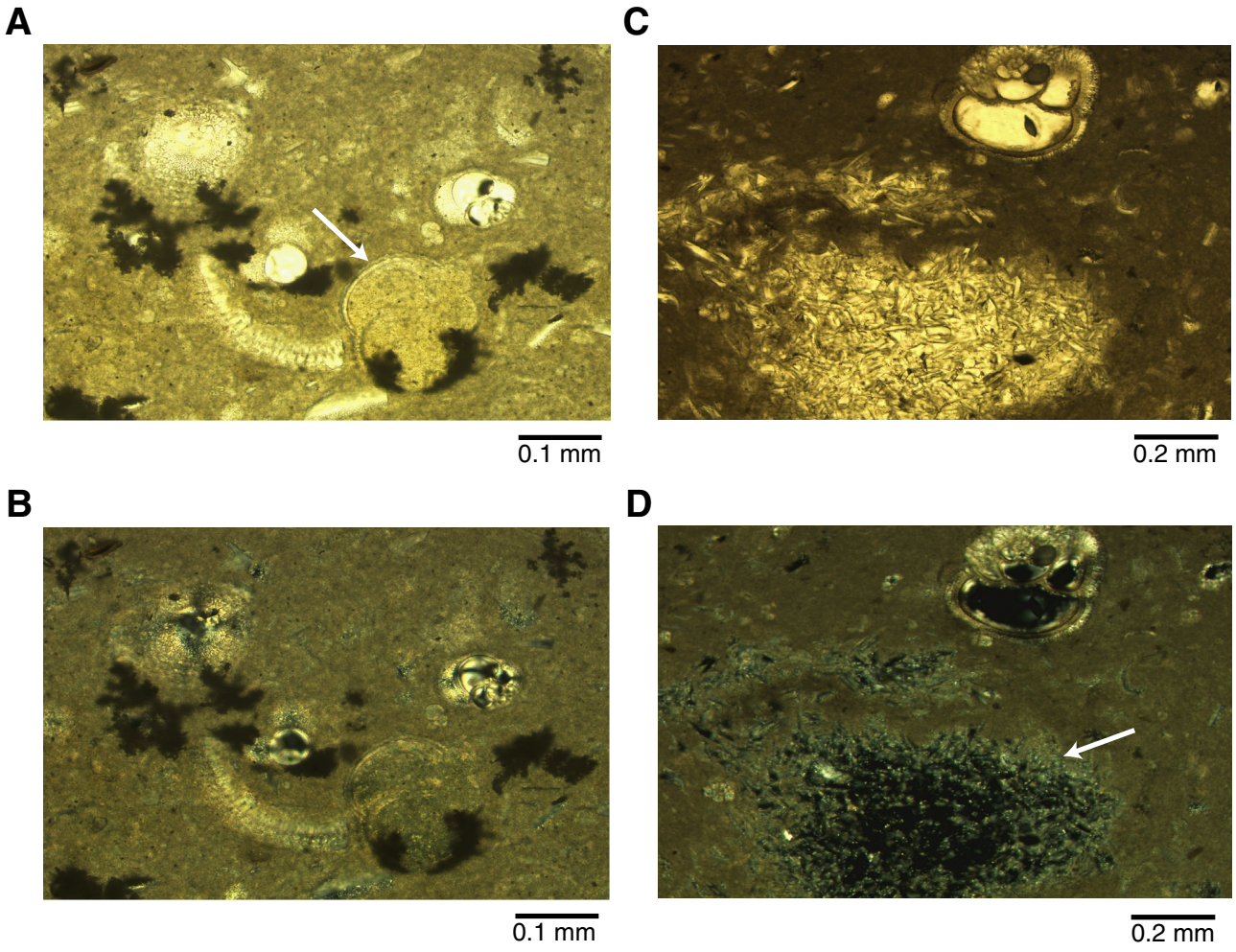

Figure F41

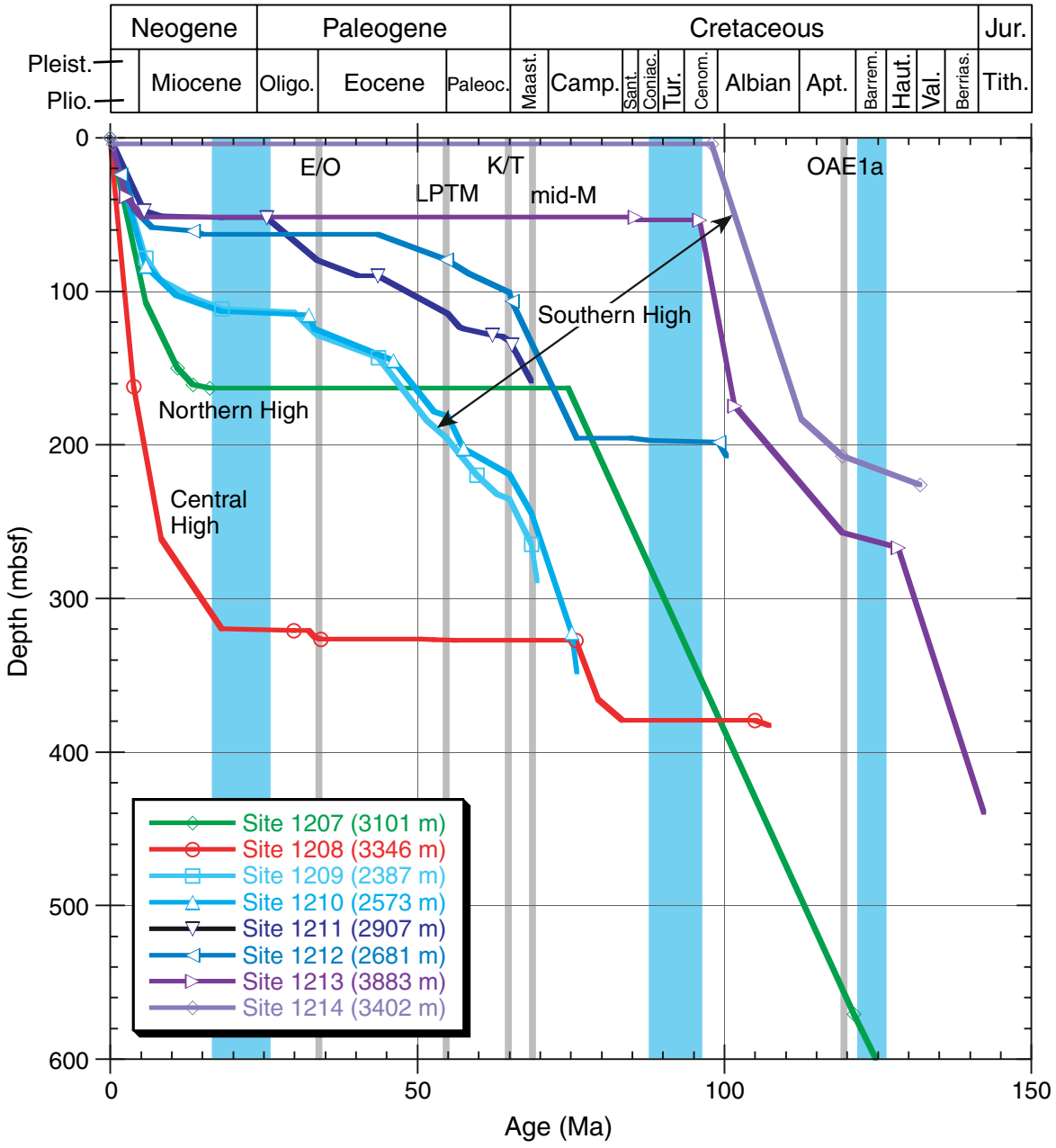
Neogene
Paleogene
Cretaceous
Jur.
Pleist.
Plio.
Miocene
Oligo.
Eocene
Paleoc.
Maast.
Camp.
Sant.
Coniac.
Tur.
Cenom.
Albian
Apt.
Barrem.
Haut.
Val.
Berrias.
Tith.
E/O
K/T
LPTM
mid-M
OAE1a
Southern High
Northern High
Central High
Depth (mbsf)
Age (Ma)
0
100
200
300
400
500
600
0
50
100
150
Site 1207 (3101 m)
Site 1208 (3346 m)
Site 1209 (2387 m)
Site 1210 (2573 m)
Site 1211 (2907 m)
Site 1212 (2681 m)
Site 1213 (3883 m)
Site 1214 (3402 m)

Figure F42

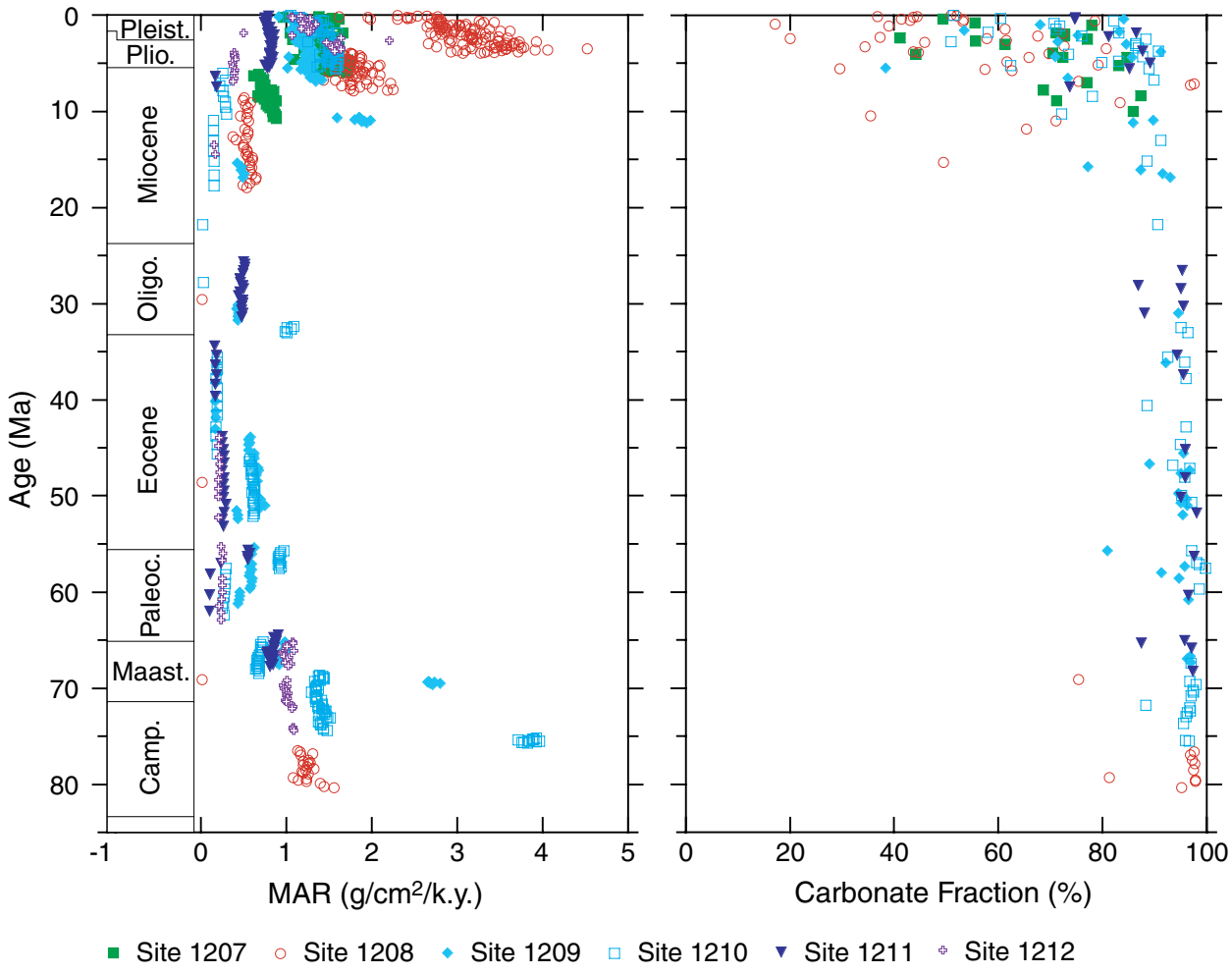
Pleist.
Plio.
Miocene
Oligo.
Eocene
Paleoc.
Maast.
Camp.
Age (Ma)
0
10
20
30
40
50
60
70
80
-1
0
1
2
3
4
5
MAR (g/cm2/k.y.)
0
20
40
60
80
100
Carbonate Fraction (%)
Site 1207
Site 1208
Site 1209
Site 1210
Site 1211
Site 1212

Figure F43

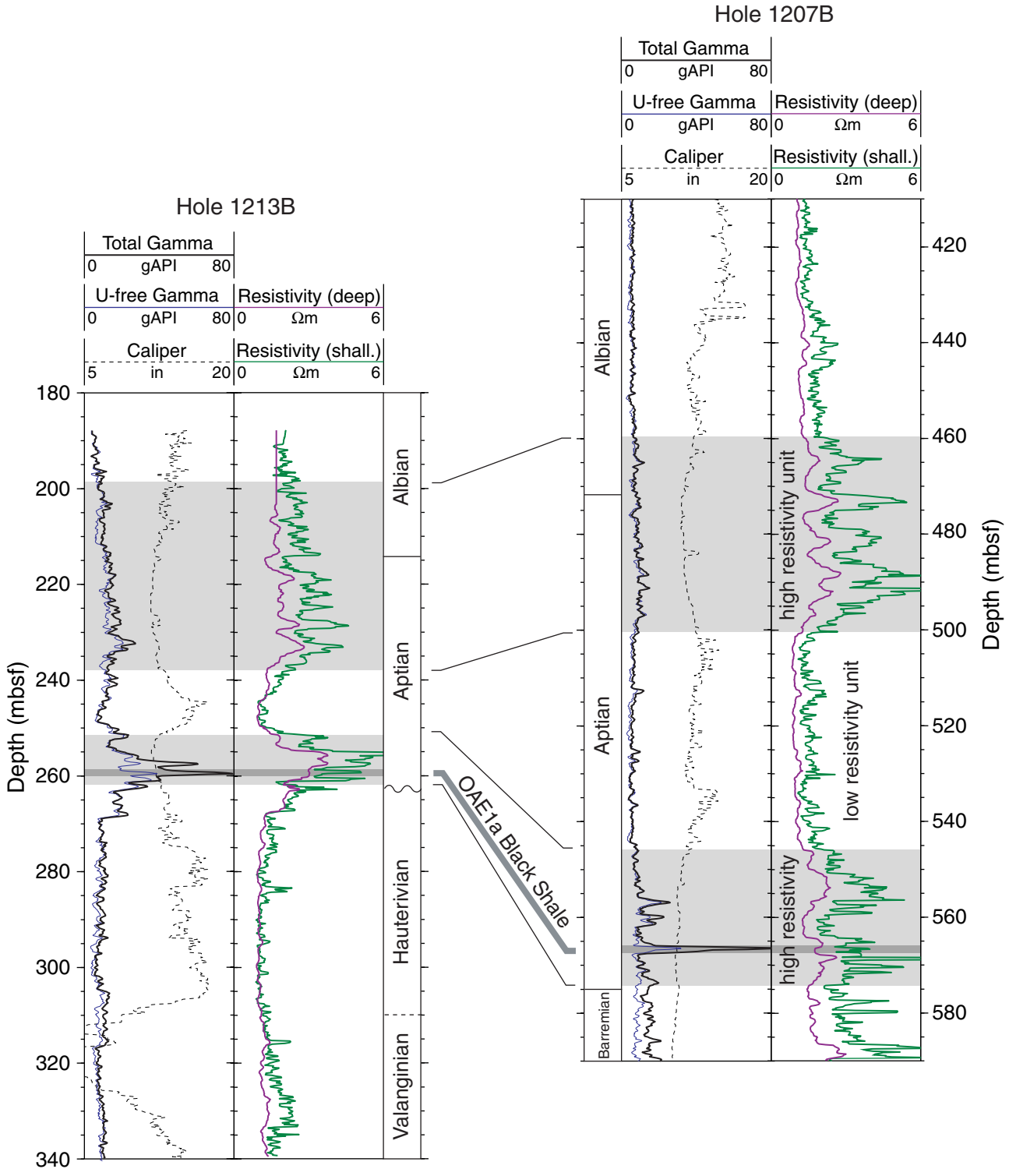
Hole 1213B
Total Gamma
0 gAPI 80
U-free Gamma
0 gAPI 80
Resistivity (deep)
0 Ωm 6
Caliper
5 in 20
Resistivity (shall.)
0 Ωm 6
Depth (mbsf)
180
200
220
240
260
280
300
320
340
Albian
Aptian
Hauterivian
Valanginian
Hole 1207B
Total Gamma
0 gAPI 80
U-free Gamma
0 gAPI 80
Resistivity (deep)
0 Ωm 6
Caliper
5 in 20
Resistivity (shall.)
0 Ωm 6
Albian
Aptian
Barremian
high resistivity unit
low resistivity unit
high resistivity
OAE1a Black Shale
420
440
460
480
500
520
540
560
580
Depth (mbsf)

Figure F44

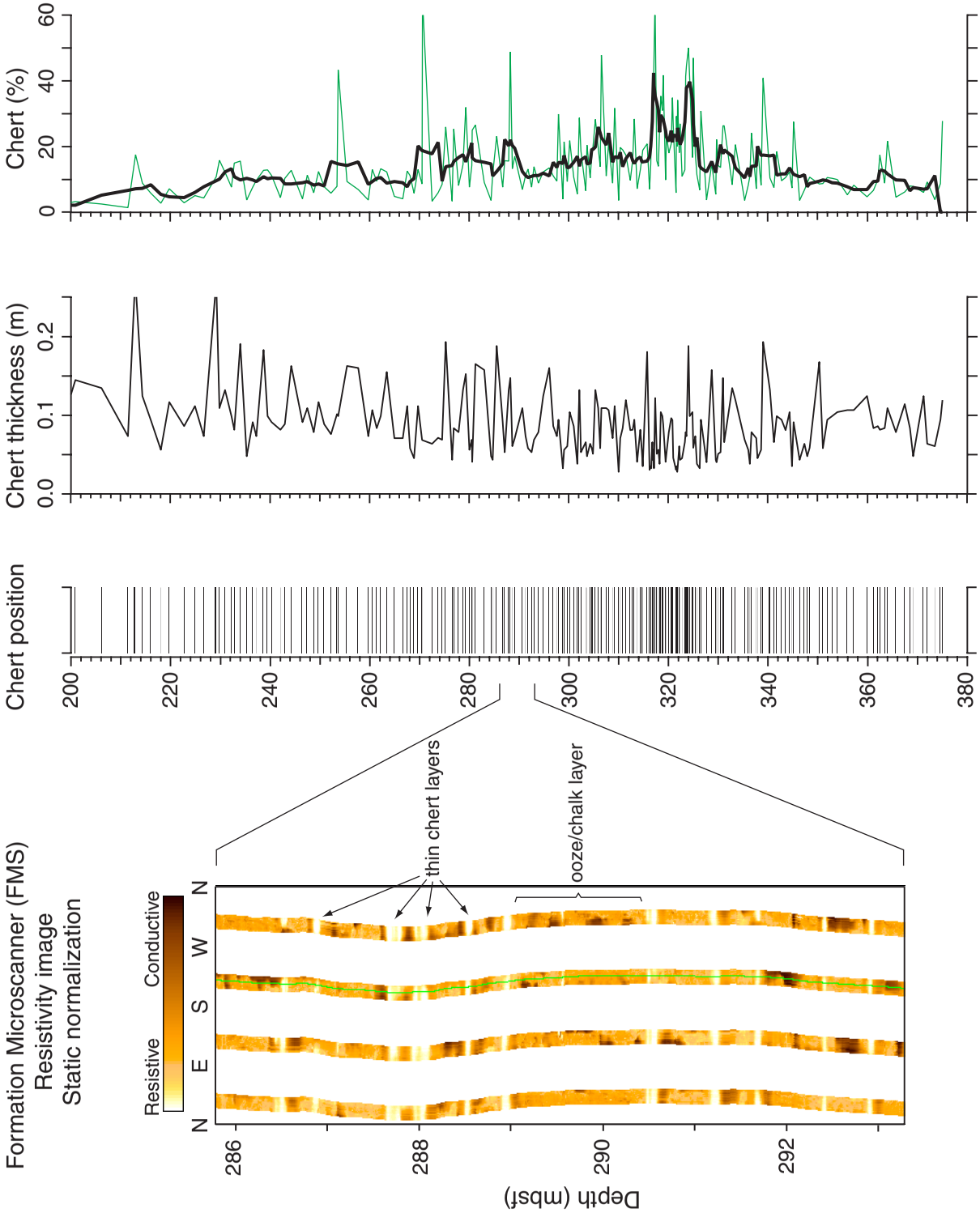
Chert (%)
0
20
40
60
Chert thickness (m)
0.0
0.1
0.2
Chert position
200
220
240
260
280
300
320
340
360
380
thin chert layers
ooze/chalk layer
Formation Microscanner (FMS)
Resistivity image
Static normalization
Resistive
Conductive
N
E
S
W
N
286
288
290
292
Depth (mbsf)

Figure F45

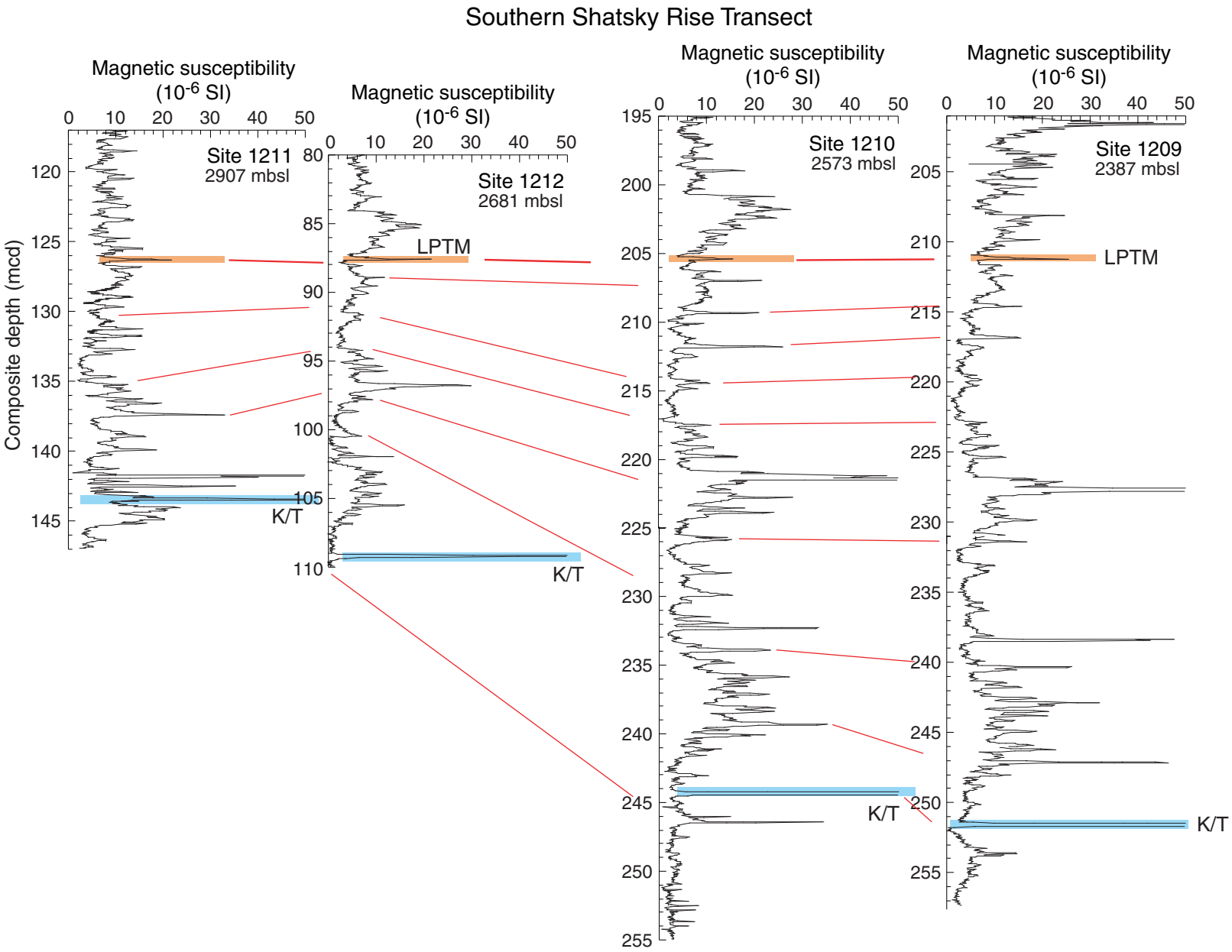
Southern Shatsky Rise Transect
Magnetic susceptibility
(10-6 SI)
Site 1211
2907 mbsl
Site 1212
2681 mbsl
Site 1210
2573 mbsl
Site 1209
2387 mbsl
LPTM
K/T
Composite depth (mcd)

Figure F46

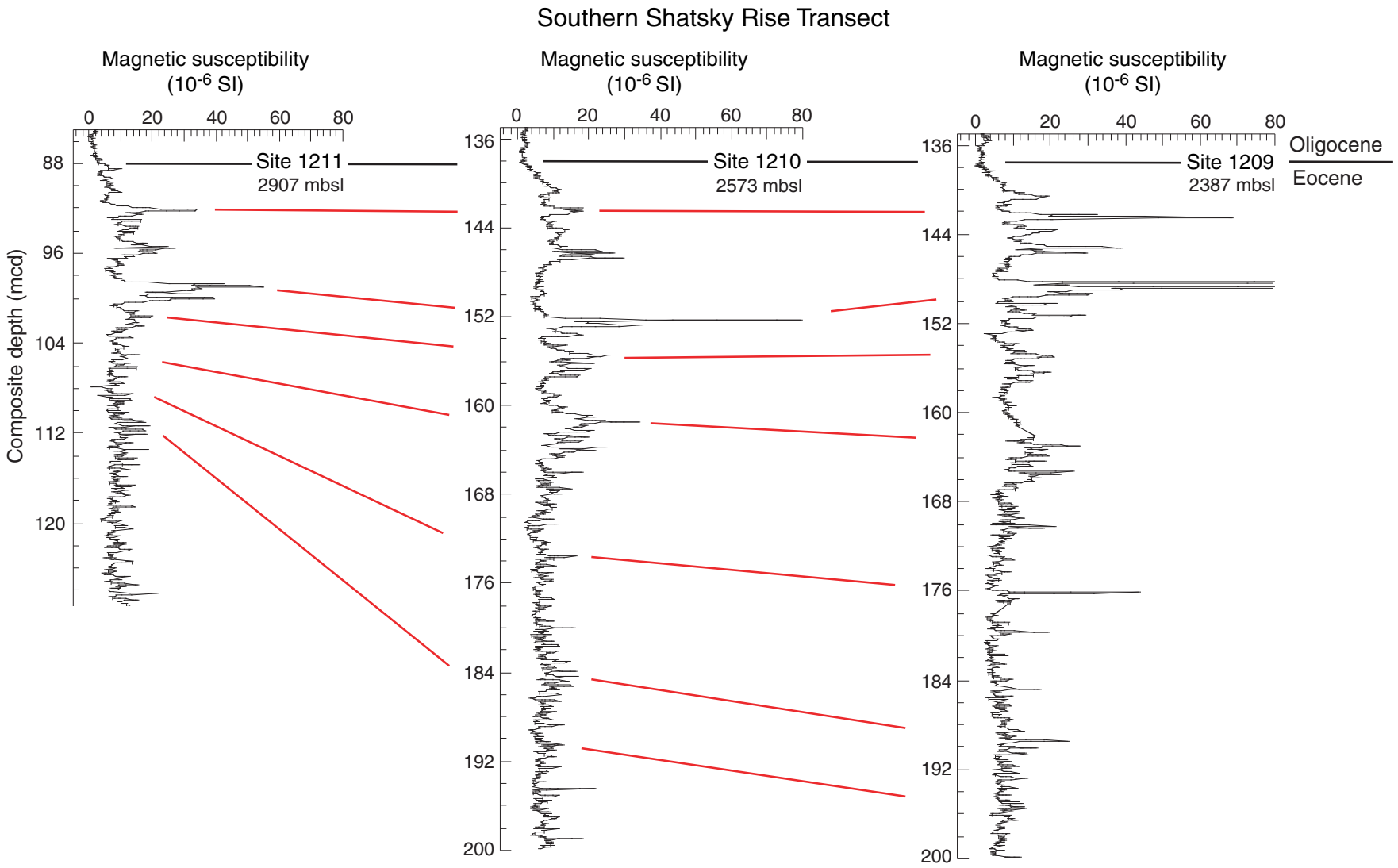
Southern Shatsky Rise Transect
Magnetic susceptibility
(10-6 SI)
0
20
40
60
80
Site 1211
2907 mbsl
Site 1210
2573 mbsl
Site 1209
2387 mbsl
Oligocene
Eocene
Composite depth (mcd)
88
96
104
112
120
136
144
152
160
168
176
184
192
200

Figure F47

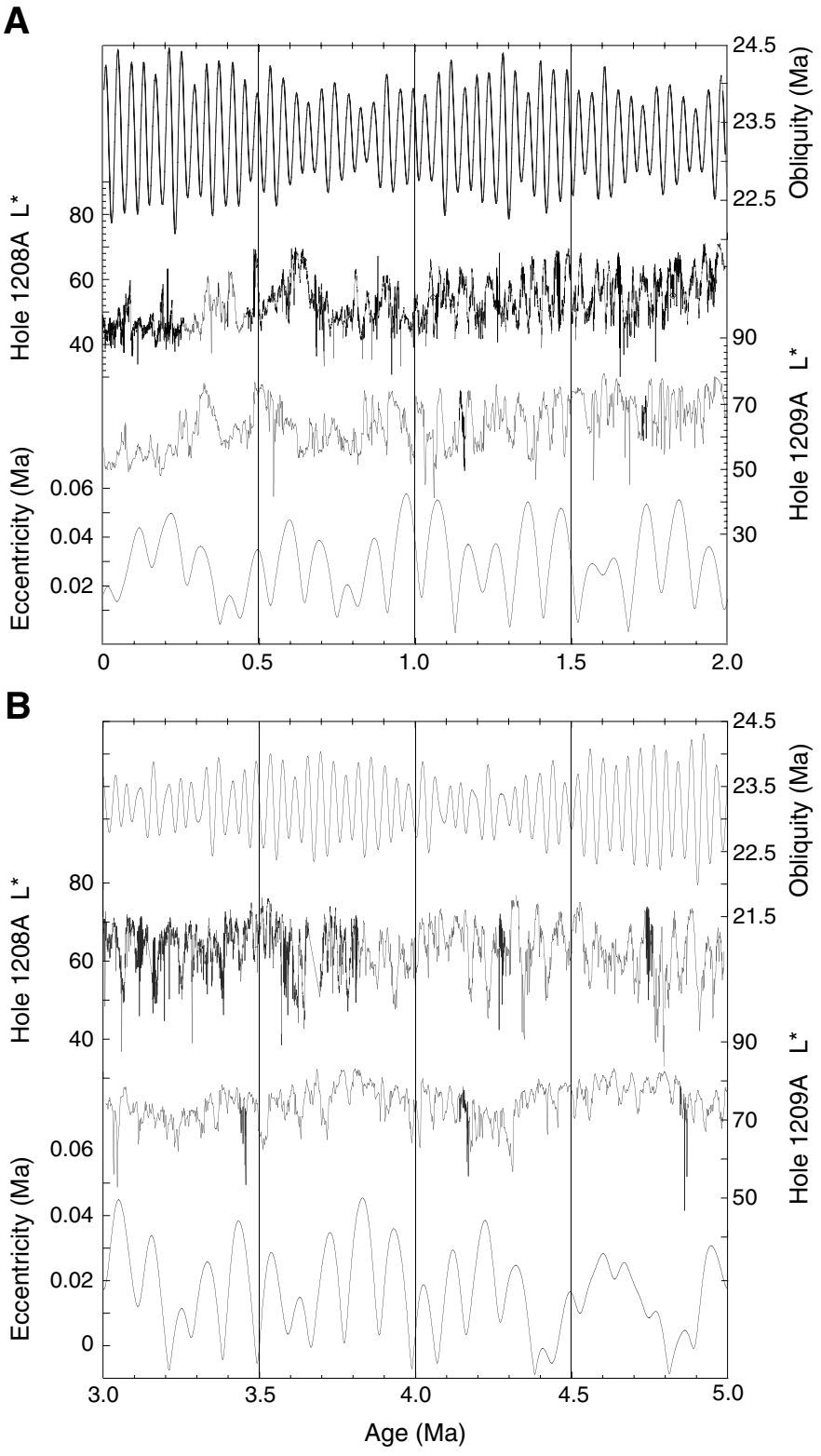
A
B
Hole 1208A L*
Obliquity (Ma)
Hole 1209A L*
Eccentricity (Ma)
Age (Ma)
24.5
23.5
22.5
21.5
80
60
40
90
70
50
30
0.06
0.04
0.02
0
0
0.5
1.0
1.5
2.0
3.0
3.5
4.0
4.5
5.0

Figure F48

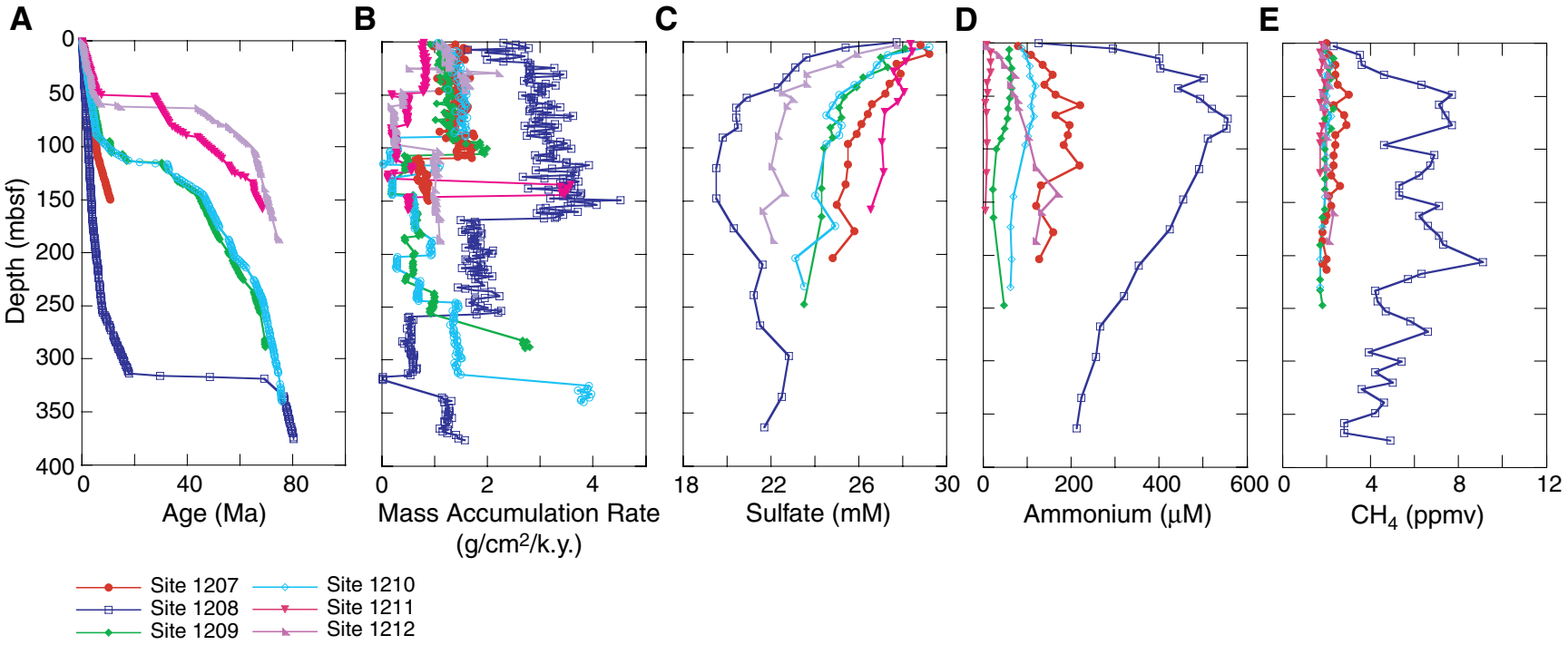
A
B
C
D
E
Depth (mbsf)
0
50
100
150
200
250
300
350
400
0
40
80
Age (Ma)
0
2
4
Mass Accumulation Rate
(g/cm2/k.y.)
18
22
26
30
Sulfate (mM)
0
200
400
600
Ammonium (µM)
0
4
8
12
CH4 (ppmv)
Site 1207
Site 1208
Site 1209
Site 1210
Site 1211
Site 1212

Figure F49

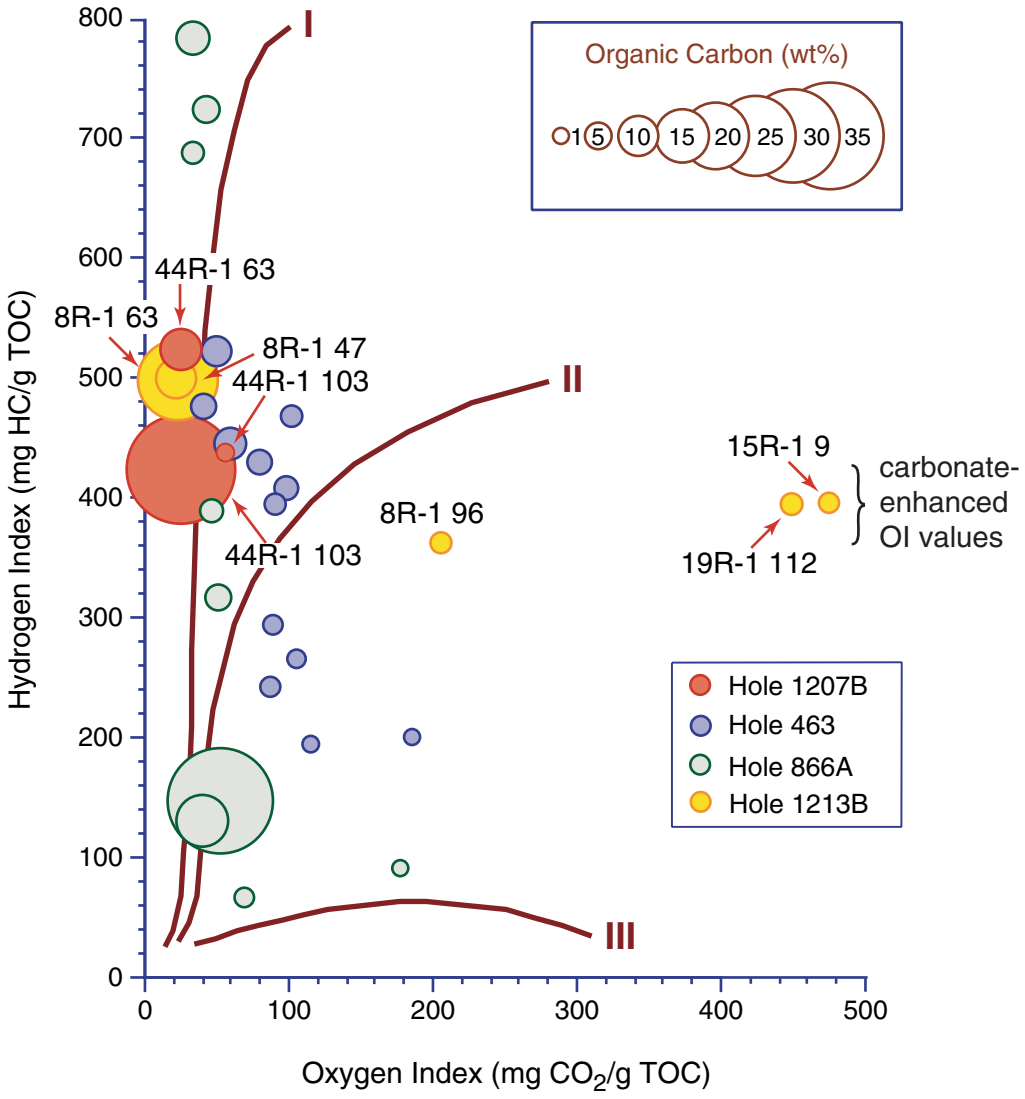
Organic Carbon (wt%)
1
5
10
15
20
25
30
35
I
II
III
44R-1 63
8R-1 63
8R-1 47
44R-1 103
8R-1 96
44R-1 103
15R-1 9
19R-1 112
carbonate-enhanced OI values
Hole 1207B
Hole 463
Hole 866A
Hole 1213B
Hydrogen Index (mg HC/g TOC)
Oxygen Index (mg CO2/g TOC)
800
700
600
500
400
300
200
100
0
0
100
200
300
400
500

Figure F50

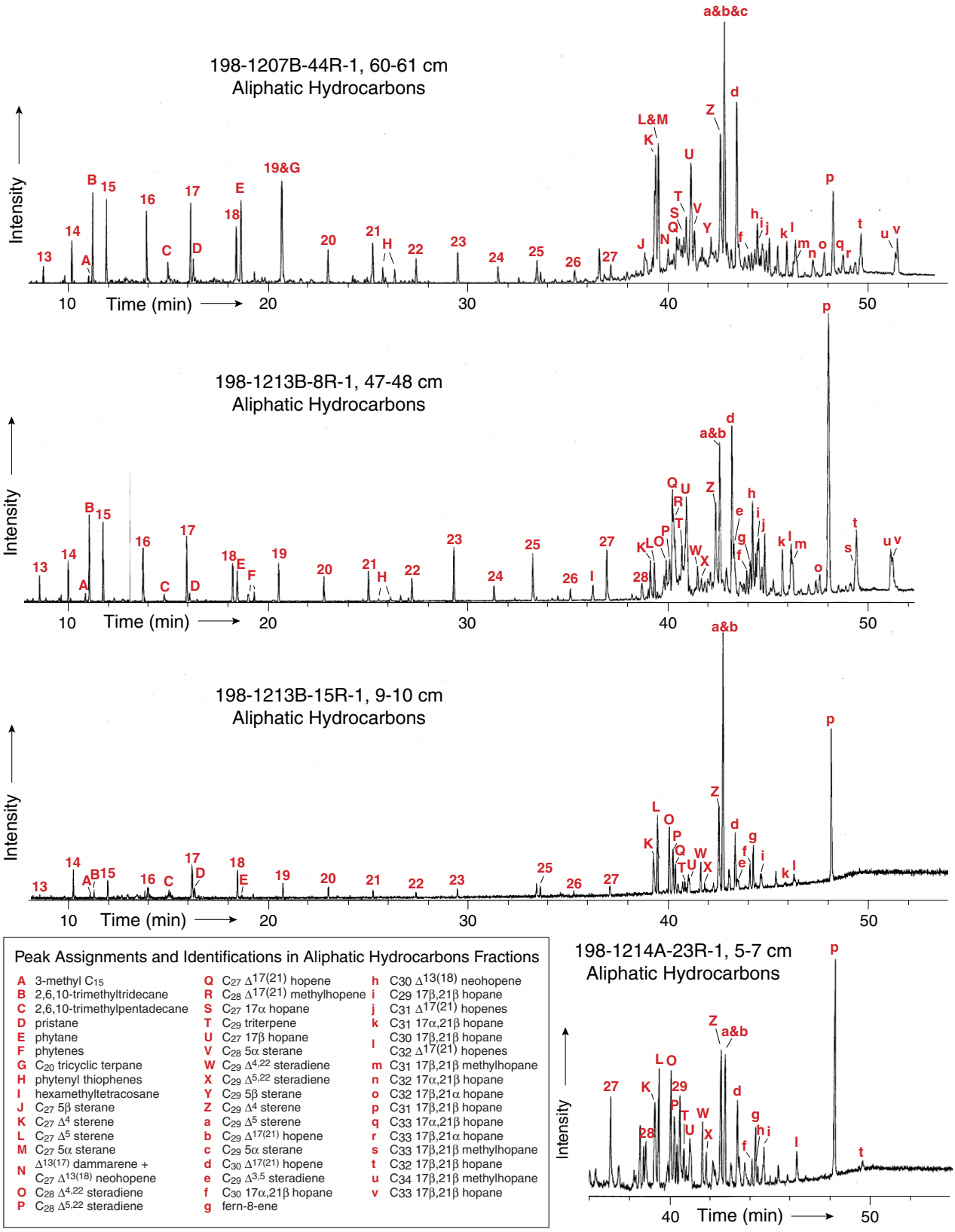
198-1207B-44R-1, 60-61 cm
Aliphatic Hydrocarbons
198-1213B-8R-1, 47-48 cm
Aliphatic Hydrocarbons
198-1213B-15R-1, 9-10 cm
Aliphatic Hydrocarbons
198-1214A-23R-1, 5-7 cm
Aliphatic Hydrocarbons
Intensity
Time (min)
Peak Assignments and Identifications in Aliphatic Hydrocarbons Fractions
A 3-methyl C15
B 2,6,10-trimethyltridecane
C 2,6,10-trimethylpentadecane
D pristane
E phytane
F phytenes
G C20 tricyclic terpane
H phytenyl thiophenes
I hexamethyltetracosane
J C27 5β sterane
K C27 Δ4 sterene
L C27 Δ5 sterene
M C27 5α sterane
N Δ13(17) dammarene + C27 Δ13(18) neohopene
O C28 Δ4,22 steradiene
P C28 Δ5,22 steradiene
Q C27 Δ17(21) hopene
R C28 Δ17(21) methylhopene
S C27 17α hopane
T C29 triterpene
U C27 17β hopane
V C28 5α sterane
W C29 Δ4,22 steradiene
X C29 Δ5,22 steradiene
Y C29 5β sterane
Z C29 Δ4 sterene
a C29 Δ5 sterene
b C29 Δ17(21) hopene
c C29 5α sterane
d C30 Δ17(21) hopene
e C29 Δ3,5 steradiene
f C30 17α,21β hopane
g fern-8-ene
h C30 Δ13(18) neohopene
i C29 17β,21β hopane
j C31 Δ17(21) hopenes
k C31 17α,21β hopane
l C30 17β,21β hopane + C32 Δ17(21) hopenes
m C31 17β,21β methylhopane
n C32 17α,21β hopane
o C32 17β,21α hopane
p C31 17β,21β hopane
q C33 17α,21β hopane
r C33 17β,21α hopane
s C33 17β,21β methylhopane
t C32 17β,21β hopane
u C34 17β,21β methylhopane
v C33 17β,21β hopane

Figure F51

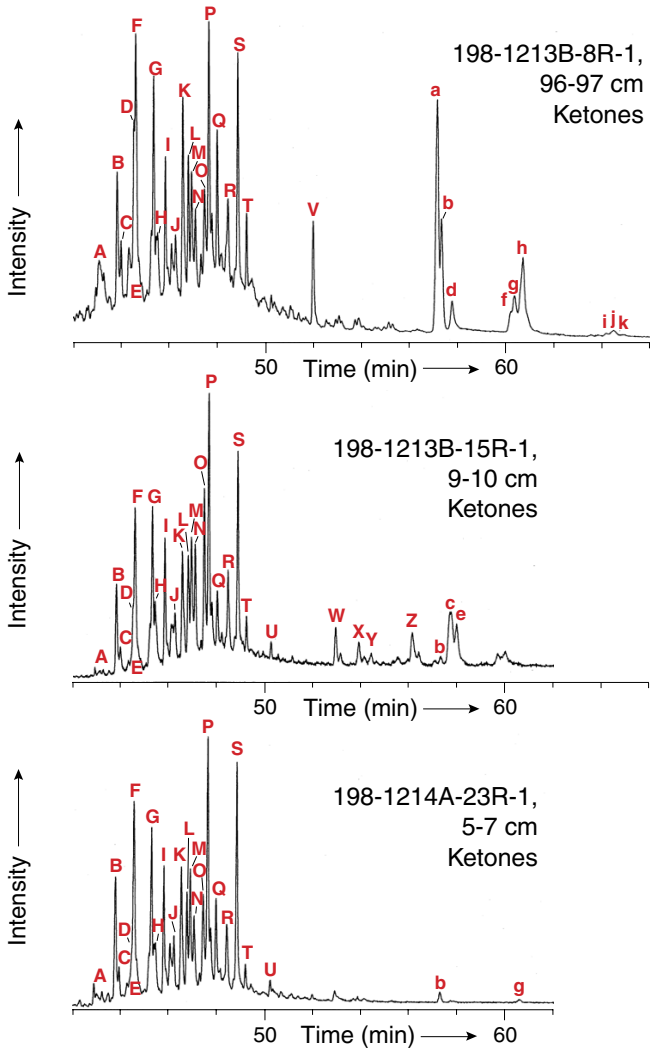

Peak Assignments and Identifications in Ketones Fractions

A	β-, γ-tocopherol	T	C_{30} triterpenone + C_{30} Δ^{22} 4-methyl 5α stanone
B	unknown	U	C_{30} 17β,21β hopanone
C	C_{27} 5β stanone	V	C_{32} 17β,21β methylhopanyl methyl ether
D	C_{27} 17β hopanone	W	C_{27} Δ^5 stenyl ether
E	α-tocopherol	X	C_{28} stenyl ether
F	C_{27} 5α stanone	Y	C_{27} Δ^5 stenyl ether
G	C_{28} Δ^{22} stanone	Z	C_{29} stenyl ether
H	C_{28} 4-methyl 5α stanone	a	C_{34} 17β,21β methylhopanone
I	C_{27} Δ^4 stenone	b	C_{33} 17β,21β hopanone
J	C_{28} 5α stanone	c	C_{29} Δ^{22} stenyl ether
K	C_{28} $\Delta^{4,22}$ stenone	d	$C_{37:2}$ methylalkenone
L	C_{29} Δ^{22} stanone	e	nonyl C_{29} stenyl ether
M	C_{29} 5β stanone	f	C_{35} 17β,21β methylhopanone
N	C_{29} 4-methyl 5α stanone	g	C_{34} 17β,21β hopanone
O	C_{30} Δ^{22} 4-methyl 5α stanone + C_{28} Δ^4 stenone	h	$C_{38:2}$ ethylalkenone
P	C_{29} 5α stanone	i	C_{36} 17β,21β methylhopanone
Q	C_{29} $\Delta^{4,22}$ stenone	j	C_{35} 17β,21β hopanone
R	C_{30} 4-methyl 5α stanone	k	$C_{39:2}$ methylalkenone
S	C_{29} Δ^4 stenone		

Figure F51 (continued)

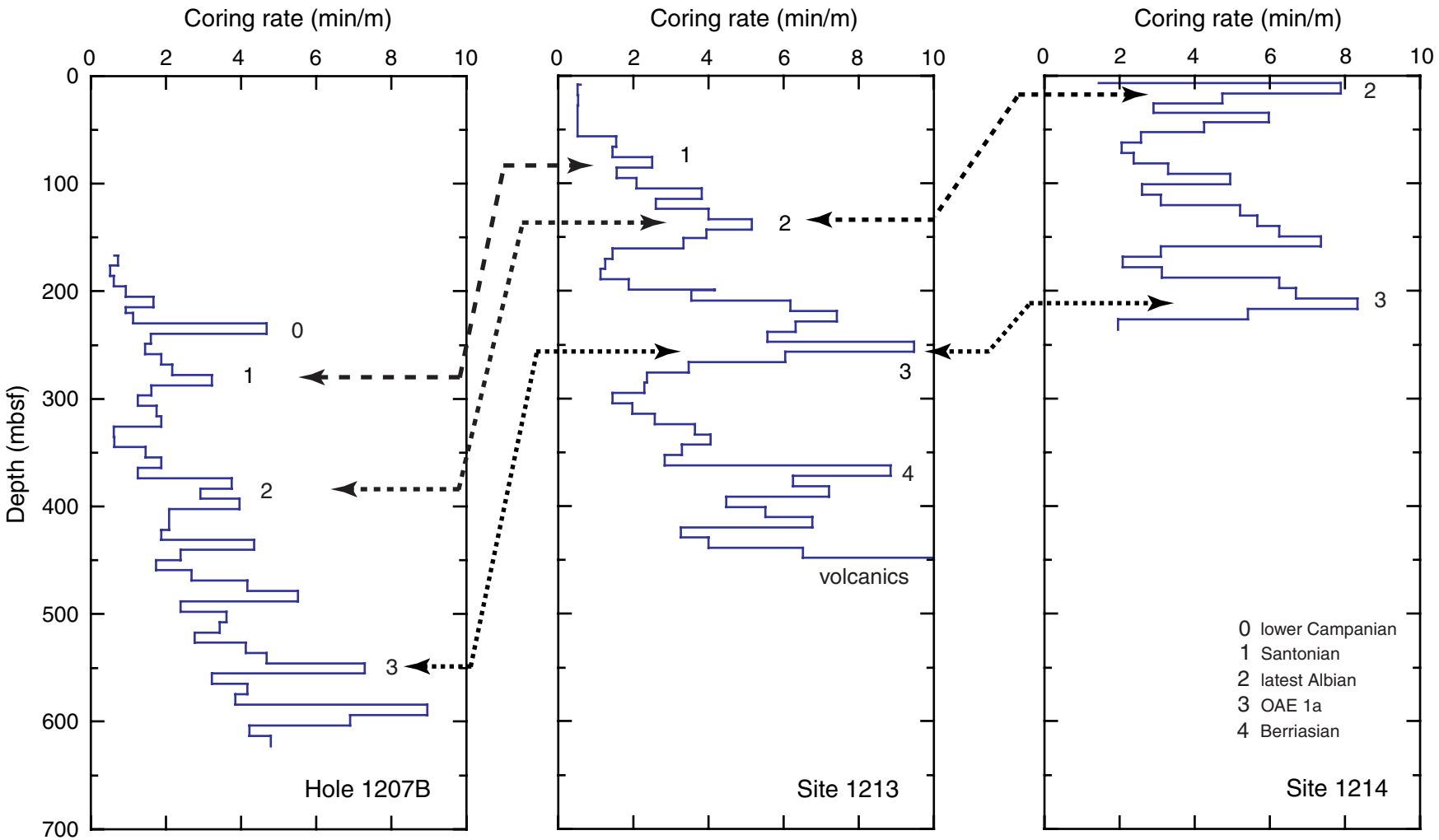
Coring rate (min/m)
Coring rate (min/m)
Coring rate (min/m)
Depth (mbsf)
Hole 1207B
Site 1213
Site 1214
volcanics
0 lower Campanian
1 Santonian
2 latest Albian
3 OAE 1a
4 Berriasian

Figure F52

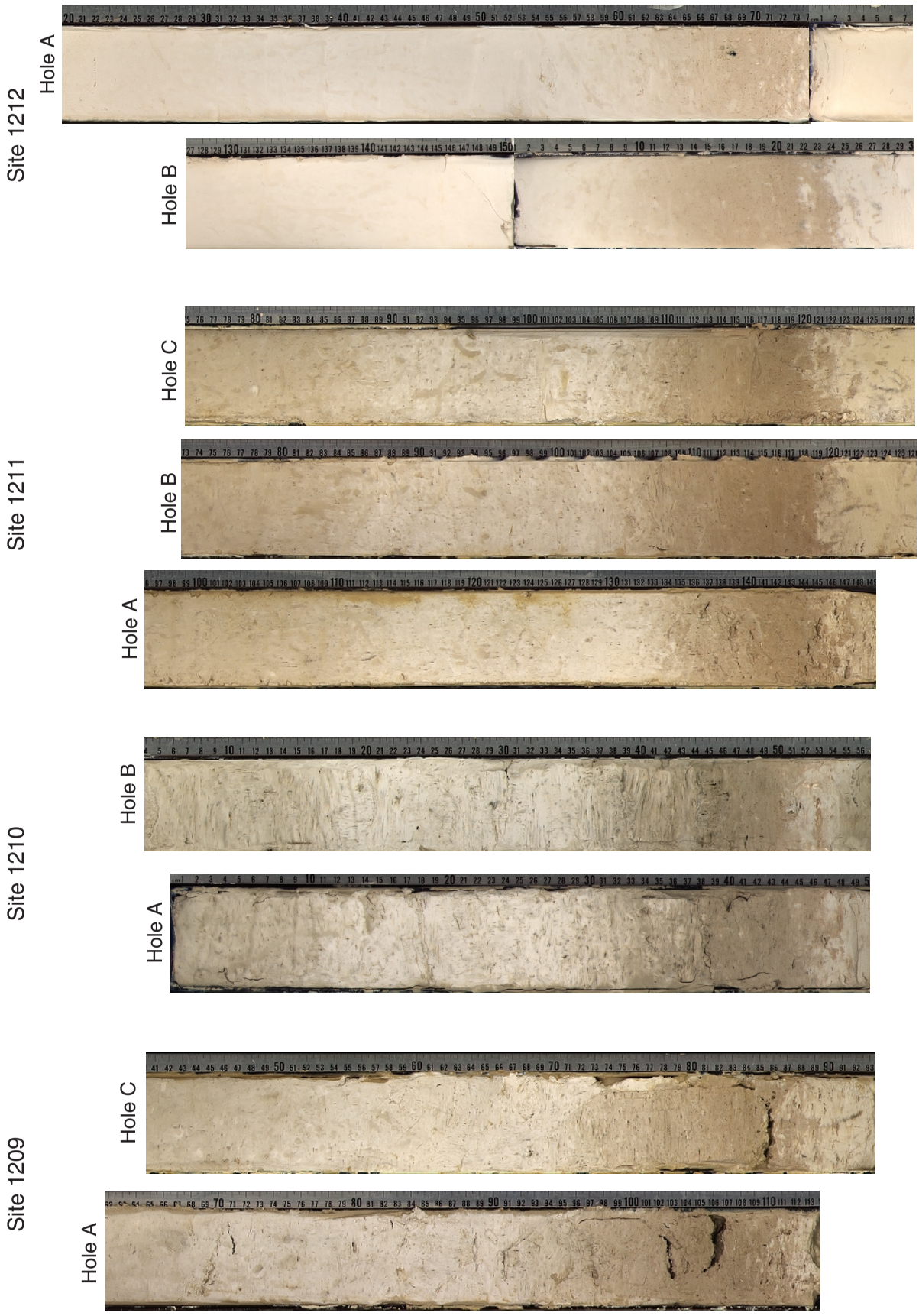
Site 1212
Hole A
Hole B
Site 1211
Hole C
Hole B
Hole A
Site 1210
Hole B
Hole A
Site 1209
Hole C
Hole A

Figure F53

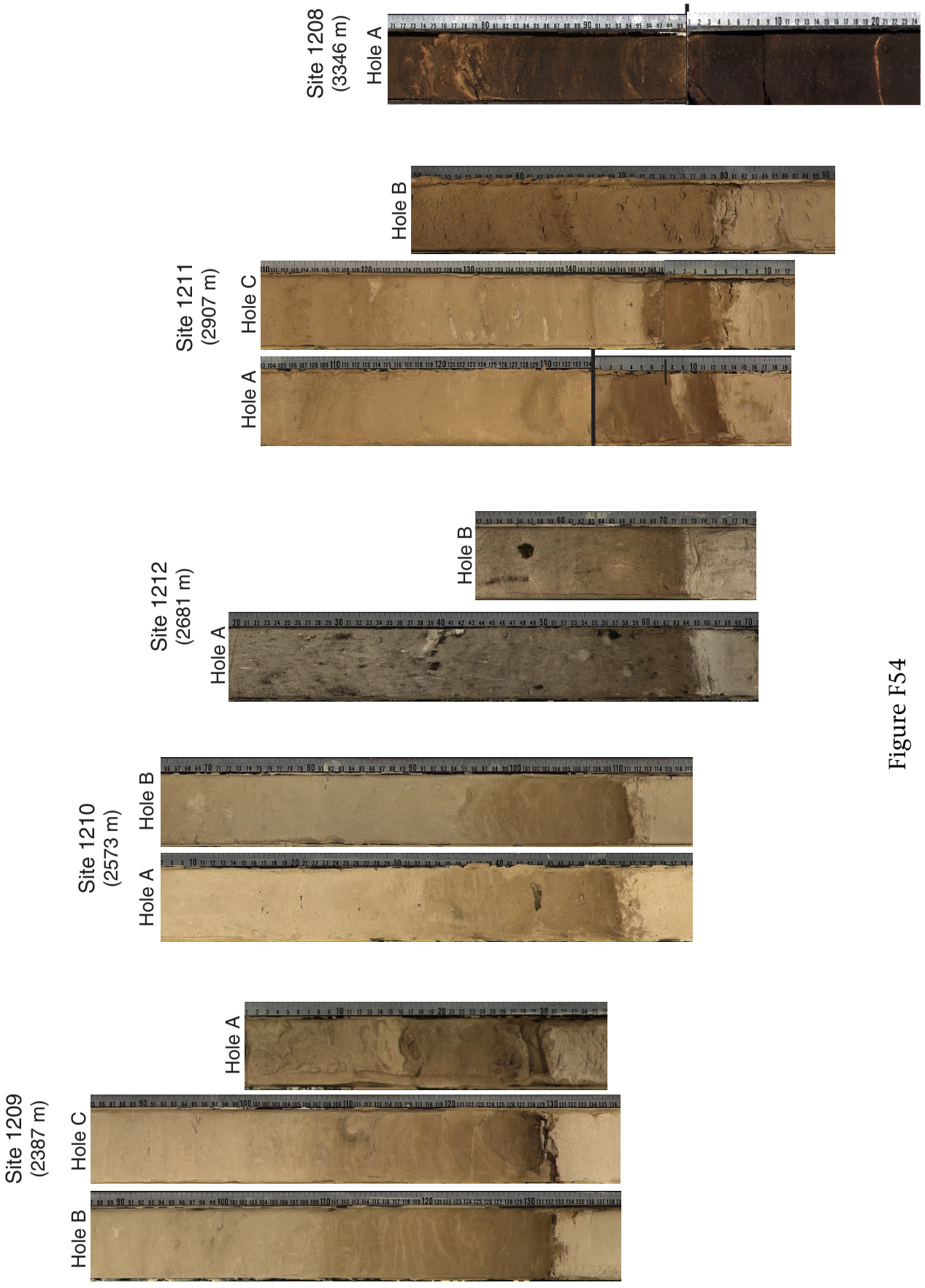
Site 1208
(3346 m)
Hole A
Hole B
Site 1211
(2907 m)
Hole C
Hole A
Site 1212
(2681 m)
Hole B
Hole A
Site 1210
(2573 m)
Hole B
Hole A
Site 1209
(2387 m)
Hole A
Hole C
Hole B

Figure F54

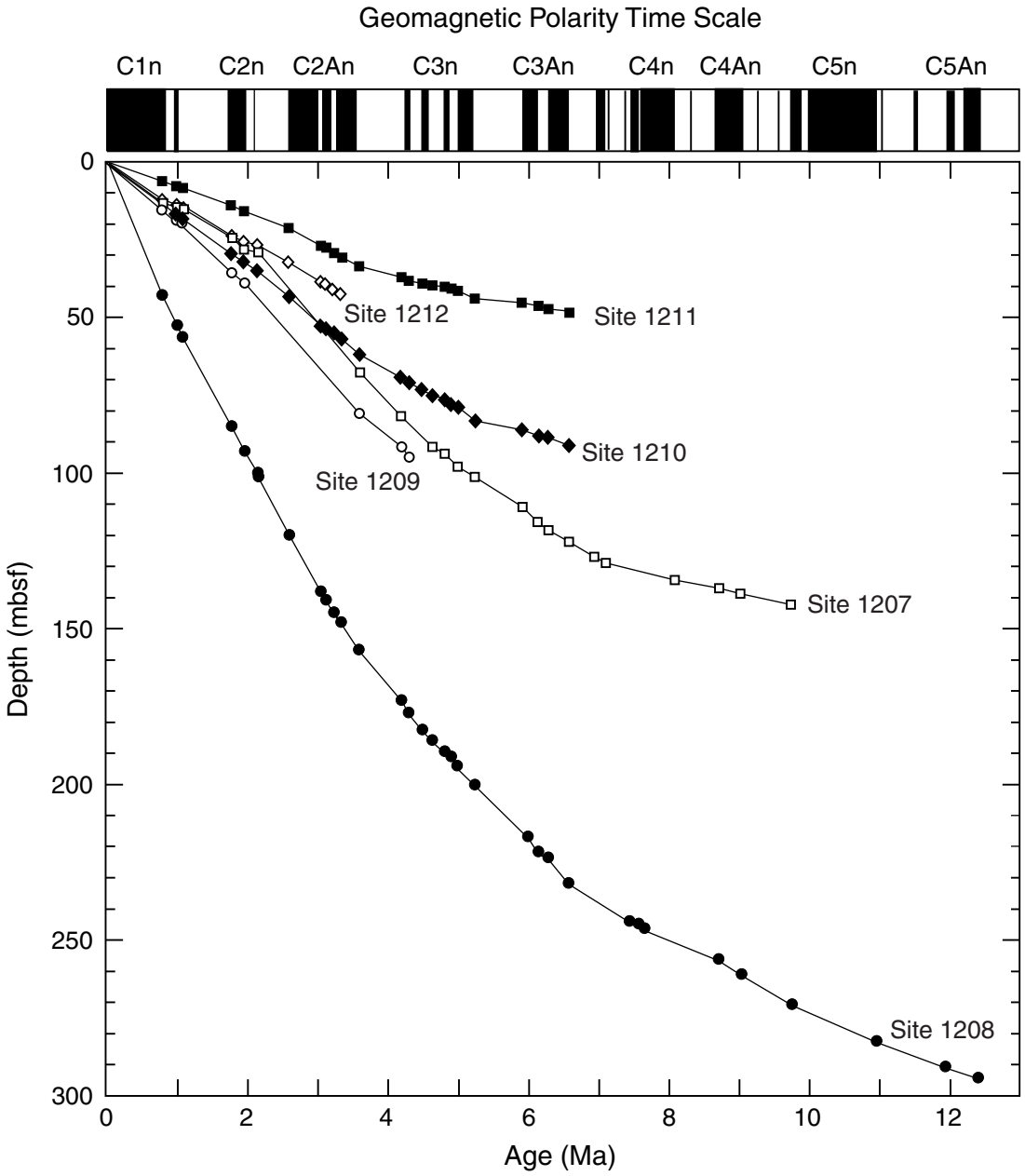
Geomagnetic Polarity Time Scale
C1n
C2n
C2An
C3n
C3An
C4n
C4An
C5n
C5An
Site 1212
Site 1211
Site 1210
Site 1209
Site 1207
Site 1208
Depth (mbsf)
Age (Ma)
0
50
100
150
200
250
300
0
2
4
6
8
10
12

Figure F55

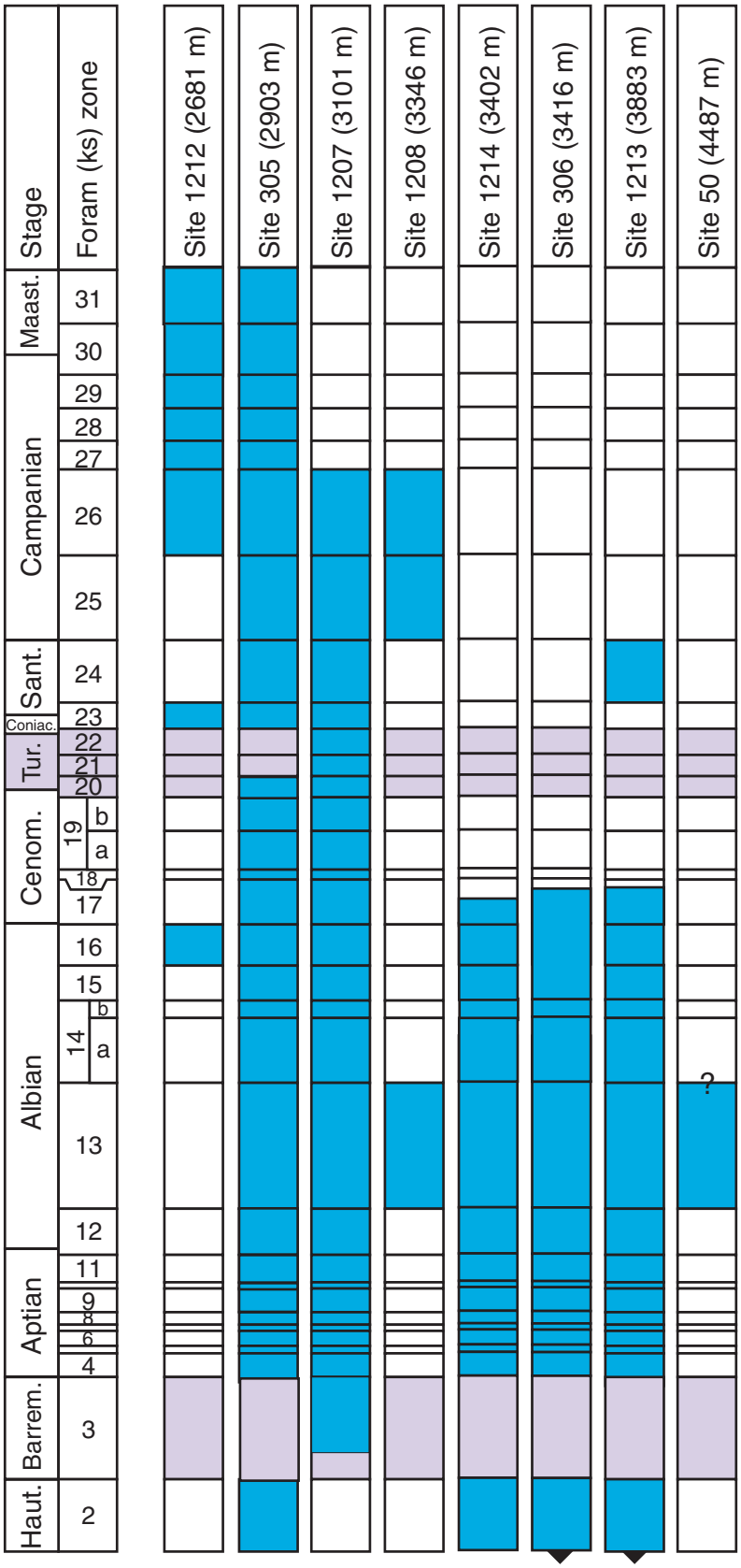
Stage
Foram (ks) zone
Maast.
Campanian
Sant.
Coniac.
Tur.
Cenom.
Albian
Aptian
Barrem.
Haut.
31
30
29
28
27
26
25
24
23
22
21
20
19
b
a
18
17
16
15
14
13
12
11
9
6
4
3
2
Site 1212 (2681 m)
Site 305 (2903 m)
Site 1207 (3101 m)
Site 1208 (3346 m)
Site 1214 (3402 m)
Site 306 (3416 m)
Site 1213 (3883 m)
Site 50 (4487 m)
?

Figure F56